

Important Notice

This copy may be used only for the purposes of research and private study, and any use of the copy for a purpose other than research or private study may require the authorization of the copyright owner of the work in question. Responsibility regarding questions of copyright that may arise in the use of this copy is assumed by the recipient.

UNIVERSITY OF CALGARY

Multicomponent seismic modeling and analysis for CO₂ storage in the Redwater reef,
Alberta, Canada

by

Taher M. Sodagar

A THESIS

SUBMITTED TO THE FACULTY OF GRADUATE STUDIES
IN PARTIAL FULFILMENT OF THE REQUIREMENTS FOR THE
DEGREE OF DOCTOR OF PHILOSOPHY

DEPARTMENT OF GEOSCIENCE

CALGARY, ALBERTA

April, 2011

© Taher M. Sodagar 2011

UNIVERSITY OF CALGARY
FACULTY OF GRADUATE STUDIES

The undersigned certify that they have read, and recommend to the Faculty of Graduate Studies for acceptance, a thesis entitled "Multicomponent seismic modeling and analysis for CO₂ storage in the Redwater reef, Alberta, Canada" submitted by Taher M. Sodagar in partial fulfilment of the requirements of the degree of DOCTOR OF PHILOSOPHY.

Supervisor, Dr. Don C. Lawton, Department of Geoscience.

Dr. Larry R. Lines, Department of Geoscience.

Dr. Rob J. Ferguson, Department of Geoscience.

Dr. Brij B. Maini, Department of Chemical and Petroleum Engineering.

*External Examiner, Dr. Richard J. Chalaturnyk,
University of Alberta.*

April 20, 2011

Date

Abstract

The Devonian Redwater reef, in Alberta, Canada, is being evaluated for geological storage of CO₂ for the Heartland Area Redwater CO₂ Storage Project (HARP). The reef complex is one of the largest Devonian reefs in the Western Canadian Sedimentary Basin and is the third largest oil reservoir in Canada. It is located close to large sources of CO₂ in the Redwater-Fort Saskatchewan-Edmonton region. The study characterized the Redwater reef, identified the reef margin, and mapped the facies variations within the reef. The seismic response of the reef to the CO₂ saturation in the Leduc Formation was investigated. Fluid substitution and seismic modeling were undertaken to generate PP and PS synthetic seismic data to study the consequences of CO₂ saturation on the seismic response of the various reef facies and formations below the reef, based on seismic attributes and character.

Common shot ray tracing and finite-difference modeling was undertaken to evaluate variations in the seismic response of the Redwater reef across the southern margin of the reef for CO₂ saturation in the Upper Leduc interval. The input geological model was based on well data and depth-converted seismic data from the interpretation of legacy 2D seismic lines in the area. Seismic reflections display positive structure below the reef in time sections due to the lateral velocity change from on-reef to off-reef, but are corrected in the depth sections.

Terminations and the lateral position of the Upper Leduc and Middle Leduc events are clear on the pre-stack time-migrated sections and a modest improvement on the depth-

migrated sections. Higher amplitudes at the base of Upper-Leduc member are evident near the reef margin due to the higher porosity of the foreslope facies in the reef rim compared to the tidal flat lagoonal facies within the center of the reef.

The 2D and 3D time-lapse multicomponent seismic modeling predicted a significant amplitude difference for the seismic data before and after CO₂ saturation, particularly for reflections from the Upper Leduc, the top of the reef rim, and the Mid Leduc member. The results show that it is feasible to map CO₂ saturation of at level 40% within the Redwater Leduc Reef through multichannel seismic surveys.

Acknowledgements

First and forever, I thank ALLAH, the merciful, for providing me the patience, support and opportunity to proceed in my high education. Second, I would like to recognize a few of people who made this thesis possible. The author would like to thank the University of Calgary and the Consortium for Research in Elastic Wave Exploration Seismology (CREWES) committed sponsors, dedicated staff and devoted students. He is grateful to Saudi Aramco for PhD program sponsorship and support. The author expresses his deep appreciation to the Dr. Don Lawton for his extreme help, advice, comments, guidance, patience, and continuous supervision during this work. The author is also thankful for his efforts and valuable time to let him understand more science and get from his wide knowledge. Special thanks are given to Helen Isaac, Kevin Hall, Rolf Maier, Han-Xing Lu, Abdullah Al-Shuhail, Faranak Mahmoudian and CREWES staff and students for their technical support, kind help, valuable discussions, and bright suggestions and ideas. Thanks to Laura Baird and Cathy Hubbell for their precious help and advice.

Data for this project was acquired through funding provided by the Alberta Energy Research Institute and ARC Resources. Software for the modeling, processing and interpretation of the data was provided to the University of Calgary by NORSAR Innovation AS, Landmark Graphics Corporation, Paradigm, and Seismic Micro-Technology. Software for the fluid replacement modeling and synthetic generating of the well data was provided by Hampson-Russell Software and Accumap.

Dedication

I would like to dedicate my thesis to my parents who help, support, advice, and pray for me. They always encourage me to proceed in my career and academy. I also dedicate it to my children, Mohammad, Omar, Lama, and Jana, for being good children, so that I could focus on my study. My last special dedication goes to my lovely wife, Amal NoorSaeed for her support, patience and understanding through my study, which has helped me reach the final page.

Table of Contents

Approval Page	ii
Abstract	iii
Acknowledgements	v
Dedication	vi
Table of Contents	vii
List of Tables.....	x
List of Figures and Illustrations	xi
List of Symbols and Abbreviations	xxii
Epigraph.....	xxiii
CHAPTER ONE: INTRODUCTION	1
1.1 Motivation of this dissertation.....	1
1.2 Background of international CCS projects.....	2
1.3 Dissertation significance	3
1.4 Objectives of the dissertation	4
1.5 Area of study	5
1.6 Geological background	6
1.6.1 Regional geologic and stratigraphic settings.....	6
1.6.2 Evolution and framework of the study area	8
1.6.3 The Redwater reef facies.....	11
1.6.4 Reservoir quality and rock properties	13
1.6.5 Reservoir pressure and formation water	14
1.6.6 Hydrogeological characteristics	14
1.7 Dissertation structure	15
1.8 Software used in the research program.....	16
CHAPTER TWO: SEISMIC INTERPRETATION OF THE REDWATER LEDUC REEF.....	18
2.1 Introduction	18
2.2 Methodology.....	18
2.2.1 Surface Seismic and Well Log Datasets	18
2.2.2 Seismic Data Reprocessing	20
2.2.3 Software	22
2.2.4 Synthetic Seismograms and correlation to seismic data	22
2.3 Seismic Section Interpretation.....	23
2.4 Map Interpretation	31
2.5 DISCUSSION AND CONCLUSIONS	38
CHAPTER THREE: WELL-BASED FLUID SUBSTITUTION SEISMIC MODELING IN REDWATER REEF.....	41
3.1 Introduction	41
3.2 Methodology.....	41
3.2.1 Synthetic Seismogram Generation	41
3.2.2 Fluid Substitution Seismic Modeling	42
3.3 Results.....	46

3.4 Discussion	57
CHAPTER FOUR: MULTICHANNEL TIME-LAPSE SEISMIC MODELING OF CO₂ FLUID SUBSTITUTION IN THE REDWATER LEDUC REEF.....	
4.1 Introduction	59
4.2 Methodology.....	60
4.2.1 Common Shot Surface Seismic Modeling	60
4.2.2 Seismic Survey Parameters	62
4.2.3 Seismic Data Processing	64
4.2.4 Software	65
4.3 Results – Line A	65
4.3.1 Baseline Modeling - ray traced data	67
4.3.2 Baseline Modeling - finite difference data.....	69
4.3.3 CO ₂ Fluid Substitution, Line A	73
4.3.3.1 CO ₂ replacement in the Upper Leduc member	73
4.3.3.2 CO ₂ saturation in the entire Leduc formation	79
4.3.3.3 CO ₂ saturation in the Leduc rim target zone only	85
4.4 Results – Line B	90
4.4.1 East-west Model including Duvernay Embayment	90
4.4.2 East-west Geological Model after CO ₂ Fluid Replacement.....	97
4.5 Results – Time-lapse of converted wave seismic modeling	103
4.5.1 Baseline Modeling, Line A	103
4.5.2 CO ₂ Fluid Substitution, Line A	108
4.6 Conclusions	113
CHAPTER FIVE: 4D MULTICOMPONENT SEISMIC MODELING OF CO₂ FLUID SUBSTITUTION IN THE REDWATER DEVONIAN REEF	
5.1 Introduction	115
5.2 Methodology.....	117
5.2.1 Common Shot Surface Seismic Modeling	117
5.2.2 Seismic Survey Parameters	118
5.2.3 Seismic Data Processing	124
5.2.4 Software	124
5.3 Results	125
5.3.1 Seismic section interpretation	126
5.3.1.1 Post-stack time migrated seismic section interpretation.....	126
5.3.1.2 Pre-stack time migrated seismic section interpretation	133
5.3.1.3 Pre-stack depth migrated seismic section interpretation	138
5.3.2 Seismic attribute map interpretation	143
5.3.2.1 PSTM amplitude map interpretation	144
5.3.2.2 PSDM amplitude map interpretation.....	150
5.4 Conclusions	157
CHAPTER SIX: DISCUSSION AND CONCLUSIONS	
6.1 Introduction	159
6.2 CO ₂ storage capacity in the Redwater Leduc reef.....	159
6.3 Discussion about assumptions used in the Dissertation.....	164

6.4 Conclusions	167
6.4.1 Surface 2D seismic data interpretation	167
6.4.2 Well-based fluid substitution seismic modeling.....	168
6.4.3 Time-lapse 2D and 3D multicomponent seismic modeling of CO ₂ fluid substitution in the Redwater Leduc reef.....	169
6.5 Recommendations for future work	170
REFERENCES.....	172

List of Tables

Table 2.1: Processing flow and parameters of the reprocessed 2D seismic data in the Redwater area.	21
Table 2.2: Interval velocities computed from sonic logs for targeted intervals.....	34
Table 3.1: Results of the well 16-08-57-23W4 before and after CO ₂ fluid substitution within of the entire thickness of the Leduc Formation, with average porosity of 6%.	50
Table 3.2: Results of the well 11-08-57-22W4 before and after CO ₂ fluid substitution within of the entire thickness of the Leduc Formation, with average porosity of 4%.	53
Table 4.1: Survey design parameters used for the 2D seismic modeling in the Redwater area for both Line A and B.	64
Table 5.1: 3D survey design parameters used for the 3D seismic modeling in the Redwater reef area.	123
Table 6.1: Redwater reef calculated CO ₂ storage capacity with different scenarios	164

List of Figures and Illustrations

Figure 1.1: World energy-related carbon dioxide emissions by fuel type (EIA, 2010).	2
Figure 1.2: Alberta map showing the location of Study area and the wells penetrating the Lower Leduc formation (Lawton and Sodagar, 2009 and Sodagar and Lawton, 2009).....	6
Figure 1.3: Stratigraphic cross section from northwest (basinward) to central (cratonward) Canada presenting the regional stratigraphic settings. The highlighted box is shown in detail in next figure (from Atchley et al., 2006).	7
Figure 1.4: Sequence stratigraphic cross section across central Alberta showing the Devonian sequences and formation subdivisions (from Atchley et al., 2006).....	8
Figure 1.5: General stratigraphy and hydrostratigraphy presenting the aquifer and aquitard in the study area (Bachu et al., 2008).	9
Figure 1.6: Cooking Lake Formation platform map demonstrating outlines of Redwater Leduc reef and Woodbend Group boundaries (from Gunter and Bachu, 2007).	10
Figure 1.7: West to east cross section illustrating the Leduc formation Redwater reef and adjacent formations (from Gunter and Bachu, 2007).....	12
Figure 1.8: Southwest to Northeast cross section presenting the Redwater Leduc reef complex divisions, Duvernay embayment, and Cooking Lake platform (after Gunter et al., 2009).	12
Figure 1.9: Core photograph of the Redwater Leduc formation showing the rock composition and porosity of the well 05-04-58-21W4 (Geoscience Dept. Lab).....	13
Figure 1.10: Southwest to northeast dip cross section showing the Redwater reef and also the separation of the Upper Mannville and shallower aquifers from the Lower Mannville and deeper aquifers (from Bachu et al., 2008).....	15
Figure 2.1: Redwater reef map showing all wells. Those wells that penetrate the Cooking Lake Formation and have sonic logs are highlighted in red.	19
Figure 2.2: Map showing the outline of the Redwater reef and the distribution of all the 2D seismic data available for the project. The black filled circles show the locations of wells that penetrate the Cooking Lake Formation and which have sonic and density logs.	20
Figure 2.3: Zero-phase Ricker 35Hz wavelet in time and frequency domain.	23
Figure 2.4: Sonic, density logs and synthetic of the well 11-08-57-22W4 correlated with seismic line with picked key horizons. This is an on-reef well.	25

Figure 2.5: Sonic, density logs and synthetic of the well 16-01-56-22W4 correlated with seismic line with picked key horizons. This is an off-reef well.	26
Figure 2.6: Sonic, density logs and synthetic of the well 11-24-56-24W4 correlated with seismic line with picked key horizons. This is an off-reef well with shale embayment of the Duvernay Formation.	27
Figure 2.7: Sonic, density logs and synthetic of the well 01-25-57-24W4 correlated with seismic line with picked key horizons. This is an off-reef well.	28
Figure 2.8: Interpreted north-south seismic section. This line shows the reef edge clearly and the Duvernay event terminating close to the reef margin.	29
Figure 2.9: Interpreted north-south seismic section. This line shows Duvernay embayment event encroaching into the reef buildup near the south end.	30
Figure 2.10: Interpreted west-east seismic section. This line shows Duvernay embayment event encroaching into the reef buildup from the west.	30
Figure 2.11: Interpreted west-east seismic section. This line shows the reef edge and the Dolomitization event at the west margin of the reef.	31
Figure 2.12: Time structure map of the Mannville Formation with the Devonian Leduc reef edge outlined except the eastern boundary marks the edge of data.	34
Figure 2.13: Time structure map of the Nisku Formation with the Devonian Leduc reef edge outlined except the eastern boundary marks the edge of data.	35
Figure 2.14: Time structure map of the Upper Leduc Formation with the Leduc reef edge outlined except the eastern boundary marks the edge of data.	35
Figure 2.15: Time structure map of Duvernay Fm with the embayment outlined between the brown and blue lines. The eastern boundary marks the edge of data.	36
Figure 2.16: Time structure map of top of Beaverhill Lake Formation with the reef edge outlined except the eastern boundary marks the edge of data.	36
Figure 2.17: Depth structure map of the Upper Leduc Formation with the Leduc reef edge outlined except the eastern boundary marks the edge of data.	37
Figure 2.18: Isochron map between Leduc and Beaverhill Lake Formations with the reef edge outlined except the eastern boundary is the edge of data.	37
Figure 2.19: Isopach map between Leduc and Beaverhill Lake Formations with the reef edge outlined except the eastern boundary marks the edge of data.	38

Figure 3.1: Redwater reef map showing all wells. Those that penetrate the Cooking Lake Formation and have sonic logs are in red color. Wells 11-08 and 1-08 were used for fluid substitution modeling.	42
Figure 3.2: Temperature and pressure phase diagram for pure carbon dioxide (Span et al., 1996, cited by Piri et al., 2005).	45
Figure 3.3: Sonic, density, and gamma ray logs and synthetic seismograms from well 11-08-57-22W4 with normal and reverse polarities.	48
Figure 3.4: Sonic, density, and gamma ray logs and synthetic seismograms from well 16-08-57-23W4 with normal and reverse polarities.	48
Figure 3.5: The relationship between the P-wave and S-wave velocity changes and CO ₂ saturation for well 16-08-57-23W4.	49
Figure 3.6: Zero-offset synthetic seismic traces for well 16-08-57-23W4, with CO ₂ fluid substitution from 0% (left) to 100% (right) in each panel. (A) wiggle-trace display, (B) color amplitude with wiggle-trace overlay, and (C) interval velocity with wiggle-trace overlay.	51
Figure 3.7: Zero-offset synthetic seismic traces of the well 16-08-57-23W4 before and after fluid substitution. (A) absolute amplitudes, and (B) amplitude difference compared to 0% saturation.	52
Figure 3.8: The relationship between the P-wave and S-wave velocity changes and various CO ₂ saturations of the well 11-08-57-22W4.	54
Figure 3.9: Zero-offset synthetic seismic traces for well 11-08-57-22W4, with CO ₂ fluid substitution from 0% (left) to 100% (right) in each panel. (A) wiggle-trace display, (B) color amplitude with wiggle-trace overlay, and (C) interval velocity with wiggle-trace overlay.	55
Figure 3.10: Zero-offset synthetic seismic traces of the well 11-08-57-22W4 before and after fluid substitution. (A) absolute amplitudes, and (B) amplitude difference compared to 0% saturation.	56
Figure 4.1: Redwater reef map showing available wells. Those wells that penetrate the Cooking Lake Formation and have sonic logs are highlighted in red. The red and blue lines are the location of 2D geological models.	61
Figure 4.2: 2D geological model along Line A, where crosses the southern margin of the Redwater reef, showing the formations included in the model.	63
Figure 4.3: Density values of the 2D model along Line A.	63
Figure 4.4: P-wave velocities of the 2D model along Line A.	64

Figure 4.5: Ray tracing numerical seismic shot gather data from the Line A.	66
Figure 4.6: Finite difference numerical seismic shot gather from the Line A.	66
Figure 4.7: 2D ray traced numerical seismic section after CDP stack, Line A, with interfaces identified on the section.	68
Figure 4.8: 2D ray traced numerical seismic section after post-stack time migration, Line A, with interfaces identified on the section.	68
Figure 4.9: 2D ray traced numerical seismic section after pre-stack time migration, Line A.....	70
Figure 4.10: 2D ray traced numerical seismic section after pre-stack depth migration, Line A. Note the litho-facies impedance contrast at the base of Upper Leduc as well as thinning at the top of the reef rim.	70
Figure 4.11: Colored pre-stack depth migrated section from Line A, with interfaces identified, showing the litho-facies impedance contrast at the top and base of Upper Leduc as well as thinning across the top of the reef rim.	71
Figure 4.12: Interpreted north-south seismic section near Line A. This line shows the reef edge clearly and the Duvernay event terminating close to the reef margin. It illustrates litho-facies impedance contrast at the top and base of Upper Leduc as well as thinning across the top of the reef rim.	71
Figure 4.13: Colored velocity model super-imposed on pre-stack depth migration seismic section, Line A.	72
Figure 4.14: 2D finite difference numerical seismic section after pre-stack time migration, Line A, with interfaces identified on the section.	72
Figure 4.15: 2D finite difference numerical seismic section after pre-stack depth migration, Line A, showing litho-facies impedance contrast at the base of Upper Leduc as well as thinning across the top of the reef rim.	73
Figure 4.16: 2D geological model with CO ₂ fluid substitution in the Upper Leduc member along Line A, across the southern margin of the Redwater reef, showing P-wave interval velocities of the various formations.....	74
Figure 4.17: 2D ray traced numerical seismic section after CO ₂ fluid substitution and PSTM, Line A.....	76
Figure 4.18: 2D ray traced numerical seismic section after CO ₂ fluid substitution and PSDM, Line A.	76
Figure 4.19: 2D finite difference numerical seismic section after CO ₂ fluid substitution and PSTM, Line A.	77

Figure 4.20: 2D finite difference numerical seismic section after CO ₂ fluid substitution and PSDM, Line A.	77
Figure 4.21: Time-lapse difference seismic section before and after CO ₂ substitution in the Upper Leduc member, Line A (ray trace modeling and PSDM).	78
Figure 4.22: Time-lapse difference seismic section before and after CO ₂ substitution in the Upper Leduc member, Line A (finite difference modeling and PSDM).	78
Figure 4.23: Colored velocity model super-imposed on the PSDM seismic section after CO ₂ fluid substitution, Line A.	79
Figure 4.24: 2D geological model with CO ₂ fluid substitution in the entire Leduc Formation along Line A, across the southern margin of the Redwater reef, showing P-wave interval velocities of the various formations.	81
Figure 4.25: 2D ray traced numerical seismic section after CO ₂ fluid substitution in the entire Leduc Formation and PSTM, Line A.	82
Figure 4.26: 2D ray traced numerical seismic section after CO ₂ fluid substitution in the entire Leduc Formation and PSDM, Line A.	82
Figure 4.27: 2D finite difference numerical seismic section after CO ₂ fluid substitution in the entire Leduc Formation and PSTM, Line A.	83
Figure 4.28: 2D finite difference numerical seismic section after CO ₂ fluid substitution in the entire Leduc Formation and PSDM, Line A.	83
Figure 4.29: Time-lapse difference seismic section before and after CO ₂ substitution in the entire Leduc Formation, Line A (ray trace modeling and PSDM).	84
Figure 4.30: Time-lapse difference seismic section before and after CO ₂ substitution in the entire Leduc Formation, Line A (finite difference modeling and PSDM).	84
Figure 4.31: 2D geological model with CO ₂ fluid substitution in the rim of Upper Leduc member along Line A, across the southern margin of the Redwater reef, showing P-wave interval velocities of the various formations.	86
Figure 4.32: 2D ray traced numerical seismic section after CO ₂ fluid substitution in the rim of Upper Leduc member and PSTM, Line A.	87
Figure 4.33: 2D ray traced numerical seismic section after CO ₂ fluid substitution in the rim of Upper Leduc member and PSDM, Line A.	87
Figure 4.34: 2D finite difference numerical seismic section after CO ₂ fluid substitution in the rim of Upper Leduc member and PSTM, Line A.	88

Figure 4.35: 2D finite difference numerical seismic section after CO ₂ fluid substitution in the rim of Upper Leduc member and PSDM, Line A.	88
Figure 4.36: Time-lapse difference seismic section before and after CO ₂ substitution in the rim target zone, Line A (ray trace modeling and PSDM).	89
Figure 4.37: Time-lapse difference seismic section before and after CO ₂ substitution in the rim target zone, Line A (finite difference modeling and PSDM).	89
Figure 4.38: 2D geological model along Line B, where crosses the eastern margin of the Redwater reef, showing the formations included in the model.	91
Figure 4.39: Density values of the 2D model along Line B.	91
Figure 4.40: P-wave velocities of the 2D model along Line B.	92
Figure 4.41: 2D ray traced numerical seismic section after pre-stack time migration, Line B. Arrow shows Duvernay embayment event encroaching into the reef.	94
Figure 4.42: 2D ray traced numerical seismic section after pre-stack depth migration, Line B. Note the litho-facies impedance contrast at the base of Upper Leduc and Duvernay invasion as well as thinning at the top of the reef rim.	94
Figure 4.43: Colored pre-stack depth migrated section from Line B, showing the litho-facies impedance contrast at the top, base of Upper Leduc and Duvernay invasion as well as thinning across the top of the reef rim.	95
Figure 4.44: Interpreted west-east seismic section near Line B. This line shows the reef edge clearly and a limited Duvernay embayment event encroaching into the reef buildup from the west. Tie with well 11-24 is shown.	95
Figure 4.45: Colored velocity model super-imposed on pre-stack depth migration seismic section, Line B.	96
Figure 4.46: 2D finite difference numerical seismic section after pre-stack time migration, Line B, with interfaces identified on the section.	96
Figure 4.47: 2D finite difference numerical seismic section after pre-stack depth migration, Line B, showing the Duvernay embayment event encroaching into the reef buildup.	97
Figure 4.48: 2D geological model with CO ₂ fluid substitution in the Upper Leduc member along Line B, across the eastern margin of the Redwater reef, showing P-wave interval velocities of the various formations.	98
Figure 4.49: 2D ray traced numerical seismic section after CO ₂ fluid substitution and PSTM, Line B.	100

Figure 4.50: 2D ray traced numerical seismic section after CO ₂ fluid substitution and PSDM, Line B.	100
Figure 4.51: 2D finite difference numerical seismic section after CO ₂ fluid substitution and PSTM, Line B.	101
Figure 4.52: 2D finite difference numerical seismic section after CO ₂ fluid substitution and PSDM, Line B.	101
Figure 4.53: Time-lapse difference seismic section before and after CO ₂ substitution in the Upper Leduc member, Line B (ray trace modeling and PSDM).	102
Figure 4.54: Time-lapse difference seismic section before and after CO ₂ substitution in the Upper Leduc member, Line B (finite difference modeling and PSDM).	102
Figure 4.55: Colored velocity model super-imposed on the PSDM seismic section after CO ₂ fluid substitution, Line B.	103
Figure 4.56: Radial component of converted wave (PS) ray tracing numerical shot gather after geometry and sorting from the Line A model.	105
Figure 4.57: Radial component of converted wave (PS) ray tracing numerical shot gather after geometry sorting and trailing trace polarity reverse from the Line A model.	106
Figure 4.58: Radial component of converted wave (PS) seismic section after pre-stack time migration, Line A, with interfaces identified on the section.	106
Figure 4.59: Radial component of converted wave (PS) seismic section after pre-stack depth migrated section, Line A.	107
Figure 4.60: PS colored pre-stack depth migrated section from Line A, showing the litho-facies impedance contrast at the top and base of Upper Leduc as well as thinning across the top of the reef rim.	107
Figure 4.61: Registration and Comparison of the events between the PP wave and PS wave PSTM seismic sections from the Line A.	108
Figure 4.62: Comparison and matching the events between PP wave and PS wave PSDM seismic sections from the Line A.	108
Figure 4.63: Radial converted wave seismic section after CO ₂ fluid substitution and PSTM, Line A.	110
Figure 4.64: Radial converted wave seismic section after CO ₂ fluid substitution and PSDM, Line A.	110

Figure 4.65: Registration and Comparison of the events between the PP wave and PS wave PSTM seismic sections from the Line A, after CO ₂ replacement in the Upper Leduc member.....	111
Figure 4.66: Comparison and matching the events between PP wave and PS wave PSDM seismic sections from the Line A, after CO ₂ replacement in the Upper Leduc member.	112
Figure 4.67: Time-lapse difference seismic section before and after CO ₂ substitution in the Upper Leduc member, Line A (radial converted wave ray trace modeling and PSDM).	112
Figure 5.1: Redwater reef map showing the wells that penetrate the Cooking Lake Formation and have sonic logs and also showing the distribution of all the 2D seismic data available for the project. The colours depict different vintages of data purchased. The location of the synthetic 3D survey is shown in the southern margin of the Redwater reef. The eastern boundary marks the edge of data, not the edge of the reef.....	116
Figure 5.2: 3D view of the gridded depth structure maps of the Redwater reef, showing the Leduc, Duvernay, Cooking Lake, and Beaverhill Lake formations that included in the 3D model.....	119
Figure 5.3: 3D geological model at the southern margin of the Redwater reef, showing the formations included in the model.....	120
Figure 5.4: 3D geological model at the southern margin of the Redwater reef, showing densities of the various formations (brine saturation).....	121
Figure 5.5: 3D geological model at the southern margin of the Redwater reef, showing densities of the various formations after CO ₂ saturation in Upper Leduc member.....	121
Figure 5.6: 3D geological model at the southern margin of the Redwater reef, showing P-wave interval velocities of the various formations (brine saturation). ..	122
Figure 5.7: 3D geological model at the southern margin of the Redwater reef, showing P-wave interval velocities of the various formations after CO ₂ saturation in Upper Leduc member.....	122
Figure 5.8: 3D survey design showing the source and receiver layout, parallel source and receiver lines every 200m, the source line in the east-west direction and shot every 100m, the receiver line in north-south direction, and the station every 50m.	123
Figure 5.9: 3D ray tracing numerical seismic shot gather data.....	125
Figure 5.10: 3D ray traced numerical seismic volume (A) after CDP stack and (B) after post-stack time migration.	127

Figure 5.11: Vertical component (PP) seismic section (inline 48) after post-stack time migration, with interfaces identified on the section.	130
Figure 5.12: Vertical component (PP) seismic section (crossline 46) after post-stack time migration, with interfaces identified on the section.	130
Figure 5.13: Vertical component (PP) post-stack time migrated seismic section (crossline 46) after CO ₂ fluid substitution in Upper Leduc member.	131
Figure 5.14: PP difference after post-stack time migration (crossline 46) before and after CO ₂ fluid substitution.	131
Figure 5.15: Radial component (PS) seismic section (crossline 46) after post-stack time migration, with interfaces identified on the section.	132
Figure 5.16: Radial component (PS) post-stack time migrated seismic section (crossline 46) after CO ₂ fluid substitution in Upper Leduc member.	132
Figure 5.17: PS difference after post-stack time migration (crossline 46) before and after CO ₂ fluid substitution. Color amplitude scale is 2 times of PP.	133
Figure 5.18: Vertical component (PP) seismic section (crossline 46) after pre-stack time migration, with interfaces identified on the section.	135
Figure 5.19: Vertical component (PP) pre-stack time migrated seismic section (crossline 46) after CO ₂ fluid substitution in Upper Leduc member.	135
Figure 5.20: PP difference after pre-stack time migration (crossline 46) before and after CO ₂ fluid substitution.	136
Figure 5.21: Radial component (PS) seismic section (crossline 46) after pre-stack time migration, with interfaces identified on the section.	137
Figure 5.22: Radial component (PS) pre-stack time migrated seismic section (crossline 46) after CO ₂ fluid substitution in Upper Leduc member.	137
Figure 5.23: PS difference after pre-stack time migration (crossline 46) before and after CO ₂ fluid substitution. Color scale is 4 times of PP.	138
Figure 5.24: Vertical component (PP) seismic section (crossline 46) after pre-stack depth migration, with interfaces identified on the section.	140
Figure 5.25: Vertical component (PP) pre-stack depth migrated seismic section (crossline 46) after CO ₂ fluid substitution in Upper Leduc member.	140
Figure 5.26: PP difference after pre-stack depth migration (crossline 46) before and after CO ₂ fluid substitution.	141

Figure 5.27: Radial component (PS) seismic section (crossline 46) after pre-stack depth migration, with interfaces identified on the section.	142
Figure 5.28: Radial component (PS) pre-stack depth migrated seismic section (crossline 46) after CO ₂ fluid substitution in Upper Leduc member.	142
Figure 5.29: PS difference after pre-stack depth migration (crossline 46) before and after CO ₂ fluid substitution.	143
Figure 5.30: Amplitude map of Leduc horizon of (PP) PSTM seismic data. The pink color line is the Redwater reef southern edge.	146
Figure 5.31: Amplitude map of Leduc horizon of (PP) PSTM seismic data after CO ₂ fluid substitution in Upper Leduc member.	146
Figure 5.32: Amplitude map of Leduc horizon of PP difference after PSTM before and after CO ₂ saturation.	146
Figure 5.33: Amplitude map of Mid-Leduc horizon of (PP) PSTM seismic data.	147
Figure 5.34: Amplitude map of Mid-Leduc horizon of (PP) PSTM seismic data after CO ₂ fluid substitution in Upper Leduc member.	147
Figure 5.35: Amplitude map of Mid-Leduc horizon of PP difference after PSTM before and after CO ₂ saturation.	147
Figure 5.36: Amplitude map of Leduc horizon of (PS) PSTM seismic data.	148
Figure 5.37: Amplitude map of Leduc horizon of (PS) PSTM seismic data after CO ₂ fluid substitution in Upper Leduc member.	148
Figure 5.38: Amplitude map of Leduc horizon of PS difference after PSTM before and after CO ₂ saturation.	148
Figure 5.39: Amplitude map of Mid-Leduc horizon of (PS) PSTM seismic data.	149
Figure 5.40: Amplitude map of Mid-Leduc horizon of (PS) PSTM seismic data after CO ₂ fluid substitution in Upper Leduc member.	149
Figure 5.41: Amplitude map of Mid-Leduc horizon of PS difference after PSTM before and after CO ₂ saturation.	149
Figure 5.42: Amplitude map of Leduc horizon of (PP) PSDM seismic data.	152
Figure 5.43: Amplitude map of Leduc horizon of (PP) PSDM seismic data after CO ₂ fluid substitution in Upper Leduc member.	152
Figure 5.44: Amplitude map of Leduc horizon of PP difference after PSDM before and after CO ₂ saturation.	152

Figure 5.45: Amplitude map of Mid-Leduc horizon of (PP) PSDM seismic data.	153
Figure 5.46: Amplitude map of Mid-Leduc horizon of (PP) PSDM seismic data after CO ₂ fluid substitution in Upper Leduc member.	153
Figure 5.47: Amplitude map of Mid-Leduc horizon of PP difference after PSDM before and after CO ₂ saturation.	153
Figure 5.48: Amplitude map of Leduc horizon of (PS) PSDM seismic data.	154
Figure 5.49: Amplitude map of Leduc horizon of (PS) PSDM seismic data after CO ₂ fluid substitution in Upper Leduc member.	154
Figure 5.50: Amplitude map of Leduc horizon of PS difference after PSDM before and after CO ₂ saturation.	154
Figure 5.51: Amplitude map of Mid-Leduc horizon of (PS) PSDM seismic data.	155
Figure 5.52: Amplitude map of Mid-Leduc horizon of (PS) PSDM seismic data after CO ₂ fluid substitution in Upper Leduc member.	155
Figure 5.53: Amplitude map of Mid-Leduc horizon of PS difference after PSDM before and after CO ₂ saturation.	155
Figure 5.54: Fold distribution maps of (A) PP and (B) PS acquisition survey with maximum offset of 1500m.	156
Figure 6.1: Redwater reef map showing all wells. Those wells that penetrate the Cooking Lake Formation and have sonic logs are highlighted in red. The blue color line presents the Redwater reef margin, the dashed red line outlines the reef water-leg scope and the dotted green line delineates the Redwater reef rim in the water-leg region.	163

List of Symbols and Abbreviations

Symbol	Definition
2D	Two-dimensional
3C	Three-component
3D	Three-dimensional
4D	Four-dimensional
ACP	Asymptotic conversion point
CCS	Carbon capture and storage
CDP	Common depth point
CMP	Common midpoint
CO ₂	Carbon Dioxide
EOR	Enhanced oil recovery
GHG	Greenhouse gas
HARP	Heartland area Redwater project
Hz	Hertz
K	Bulk modulus
MPa	MegaPascal
NMO	Normal moveout
OOIP	Original oil in place
P _c	Critical pressure
PSDM	Pre-stack depth migration
PSTM	Pre-stack time migration
P-wave	Compressional wave
rms	Root mean square
S-wave	Shear wave
SRD	Seismic reference datum
T _c	Critical temperature
V _p	Compressional wave velocity
V _s	Shear wave velocity
WCSB	Western Canada sedimentary basin
∅	Rock porosity
ρ	Rock density
μ	Shear modulus
ΔT	Two-way time delay

Epigraph

And they ask you, [O Muhammad], about the soul. Say, "The soul is of the affair of my Lord. And mankind have not been given of knowledge except a little".

The Holy Qur'an, (chapter 17: verse 85), translation of Sahih International.

Chapter One: **INTRODUCTION**

1.1 Motivation of this dissertation

Growing emissions of Carbon Dioxide (CO₂) have caused the atmospheric concentration of this greenhouse gas (GHG) to increase by approximately 32% between 1850 and 1994 (Houghton et al., 1994). Recent studies confirmed that CO₂ is a major GHG contributing to climate change, known as global warming, and formed 77% of the total GHGs emitted in 2000 (Del Pino et al., 2006). The global warming problem occurs due to the increase in concentration of these GHGs causing more heat to be trapped in the earth's atmosphere (IPCC, 2005). The world energy-related carbon dioxide emissions are increasing and projected to be increased in the future (Figure 1.1).

The Alberta Basin is one of the Canada's major petroleum sedimentary basins and has one of the world's largest commercial opportunities for reducing CO₂ emissions into the atmosphere. It could be done through Carbon Capture and Storage (CCS) in subsurface deep geological formations (Gunter and Bachu, 2007). Most emissions of CO₂ are from large stationary sources, such as thermal power plants, refineries, oil sand plants, and cement plants (Bachu, 2000) which some are close to the area studied in this thesis.

Generally, the initial target of CCS is for permanent Storage of CO₂ or increase in oil production through enhanced oil recovery (EOR). This is of great importance and significance as Canada has the second largest oil reserve in the world and has a major role to play in Canada's global warming mitigation efforts (Gunter and Bachu, 2007). It

is planned to undertake a carbon capture and permanent storage project in the Redwater Devonian Leduc reef for the Heartland Area Redwater CO₂ Storage Project (HARP).

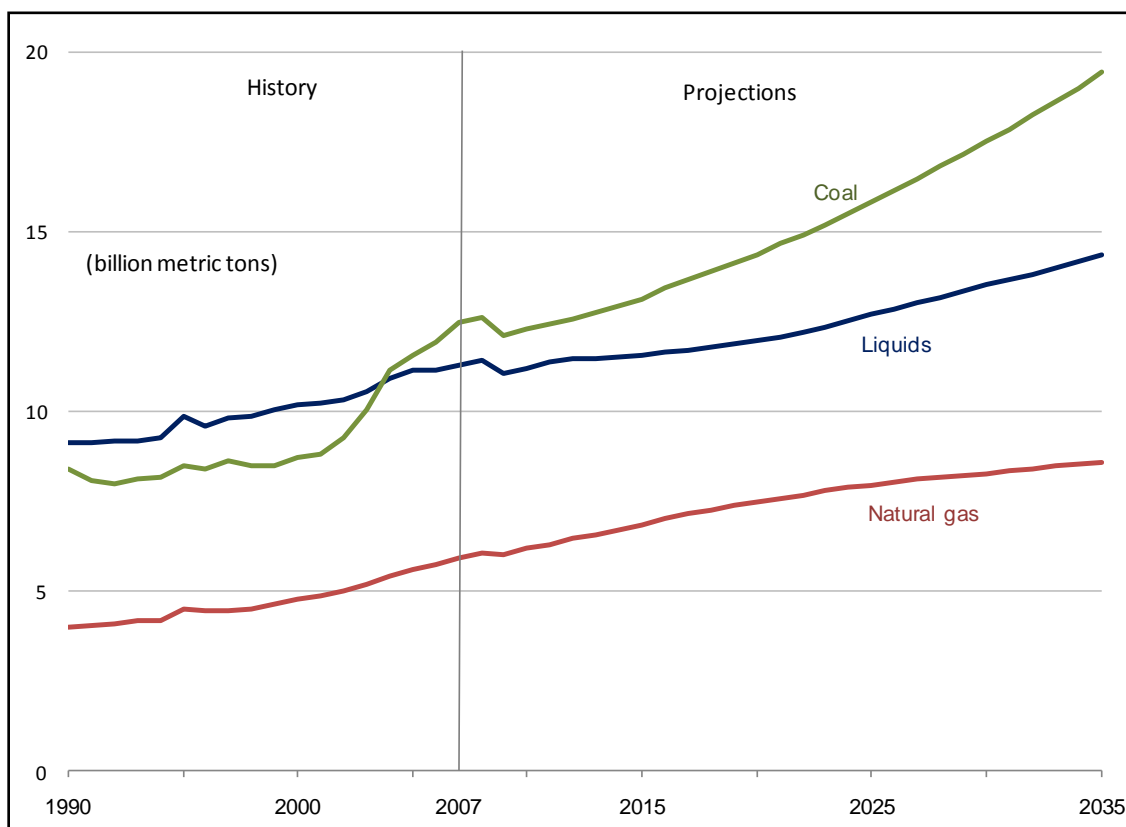


Figure 1.1: World energy-related carbon dioxide emissions by fuel type (EIA, 2010).

1.2 Background of international CCS projects

Seismic methods are one of the many geological sequestration monitoring and verification (MMV) techniques (IPCC, 2005), such as geochemical and geomechanical practices in the performance of the CCS technology. In industry, the CCS project was successfully employed in different parts of the world using the seismic analysis of time-lapse technology. Some of the implemented cases are illustrated in this thesis. In the first example, CO₂ is injected in the Sleipner field in North Sea, offshore Norway, in saline

aquifer of Utsira sand. It is 200-300m in thickness. It has 27-39% of porosity and 0.8-3 Darcy of permeability (Arts et al., 2002). The Weyburn field in Saskatchewan, Canada, is another example of CCS where oil bearing carbonates has average porosity of 15-26% and permeability of 0.1-0.3 Darcy. The thickness is 3-30m (Brown et al., 2002).

The Violet Grove in Alberta, Canada is oil bearing Cardium upper sand unit with thickness of around 6m and has 16% average porosity with 0.02 Darcy of average permeability (Dashtgard et al., 2006). In addition, the Wabamun Lake project also in Alberta that focuses on brine bearing Nisku dolostone with thickness of 50m has average porosity of 9% and 0.17 Darcy of average permeability (Michael et al., 2008). More successful examples are in the In Salah field for enhanced gas recovery (EGR) and Krechba fields in Algeria (Riddiford et al, 2003; Mathieson et al, 2008), in the Frio site in the United States for permanent storage in geological saline formation (Daley et al., 2005), and in China for enhanced coalbed methane recovery (Yu et al., 2006).

1.3 Dissertation significance

The significant of this study is to examine the suitability of the low porosity Devonian Leduc carbonate formation at Redwater reef within the Western Canada sedimentary basin (WCSB) in Alberta for the geological storage of CO₂, and for using seismic analysis for time-lapse monitoring. The various successes of time-lapse seismic analysis in the international CCS projects show the feasibility of reflection surface seismic techniques in monitoring, detecting and tracking sequestered CO₂. Therefore, a broad

range of time-lapse seismic analysis techniques will be evaluated and compared in this study.

In theory, all the analyses depend on assumption that the injected CO₂ will change the reservoir rock properties. Therefore, it will affect the seismic response which gives different seismic anomalies with various CO₂ saturations. Consequently, using fluid substitution seismic modeling and different quantitative reflection seismic interpretation methods like seismic attributes allow prediction, identification and evaluation of future CO₂ sequestration in the Leduc reef at the Redwater area. Finally, the dissertation utilizes all the available geological, geophysical, hydrogeological, geomechanical, and geochemical information to enhance our understanding of significant issues like feasibility of the Leduc reef for CCS, CO₂ storage capacity, injectivity, containment, and length of storage.

1.4 Objectives of the dissertation

There were several key objectives to this study. The first main objective was the Redwater reef site characterization to identify the reef margin, and to map facies variations within the reef, based on seismic character and by generating synthetic seismograms for the wells with sonic log that penetrated Devonian Cooking Lake formation within and around the Redwater reef. A second objective was to map the external and internal geometry of the Redwater Devonian reef for the potential geological storage of CO₂ using available 2D seismic data.

A third major objective was to identify and evaluate the future CO₂ saturation in the Devonian Leduc reservoir at the Redwater reef by using well-based fluid substitution seismic modeling approach. Finally, the fourth objective was to predict the monitoring and verification of the CO₂ saturation response by undertaking time-lapse 2D and 3D multicomponent seismic modeling for the Redwater reef before and after CO₂ fluid substitution reaching the end-state situation.

1.5 Area of study

The study area is located in the Redwater region of Alberta, northeast of Edmonton, (Anderson et al., 1989) encompassing Townships of 56 to 58 and Ranges of 20 to 24W4 (Figure 1.2). The Leduc reef at Redwater is one of the largest Devonian reefs in the Western Canada sedimentary basin (WCSB) and is the third largest oil reservoir in Canada. The original oil in place (OOIP) reserves was about 1.3 billion barrels. The Redwater reef is in the Heartland area close to large sources of CO₂ in the Redwater-Fort Saskatchewan-Edmonton region (Gunter and Bachu, 2007).

The reef complex has a triangular-rounded shape (Figure 1.2) with an area of about 600 km² (Anderson et al., 1989) and lies at depth of about 1000 m (-400 m elevation). It has a thickness of 160 to 300 m and had an original oil cap almost 50 m thick. The Redwater reef is currently under the last stages of water flooding for oil production, and this depleted oil reservoir is currently used for water disposal (Bachu et al, 2008). The downdip leg of the Leduc Formation in the reef is being assessed for a CCS project (Lawton and Sodagar, 2009 and Sodagar and Lawton, 2009).

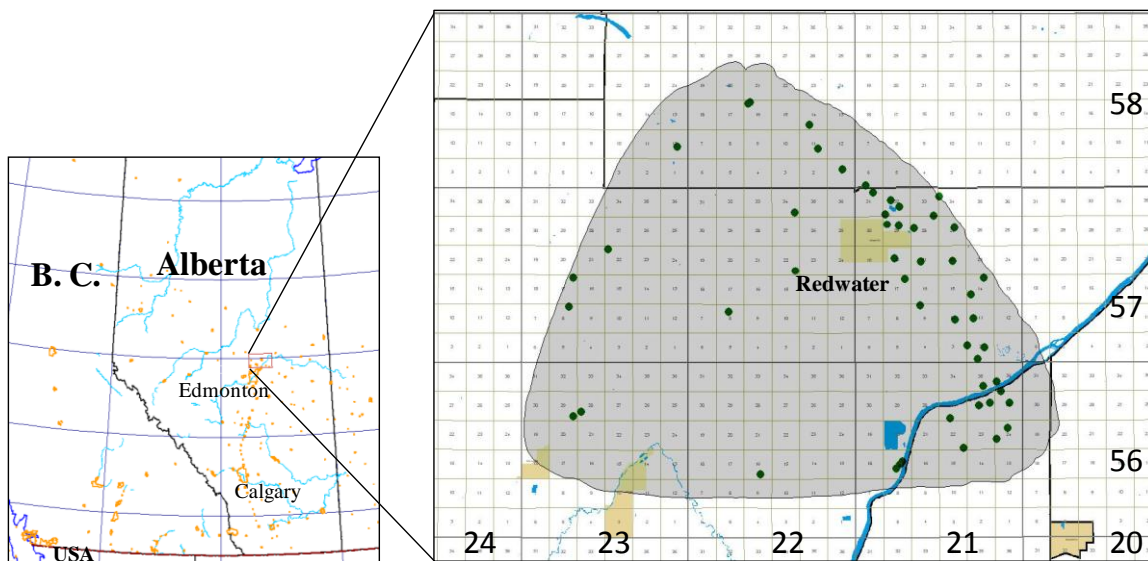


Figure 1.2: Alberta map showing the location of Study area and the wells penetrating the Lower Leduc formation (Lawton and Sodagar, 2009 and Sodagar and Lawton, 2009).

1.6 Geological background

1.6.1 Regional geologic and stratigraphic settings

Devonian reefs are present within the (1930 km long and 563 km wide) Western Canadian sedimentary basin (WCSB). The lowlands of the Precambrian shield area formed the eastern limit of the basin (Figure 1.3), while the Cordilleran miogeosyncline formed the western border (Klovan, 1974).

Three major episodes of reef growth are known during the Middle and Late Devonian in WCSB. Each of these episodes is characterized by a comparable pattern of development. Typically, the sequence base is marked by an unconformity (Figure 1.4), and followed by deposition of widespread shallow-water carbonate platform deposits. Then, biohermal

growth developed on this platform. It represents a typical transgressive-regressive sequence of events. The conditions for the reef growth are mainly dependant on depth of water, circulation, and rate of subsidence (Klovan, 1974). According to Andrichuk (1958), Klovan (1964), Mossop (1972), and Stoakes (1980), a sudden increase in subsidence rate is recorded by the invasion of dark shales into the reef interior. A gradual decrease in subsidence rate is documented by the development of massive stromatoporoid framestone along the seaward edge of the reef complex, and the creation of wide spreading shallow-water, and supratidal deposits in the back reef area.

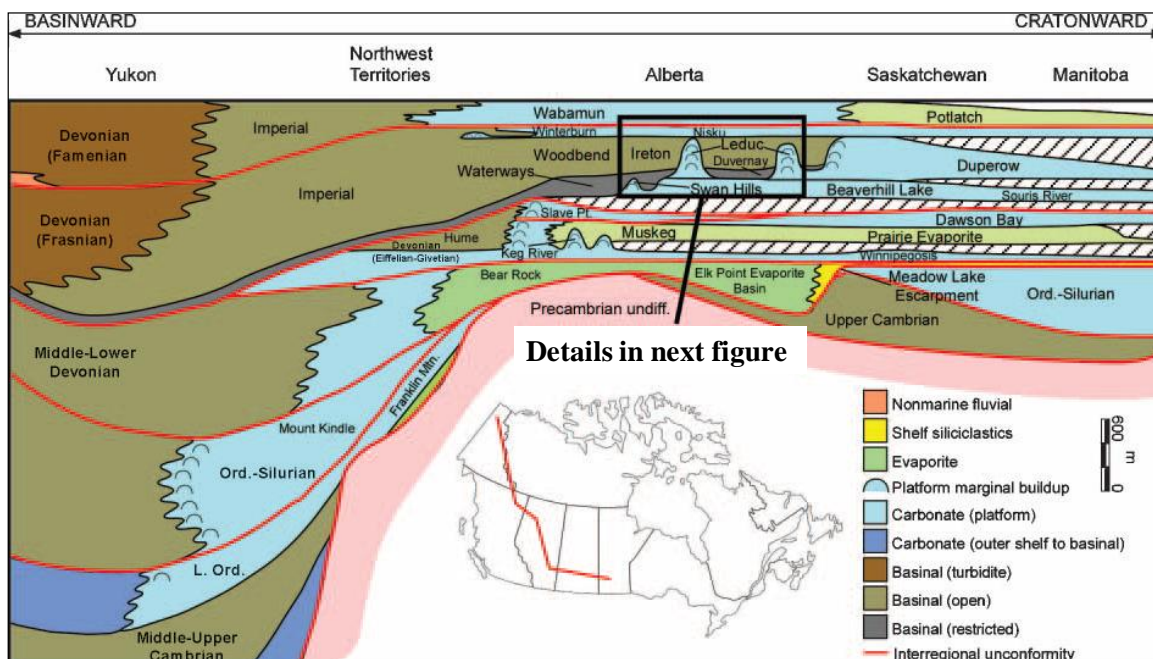


Figure 1.3: Stratigraphic cross section from northwest (basinward) to central (cratonward) Canada presenting the regional stratigraphic settings. The highlighted box is shown in detail in next figure (from Atchley et al., 2006).

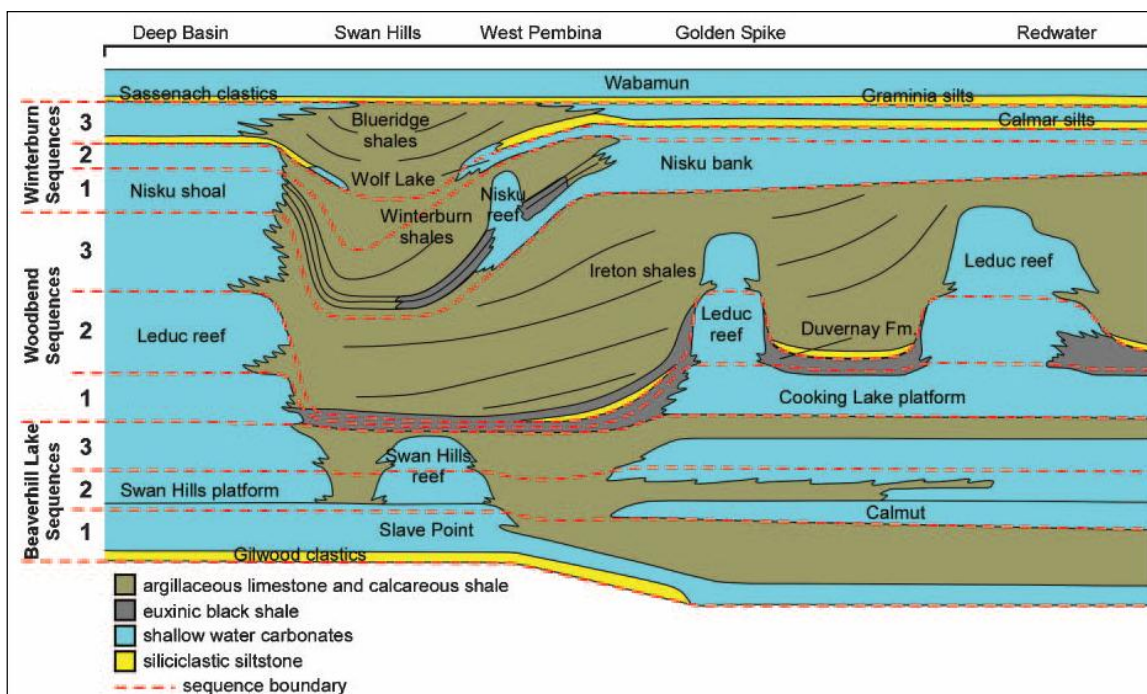


Figure 1.4: Sequence stratigraphic cross section across central Alberta showing the Devonian sequences and formation subdivisions (from Atchley et al., 2006).

1.6.2 Evolution and framework of the study area

The study area is located within the Middle to Early Upper Devonian Waterways Basin (Figure 1.5) includes deep water carbonates and calcareous shales of the Upper Beaverhill Lake Group. These units have an average thickness of 200 m with generally low porosity and permeability (Bachu et al., 2008). The Beaverhill Lake Group is conformably overlain by the Cooking Lake shelf platform carbonates, which both dip gently southwestward (Mossop, 1972 and Stoakes, 1980). The average thickness of the Cooking Lake Formation reaches up to 90 m and has a reefal margin bordering a shallow basin to the west (Figure 1.6). Later, the platform growth gradually became differentiated into a number of isolate shoals that formed a depositional high on which Leduc reef growth took place (Wendte et al., 1992).

Period	Group / Formation	Hydrostratigraphy	
Cretaceous	Colorado Gp.	Colorado aquitard system	
	Mannville Gp.	Upper Mannville aquifer	
	Upper Mannville Undifferentiated channel sandstones	Clearwater - Upper Mannville aquitard	
	Clearwater Upper Lower Eillerslie/Basal Quartz	Lower Mannville aquifer	
Jurassic	Fernie	Fernie aquitard	
Mississippian	Rundle	Mississippian aquifer	
	Banff		
	Exshaw		
Devonian	Wabamun Gp.	Wabamun - Winterburn aquifer	
	Winterburn Gp.	Graminia	
		Nisku	
	Woodbend Gp.	Ireton	Ireton aquitard
		Leduc	Cooking Lake aquifer
		Duvernay	
		Cooking Lk. / Majeau Lk.	
Beaverhill Lake Gp.	Waterways	Waterways aquitard	
	Elk Point Gp.	Elk Point aquitard	

Aquifer
 Aquitard

Figure 1.5: General stratigraphy and hydrostratigraphy presenting the aquifer and aquitard in the study area (Bachu et al., 2008).

Away from the Leduc reef buildup, the Cooking Lake platform is overlain directly by basinal sediments made up of the interbedded dark brown, organic rich shales, dark brown calcareous shales and dense argillaceous limestones of the Duvernay Formation (Figure 1.7) (Klovan, 1964 and Stoakes, 1980). Its thickness ranges from about 70 m in the northeastern part to about 30 m in the west. The Duvernay Formation is overlain by

calcareous shales and argillaceous carbonates of the Ireton Formation (Figure 1.7) where thickness ranges from about 150 m in the East Shale Basin to over 250 m in the southwestern part (Bachu et al., 2008). The Ireton Formation represents the final infilling of the basin in the study area and is a regional aquitard and caprock to the oil in the reef reservoir (Wendte et al., 1992).

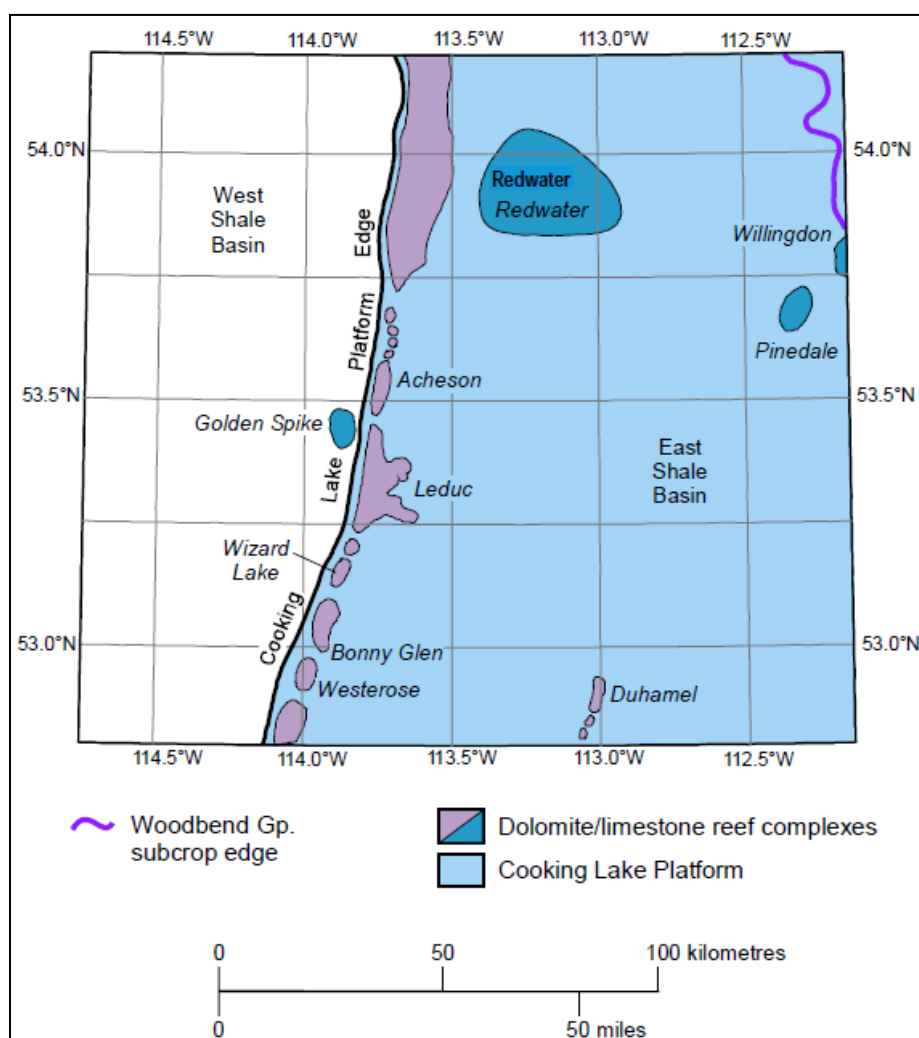


Figure 1.6: Cooking Lake Formation platform map demonstrating outlines of Redwater Leduc reef and Woodbend Group boundaries (from Gunter and Bachu, 2007).

1.6.3 The Redwater reef facies

The Redwater Leduc reef is capped by shales of the Ireton Formation, which are 10-50 m thick directly above the reef (Figure 1.7). The reef developed on the Cooking Lake Formation platform carbonates (Figure 1.6) (Bachu et al., 2008). The total thickness of the Leduc reef is up to 290 meters and grew as a bulky isolated carbonate atoll, surrounded by shallow water (Mossop, 1972). The depositional facies of the reef are subdivided into foreslope, reef margin and interior lagoon units (Stoakes, 1980). The Redwater Leduc reef complex is divided into Lower, Middle and Upper Leduc members (Figure 1.8). The marine embayment is the key to differentiate between these subdivisions. The embayment incursion is between the Lower Leduc and Upper Leduc units (Figure 1.7 and Figure 1.8), and the embayment is present on both the eastern side and the western side with a lesser extent within the reef buildup (Wendte et al., 1992).

The Lower Leduc developed on top of the depositional high of the underlying Cooking Lake Formation (Klovan, 1964). It is comprised of a low porosity, mud dominated unit with a narrow reefal fringe (Figure 1.8). A transgression ended the Lower Leduc deposition and the Middle Leduc constitutes a number of backstepping reef cycles, including the maximum advance of the marine embayment into the Redwater reef (Stoakes, 1980). The Middle Leduc is characterized by a thin condensed interval of basinal laminate deposition at the bottom of the embayment (Mossop, 1972). Along the eastern reef margin, the Upper Leduc (best known within the oilfield) exhibits a series of discrete elongated shoals oriented in a northeast southwest direction parallel to the interpreted tradewind direction (Wendte et al., 1992).

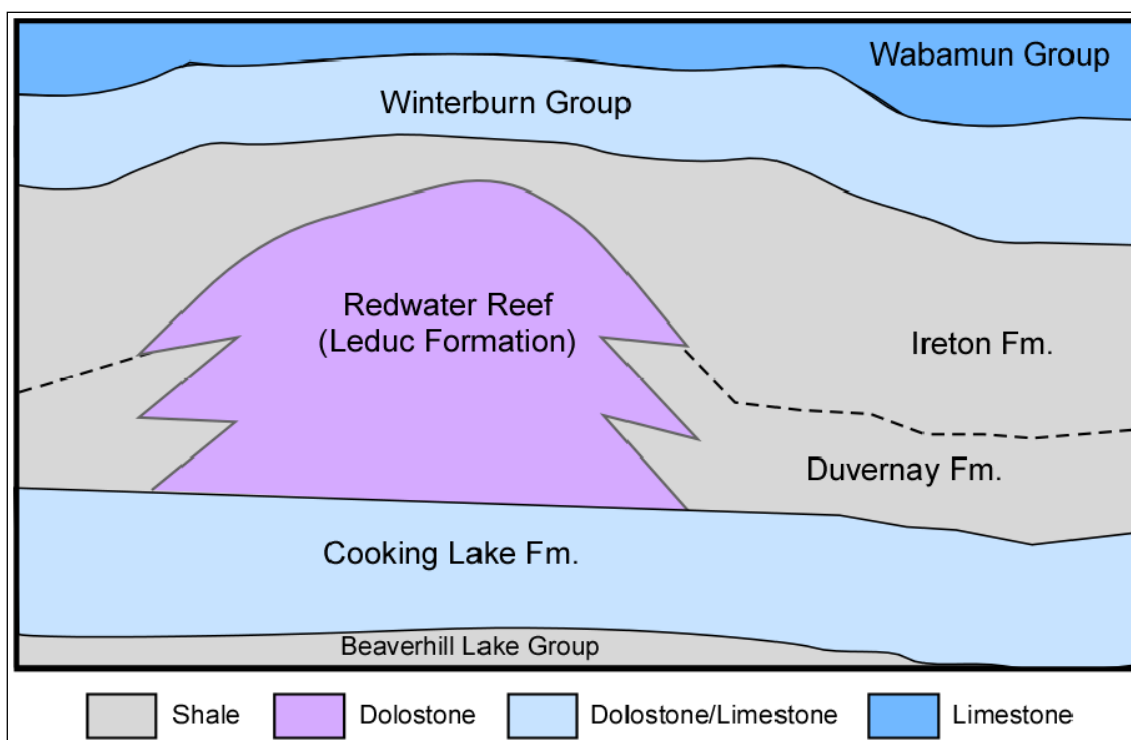


Figure 1.7: West to east cross section illustrating the Leduc formation Redwater reef and adjacent formations (from Gunter and Bachu, 2007).

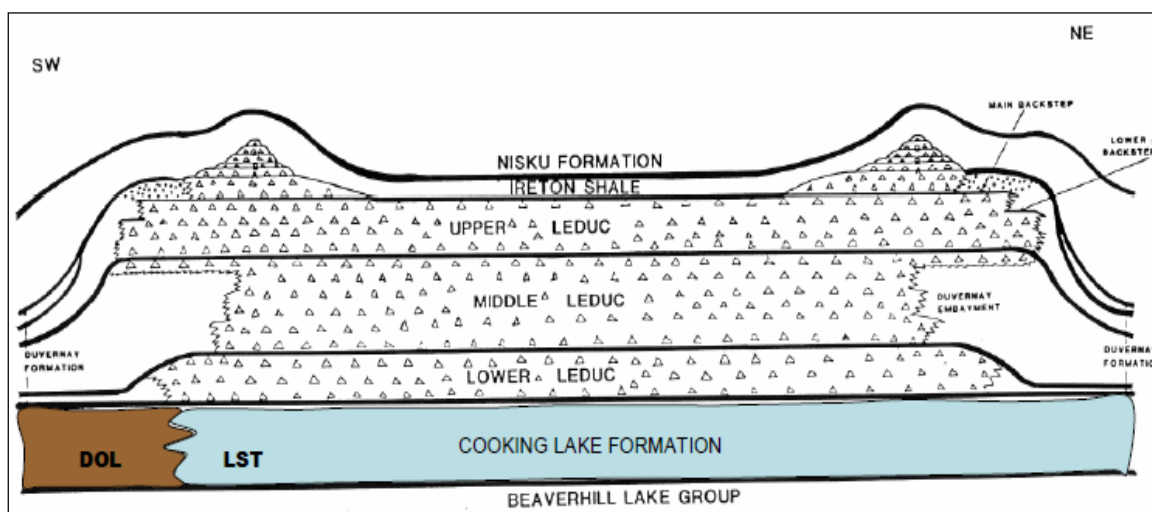


Figure 1.8: Southwest to Northeast cross section presenting the Redwater Leduc reef complex divisions, Duvernay embayment, and Cooking Lake platform (after Gunter et al., 2009).

1.6.4 Reservoir quality and rock properties

The Devonian Leduc Formation carbonates of the Redwater reef consists mostly of 84% medium to light-gray fossiliferous limestone, with 15% of minor amounts of secondary, patchy replacement dolomite (Gunter and Bachu, 2007). In addition, there are traces of iron minerals and anhydrite (Figure 1.9). The porosity commonly ranges between 1 and 17%, and the average porosity taken from the field is around 7% (Bachu et al., 2008). Porosity consists primarily of intercrystalline, moldic, and fracture porosity. The permeability ranges from 0.01 to 4000 md horizontally and 0.02 to 670 md vertically (Gunter and Bachu, 2007).



Figure 1.9: Core photograph of the Redwater Leduc formation showing the rock composition and porosity of the well 05-04-58-21W4 (Geoscience Dept. Lab).

1.6.5 Reservoir pressure and formation water

The initial pressure of Redwater pool was 7.4 MPa (coincidentally nearly equal to the CO₂ critical pressure $P_c=7.38$ MPa) and temperature of 34°C (a little higher than the CO₂ critical temperature $T_c=31.1$ °C). The density of formation water in the Cooking Lake aquifer in the study area is 1083 kg/m³ (Bachu et al., 2008). Salinity in the Redwater area ranges from 85,000 to 140,000 mg/l. The formation water in the reef is NaCl type with 107,000 mg/l TDS (Total Dissolved Solids). The reef experiences a strong water drive from the underlying highly-permeable Cooking Lake aquifer (Bachu et al., 2008).

1.6.6 Hydrogeological characteristics

The aquifers in the Upper Devonian Cooking Lake strata to Lower Cretaceous Mannville sequence show a similar flow pattern on a regional scale (Gunter and Bachu, 2007). The updip flow is from the southwest and downdip flow from the northeast converging into normally northwest channel flow in the Redwater area (Gunter and Bachu, 2007). The lower hydraulic heads in the Wabamun, Winterburn and Cooking Lake aquifers and the existence of Leduc reefs suggest hydraulic communication and downward flow from the Lower Mannville Aquifer into the Cooking Lake Aquifer (Gunter and Bachu, 2007). The Clearwater Upper Mannville aquitard is an efficient barrier to cross formation flow (Figure 1.5 and Figure 1.10). It is hydraulically separating the Upper Mannville Aquifer and the shallower formations from the Lower Mannville aquifer and the deeper underlying Devonian aquifers (Gunter and Bachu, 2007).

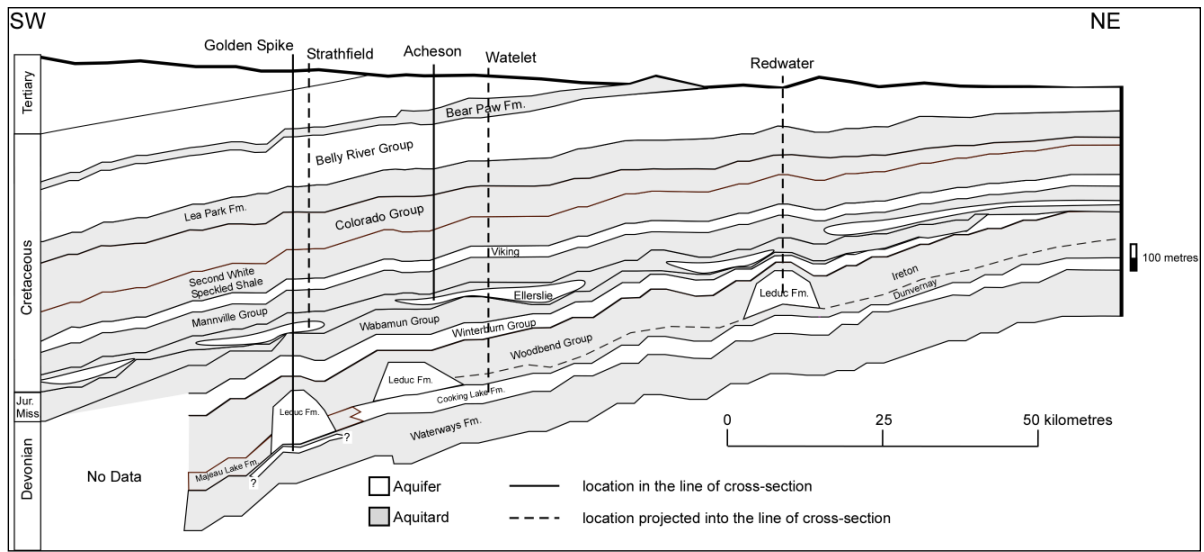


Figure 1.10: Southwest to northeast dip cross section showing the Redwater reef and also the separation of the Upper Mannville and shallower aquifers from the Lower Mannville and deeper aquifers (from Bachu et al., 2008).

1.7 Dissertation structure

Chapter one presents an introduction to the dissertation by describing the motivations behind this thesis, main objectives, and significance of this study. It gives summary of some of the successful international CCS projects in the world and in Canada. Also, it reviews the background and geological setting of the study area. It illustrates in details the Redwater reef facies, properties, reservoir quality and hydrogeological characteristics. Chapter two describes the 2D seismic data quality and the reprocessing work flows. It shows the synthetic seismograms of the wells that deeper than the target Leduc Formation and then tie them to the seismic data at well locations. In addition, it presents a detailed interpretation of the seismic sections and structure maps of the Redwater reef. Chapter three discusses the well-based fluid substitution seismic modeling using Gassmann approach explaining in details the steps to acquire the new P-wave velocity

and S-wave velocity after CO₂ fluid substitution. It provides the relationship between the CO₂ saturations and the density, P-wave and S-wave velocities, reflection amplitudes and time shifts. In chapter four, the interpretation of time-lapse seismic modelling of CO₂ fluid substitution in the Redwater Leduc Reef is reviewed using ray tracing and finite difference methods. It evaluates the seismic modelling of CO₂ fluid substitution in the Upper Leduc member, reef rim only and entire Leduc Formation as well as modeling of the Duvernay Embayment in the Redwater reef. The analysis of the time-lapse of converted wave seismic modeling of CO₂ fluid replacement in the Redwater Devonian Reef is also presented in chapter four. It shows the seismic survey parameters to acquire the PS synthetic seismograms and the processing work flow to reach the best seismic data. Chapter five furthermore demonstrates the 4D multicomponent seismic modeling of CO₂ fluid substitution zoomed in the southern part of the Redwater Reef. It illustrates the 3D seismic survey parameters to obtain the 3D multicomponent synthetic seismograms and the processing flow to achieve the optimum 3D seismic data volumes. Finally, chapter six provides the conclusions attained in this dissertation and recommends future work. It also gives an estimate of CO₂ storage capacity in the Redwater Leduc reef and Cooking Lake Formation below the reef.

1.8 Software used in the research program

IHS Accumap and GeoSyn software were used to examine and to generate the synthetic seismograms for the wells provided to the University of Calgary in the Redwater reef area for HARP project. Hampson-Russell Pro4D software was utilized for the well-based fluid replacement modeling. Kingdom Suite software was used to interpret the 2D and 3D

seismic data, generate synthetic seismograms, grid interpreted data, convert the horizons from time to depth and create the suite of maps. NORSAR Innovation AS (NORSAR2D and NORSAR3D) software was used to create the 2D and 3D interface blocks, perform common shot ray tracing, and generate the multicomponent synthetic shot gather seismic data. Landmark Graphics Corporation ProMax software was used for finite difference modeling, geometry sorting, polarity reversal for PS data, velocity conversion and post-stack time migration, pre-stack time migration, and 2D pre-stack depth migration. Paradigm GeoDepth software was utilized for 3D pre-stack depth migration for multicomponent synthetic seismic data.

Chapter Two: **SEISMIC INTERPRETATION OF THE REDWATER LEDUC REEF**

2.1 Introduction

The main topic covered in this chapter was to use available seismic data to map the external and internal geometry of the Redwater Devonian reef for the potential geological storage of CO₂. This phase of the study concentrated on reprocessing the available 2D seismic data and undertaking a detailed interpretation of it to identify the reef margin, and to map facies variations within the reef based on seismic character, constrained by synthetic seismograms generated from available wells with sonic logs.

2.2 Methodology

2.2.1 Surface Seismic and Well Log Datasets

A large number of wells penetrate the Upper Leduc member in the study area, especially on the eastern margin of the Redwater reef, but only a small number of wells penetrate the Cooking Lake Formation and few of these have sonic and density logs. Figure 2.1 shows three wells inside the reef (10-27-57-21W4, 11-08-57-22W4 and 16-08-57-23W4) and six wells off-reef (16-25-57-20W4, 10-02-59-22W4, 01-25-57-24W4, 11-24-65-24W4, 06-05-56-23W4 and 16-01-56-22W4) that penetrate the Cooking Lake Formation in the general study area. Of these, two on-reef and four off-reef wells were used to tie the surface seismic data to formation tops using zero-offset synthetic seismograms.

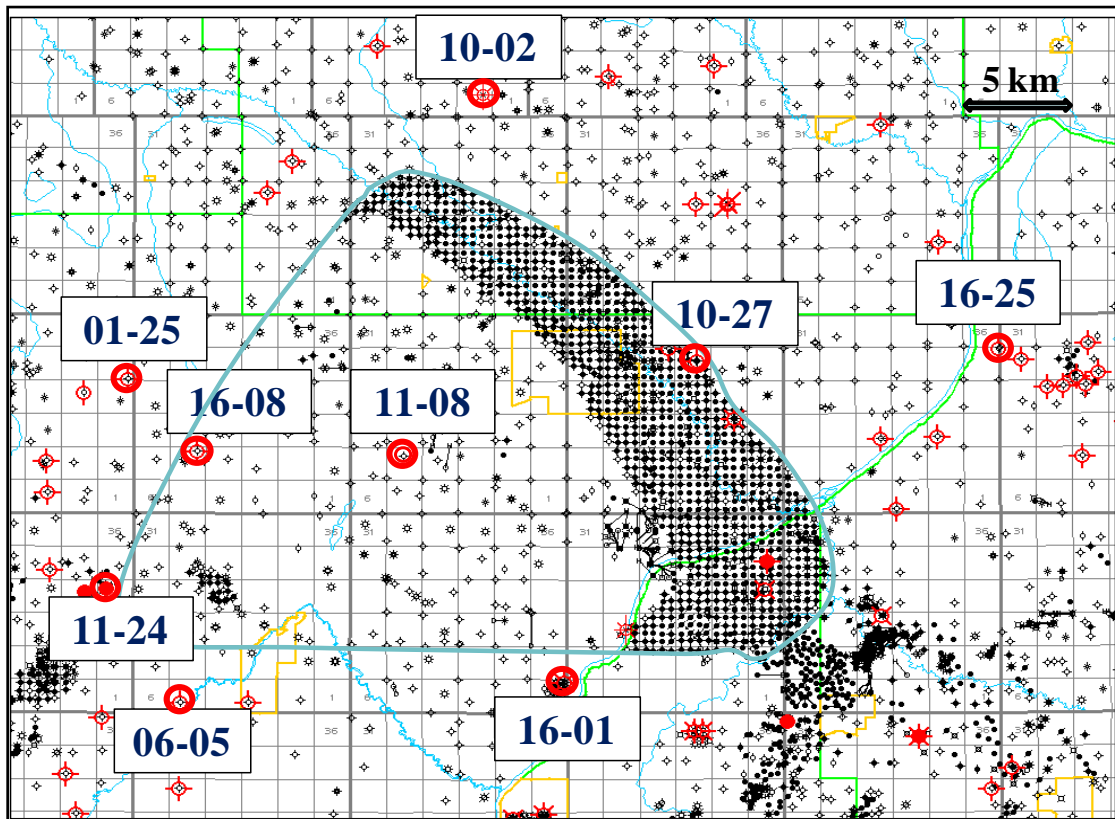


Figure 2.1: Redwater reef map showing all wells. Those wells that penetrate the Cooking Lake Formation and have sonic logs are highlighted in red.

These well data were also used for fluid substitution modeling and rock physics analysis to predict the seismic response of CO₂ injection into the Leduc Formation.

Approximately 400 line-km of different vintages of 2-D seismic data were interpreted and the distribution of these seismic lines is shown in Figure 2.2.

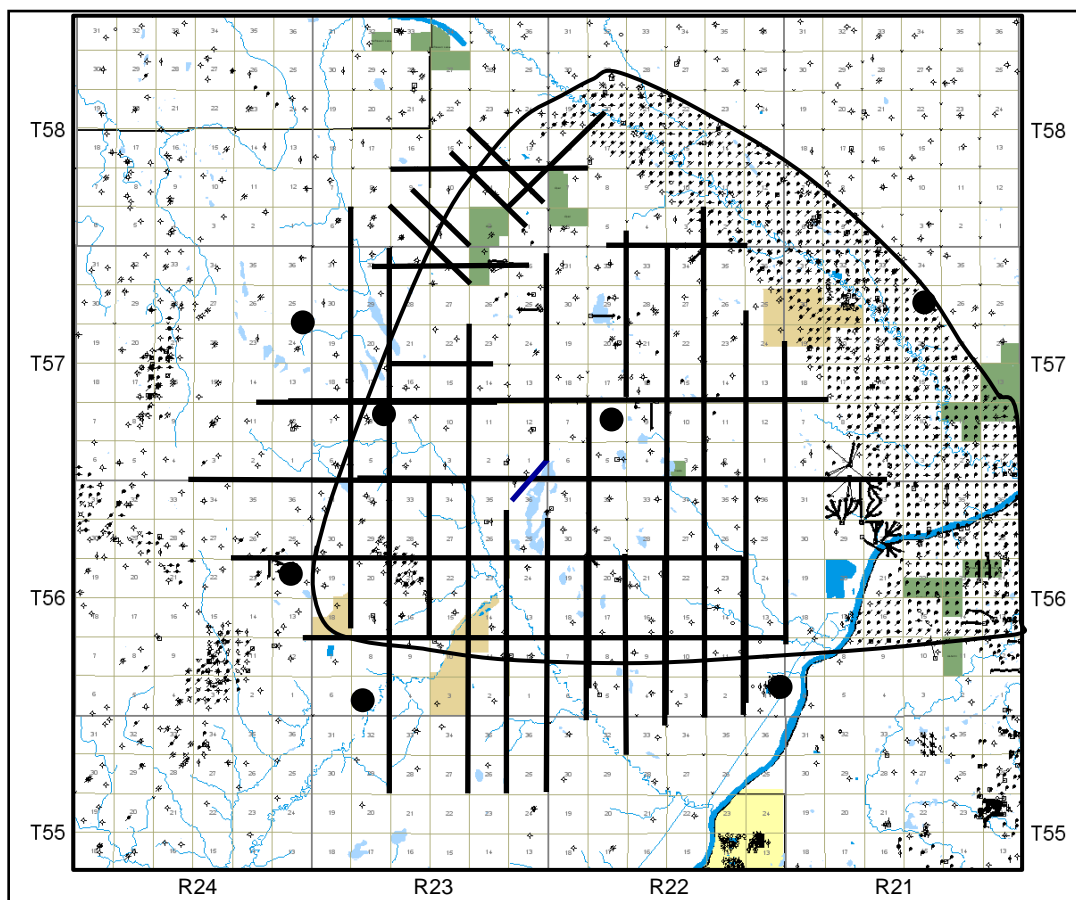


Figure 2.2: Map showing the outline of the Redwater reef and the distribution of all the 2D seismic data available for the project. The black filled circles show the locations of wells that penetrate the Cooking Lake Formation and which have sonic and density logs.

2.2.2 Seismic Data Reprocessing

The original seismic data were acquired and processed in the 1980's by various companies. The seismic lines at the south, southwest, and northwest edges of the reef were reprocessed, following a processing flow outlined in Table 2.1. Lines restricted to the interior of the reef were not reprocessed, but were post-stack migrated locally at the University of Calgary and bulk-shifted to the same datum as the reprocessed reef-margin data. The objective of the reprocessing was to improve the static solution and enhance

imaging of the reef edge as well as the internal reef facies and geometry near the reef margin. The reprocessed data showed significant improvement in resolution and coherency of events over the original sections and yielded more confidence in the delineation of significant features within the reef, particularly embayments in the reef margin and localized area of dolomitization (Sodagar and Lawton, 2010h).

Table 2.1: Processing flow and parameters of the reprocessed 2D seismic data in the Redwater area.

PROCESSING FLOW	PARAMETERS
Demultiplex	2 ms. sample rate
Amplitude Recovery	(T) Exp (BT), B= 0.0008
Deconvolution Type	Adaptive 5 component surface consistent signature with zero phase frequency domain offset component
Deconvolution Gate	250-1500 ms. at 0 offset, 900- 1600 ms at 1500 m. offset
Structural Corrections	Datum elevation= 725m., Datum velocity= 2150m./Sec., Processing datum= -100ms.
Analysis	Preliminary velocities and statics
Statics and Trace Kills	Surface stack residual
Velocity Analysis and Final Moveout	Interval= 30 CDPs
Mean Scaling	Window: 500-1500 ms.
Time-Variant Scaling	Window: 0-500 ms.
Mute	Distance (m.) 330 1500 Time (ms.) 550 1150
Statics	Surface consistent residual, Window: 500-1500
Trace Gather	Offset Range: 0-1500 m., Maximum fold: 14
Statics	CDP cross correlation, Window: 500-1500 ms.
Stack	Cross correlation weighted
F-X Noise Reduction	Block size: 150 traces, %model: 60% Prediction filter: 10 traces, PW: 10% 300 ms. Window, 100 ms. Overlap
F-D Migration	100% theoretical velocities
Filter	10/14 - 75/85 Hz.
Equalization	Mean window: 500-1500 ms.

2.2.3 Software

ProMax software was used for the post-stack migration, and Kingdom Suite software was used to interpret the 2D seismic data, generate synthetic seismograms, grid interpreted data and create the suite of maps. Data reprocessing was undertaken by Divestco.

2.2.4 Synthetic Seismograms and correlation to seismic data

The first step in seismic data interpretation was to correlate the formation tops at well locations from synthetic seismogram to the 2D surface seismic data. Synthetic seismograms were generated for the wells that penetrated the Devonian Cooking Lake Formation, which is deeper than the target Leduc Formation. Only the primary reflection events were modeled, using logs from two wells inside the Redwater reef and from four wells off-reef. Tests with different wavelets showed that a good match between the synthetic seismograms and the 2D surface seismic data was a zero-phase 35 Hz Ricker wavelet (Figure 2.3). Also, seismic wavelets for some of the synthetic seismograms were extracted from the reprocessed 2D surface seismic data at the well locations.

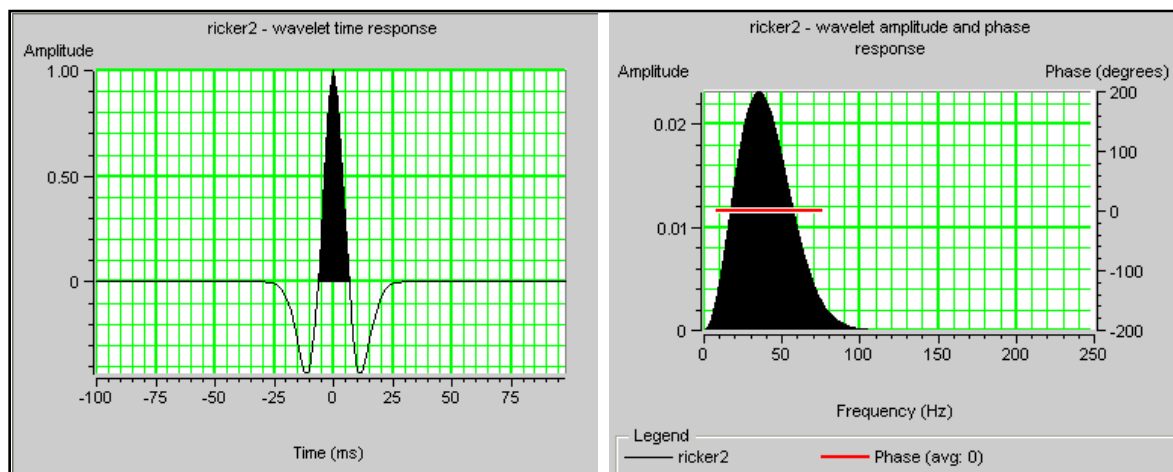


Figure 2.3: Zero-phase Ricker 35Hz wavelet in time and frequency domain.

2.3 Seismic Section Interpretation

The two wells within the Redwater reef that were used to generate synthetic seismograms were 11-08-57-22W4 (near the centre of the reef), and 16-08-57-23W4 (near the west margin of the reef). The off-reef wells were 01-25-57-24W4, 11-24-65-24W4, 06-05-56-23W4 and 16-01-56-22W4, all of which are west or south of the reef. Well 10-27-57-21W4 (on the east edge of the reef) has a shale embayment correlative with the Duvernay Formation. However, since there are no seismic data available close to well 10-27-57-21W4, synthetic seismograms were not tied to seismic data, but did provide useful information about the expected seismic character of the embayment to assist in the data interpretation.

Figure 2.4 to Figure 2.7 illustrate synthetic seismograms tied to the corresponding surface seismic data. They tied reasonably well with the surface seismic data for the key horizons. In all of the seismograms, the Nisku event is a fairly strong peak, the Ireton

shale is a trough and the Cooking Lake Formation correlates to a moderate amplitude peak on-reef but has higher amplitude in off-reef wells (Figure 2.4 to Figure 2.7). This is because the Cooking Lake carbonate, when overlain by Ireton shale, represents a large impedance contrast and generates a high-amplitude reflection.

After correlation with synthetic seismograms, the migrated seismic lines were interpreted, with the following key horizons being picked: Mannville, Nisku, Leduc, Mid-Leduc, Cooking Lake, Beaverhill Lake, and Lower Beaverhill Lake Formations. The Second White Speckled shale, Base Fish Scales Zone, Ireton, Elk Point, and the Basement events were picked where possible. All the horizons dip gently to the southwest in the 2D seismic datasets and no observable faults were identified in the region of the study area covered by the 2D lines.

Figure 2.8 to Figure 2.10 show samples of the 2D seismic data. Shotpoints and the location of these seismic data cannot be included on the sections or maps due to data licencing agreements. The 2D seismic lines clearly define the upper margin of the Redwater Reef (Upper Leduc Fm) and the Mid-Leduc event was used to formally map the lateral extent of the reef buildup. On some lines, the Duvernay embayment was mapped as a moderate amplitude event that is approximately correlative with the mid-Leduc event and extends into the buildup.

From the geological studies for the HARP Project (Stoakes and Foellmer personal communication, 2008), dolomitization of the Cooking Lake Formation and the Lower

Leduc and part of the Middle Leduc formations is observed in cores from wells in the west side of the reef (e.g. well 16-08). Interpretation of the 2D seismic lines in the west side of the reef suggests that dolomitization causes a loss of coherent reflectivity of these units (Figure 2.11). This character was mapped along some other seismic lines along the western and northwestern parts of the reef (Sodagar and Lawton, 2010h).

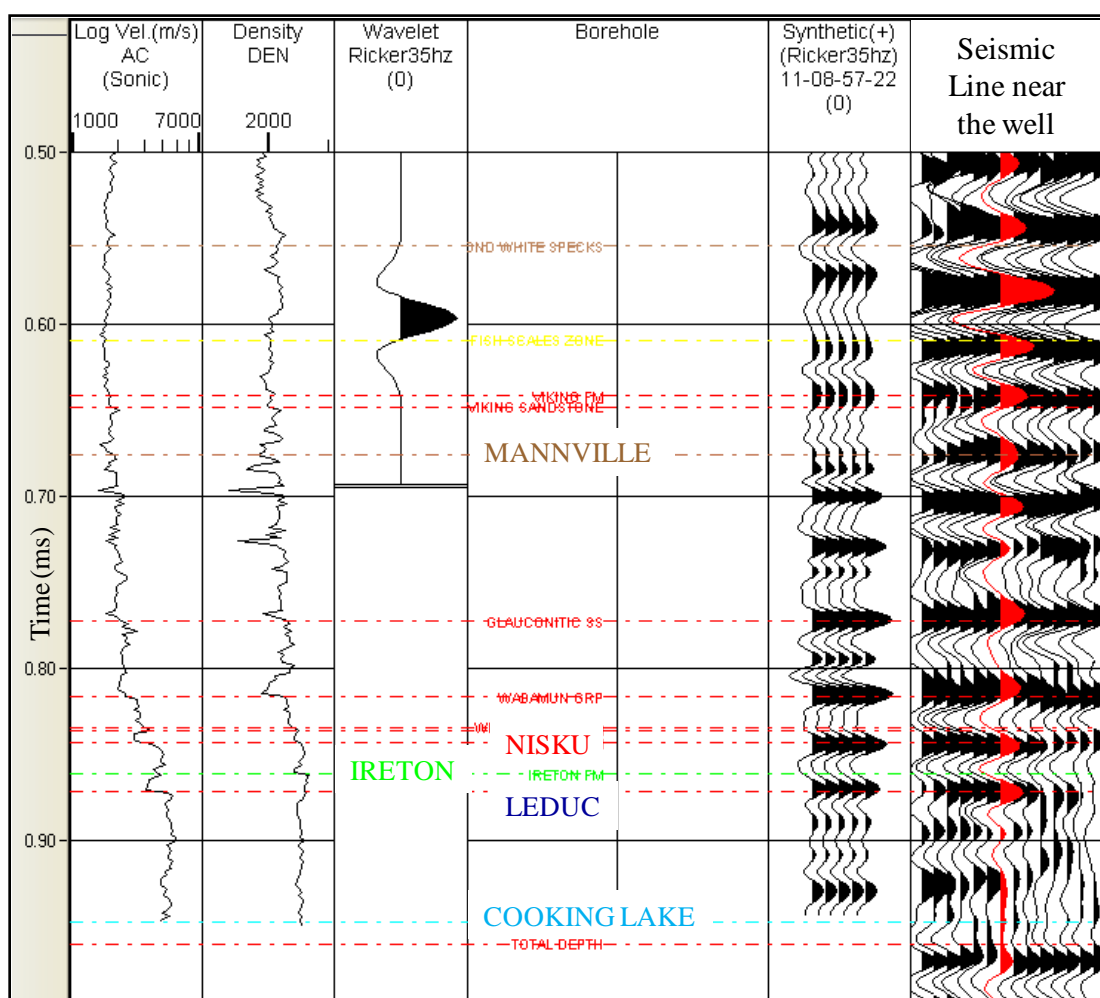


Figure 2.4: Sonic, density logs and synthetic of the well 11-08-57-22W4 correlated with seismic line with picked key horizons. This is an on-reef well.

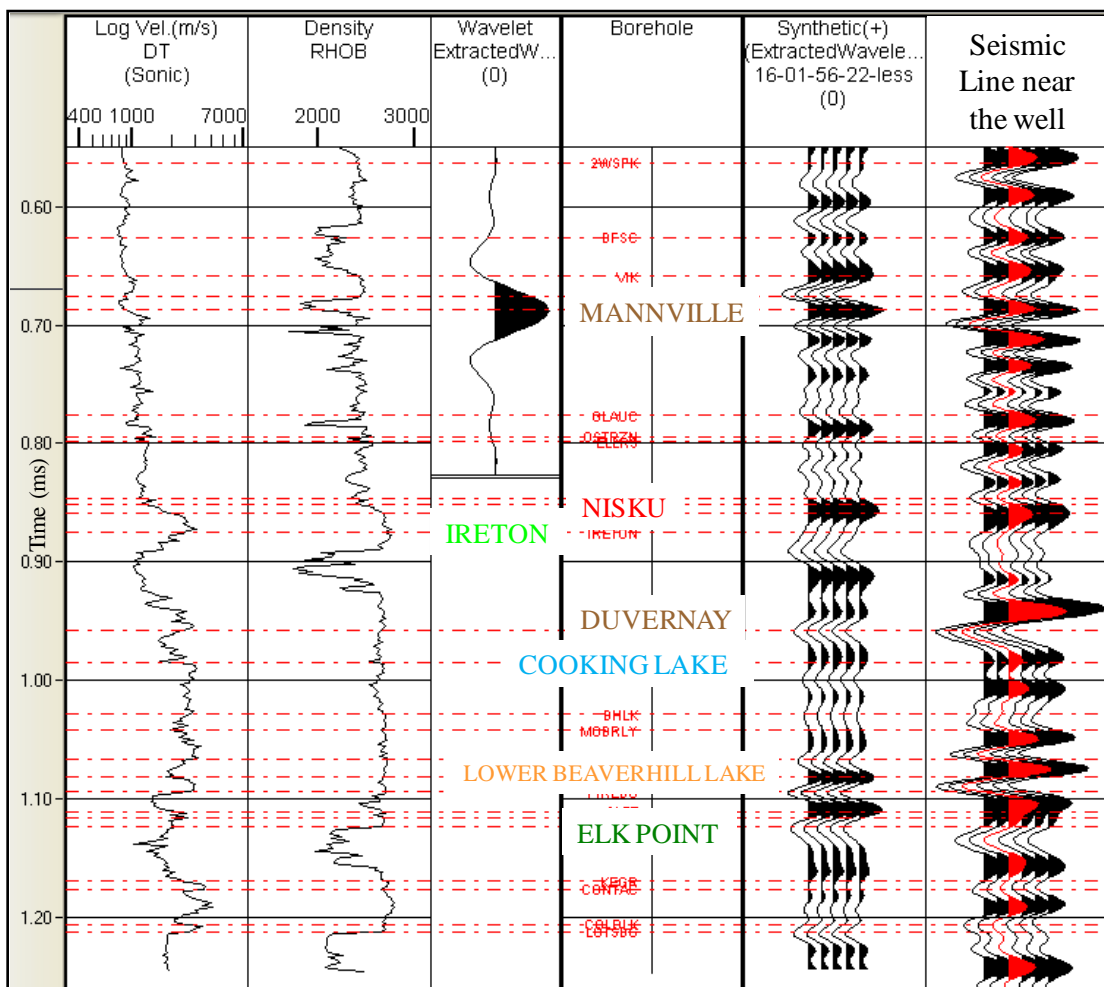


Figure 2.5: Sonic, density logs and synthetic of the well 16-01-56-22W4 correlated with seismic line with picked key horizons. This is an off-reef well.

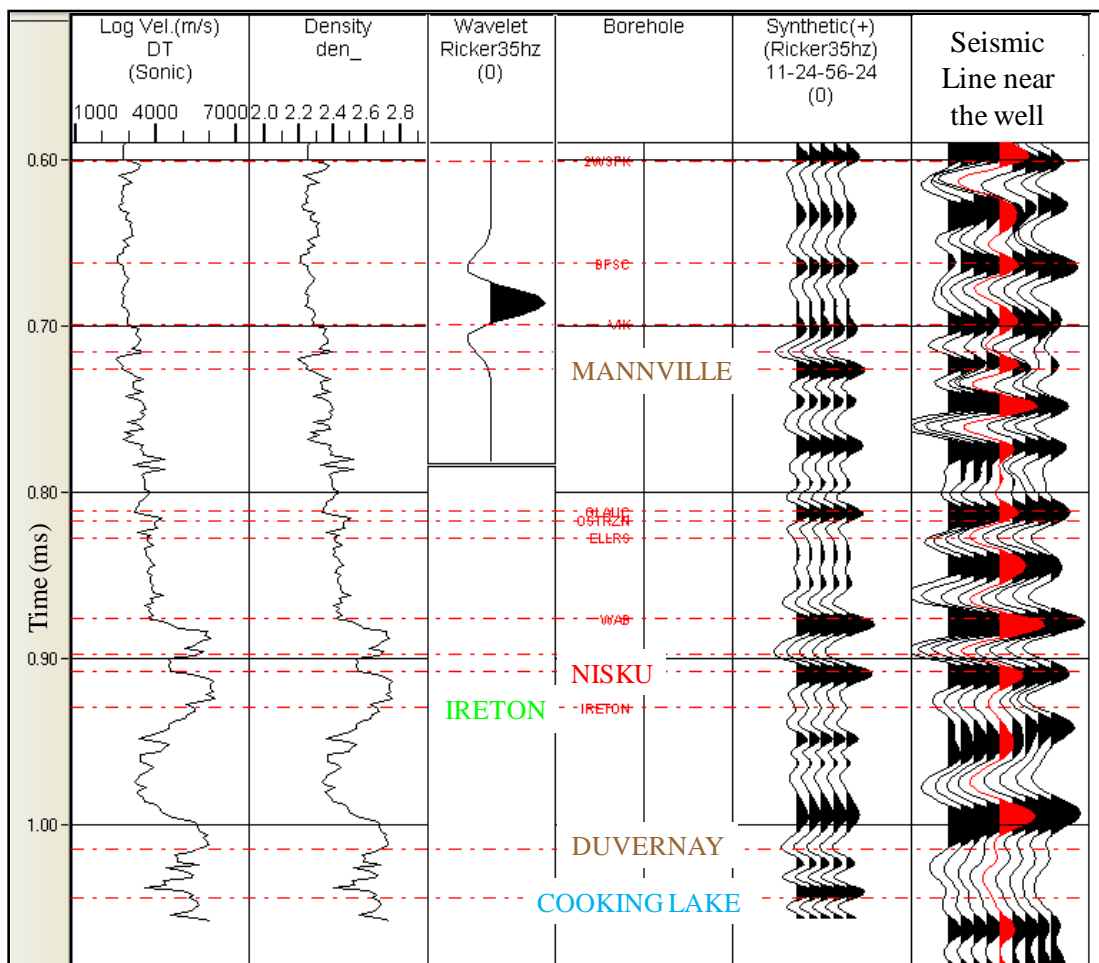


Figure 2.6: Sonic, density logs and synthetic of the well 11-24-56-24W4 correlated with seismic line with picked key horizons. This is an off-reef well with shale embayment of the Duvernay Formation.

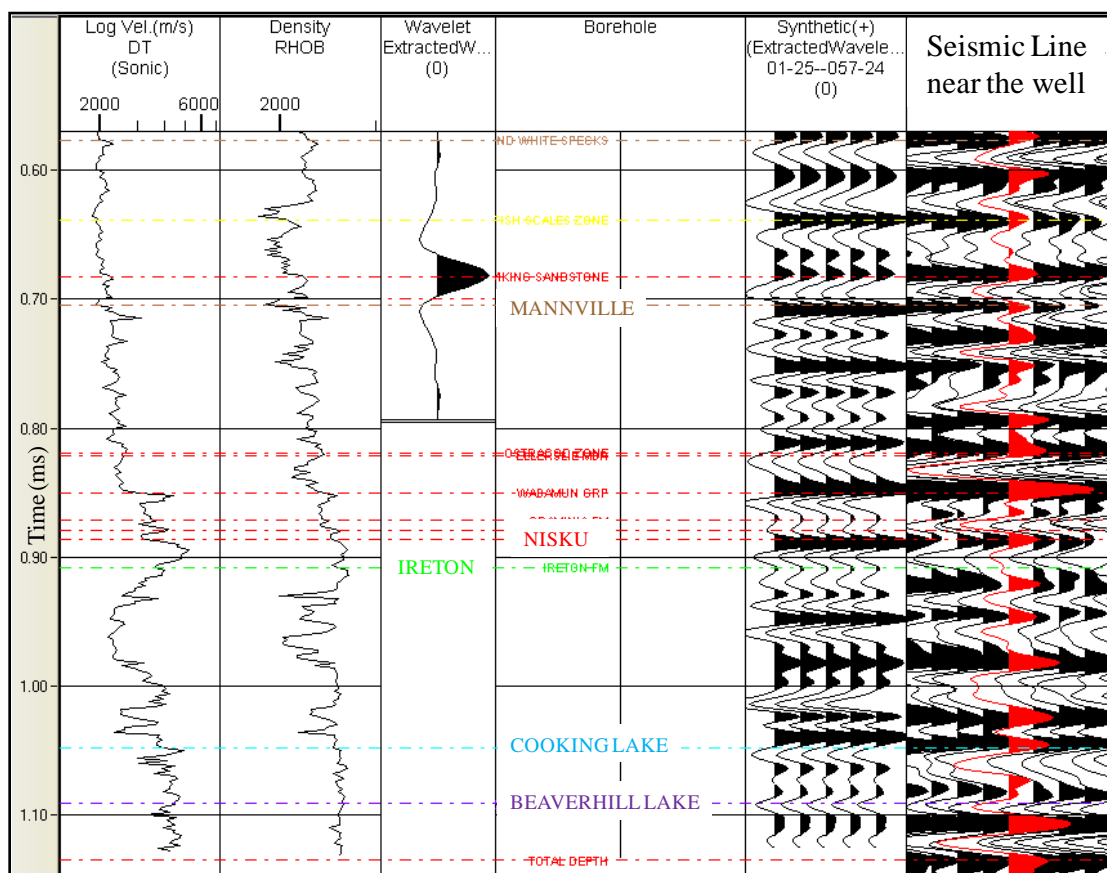


Figure 2.7: Sonic, density logs and synthetic of the well 01-25-57-24W4 correlated with seismic line with picked key horizons. This is an off-reef well.

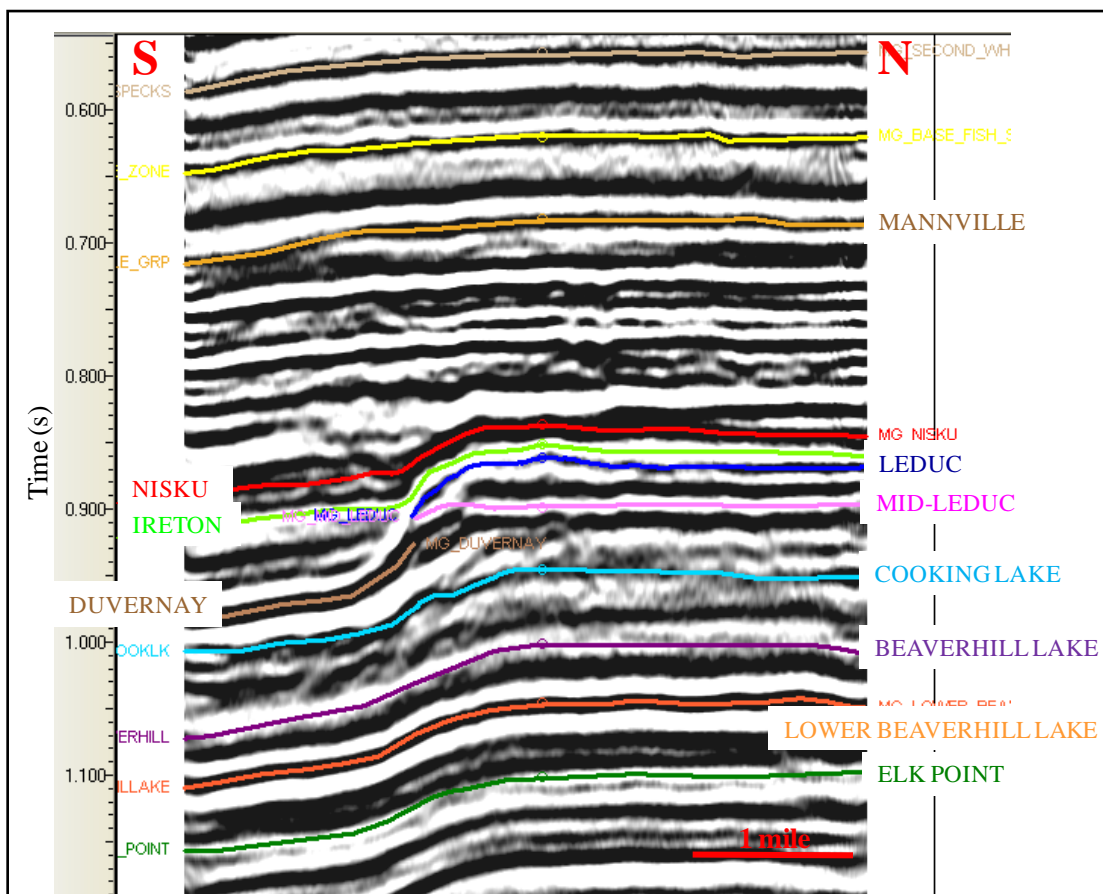


Figure 2.8: Interpreted north-south seismic section. This line shows the reef edge clearly and the Duvernay event terminating close to the reef margin.

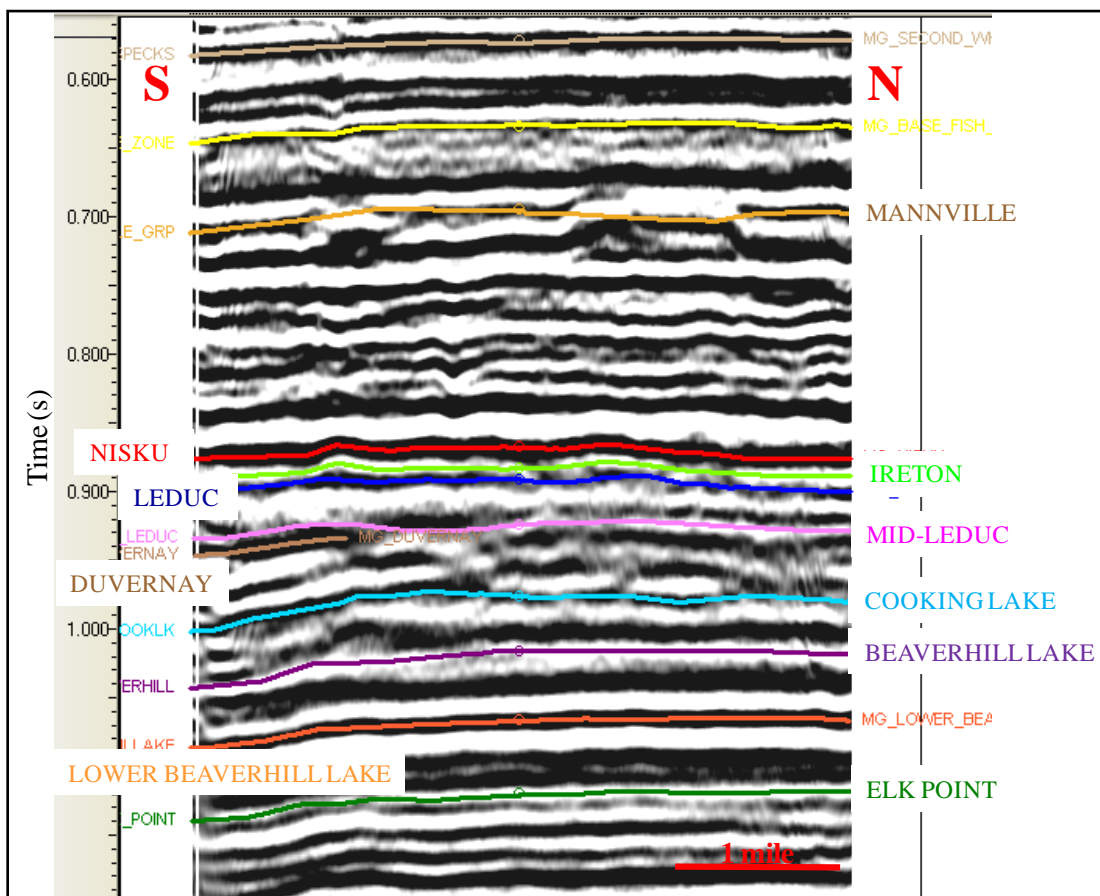


Figure 2.9: Interpreted north-south seismic section. This line shows Duvernay embayment event encroaching into the reef buildup near the south end.

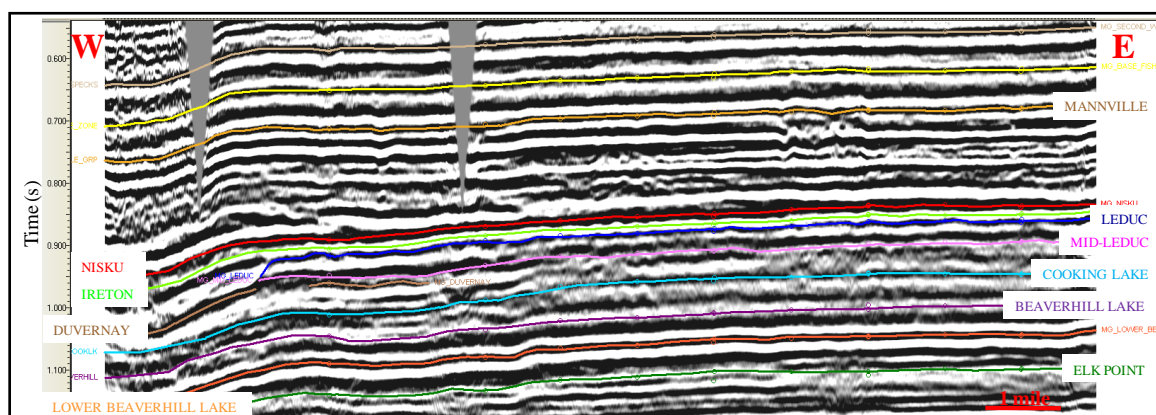


Figure 2.10: Interpreted west-east seismic section. This line shows Duvernay embayment event encroaching into the reef buildup from the west.

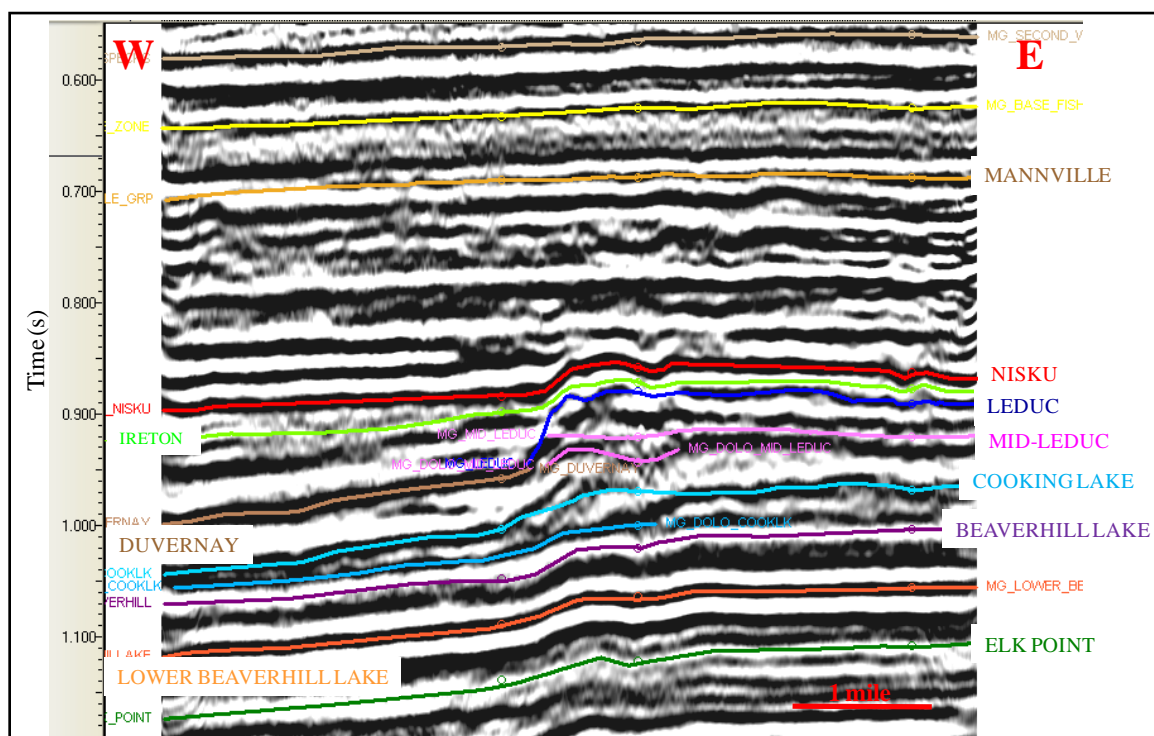


Figure 2.11: Interpreted west-east seismic section. This line shows the reef edge and the Dolomitization event at the west margin of the reef.

2.4 Map Interpretation

After the seismic sections had been interpreted, the time picks of all horizons were gridded and contoured, producing time structure maps. Note that for all of the map views, the eastern boundary line marks the edge of data, not the eastern reef margin, whereas the northwestern and southern boundaries do represent the interpreted reef margin at the mid-Leduc level. Examples of time structure maps for the Mannville, Nisku and Upper Leduc formations are shown in Figure 2.12 to Figure 2.14 respectively. The Mannville time structure map (Figure 2.12) shows generally a dip to the southwest and the Nisku time structure map (Figure 2.13) shows also a dip to the southwest, with some drape evident over the flanks of the reef. The time structure map of the Upper Leduc Formation (Figure

2.14) illustrates rim buildup in the north-west, south-west, and southern sides of the reef.

The Middle Leduc time structure map was used to define the lateral extent of the reef.

Figure 2.15 show the Duvernay Fm time structure map. It shows the regional off-reef pick and also the embayment inside the reef along the north-west and south-west sides.

The interpreted Duvernay embayment does not extend along the south side of the reef.

Time structure map for the Beaverhill Lake Formation is shown in Figure 2.16. This map demonstrates positive time structure of these reflections below the reef due to a lateral velocity change between on-reef carbonates and off-reef shales but the geological data confirms that it is almost flat in depth. The Basement event time structure map is smooth away from the reef edges and no significant local basement highs were mapped from the seismic data.

For depth interpretations, a single interval velocity function was used for depth conversion of the Nisku, Leduc, Cooking Lake, and Beaverhill Lake events. Interval velocities from all available sonic logs from wells for these intervals were compiled for a simple vertical time-to-depth conversion. It was achieved by computing the mean (standard average) of velocities for each formation interval at each well. Then, the average (arithmetic mean) was again taken for all the wells for every formation interval. The difference between the harmonic mean and arithmetic mean is small since the values are close to each other. Table 2.2 demonstrates the mean interval velocities that were used in depth conversions for the targeted formations. It also shows the standard deviation (how much variation from the mean) of the velocities which indicate low

standard deviation values implying that the velocities are very close to the mean. The Nisku depth structure map is similar to the time structure map and shows generally a dip to the southwest, with some drape evident over the flanks of the reef. The depth structure map of the Upper Leduc Formation (Figure 2.17) illustrates rim buildup in the north-west, south-west, and southern sides of the reef. The errors in the calculated depth were estimated between 3-9 m at the well locations for the key formations.

Isochron maps (defined as differenced time structure maps) between the Upper Leduc and Cooking Lake formations and also between the Upper Leduc and Beaverhill Lake formations (Figure 2.18) also demonstrate the thickening of the rim of the reef and thinning in the central region of the reef which is corroborated by well data elsewhere around the reef rim. Isopach maps (defined as differenced depth structure maps) between the Upper Leduc and Cooking Lake formations and also between the Upper Leduc and Beaverhill Lake formations (Figure 2.19) also demonstrate the thickening of the rim of the reef and thinning in the central region of the reef.

Depth structure maps for the Cooking Lake and Beaverhill Lake formations illustrate generally a dip to the southwest and compensate for the velocity pull-up due to a lateral velocity change. They also demonstrate negative depth structure of these reflections below the reef embayment because of the simplification of using a single interval velocity technique for depth conversion for the Upper, Mid and Lower Leduc Formations (averaged from the logs). Therefore, the average velocity is less below the reef embayment due to the presence of shales instead of carbonates. Since no wells

penetrated the embayment along the southwest edge of the reef, no velocity control is present.

Table 2.2: Interval velocities computed from sonic logs for targeted intervals.

Formation interval	Interval velocity (m/s)	Standard deviation (m/s)
Surface to Nisku	2450	70
Nisku to Leduc/Cooking Lake	4400	150
Leduc to Cooking Lake	5760	30
Cooking Lake to Beaverhill Lake	5513	160

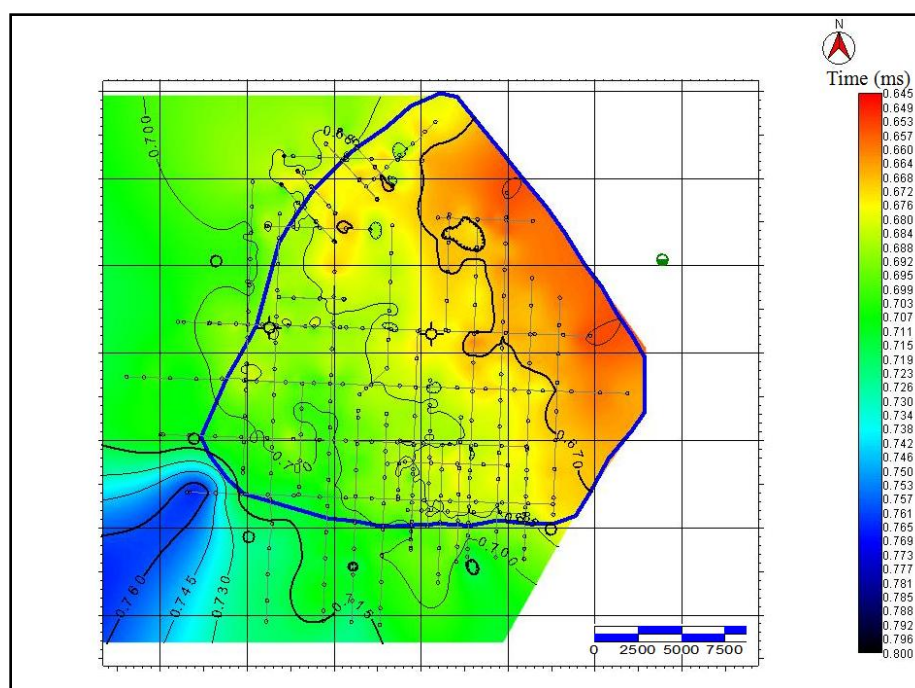


Figure 2.12: Time structure map of the Mannville Formation with the Devonian Leduc reef edge outlined except the eastern boundary marks the edge of data.

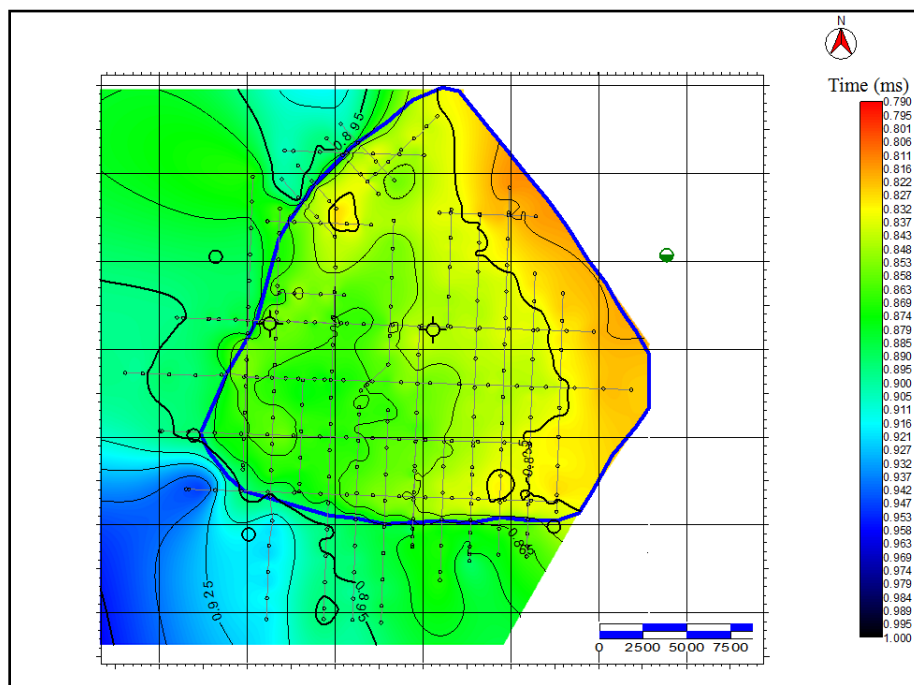


Figure 2.13: Time structure map of the Nisku Formation with the Devonian Leduc reef edge outlined except the eastern boundary marks the edge of data.

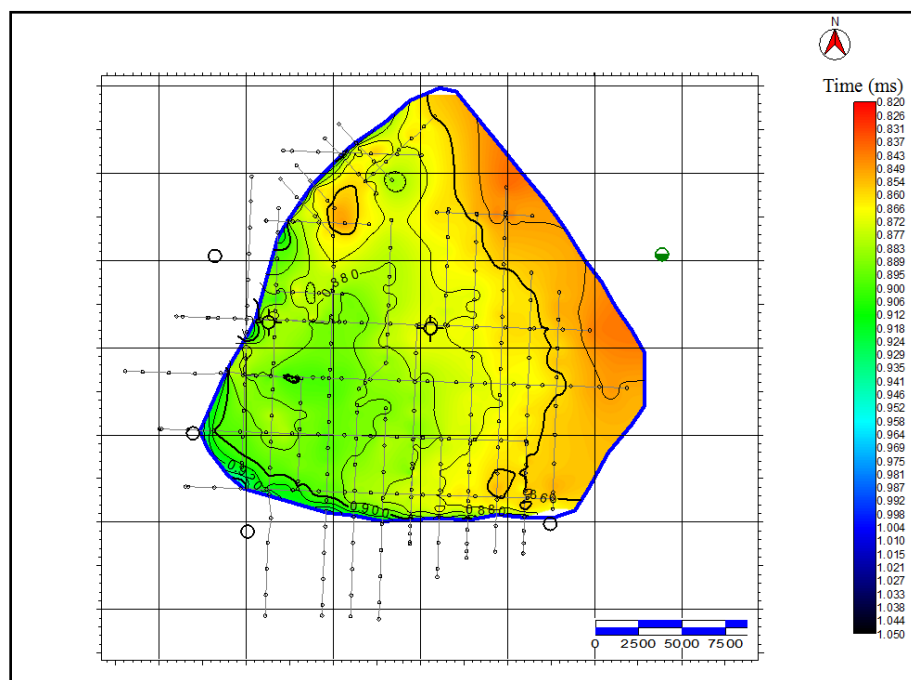


Figure 2.14: Time structure map of the Upper Leduc Formation with the Leduc reef edge outlined except the eastern boundary marks the edge of data.

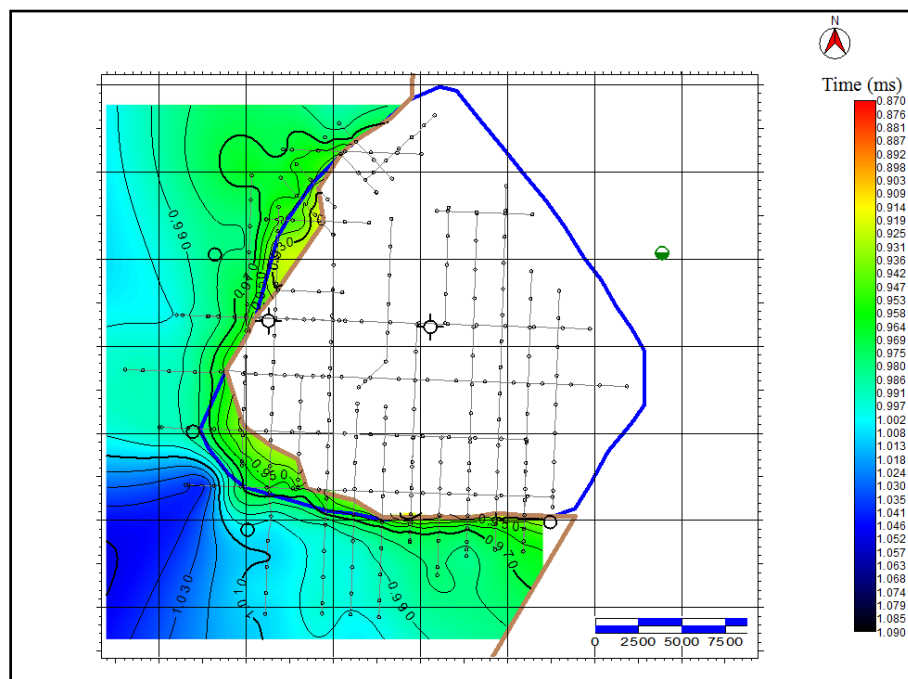


Figure 2.15: Time structure map of Duvernay Fm with the embayment outlined between the brown and blue lines. The eastern boundary marks the edge of data.

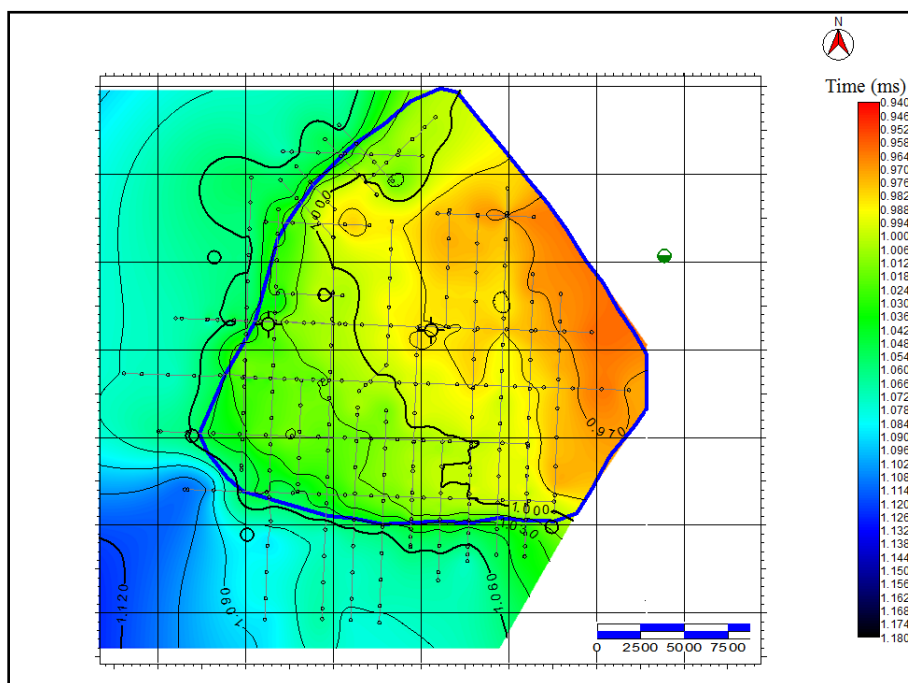


Figure 2.16: Time structure map of top of Beaverhill Lake Formation with the reef edge outlined except the eastern boundary marks the edge of data.

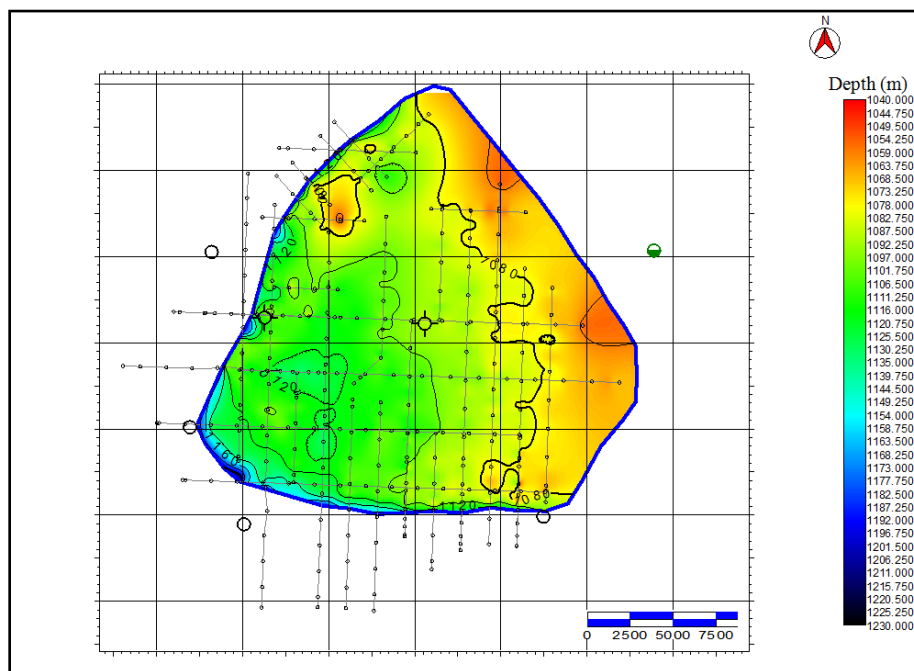


Figure 2.17: Depth structure map of the Upper Leduc Formation with the Leduc reef edge outlined except the eastern boundary marks the edge of data.

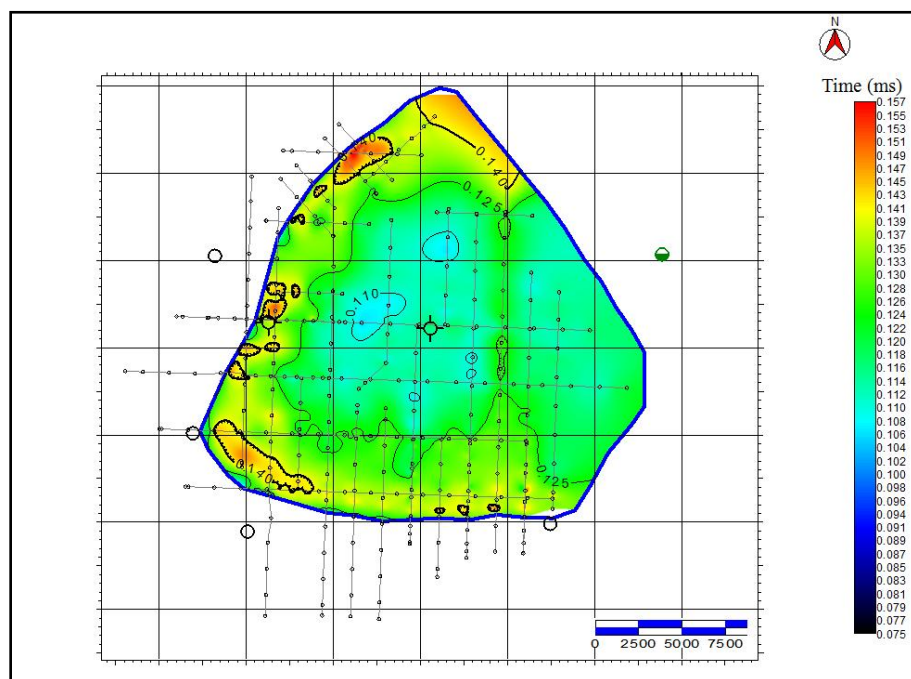


Figure 2.18: Isochron map between Leduc and Beaverhill Lake Formations with the reef edge outlined except the eastern boundary is the edge of data.

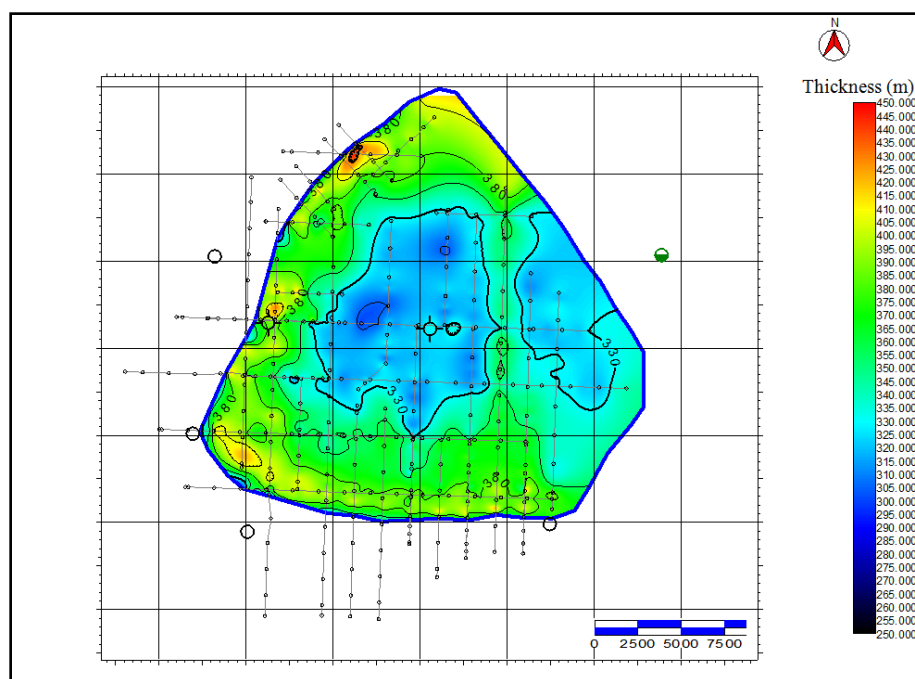


Figure 2.19: Isopach map between Leduc and Beaverhill Lake Formations with the reef edge outlined except the eastern boundary marks the edge of data.

2.5 DISCUSSION AND CONCLUSIONS

Interpretation of 400 line km of vintage 2D seismic data was undertaken for this study. Prior to interpretation, the data were reprocessed through to post-stack time migration to improve the lateral position of reflectors and to correctly image the reef edges. Overall, the data quality is good. Six wells were used to generate zero-offset synthetic seismograms to tie the seismic data to formation tops. Two of these wells are inside the reef and four are off-reef. The correlation between the synthetic seismograms and the migrated seismic data were good.

For the interpretation of the seismic data, the key horizons picked were the Mannville, Nisku, Leduc, Mid-Leduc, Cooking Lake, Beaverhill Lake, Lower Beaverhill Lake formations. An interpreted Basement event was also picked. Generally, all the horizons picked dip towards the south-west and no observable faults in the study area were identified. Time structure maps of formations younger than the Leduc Formation exhibit compactional drape over the reef by 30 ms, and this decreases upwards.

Reflections from below the reef exhibit significant positive time structure and appear as highs in time structure maps by 55 ms. This structure is apparent only and is due to high velocities of on-reef carbonate strata (Leduc Formation.) being juxtaposed beside lower velocity off-reef shales of the Ireton Formation. Converted depth maps generally compensated for the velocity pull up. However, they demonstrate slight negative depth structure below the reef embayment because of the use of only a single interval velocity technique for depth conversion, due to lack of wells penetrating the embayment where seismic data are available. The average velocity is lower within the reef embayment due to the presence of shales instead of carbonates.

Terminations of the Upper Leduc and Middle Leduc events are clear on the 2D seismic lines and the latter pick was used to define the reef margin. Isochron and Isopach maps between the Upper Leduc and deeper formations delineate thickening of the reef around the rim on the western and southern sides, and thinning in the central part of the reef. This was corroborated with well data.

A Duvernay embayment was mapped encroaching into the reef along part of the north-western reef flank, and also around the southwestern corner of the reef. The embayment was evidenced by a high-amplitude reflection within the reef interval. Elsewhere, the internal reflectivity of the reef is generally low and uncharacteristic. A loss of coherence in reflectivity along some seismic lines near the western edge of the reef was interpreted to be an indicator of dolomitization in the Middle Leduc and Cooking Lake formations.

Chapter Three: **WELL-BASED FLUID SUBSTITUTION SEISMIC MODELING IN REDWATER REEF**

3.1 Introduction

The Alberta Basin exhibits one of the world's largest commercial opportunities for reducing CO₂ emissions into the atmosphere (Gunter and Bachu, 2007). It can be done through carbon capture and storage (CCS) in deep subsurface geological formations such as the Leduc Formation at the Redwater reef. In this chapter, synthetic seismograms were generated for the wells that penetrate the Devonian Cooking Lake Formation within the Redwater reef and which have sonic and density logs. The initial objective was to evaluate the seismic response to CO₂ saturation in the Devonian Leduc reservoir at the Redwater reef using uniform fluid substitution seismic modeling.

3.2 Methodology

3.2.1 Synthetic Seismogram Generation

In order to generate synthetic seismograms, two wells were selected that penetrate the Devonian Cooking Lake Formation, which is deeper than our target Leduc Formation (Figure 3.1). These wells are within the Redwater reef complex, one in the center of the reef and another near the west edge of the reef. Only the primary reflection events were modeled, so there are no multiple reflections included. GeoSyn Software package was used for generating zero-offset (P-P) synthetics using zero-phase 35 Hz Ricker wavelet for these wells, using P-wave, density, and S-wave logs. In our case, there is no S-wave log, so this was created using the average of global empirical relationship of $V_p / V_s = 1.9$ for carbonates and for WCSB (Bakhorji and Schmitt, 2008) due to limitation to real data in Redwater area, where V_s is the S-wave velocity and V_p is the P-wave velocity.

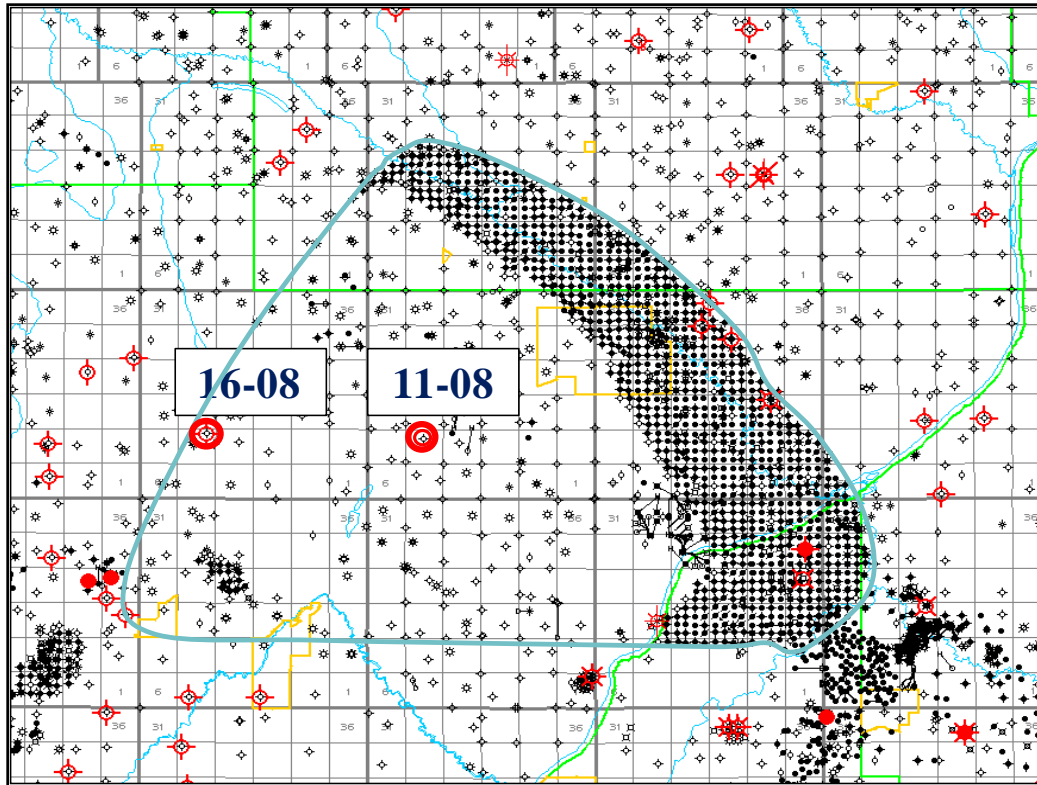


Figure 3.1: Redwater reef map showing all wells. Those that penetrate the Cooking Lake Formation and have sonic logs are in red color. Wells 11-08 and 1-08 were used for fluid substitution modeling.

3.2.2 Fluid Substitution Seismic Modeling

The most common method for fluid substitution modeling is based on Gassmann (1951). He used the rock porosity, the porous rock frame bulk modulus, the mineral matrix bulk modulus, and the pore fluid bulk modulus to calculate the fluid-saturated porous rock bulk modulus (Smith et al., 2003):

$$K_{sat} = K^* + \frac{\left[1 - \frac{K^*}{K_o}\right]^2}{\frac{\phi}{K_{fl}} + \frac{(1-\phi)}{K_o} + \frac{K^*}{K_o^2}}$$

where,

K_{sat} is the saturated rock bulk modulus (un-drained of pore fluids),

K^* is the porous rock frame bulk modulus (drained pore fluid, but not the dry bulk modulus),

K_o is the mineral matrix bulk modulus,

K_{fl} is the pore fluids bulk modulus, and

\emptyset is the rock porosity.

It is expected that shear modulus (μ) of the rock is not affected by fluid substitution, so we assume that:

$$\mu_{\text{sat}} = \mu^*$$

where,

μ_{sat} is the saturated rock shear modulus, and

μ^* is the porous rock frame shear modulus.

Since the P-wave velocity and bulk density (ρ_b), are measured from well logs, and the S-wave velocity is assumed ($V_p/V_s = 1.9$), then the saturated rock bulk and shear moduli can be calculated from the following two equations (Smith et al., 2003):

$$K_{\text{sat}} = \rho_b [V_p^2 - (4/3) V_s^2]$$

$$\mu_{\text{sat}} = \rho_b V_s^2$$

To calculate the porous rock frame bulk modulus, three parameters need to be determined. These are the rock porosity (\emptyset), the rock matrix bulk modulus (K_o), and the fluid bulk modulus (K_{fl}). Since the in-situ fluid in the reservoir is the formation water, the density and modulus of the formation water are then 1072 kg/m^3 and 2.8575 GPa

respectively, calculated using the equations of Batzle and Wang (1992) for brine reservoir. Also, since the Leduc Formation is a carbonate reservoir, the density, bulk modulus, and shear modulus of the carbonates are then 2736 kg/m³, 78.96 GPa, and 33.65 GPa respectively, determined from the two-phase materials equations by Hashin-Shtrikman (1963). The porosity can be calculated from the mass balance equation (Mavko et al., 1998):

$$\phi = (\rho - \rho_m) / (\rho_{fl} - \rho_m) \quad (\text{eq. 1})$$

where,

ρ is the measured rock density,

ρ_m is the matrix density, and

ρ_{fl} is the fluid density.

Since the three parameters (ϕ , K_o and K_{fl}) are known, the porous rock frame bulk modulus (K^*) can be computed using the backward Gassmann equation:

$$K^* = \frac{K_{sat} \left[\frac{\phi K_o}{K_{fl}} + 1 - \phi \right] - K_o}{\frac{\phi K_o}{K_{fl}} + \frac{K_{sat}}{K_o} - 1 - \phi}$$

Finally, the in-situ reservoir fluid can be replaced with CO₂ and therefore, the fluid density and bulk modulus (ρ_{fl} and K_{fl}) can be changed to the new fluid density and bulk modulus. These were calculated by the following simple volumetric mix of the end-member components (Mavko et al., 1998) and Wood's (1941) equations:

$$\rho_{fl} = \rho_w S_w + \rho_c (1 - S_w)$$

$$1/K_{fl} = S_w/K_w + (1-S_w)/K_c$$

where,

S_w is the formation water saturation,

ρ_w is the formation water density,

K_w is the formation water modulus,

ρ_c is the CO_2 density which is 500 kg/m^3 under the reservoir conditions (the initial pressure of Redwater pool was 7.4 MPa and temperature of 34°C), and

K_c is the CO_2 modulus which is 0.1 GPa under the same condition.

CO_2 density and modulus were calculated using the Batzle and Wang (1992) equations for CO_2 in supercritical phase (Figure 3.2).

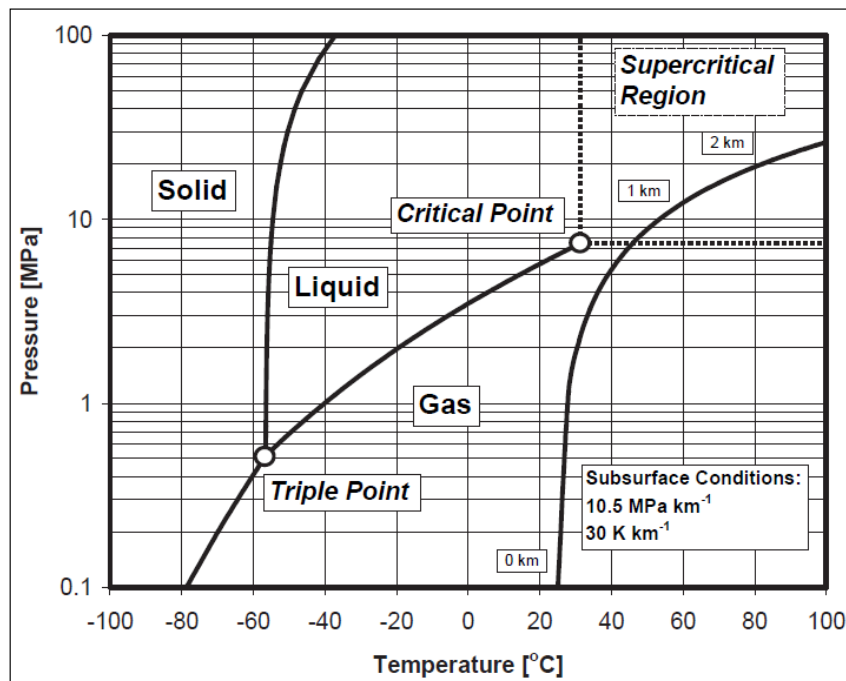


Figure 3.2: Temperature and pressure phase diagram for pure carbon dioxide (Span et al., 1996, cited by Piri et al., 2005).

Then the new saturated rock bulk modulus with the new fluid was calculated using the Gassmann equation again:

$$K^{new}_{sat} = K^* + \frac{\left[1 - \frac{K^*}{K_o}\right]^2}{\frac{\phi}{K^{new}_{fl}} + \frac{(1-\phi)}{K_o} + \frac{K^*}{K_o^2}}$$

and the new bulk density (ρ_b) with the new fluid can be obtained from the rewritten equation (1):

$$\rho_b^{new} = \rho_{fl} \phi + \rho_m (1-\phi)$$

To acquire the new P-wave velocity and S-wave velocity after fluid substitution, we apply the following two equations (Smith et al., 2003):

$$V_p^{new} = \sqrt{\frac{K^{new}_{sat} + \frac{4}{3} \mu_{sat}}{\rho_b^{new}}}$$

$$V_s^{new} = \sqrt{\frac{\mu_{sat}}{\rho_b^{new}}}$$

There are several assumptions in the application of Gassmann's equations. Firstly, the rock is assumed to be homogeneous. Secondly, all the pores are in communication, and thirdly, the pores are filled with a frictionless fluid. Fourthly, the un-drained rock-fluid system is assumed to be closed, and the pore fluid will not soften or harden the rock frame (Wang, 2001).

3.3 Results

Two wells were used to generate zero-offset synthetic seismograms (Figure 3.1). These wells are within the Redwater reef. They are 11-08-57-22W4 (in the center of the reef),

and 16-08-57-23W4 (near the west edge of the reef). There are few wells around the reef that have sonic and density logs. The on-reef wells intersected the Leduc Formation carbonates (Figure 3.3 and Figure 3.4) but the off-reef wells did not. In all of these wells, the top of the Ireton Formation has a seismic trough signature and underlying carbonate Cooking Lake Formation has a weak peak signature on-reef, but has a very strong seismic peak in the wells outside the reef. This is because the Cooking Lake carbonate overlain by Ireton shale yields a large contrast in acoustic impedance. The Leduc Formation in the on-reef wells is identified by a moderate amplitude seismic peak due to moderate contrast in P-wave velocity between Ireton Formation shales and Leduc Formation carbonates.

These two reef wells were also used for fluid substitution seismic modeling. These wells are 11-08-57-22W4 (in the tidal flat lagoonal facies of the reef), and 16-08-57-23W4 (in the foreslope facies at the rim of the reef) (Stoakes, 1980). Gassmann fluid substitution calculations for CO₂ replacing brine were computed for the entire thickness of the Leduc Formation (from 1119 to 1411 m) for well 16-08-57-23W4. Table 3.1 shows some of the computed parameters of the full thickness of the Leduc reservoir (292m) before and after CO₂ substitution assuming uniform saturation. The average porosity of the Leduc Formation at this well is around 6% (composed of 85% of Limestone and 15% of Dolomite) obtained from equation (1). A distinct P-wave velocity decrease occurs from 0% CO₂ saturation to 40% CO₂ saturation (Figure 3.5). From 40% to 100% of CO₂ saturation, the P-wave velocity increases slightly. In contrast, the S-wave velocity increases almost linearly with the CO₂ saturation (Figure 3.5).

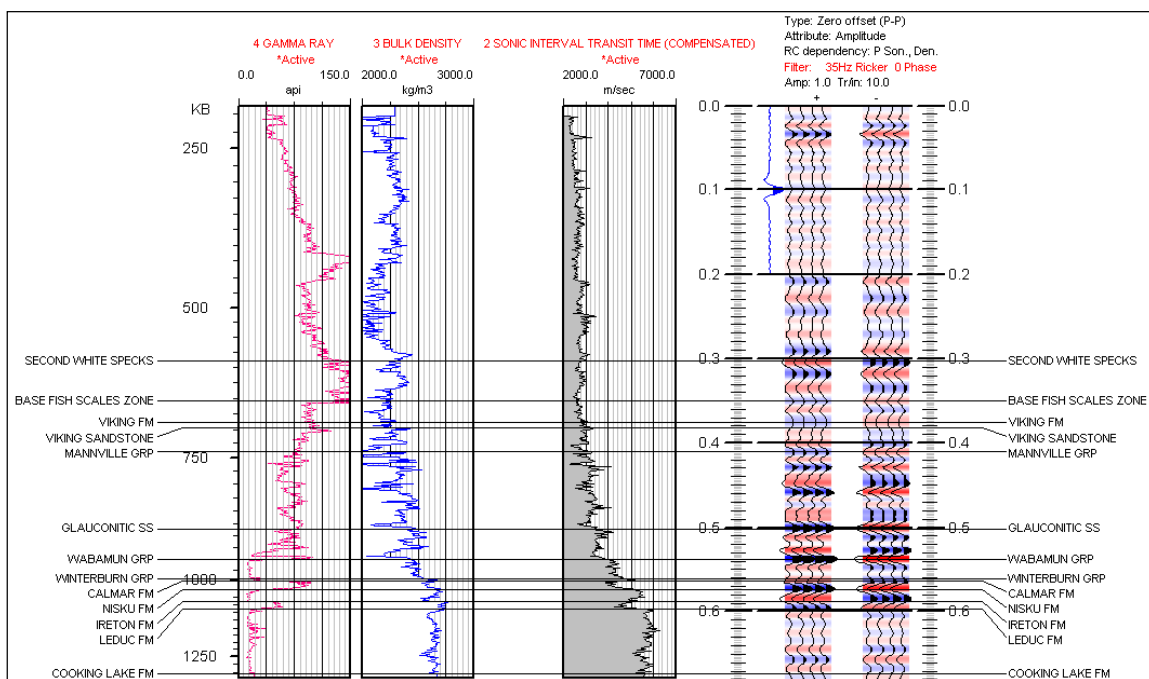


Figure 3.3: Sonic, density, and gamma ray logs and synthetic seismograms from well 11-08-57-22W4 with normal and reverse polarities.

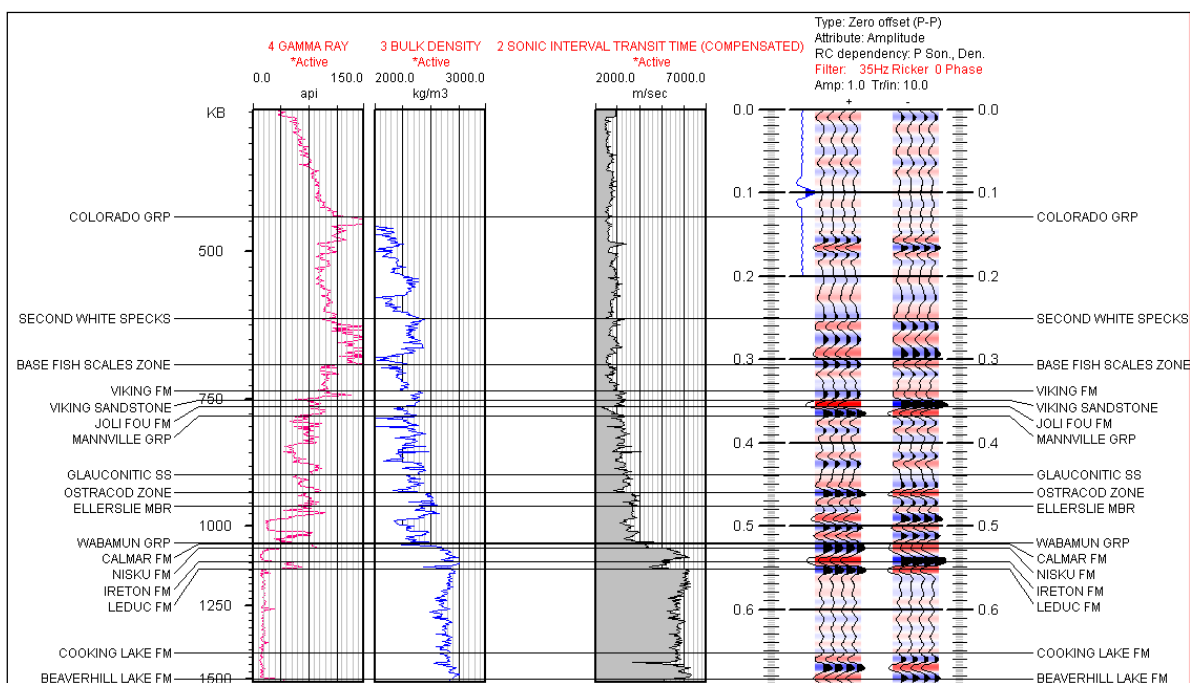


Figure 3.4: Sonic, density, and gamma ray logs and synthetic seismograms from well 16-08-57-23W4 with normal and reverse polarities.

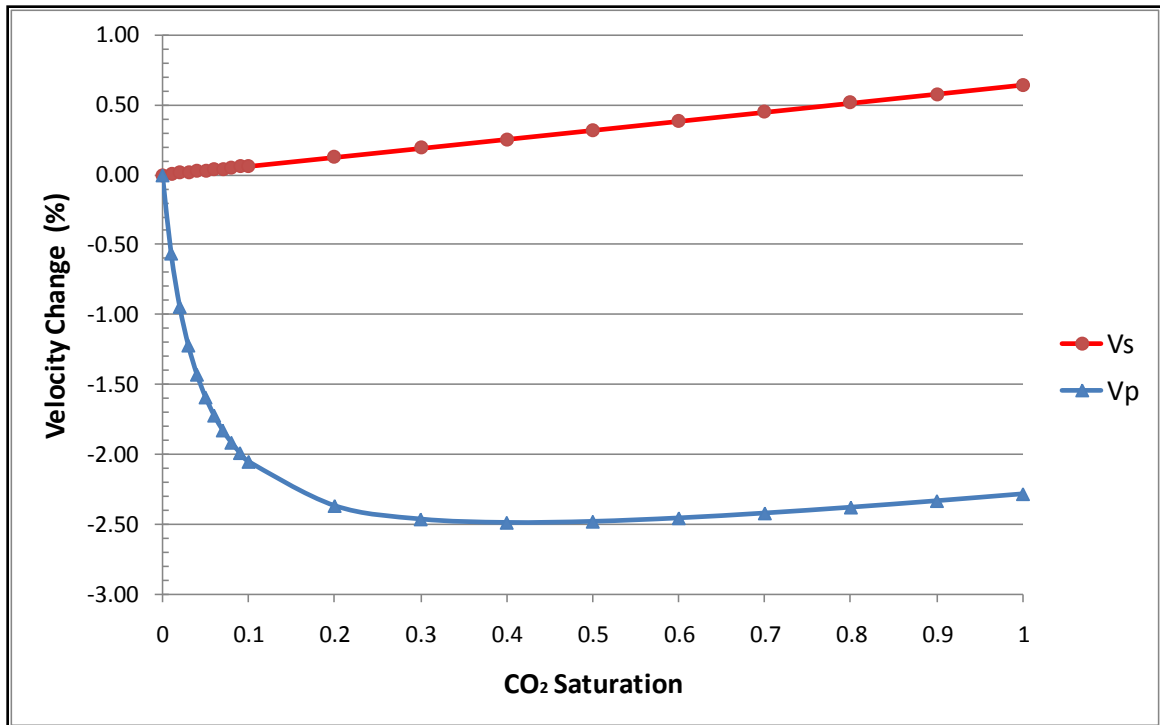


Figure 3.5: The relationship between the P-wave and S-wave velocity changes and CO₂ saturation for well 16-08-57-23W4.

Comparing the native reservoir fluid with 100% CO₂ fluid replacement, a very slight difference is observed in the rock density. The average bulk rock density changed from 2640 kg/m³ to 2600 kg/m³ (about 1.5%) after 100% CO₂ fluid replacement. The average P-wave velocity decreased by about 2.3%, from 5789 m/s to 5657 m/s and the average S-wave velocity increased by about 0.65% from 3047 m/s to 3067 m/s. Vp/Vs decreased by about 2.9% from 1.9 to 1.84 and the P-wave impedance also decreased by 3.5%. The estimated P-wave two-way time delay caused by CO₂ substitution is about 2.5 ms, calculated using the following equation:

$$\Delta T = T_2 - T_1 = 2 H (1/V_2 - 1/V_1)$$

where,

ΔT is the anticipated two-way time delay caused by CO₂ injection,

T_1 and T_2 are the P-wave two-way travel times through the Leduc Formation before and after CO₂ substitution respectively,

V_1 and V_2 are the average P-wave velocities of the Leduc Formation before and after CO₂ substitution, respectively, and

H is the total thickness of the Leduc formation (292m).

Table 3.1: Results of the well 16-08-57-23W4 before and after CO₂ fluid substitution within of the entire thickness of the Leduc Formation, with average porosity of 6%.

CO ₂ Saturation	Fluid Density (g/cc)	Rock Density (g/cc)	K _{fr} Gpa	K _{sat} Gpa	V _p m/s	V _s m/s	V _p Change %	V _s Change %	V _p /V _s Change %	Δt (ms)
0	1.07	2.64	2.86	55.75	5789	3047	0	0	0	0
0.1	1.02	2.63	0.76	52.05	5670	3049	-2.05	0.06	-2.12	2.1
0.2	0.96	2.63	0.44	51.40	5652	3051	-2.37	0.13	-2.50	2.4
0.3	0.90	2.63	0.31	51.12	5646	3053	-2.47	0.19	-2.65	2.6
0.4	0.85	2.62	0.24	50.97	5645	3055	-2.49	0.26	-2.74	2.6
0.5	0.79	2.62	0.19	50.88	5645	3057	-2.48	0.32	-2.80	2.6
0.6	0.73	2.62	0.16	50.81	5647	3059	-2.46	0.39	-2.83	2.5
0.7	0.67	2.61	0.14	50.77	5649	3061	-2.42	0.45	-2.86	2.5
0.8	0.62	2.61	0.12	50.73	5651	3063	-2.38	0.52	-2.88	2.5
0.9	0.56	2.61	0.11	50.70	5654	3065	-2.34	0.58	-2.90	2.4
1	0.50	2.60	0.10	50.68	5657	3067	-2.29	0.65	-2.91	2.4
Average	0.76	2.62	0.26	51.01	5652	3058	-2.38	0.35	-2.72	2.5

Zero-offset synthetic seismograms were generated for well 16-08-57-23W4 with CO₂ saturations increasing from 0% to 100% (at 10% increments) using Hampson-Russell

Pro4D software. There are slight changes in amplitude between 0% and 40% CO₂ saturation (Figure 3.6). In addition, there is a small velocity reduction with increasing CO₂ saturation, shown by a time delay of the Cooking Lake event. The sensitivity of the synthetic seismograms to CO₂ saturation is more clearly seen in Figure 3.7, which show synthetic seismograms (Figure 3.7 left) and amplitude difference compared to 0% CO₂ saturation (Figure 3.7 right). As CO₂ saturation greater than 40%, the amplitude difference becomes less sensitive to CO₂ saturation.

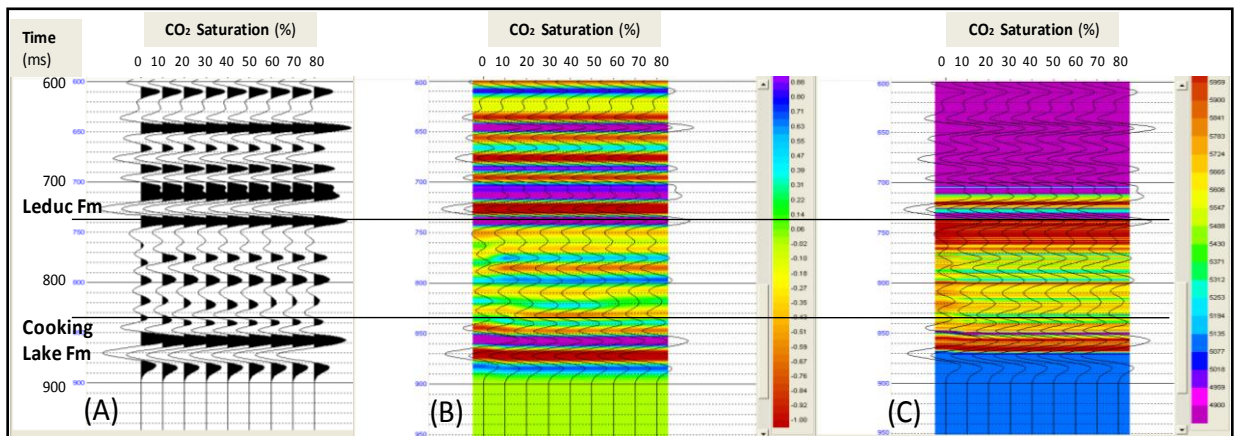


Figure 3.6: Zero-offset synthetic seismic traces for well 16-08-57-23W4, with CO₂ fluid substitution from 0% (left) to 100% (right) in each panel. (A) wiggle-trace display, (B) color amplitude with wiggle-trace overlay, and (C) interval velocity with wiggle-trace overlay.

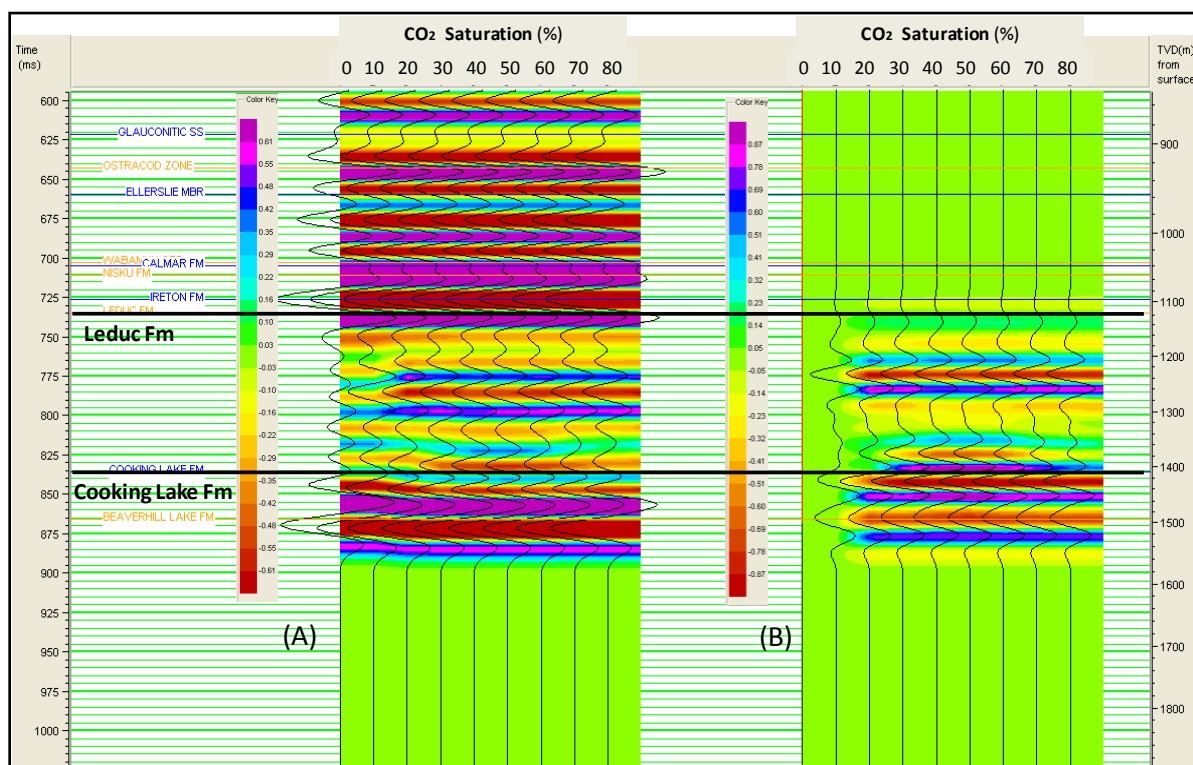


Figure 3.7: Zero-offset synthetic seismic traces of the well 16-08-57-23W4 before and after fluid substitution. (A) absolute amplitudes, and (B) amplitude difference compared to 0% saturation.

As a comparison, Gassmann fluid substitution calculations were performed for the entire thickness of the Leduc Formation (from 1086 to 1311 m) for well 11-08-57-22W4. Table 3.2 shows some of the computed parameters of the full thickness of the Leduc reservoir (225m) before and after CO₂ replacement. The average porosity of the entire Leduc Formation at this well is about 4% (composed of 100% of Limestone) calculated from equation (1). A distinct P-wave velocity decrease occurs from 0% to 40% of CO₂ saturation (Figure 3.8). From 40% to 100% CO₂ saturation, the P-wave velocity decreases slightly. In contrast, the S-wave velocity again increases almost linearly with the CO₂ saturation increasing (Figure 3.8).

Table 3.2: Results of the well 11-08-57-22W4 before and after CO₂ fluid substitution within of the entire thickness of the Leduc Formation, with average porosity of 4%.

CO2 Saturation	Fluid Density (g/cc)	Rock Density (g/cc)	K_{fi} Gpa	K_{sat} Gpa	V_p m/s	V_s m/s	V_p Change %	V_s Change %	V_p/V_s Change %	Δt (ms)
0	1.07	2.64	2.86	55.08	5747	3025	0	0	0	0
0.1	1.02	2.64	0.76	49.61	5567	3026	-3.14	0.04	-3.18	3.3
0.2	0.96	2.64	0.44	48.55	5533	3027	-3.72	0.09	-3.81	3.9
0.3	0.90	2.64	0.31	48.10	5520	3029	-3.95	0.13	-4.07	4.2
0.4	0.85	2.63	0.24	47.85	5514	3030	-4.06	0.17	-4.22	4.3
0.5	0.79	2.63	0.19	47.70	5511	3031	-4.11	0.22	-4.32	4.4
0.6	0.73	2.63	0.16	47.59	5510	3033	-4.13	0.26	-4.38	4.4
0.7	0.67	2.63	0.14	47.51	5509	3034	-4.14	0.30	-4.43	4.4
0.8	0.62	2.63	0.12	47.45	5509	3035	-4.13	0.35	-4.47	4.4
0.9	0.56	2.62	0.11	47.40	5510	3037	-4.12	0.39	-4.50	4.4
1	0.50	2.62	0.10	47.36	5511	3038	-4.10	0.44	-4.52	4.3
Average	0.76	2.63	0.26	47.91	5519	3032	-3.96	0.24	-4.19	4.2

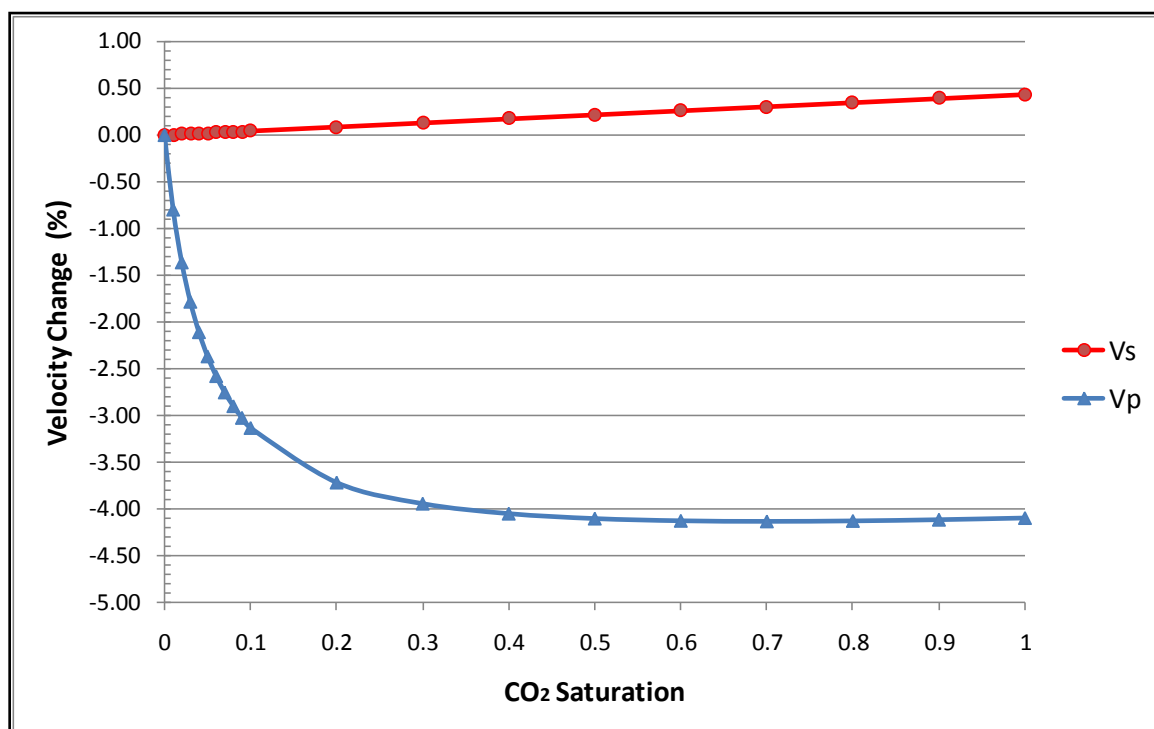


Figure 3.8: The relationship between the P-wave and S-wave velocity changes and various CO₂ saturations of the well 11-08-57-22W4.

Comparing results from the in-situ wet reservoir conditions with 100% of CO₂ fluid replacement, a very slight difference was observed again in the density. The average rock density changed from 2640 kg/m³ to 2620 kg/m³ (about a 0.75% decrease) after 100% CO₂ fluid replacement. The average P-wave velocity decreased by about 4.1% from 5747 m/s to 5511 m/s, and the average S-wave velocity increased by about 0.44% from 3025 m/s to 3038 m/s. Vp/Vs decreased by about 4.5% from 1.9 to 1.81 and the P-wave impedance also decreased by 4.9%. The estimated P-wave two-way time delay caused by CO₂ substitution is about 4.2 ms.

Zero-offset synthetic seismograms were also generated for well 11-08-57-22W4 with CO₂ replacement from 0% to 100% (in increments of 10%). There are still minor changes in amplitude between the reservoir reflections of Leduc formation before and after fluid substitution (Figure 3.9). The amplitude differences between wet and various CO₂ saturations were examined (Figure 3.10). The maximum amplitude difference changes are recognized at 40% and 50% of CO₂ saturations.

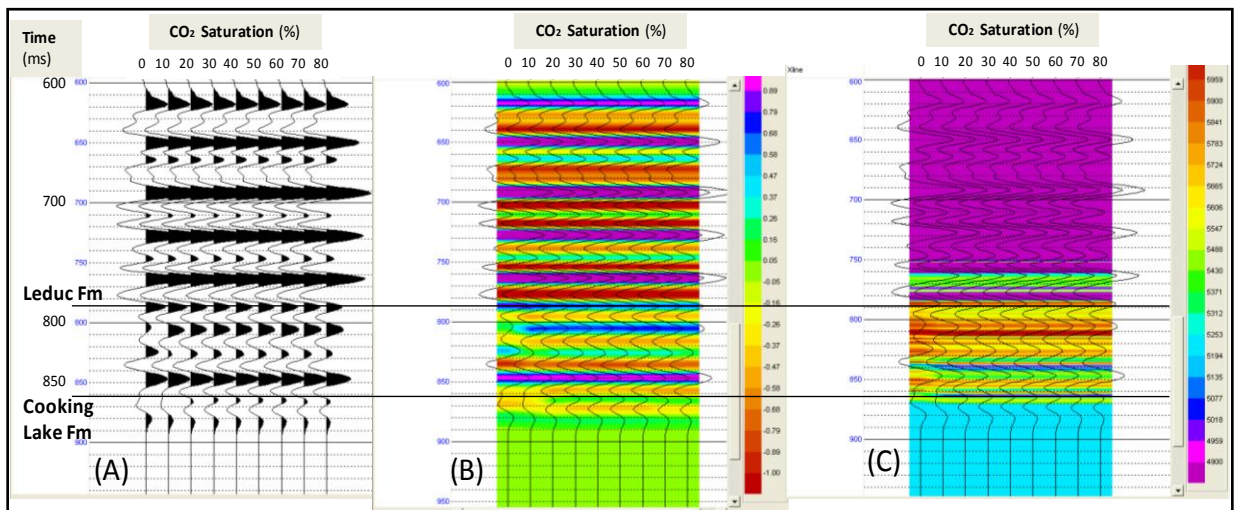


Figure 3.9: Zero-offset synthetic seismic traces for well 11-08-57-22W4, with CO₂ fluid substitution from 0% (left) to 100% (right) in each panel. (A) wiggle-trace display, (B) color amplitude with wiggle-trace overlay, and (C) interval velocity with wiggle-trace overlay.

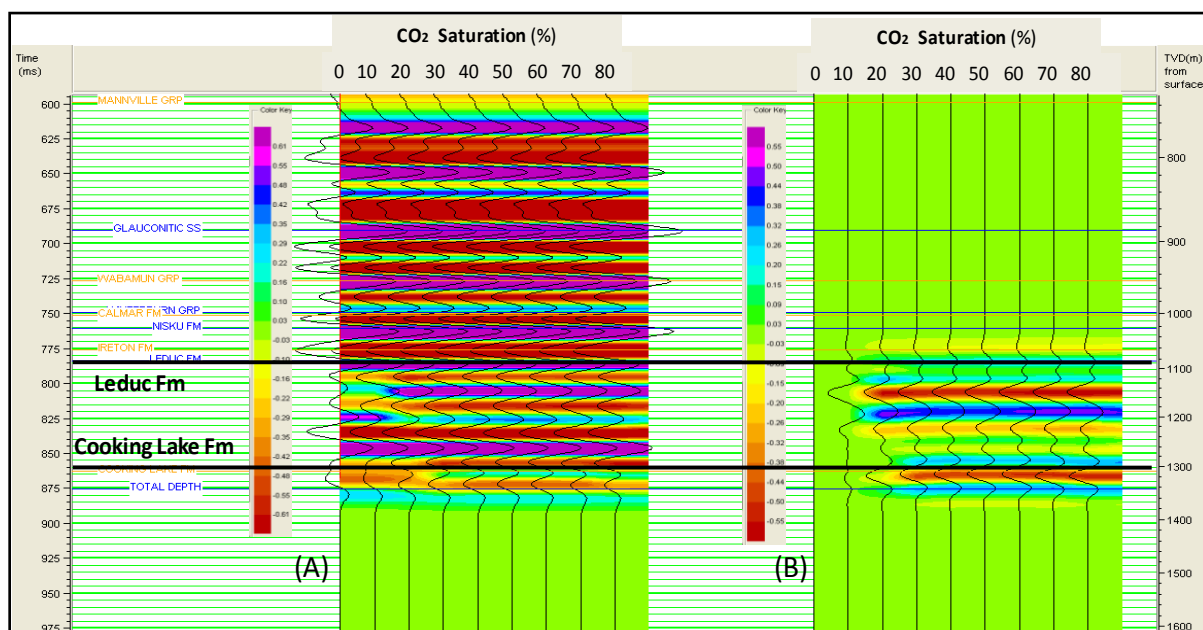


Figure 3.10: Zero-offset synthetic seismic traces of the well 11-08-57-22W4 before and after fluid substitution. (A) absolute amplitudes, and (B) amplitude difference compared to 0% saturation.

After presenting these results, some discussion is required about the assumptions that were made for the fluid substitution processes. Firstly, the shear modulus remains constant during fluid substitution when using the Gassmann's equations (Smith, 2003). This means that the shear modulus for an isotropic media is independent of pore fluids (Wang, 2001), but if the pores are not in communication or cracks happen in the reservoir, this assumption would be violated. Secondly, during the fluid substitution process an equilibrium saturation model was assumed (Wang, 2001). However, during the CO₂ injection, the equilibrium distribution of fluids will be disturbed. Therefore, it would be perhaps more sensible and realistic to employ a patchy saturation model rather than the equilibrium saturation model (Smith, 2003). Moreover, the effects of the pressure, temperature and viscosity variations in the reservoir were not taken in

consideration as well. All of these variables were not taken in the calculation of fluid substitution because of the lack of this information in Redwater reef due to termination of the HARP project which impacting the acquiring of new field data.

3.4 Discussion

Fluid replacement modeling using Gassmann equation is an effective method to model the time-lapse differences that are caused by the CO₂ injection. For the wells 16-08-57-23W4 and 11-08-57-22W4, a distinct P-wave velocity decrease occurs from 0% CO₂ saturation to 40% CO₂ saturation. From 40% to 100% of CO₂ saturation, the P-wave velocity starts increasing slightly, while the S-wave velocity increases linearly with increasing CO₂ saturation. The P-wave velocity of the Leduc reservoir is so sensitive to the CO₂ substitution especially for lower saturation. Even with small quantity like 1% saturation of CO₂, the P-wave velocity dropped considerably.

The average rock density for well 16-08-57-23W4 decreases about 1.5% after 100% CO₂ fluid replacement and the average P-wave velocity decreases by about 2.3%, whereas, the average S-wave velocity increases by about 0.65%. V_p/V_s decreases by about 2.9% and the P-wave impedance also decreases by 3.5%. The estimated P-wave two-way time delay caused by CO₂ substitution is about 2.5 ms. While, the average P-wave velocity for well 11-08-57-22W4 decreases by about 4.1% and the average S-wave velocity increases by about 0.44%. V_p/V_s decreases by about 4.5% and the P-wave impedance also decreases by 4.9%. The estimated P-wave two-way time delay caused by CO₂ substitution for well 11-08-57-22W4 is about 4.2 ms.

Synthetic seismograms were generated for the wells 16-08-57-23W4 and 11-08-57-22W4 before and after fluid substitution. There are slight changes in reflection amplitudes of the Leduc events between the wet in-situ reservoir condition and after fluid substitution modeling. The time shift observed at the base of the Leduc reservoir. The maximum time shift at the base of the Leduc reservoir and the highest amplitude difference changes are seen at between 30% and 40% CO₂ saturations.

Chapter Four: **MULTICHANNEL TIME-LAPSE SEISMIC MODELING OF CO₂ FLUID SUBSTITUTION IN THE REDWATER LEDUC REEF**

4.1 Introduction

The main objective of this part of the thesis was to characterize the reef members and formations below the reef through a 2D geological model of the Redwater reef, from the reef center to off-reef, across the southern margin of the reef. Seismic modeling was then undertaken to generate 2D synthetic seismic data to study the multichannel seismic response of Redwater different formations, particularly the Leduc reef units. Another main objective was to assess the multichannel seismic response of the reef, with uniform 40% CO₂ saturation in the Upper Leduc member interval, in the entire Leduc formation, and in only the Leduc rim target zone. Fluid substitution seismic modeling was undertaken to generate the 2D synthetic seismic data to trace the consequences of CO₂ saturation in the various facies within the reef, the reef members and formations below the reef based on seismic attributes and character when reaching the end-state situation.

One more essential objective of the study was to map Duvernay shale along with Leduc reef facies by building a 2D geological model of the Redwater reef across the eastern margin of the reef where it has Duvernay shale embayments in the Middle and Lower Leduc members, with and without 40% CO₂ saturation in the Upper Leduc member zone. Time-lapse and fluid substitution seismic modeling was then undertaken to examine the consequences of CO₂ saturation on the reef complex. Also, it was to give a comparison between the embayment and no embayment profiles.

For the 2D synthetic seismic modeling discussed in this chapter, full common-shot ray tracing (for PP and PS) and finite-difference (for PP) modeling were used to produce the numerical seismic response of the reef. The model is based on available well data and depth-converted seismic data from the seismic interpretation discussed in chapter two and discussed by Sodagar and Lawton, 2010h. The numerical seismic data were processed to evaluate the reflection image of the reef edge as well as the internal reef litho-facies.

4.2 Methodology

4.2.1 Common Shot Surface Seismic Modeling

A large number of wells penetrate the Upper Leduc Fm, especially along the eastern margin of the Redwater reef, but only a small number of wells penetrate the Cooking Lake Formation and few of these have sonic and density logs. Figure 4.1 shows three wells inside the reef and six wells off-reef that penetrate the Cooking Lake Formation in the general study area. Of these, three on-reef and four off-reef wells were used to assist in the generation of the velocity and density model used for the seismic modelling project.

2D geological models of the Redwater reef area were constructed from the interpretation of legacy 2D surface seismic data within the study area as well as the available well data. The first 2D profile (Line A) is oriented in a north-south direction and extends from the lagoonal facies within the central region of the reef to off-reef (Figure 4.1). The second 2D geological model (line B) is oriented in an east-west direction. The 2D geological models were extracted from the 3D gridded time structure maps of geological formations

including Mannville, Nisku, Ireton, Leduc, Mid-Leduc, Cooking Lake and Beaverhill Lake (Sodagar and Lawton, 2010a, b, and c). These time structure maps were converted to depth maps using a gradient velocity at the well locations. Errors in the calculated depth were within 1m at the well locations for all formations picked for the geological model.

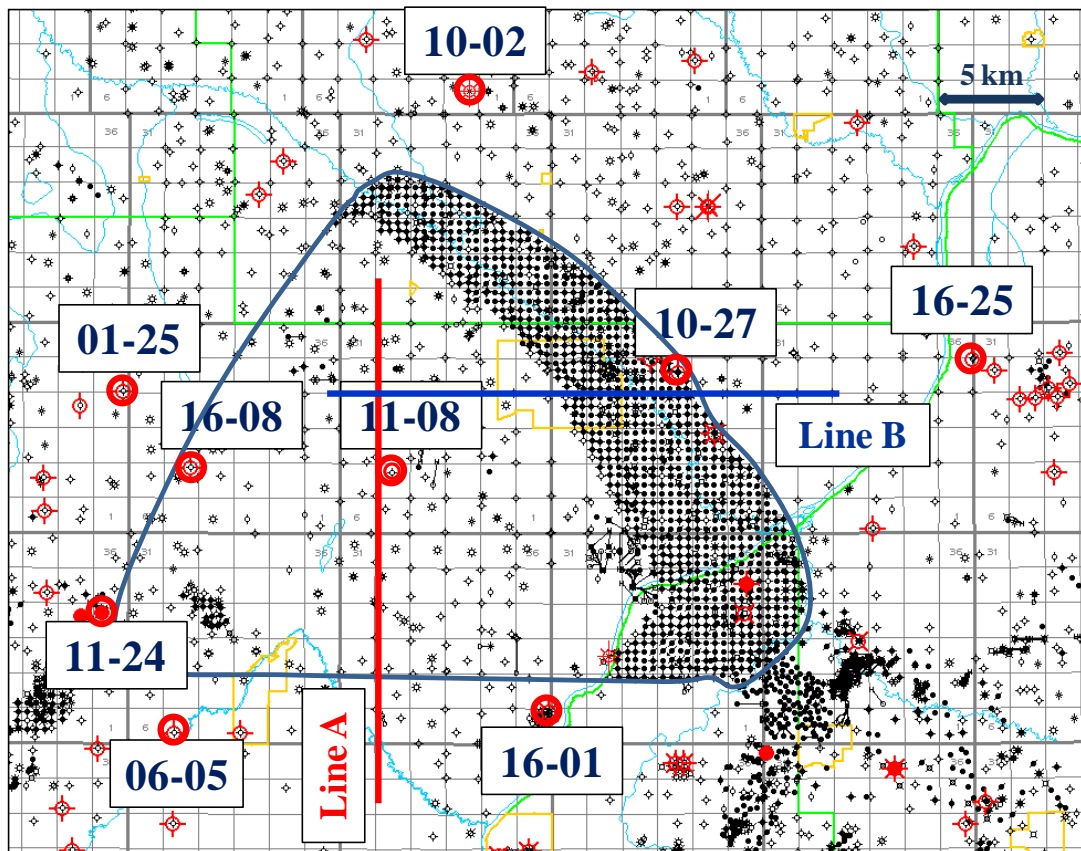


Figure 4.1: Redwater reef map showing available wells. Those wells that penetrate the Cooking Lake Formation and have sonic logs are highlighted in red. The red and blue lines are the location of 2D geological models.

The 2D geological model developed along Line A is shown in Figure 4.2. Interfaces in depth were transformed to event blocks and then P-wave velocities and densities were

assigned to these blocks using average values from the wells (Sodagar and Lawton, 2010a and h). These properties of the model are shown in Figure 4.3 and Figure 4.4. S-wave velocities were assigned using $V_p/V_s = 1.9$, calculated from a single existing dipole well on the eastern side of the reef. The reef rim region was modelled as a separate block (Figure 4.2 through Figure 4.4). In this block, the velocity and density values had a lateral gradient associated with an average porosity of 4% in the inner-reef tidal flat lagoonal facies increasing to an average porosity 9% in the foreslope facies at the rim of the reef (Figure 4.3 and Figure 4.4). For fluid substitution modeling, Leduc Formation original fluid (100% saline water) was replaced uniformly by CO_2 at a saturation level of 40%, where it has a large impact on seismic attributes (Lawton and Sodagar, 2009), in the Upper Leduc member, then in the entire Leduc formation, and also only in the Leduc rim target zone respectively. The P-wave velocities and densities after fluid substitution were calculated using Gassmann's equation (Gassmann, 1951). CO_2 saturations of greater than 40% were not evaluated since the change in seismic velocity between 40% and 100% saturation is small (Sodagar and Lawton, 2010d and 2011a).

4.2.2 Seismic Survey Parameters

Common shot ray tracing (for PP and PS) and finite-difference (for PP) modeling for primary events were performed with a shot interval of 40 m and receiver interval of 10 m from a SRD (Seismic Reference Datum) of 750 m above sea-level. The survey was undertaken with a split-spread geometry with 150 receivers on each side of the source point. Table 4.1 lists the full survey design parameters that were used in the seismic modeling. Seismic shot gathers were generated by convolving the reflectivity functions at

the computed arrival times with a zero-phase 40 Hz Ricker wavelet for PP data and a 20 Hz Ricker wavelet for the PS data (Sodagar and Lawton, 2010e, f, and g). The seismic wavelet for PP data was estimated from the reprocessed 2D surface seismic data at a well location.

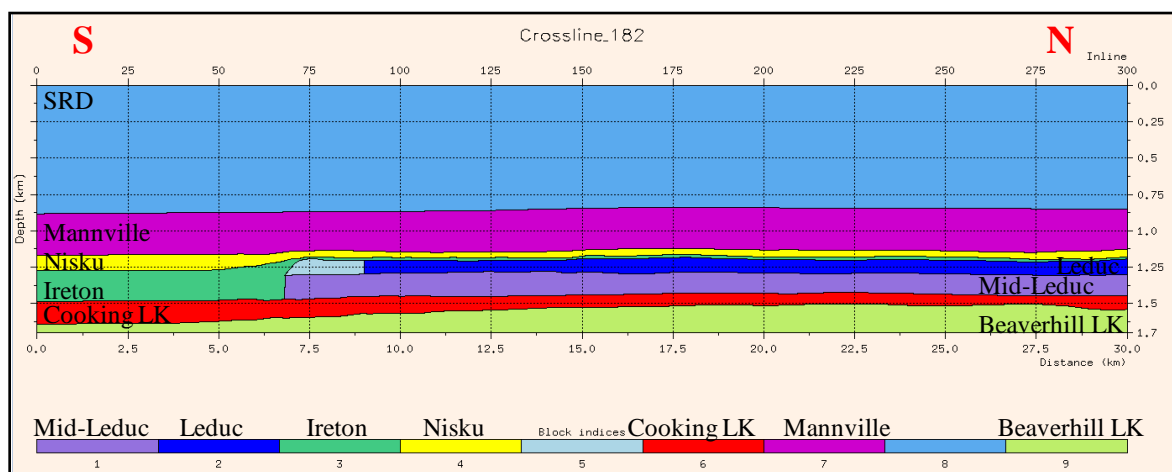


Figure 4.2: 2D geological model along Line A, where crosses the southern margin of the Redwater reef, showing the formations included in the model.

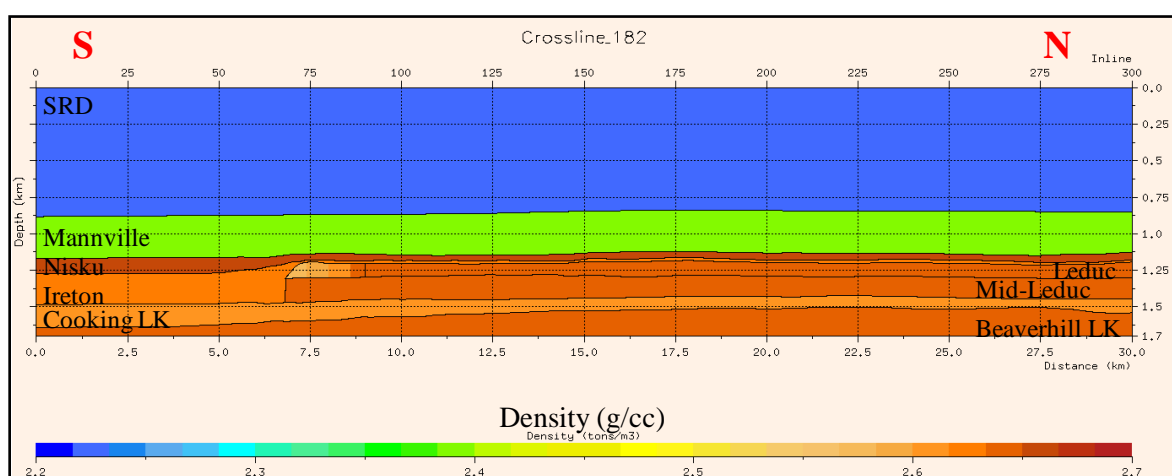


Figure 4.3: Density values of the 2D model along Line A.

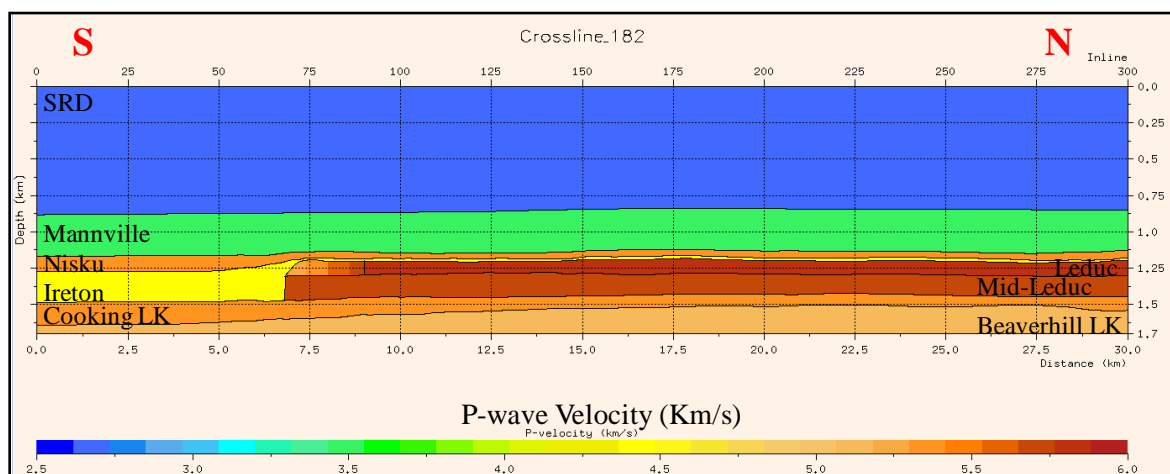


Figure 4.4: P-wave velocities of the 2D model along Line A.

Table 4.1: Survey design parameters used for the 2D seismic modeling in the Redwater area for both Line A and B.

PARAMETER	VALUES
Source interval	40 m
Receiver interval	10 m
CDP interval	5 m
Receivers per source	301
Minimum offset	10 m
Maximum offset	1500 m
Total number of shots	401
Total number of receivers	1901
Total number of traces	120701
Fold	37

4.2.3 Seismic Data Processing

The synthetic seismic data were processed and migrated to image the reef margin and the internal reef facies. This processing involved converting the trace headers from shot point to common depth point (CDP) domain, CDP gather, normal moveout (NMO) correction, and stack, followed by Kirchhoff post-stack migration for PP data (Sodagar

and Lawton, 2010a, b, and c). Processing of the PS data involved converting the trace headers from common midpoint (CMP) to ACP (Asymptotic Conversion Point) domain, reversing the polarity of trailing traces in the shot gathers, normal moveout (NMO) correction, and stack (Sodagar and Lawton, 2010e, f, and g). Kirchhoff pre-stack time migration (PSTM) and Kirchhoff pre-stack depth migration (PSDM) were undertaken for PP and PS data. The P-P and P-S velocity models used for the NMO corrections and for migration were created by converting the interval velocities from the input geological model into RMS velocities in time.

4.2.4 Software

NORSAR2D software was used to create the 2D interface blocks, perform common shot ray tracing, and generate the synthetic shot gather seismic data (NORSAR, 2007).

ProMax software was used for finite difference modeling, geometry, sorting, polarity reversal, velocity conversion and post-stack time migration, pre-stack time migration, and pre-stack depth migration.

4.3 Results – Line A

Figure 4.5 and Figure 4.6 show examples of seismic shot gathers of ray tracing and finite difference modeling methods respectively. It is noticed that ray traced shot gather is cleaner and multiple free compare to finite difference shot gather. The primary events are strong enough to be recognized in both gathers. In finite difference gather, there are multiples like the event at 1120 ms and it has artifacts coming from the reef edge diffraction.

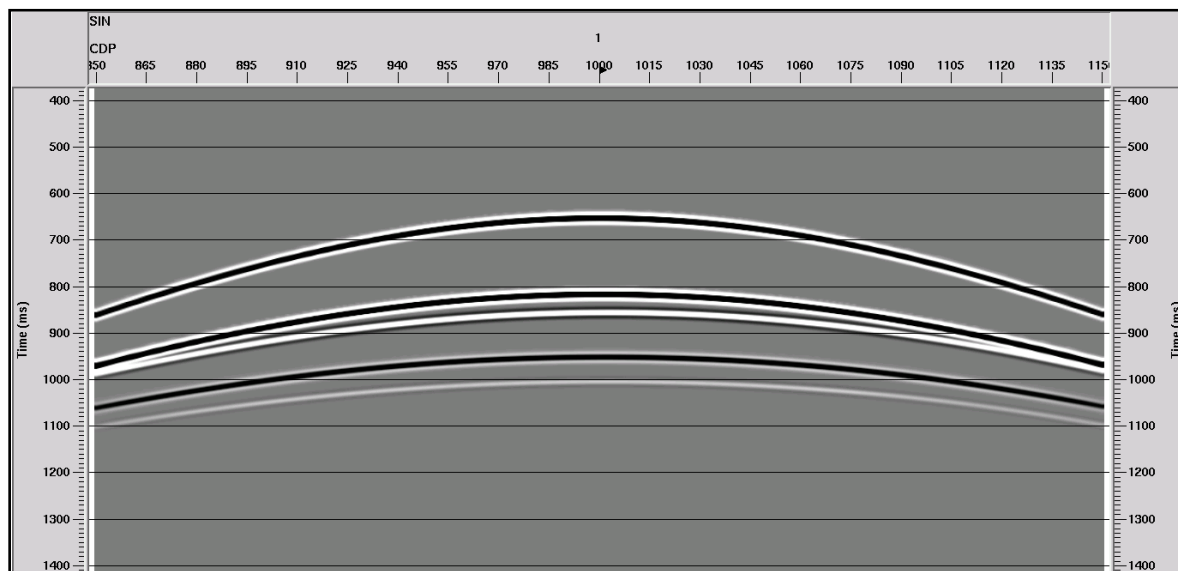


Figure 4.5: Ray tracing numerical seismic shot gather data from the Line A.

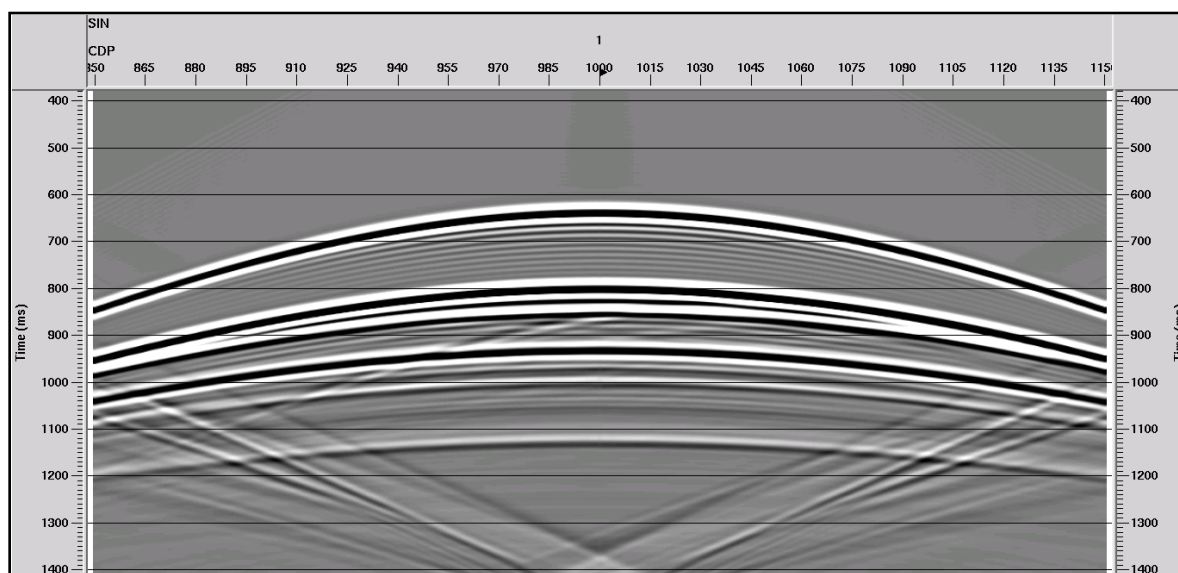


Figure 4.6: Finite difference numerical seismic shot gather from the Line A.

4.3.1 Baseline Modeling - ray traced data

Figure 4.7 and Figure 4.8 illustrate the ray traced numerical seismic data after CDP stack and after post-stack Kirchhoff migration respectively where the migration effect is clear in Figure 4.8 at the reef margin. In this section, the Mannville event is a strong peak, the Nisku event is a moderate amplitude peak, the Ireton shale event is a trough and the Cooking Lake Formation correlates to a moderate amplitude trough on-reef but has higher amplitude peak off-reef. This is because the Cooking Lake carbonates, when overlain by Ireton shale, yield a large impedance contrast and a high-amplitude reflection. The Beaverhill Lake event is fairly weak trough due to the small impedance contrast at the interface between the two carbonate units.

Reflections from the Cooking Lake and Beaverhill Lake formations exhibit positive time structure below the reef, due to a lateral velocity change from the on-reef carbonate strata (Leduc Formation) to the adjacent, lower velocity off-reef shale strata (Ireton Formation). Both formations are essentially flat in the depth model (Figure 4.2). This velocity pull-up is removed in the pre-stack depth-migrated section discussed later (Figure 4.10).

Terminations of the Upper Leduc and Middle Leduc events are clear on the 2D synthetic seismic section at the reef margin, and the Upper Leduc event shows the rim build-up. A high- amplitude reflection at the base of upper-Leduc member is evident near the reef margin and but this event becomes weaker toward the interior facies. This is due to the modelled porosity differences and consequently impedance difference between the foreslope facies in the reef rim and lagoonal facies within the central region of the reef. All the horizons dip gently to the south on the 2D synthetic seismic section.

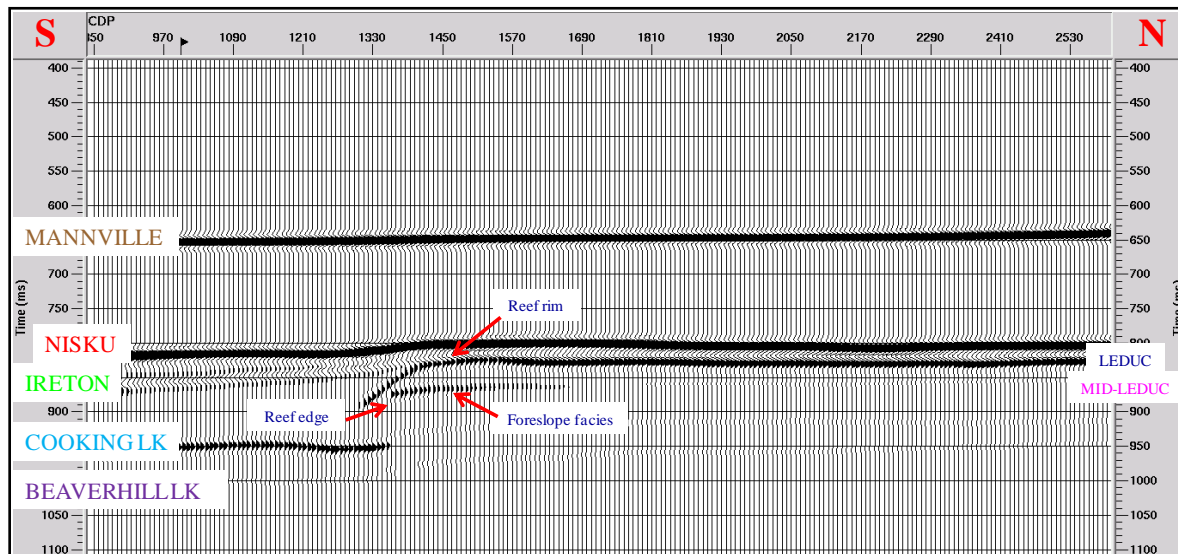


Figure 4.7: 2D ray traced numerical seismic section after CDP stack, Line A, with interfaces identified on the section.

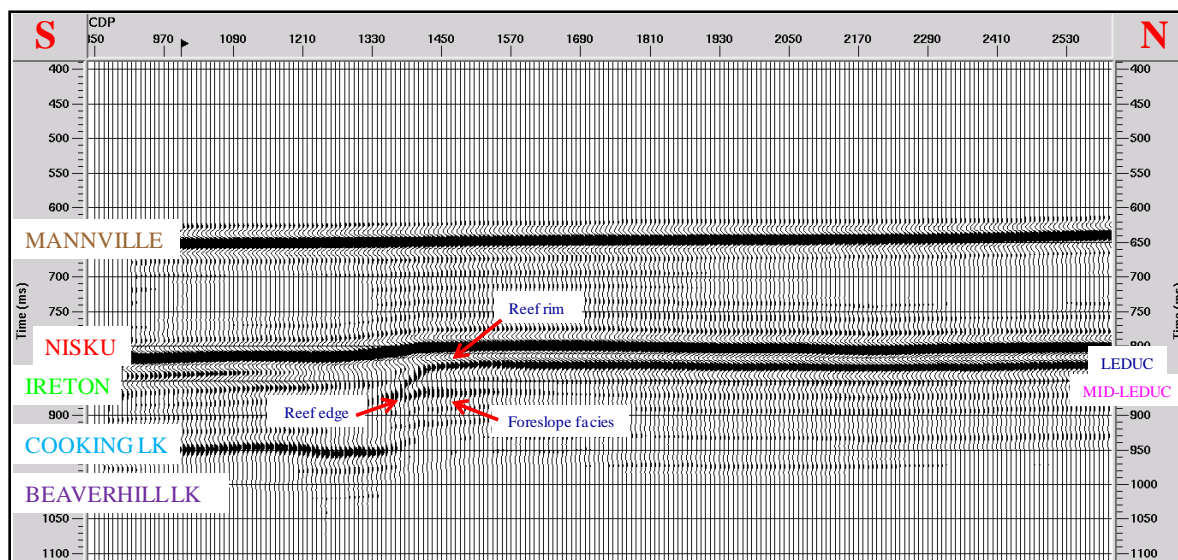


Figure 4.8: 2D ray traced numerical seismic section after post-stack time migration, Line A, with interfaces identified on the section.

Figure 4.9 and Figure 4.10 display the pre-stack time-migrated and depth-migrated seismic sections respectively, created from the ray traced data. The Mannville, Nisku, Ireton, Cooking Lake, and Beaverhill Lake formations display essentially the same seismic attributes as the post-stack time-migrated seismic section with some enhancements, especially on the depth section. Positive time structure below the reef still exists in the pre-stack time-migrated data, as expected, but corrected to almost flat in the pre-stack depth-migrated section. Reflection terminations and the lateral positions of the Upper Leduc and Middle Leduc events are enhanced after pre-stack migration, as shown in Figure 4.9 and Figure 4.10. The reef rim is clearly observable near the reef margin and the high amplitude event at the base of the Upper-Leduc member is apparent at the reef edge but diminishes toward the lagoonal facies within the central part of the reef (Figure 4.11). It is noteworthy that the amplitude variation of this event on the modelled seismic data is similar to that observed on the processed field data in this part of the reef (Figure 4.12), and thus may be a possible porosity indicator. Figure 4.13 illustrates the velocity model in color super-imposed on the pre-stack depth migration seismic section, and shows the excellent correlation between the original velocity model and the seismic depth image.

4.3.2 Baseline Modeling - finite difference data

Figure 4.14 and Figure 4.15 display the pre-stack time-migrated and depth-migrated seismic sections respectively using finite difference method. The sections display essentially the same visual seismic attributes as the sections derived from ray-trace modelling. Also, positive time structure compensated in the depth section to nearly flat.

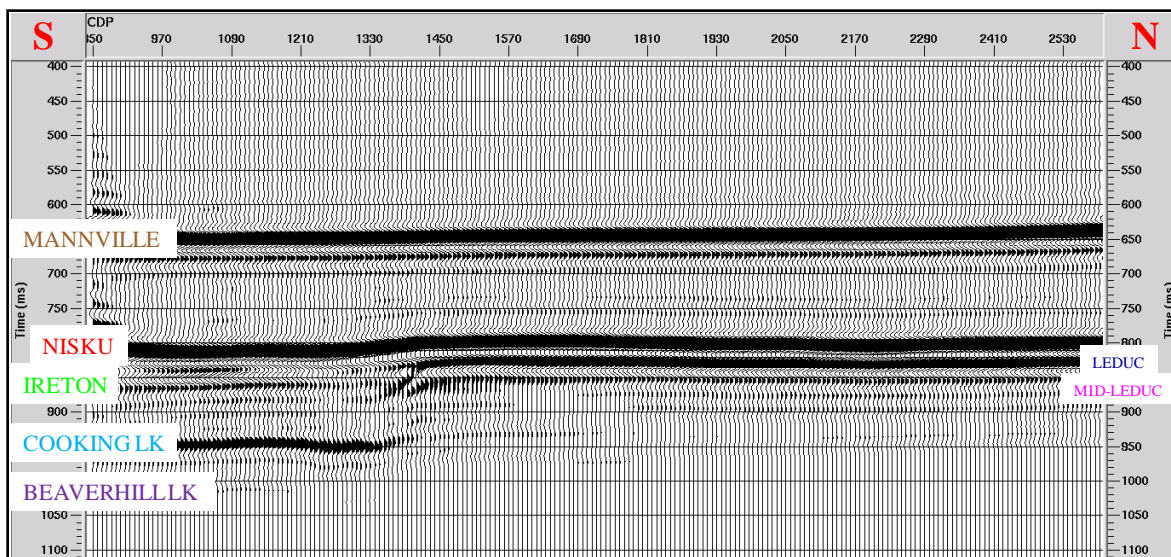


Figure 4.9: 2D ray traced numerical seismic section after pre-stack time migration, Line A.

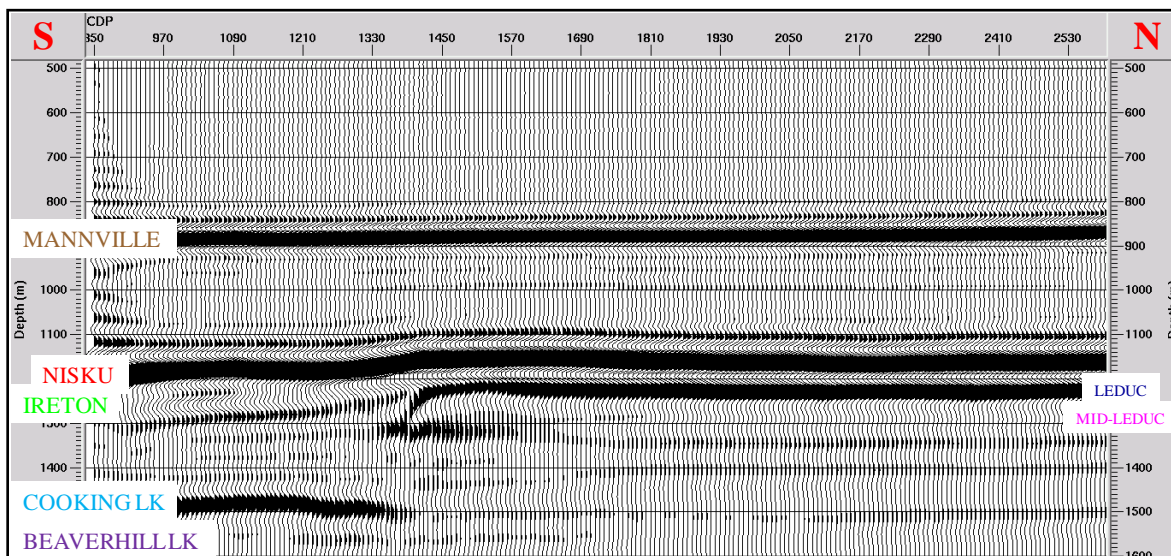


Figure 4.10: 2D ray traced numerical seismic section after pre-stack depth migration, Line A. Note the litho-facies impedance contrast at the base of Upper Leduc as well as thinning at the top of the reef rim.

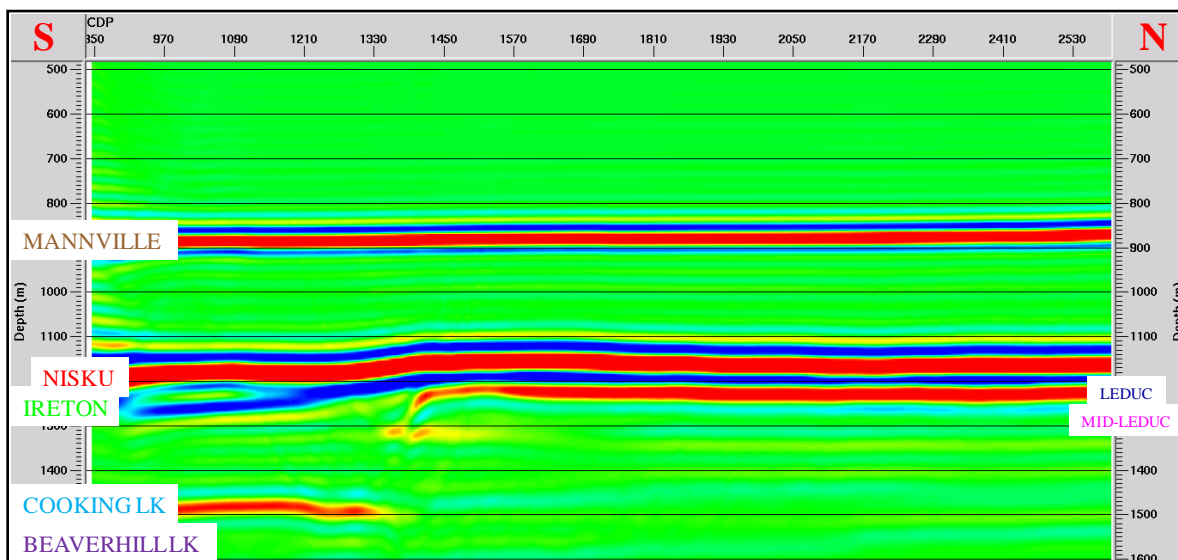


Figure 4.11: Colored pre-stack depth migrated section from Line A, with interfaces identified, showing the litho-facies impedance contrast at the top and base of Upper Leduc as well as thinning across the top of the reef rim.

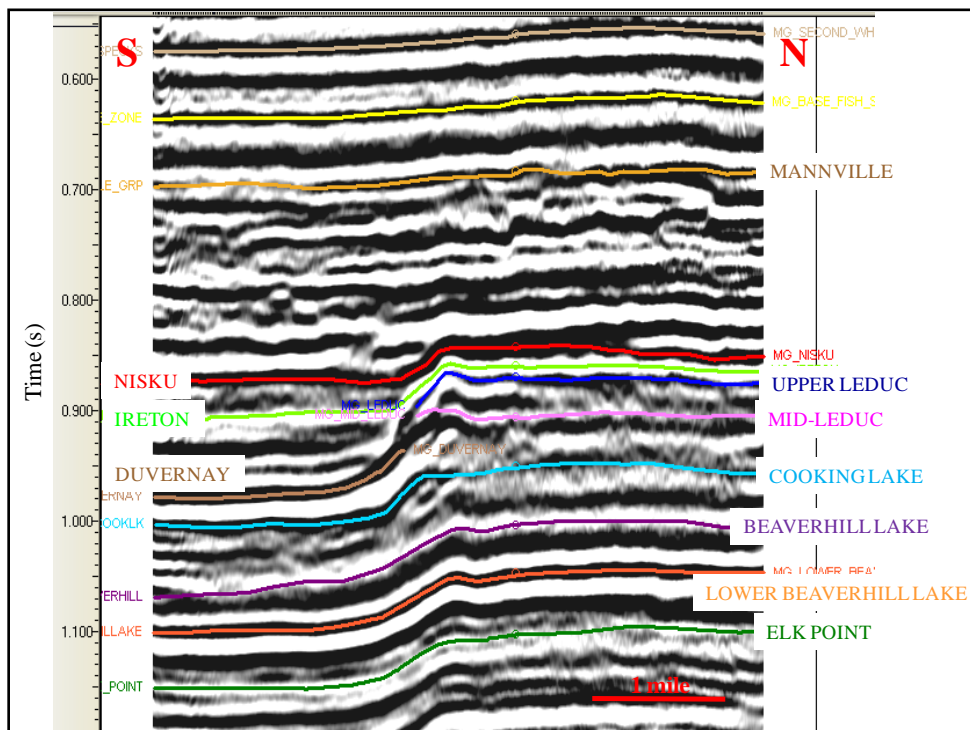


Figure 4.12: Interpreted north-south seismic section near Line A. This line shows the reef edge clearly and the Duvernay event terminating close to the reef margin. It illustrates litho-facies impedance contrast at the top and base of Upper Leduc as well as thinning across the top of the reef rim.

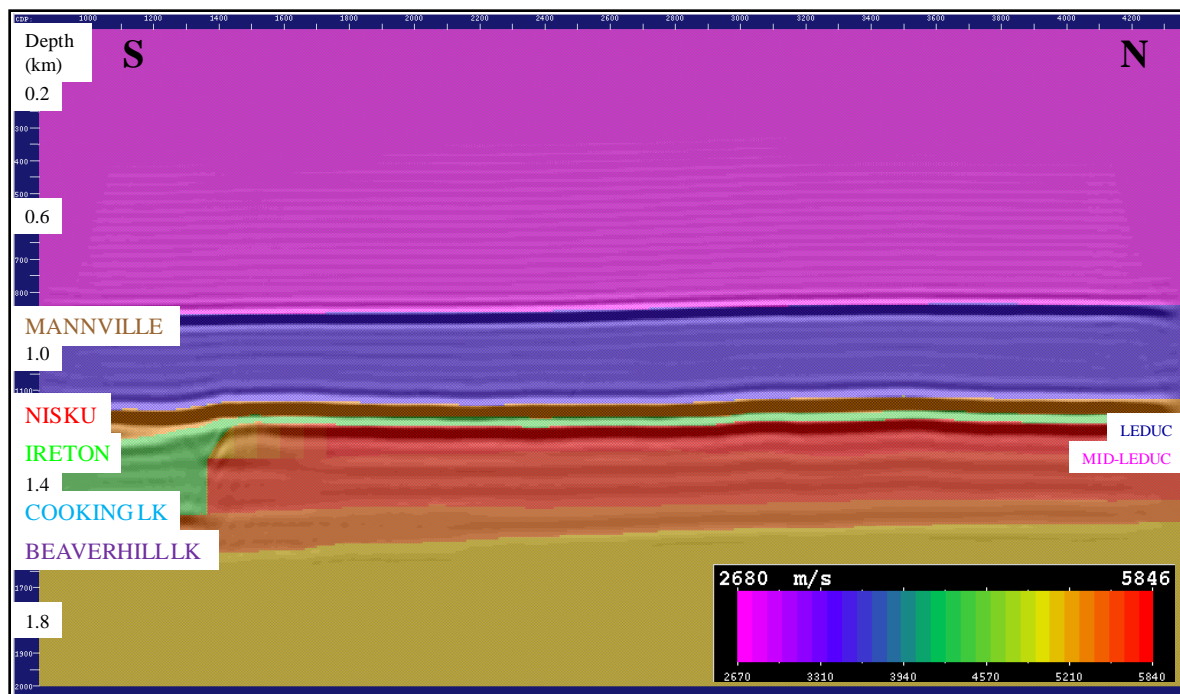


Figure 4.13: Colored velocity model super-imposed on pre-stack depth migration seismic section, Line A.

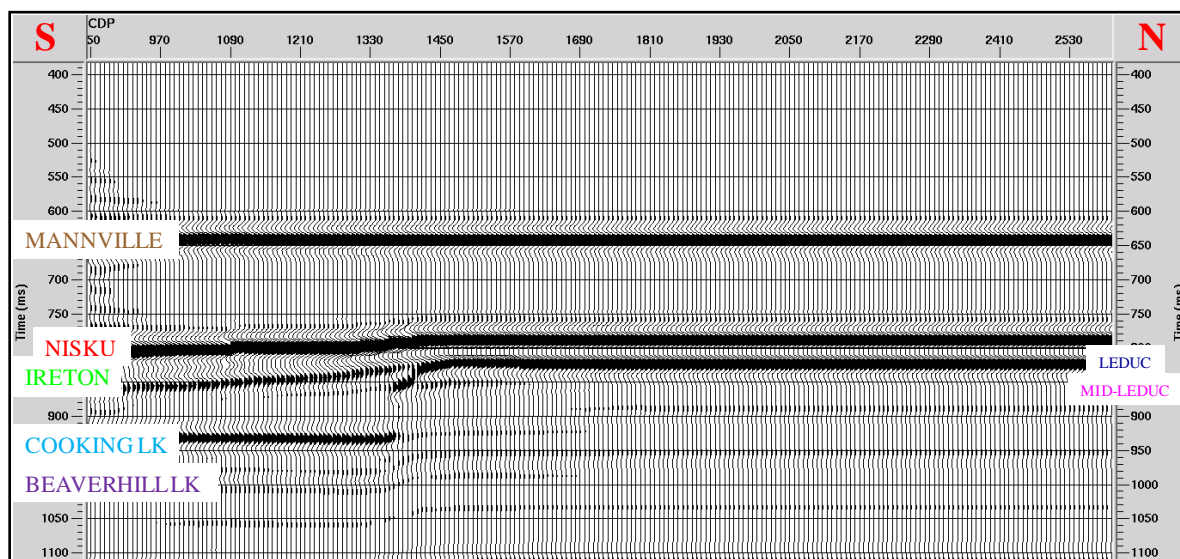


Figure 4.14: 2D finite difference numerical seismic section after pre-stack time migration, Line A, with interfaces identified on the section.

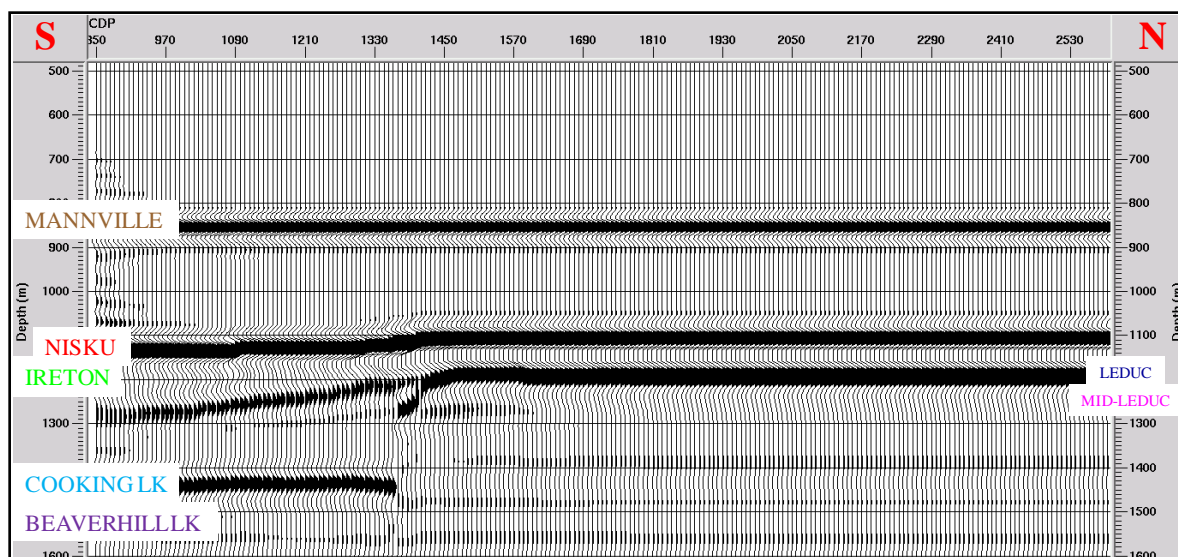


Figure 4.15: 2D finite difference numerical seismic section after pre-stack depth migration, Line A, showing litho-facies impedance contrast at the base of Upper Leduc as well as thinning across the top of the reef rim.

4.3.3 CO₂ Fluid Substitution, Line A

4.3.3.1 CO₂ replacement in the Upper Leduc member

The 2D geological model with CO₂ replacing nature pore water in the Upper-Leduc member is shown in Figure 4.16. Figure 4.17 and Figure 4.18 illustrate the pre-stack time-migrated (PSTM) and depth-migrated (PSDM) seismic sections respectively with 40% CO₂ saturation, based on ray tracing. In these sections, The Mannville, Nisku, Ireton, Cooking Lake, and Beaverhill Lake formations display essentially the same seismic attributes as the baseline seismic sections. The positive time structure below the reef exists in the pre-stack time-migrated data but is corrected in the pre-stack depth-migrated data (Figure 4.18).

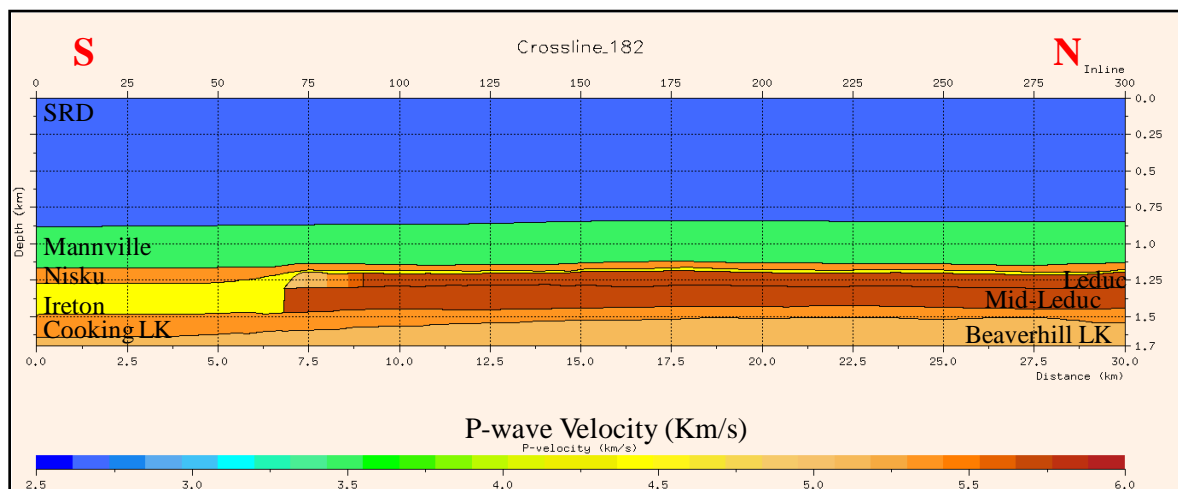


Figure 4.16: 2D geological model with CO₂ fluid substitution in the Upper Leduc member along Line A, across the southern margin of the Redwater reef, showing P-wave interval velocities of the various formations.

Terminations of the Upper-Leduc and Middle-Leduc events are apparent on the 2D synthetic seismic sections with some enhancements on the depth section at the reef margin, and the Upper Leduc event shows the rim build-up (Figure 4.17 and Figure 4.18). Due to the CO₂ saturation, a stronger and higher amplitude reflection at the base of upper-Leduc member is evident near the reef margin compared to the baseline sections. This event becomes weaker toward the interior facies due to the lateral porosity gradient and consequently velocity and density differences between the foreslope facies in the reef rim and lagoonal facies within the central region of the reef.

After 40% CO₂ saturation in the Upper Leduc Formation, the average P-wave interval velocity was found to decrease by about 3.3% and its impedance decreases by 3.6%, yielding a reflectivity difference of about 14%. The two-way travel-time delay through the Upper Leduc Formation following CO₂ substitution is about 1.6 ms. Figure 4.19 and

Figure 4.20 present the pre-stack time-migrated (PSTM) and depth-migrated (PSDM) seismic sections respectively with 40% CO₂ saturation in the Upper Leduc member zone, based on finite difference modeling. All the formations display mainly the same seismic attributes as the sections based on ray tracing. Also, positive time structure is corrected in the depth sections.

Taking the difference between two 2D seismic sections is called time-lapse seismology. In this study, a numerical timelapse study was undertaken to examine the effect of 40% CO₂ saturation on seismic reflectivity and attributes (Lawton and Sodagar, 2009). Figure 4.21 shows the time-lapse seismic section using ray trace numerical modeling and pre-stack depth migration seismic data. This difference section is before and after 40% CO₂ saturation. Notice that there are high amplitude events at the top of Upper-Leduc member, top of the rim, and base of Upper-Leduc near the reef edge as expected. In comparison, Figure 4.22 shows time-lapse seismic section produced using finite difference numerical modeling and PSDM before and after CO₂ saturation. There are small dissimilarities between the time-lapse data using the two approaches to modelling which are thought to be due primarily to the smoothing of the velocity model in the finite difference method. Also, the amplitude events at the top of the rim and base of Upper-Leduc near the reef edge are weaker in the time-lapse finite difference section compared to ray tracing. Figure 4.23 illustrates the velocity model in colour super-imposed on the pre-stack depth migration seismic section with 40% CO₂ saturation in the Upper Leduc. It shows an excellent match between the original model (formation interfaces and velocities, Figure 4.16) and the depth seismic model.

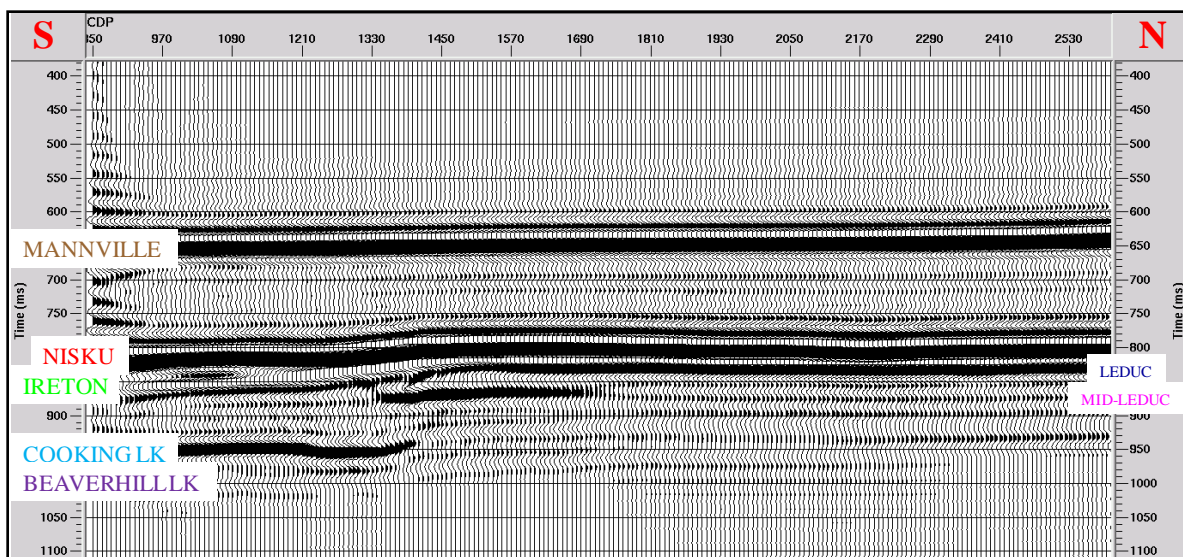


Figure 4.17: 2D ray traced numerical seismic section after CO₂ fluid substitution and PSTM, Line A.

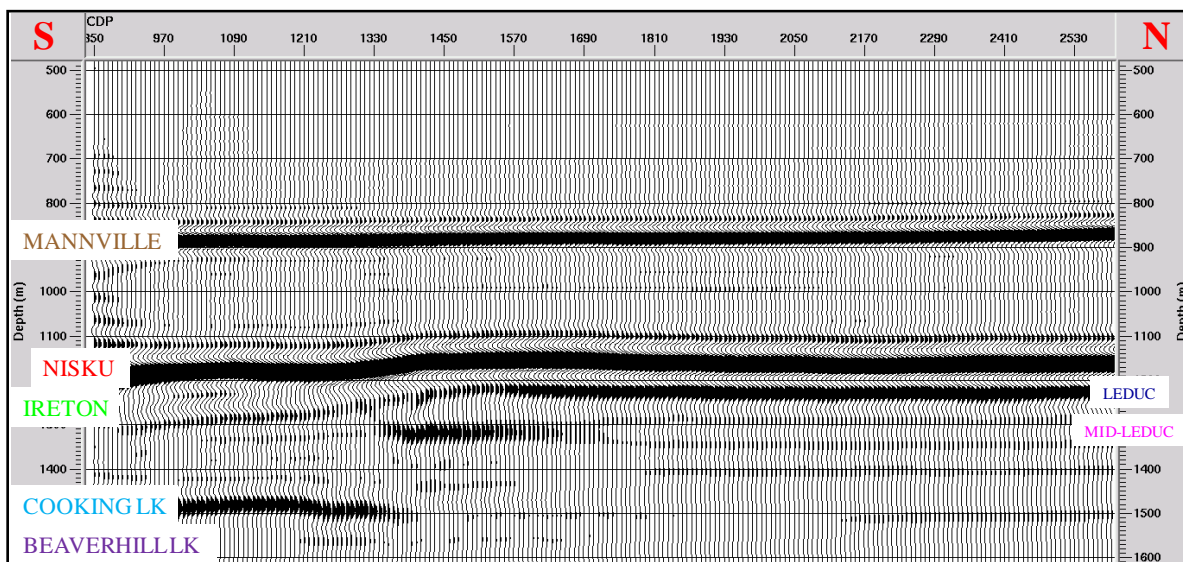


Figure 4.18: 2D ray traced numerical seismic section after CO₂ fluid substitution and PSDM, Line A.

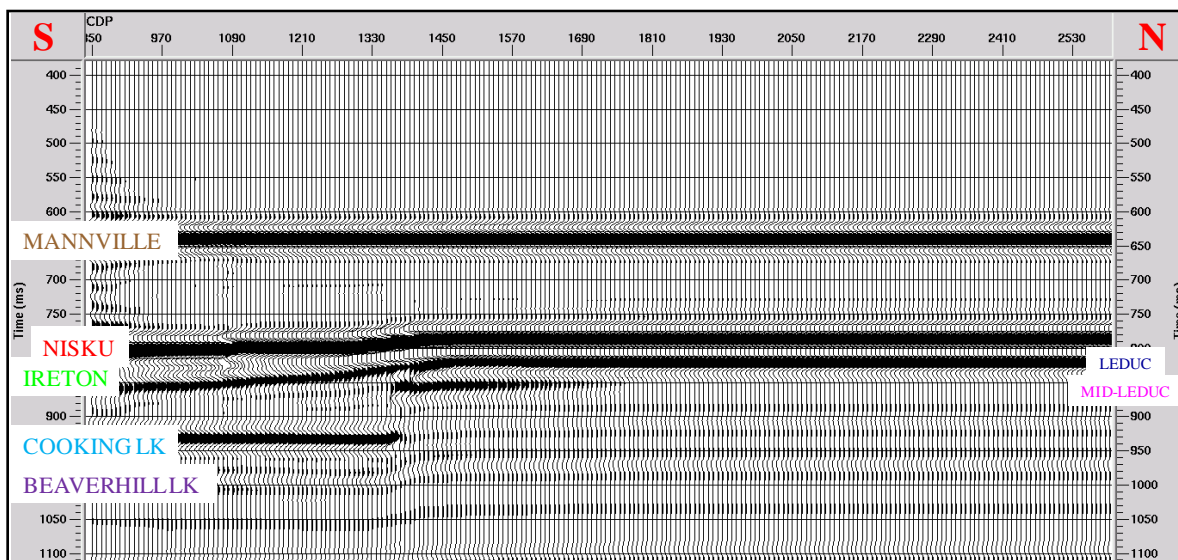


Figure 4.19: 2D finite difference numerical seismic section after CO₂ fluid substitution and PSTM, Line A.

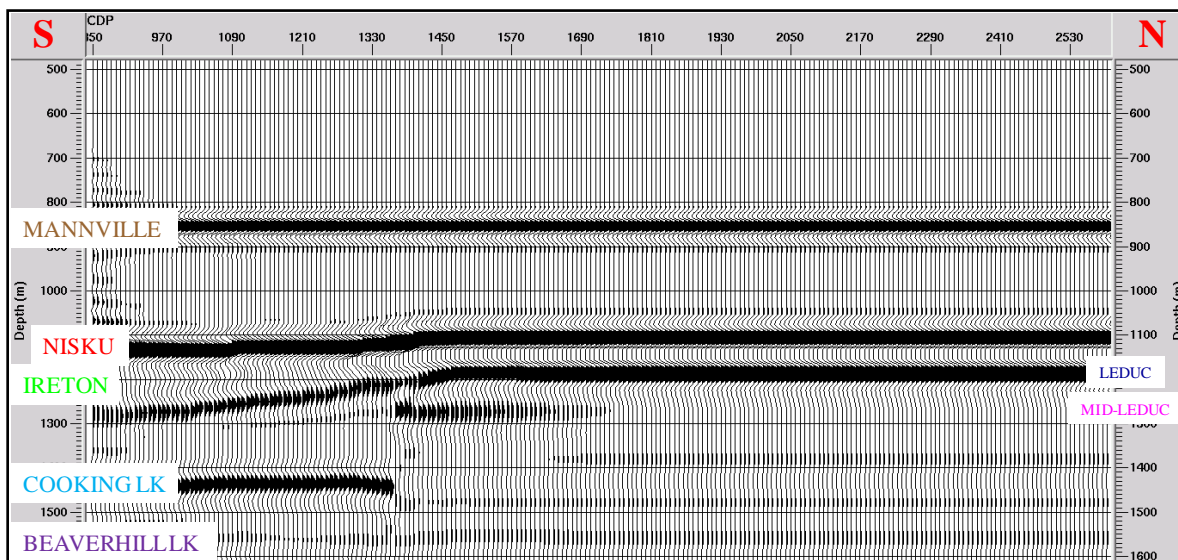


Figure 4.20: 2D finite difference numerical seismic section after CO₂ fluid substitution and PSDM, Line A.

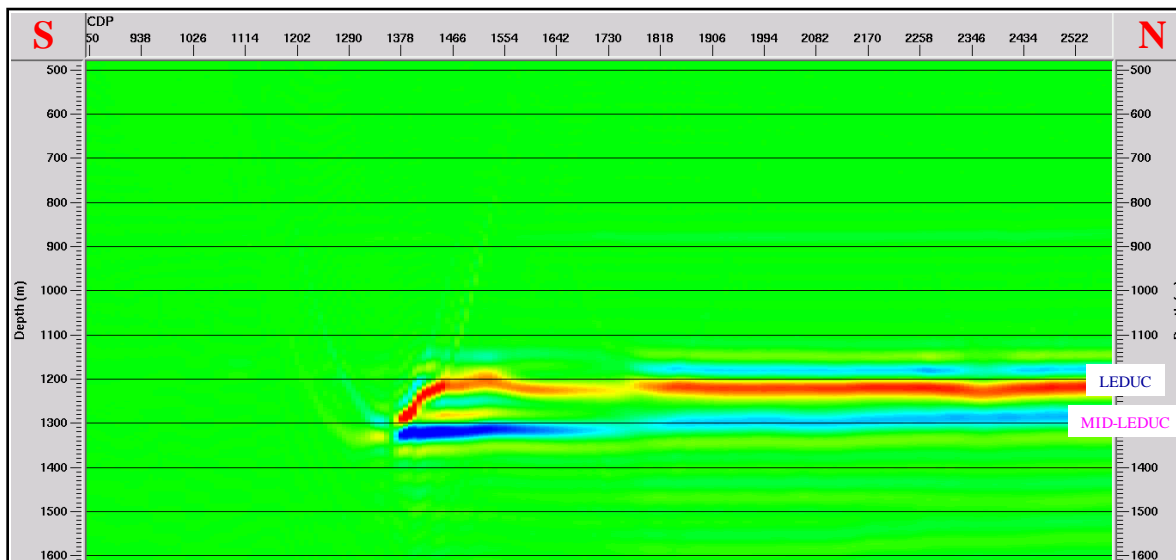


Figure 4.21: Time-lapse difference seismic section before and after CO₂ substitution in the Upper Leduc member, Line A (ray trace modeling and PSDM).

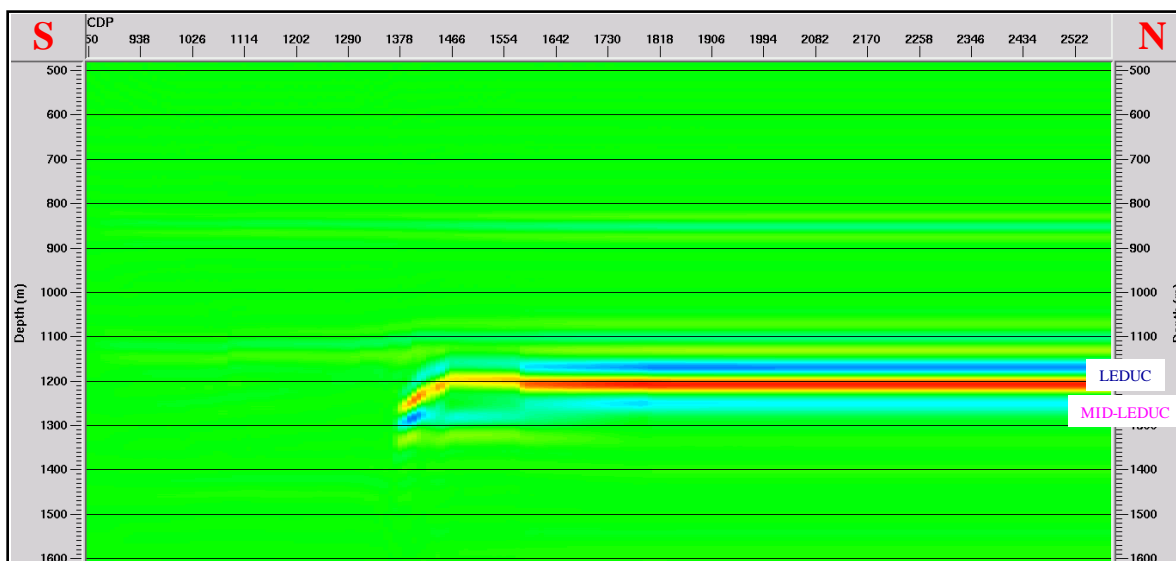


Figure 4.22: Time-lapse difference seismic section before and after CO₂ substitution in the Upper Leduc member, Line A (finite difference modeling and PSDM).

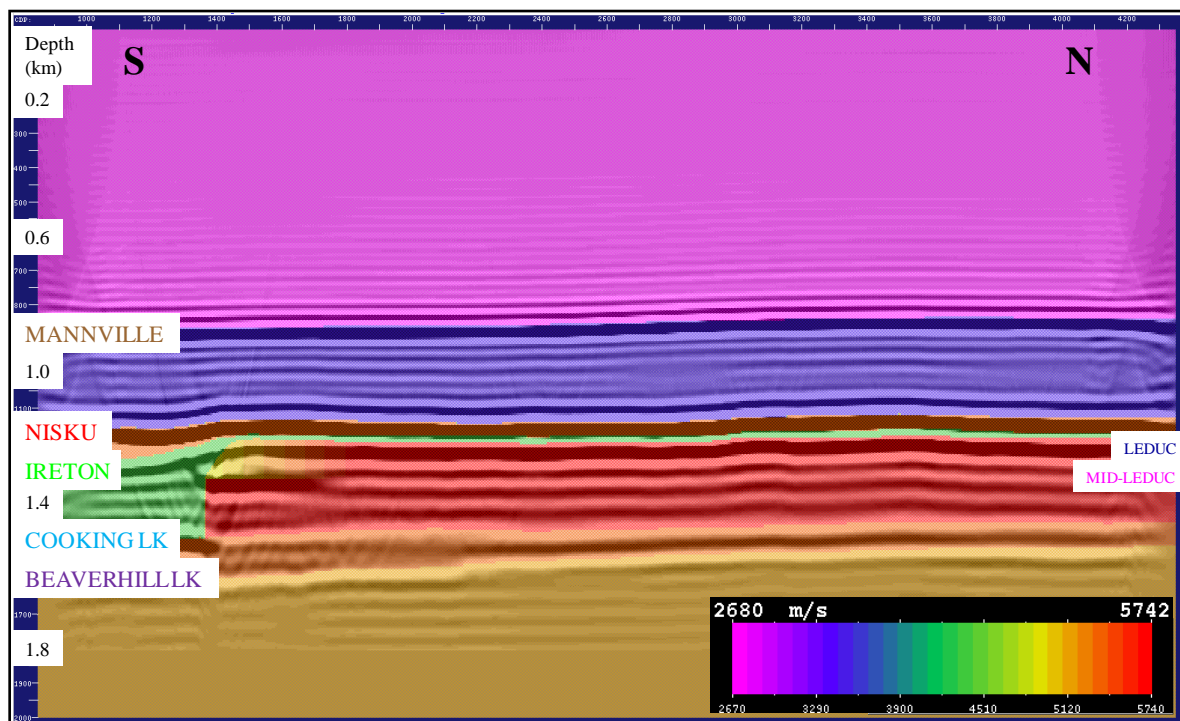


Figure 4.23: Colored velocity model super-imposed on the PSDM seismic section after CO₂ fluid substitution, Line A.

4.3.3.2 CO₂ saturation in the entire Leduc formation

The 2D geological model developed with CO₂ fluid substitution in the entire Leduc Formation displayed in Figure 4.24, showing P-wave interval velocities of the various formations. Figure 4.25 and Figure 4.26 illustrate the PSTM and PSDM seismic sections respectively with 40% CO₂ saturation in the entire Leduc Formation, based on ray trace modeling. In these sections, The Mannville, Nisku, Ireton, Cooking Lake, and Beaverhill Lake formations display essentially the same seismic attributes as the baseline seismic sections. Positive time structure below the reef also exists in the PSTM section but is corrected to almost flat in the PSDM section (Figure 4.26).

Terminations of the Upper-Leduc and Middle-Leduc events are clear on the 2D synthetic seismic sections, with some enhancements on the depth section at the reef margin, and the Upper Leduc event shows the rim build-up (Figure 4.25 and Figure 4.26). A high-amplitude reflection at the base of upper-Leduc member is clear near the reef margin and but this event becomes weaker toward the interior facies because of the porosity differences between the foreslope facies in the reef rim and lagoonal facies within the central region of the reef. Only a very low amplitude reflection at the base of Leduc member is seen compared to in-situ sections, due to CO₂ saturation, which has reduced the impedance contrast between the Leduc and Cooking Lake Formations within the reef (Figure 4.24).

Figure 4.27 and Figure 4.28 present the PSTM and PSDM seismic sections respectively generated using finite difference modeling with 40% CO₂ saturation in the full Leduc Formation. These images display essentially the same seismic attributes as the ray traced modelling sections. Also, positive time structure corrected to nearly flat in the depth section.

Time-lapse analysis was applied to evaluate the effect of CO₂ saturation in the entire Leduc Formation, based on seismic reflectivity and attributes. Figure 4.29 shows the time-lapse seismic section using ray trace numerical modeling for PSDM seismic data before and after 40% CO₂ saturation. It is noticed that there are high amplitude reflections at the top of Upper-Leduc member, top of the rim, base of Upper-Leduc near the reef edge, and base of Leduc (top of Cooking Lake) within the reef as expected. A

time-lapse seismic section was also produced after undertaking finite difference modeling for PSDM seismic data before and after CO₂ saturation (Figure 4.30). Small differences between the two time-lapse sections are due to the smoothing of the velocity model in the finite difference method. In addition, the amplitude events at the top of the rim, base of Upper-Leduc near the reef edge and the top of Cooking Lake Formation below the reef are weaker in the time-lapse finite difference seismic section compared to the time-lapse ray tracing section.

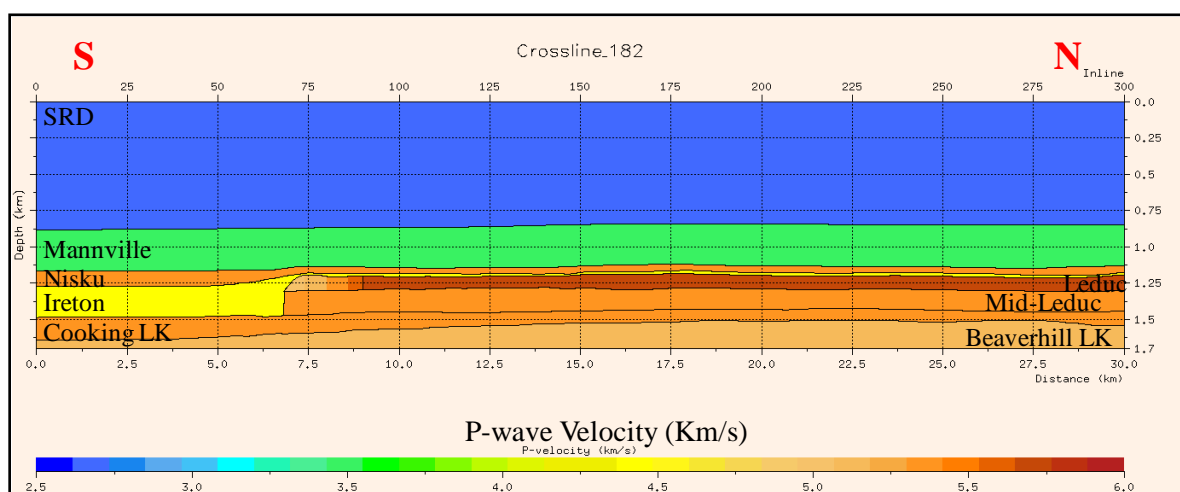


Figure 4.24: 2D geological model with CO₂ fluid substitution in the entire Leduc Formation along Line A, across the southern margin of the Redwater reef, showing P-wave interval velocities of the various formations.

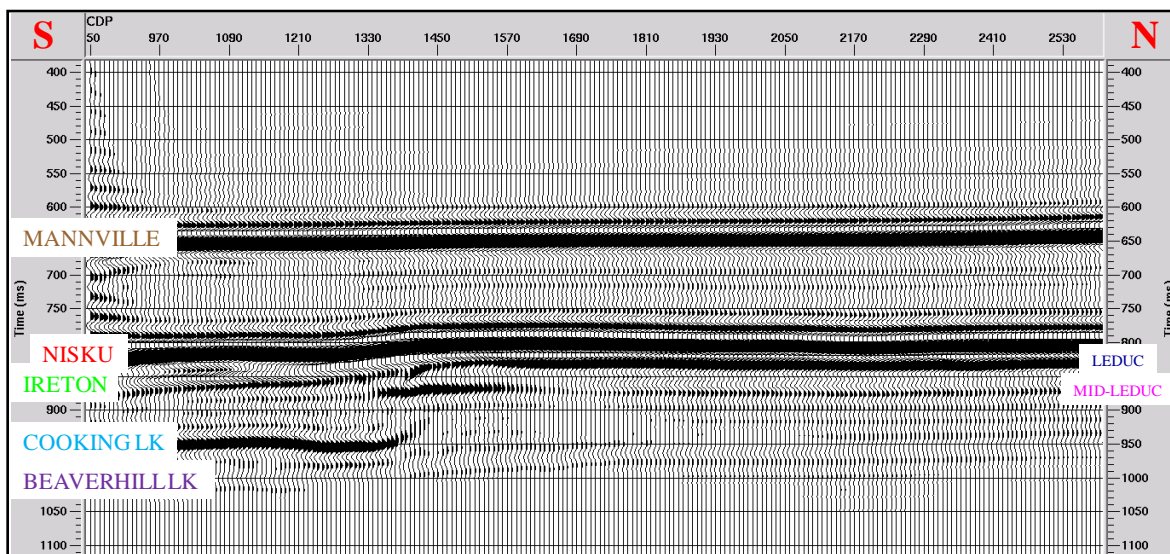


Figure 4.25: 2D ray traced numerical seismic section after CO₂ fluid substitution in the entire Leduc Formation and PSTM, Line A.

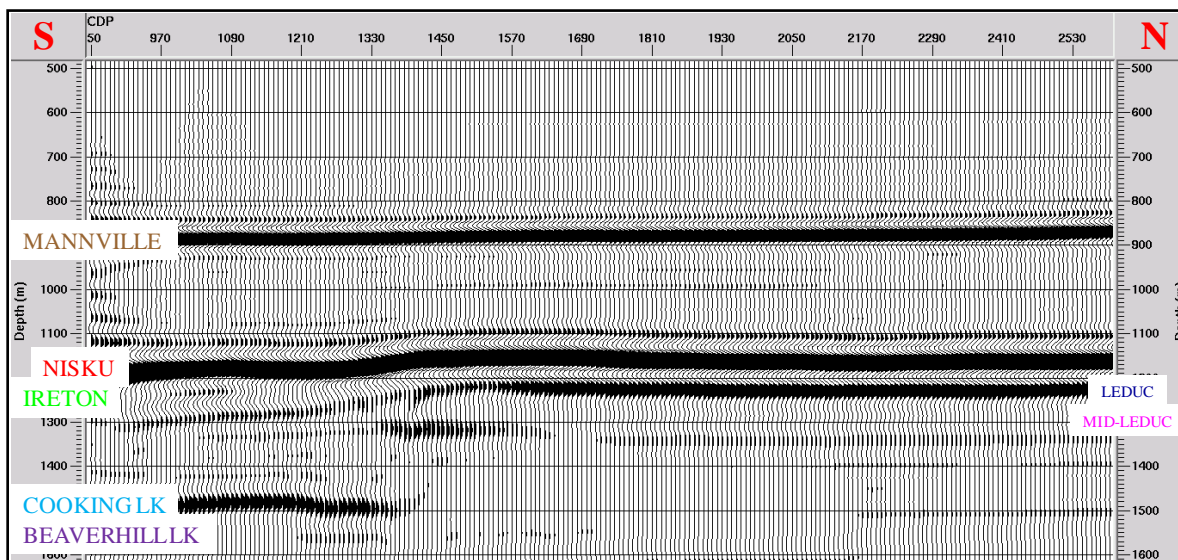


Figure 4.26: 2D ray traced numerical seismic section after CO₂ fluid substitution in the entire Leduc Formation and PSDM, Line A.

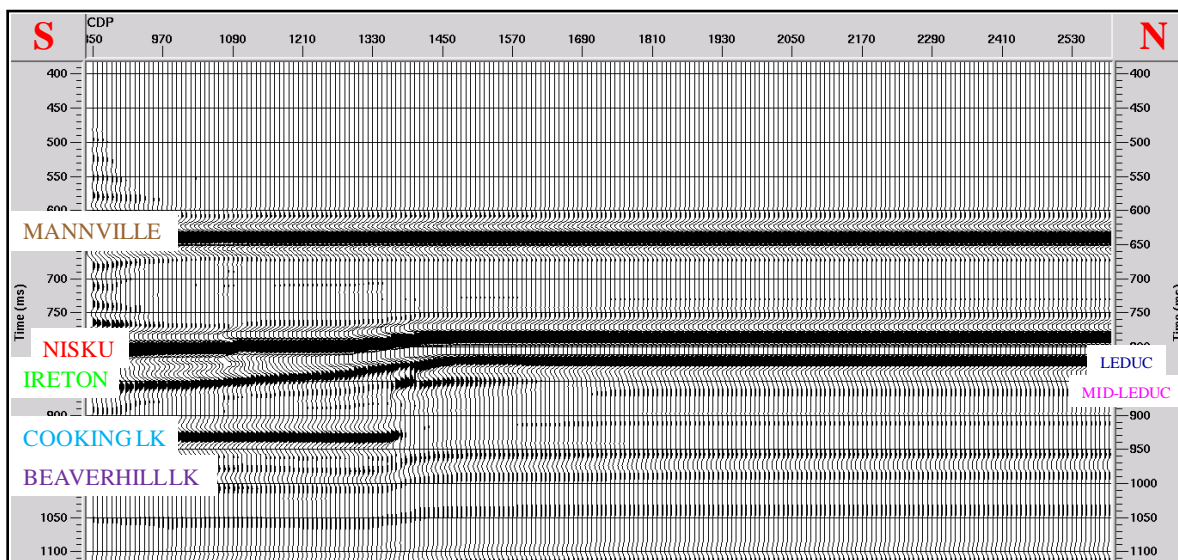


Figure 4.27: 2D finite difference numerical seismic section after CO₂ fluid substitution in the entire Leduc Formation and PSTM, Line A.

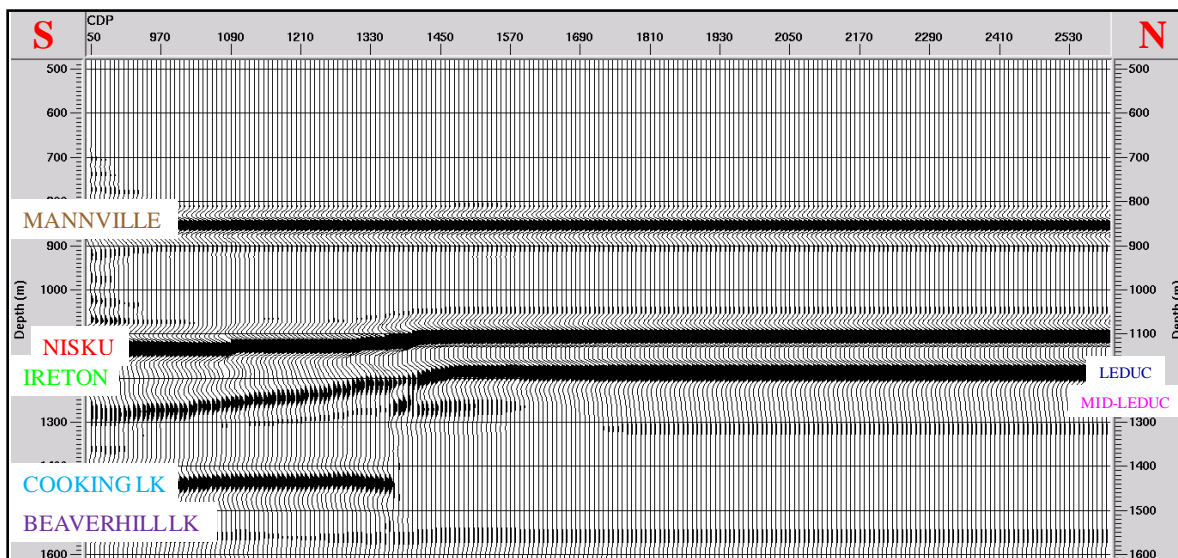


Figure 4.28: 2D finite difference numerical seismic section after CO₂ fluid substitution in the entire Leduc Formation and PSDM, Line A.

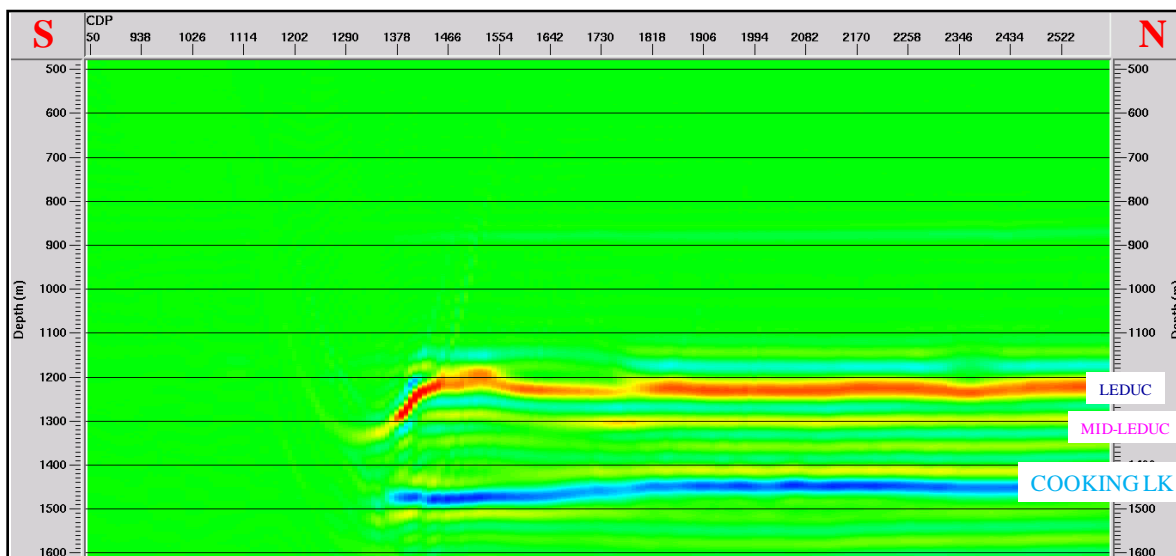


Figure 4.29: Time-lapse difference seismic section before and after CO₂ substitution in the entire Leduc Formation, Line A (ray trace modeling and PSDM).

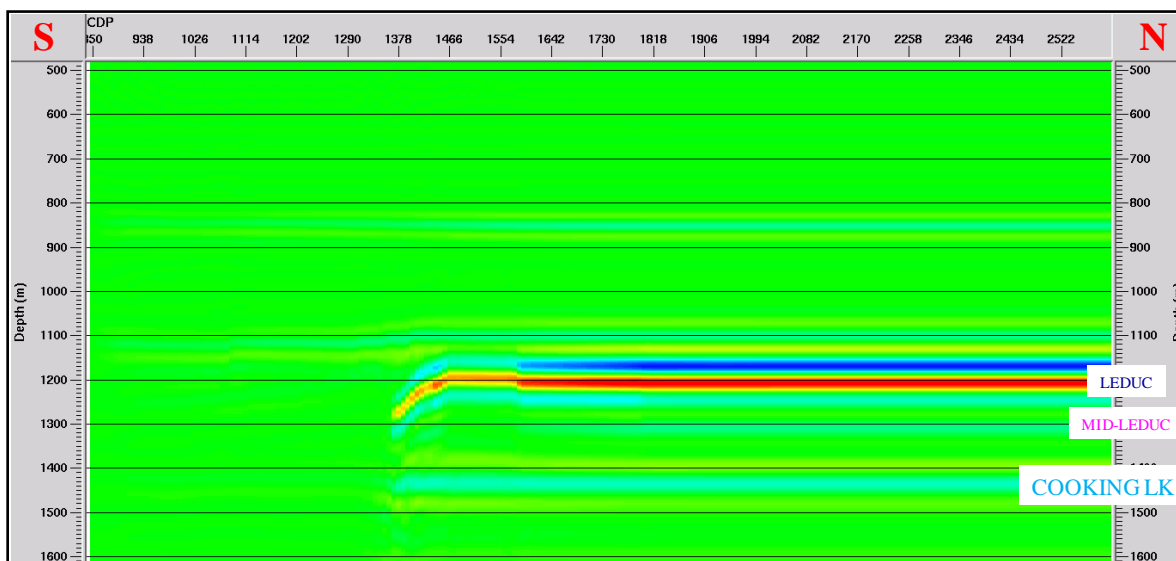


Figure 4.30: Time-lapse difference seismic section before and after CO₂ substitution in the entire Leduc Formation, Line A (finite difference modeling and PSDM).

4.3.3.3 CO₂ saturation in the Leduc rim target zone only

The 2D geological model was refined with CO₂ fluid substitution only in the rim of the Leduc member, as shown in Figure 4.31. Figure 4.32 and Figure 4.33 illustrate the PSTM and PSDM seismic sections respectively, with 40% CO₂ saturation in the Leduc rim zone interval, based on the ray tracing method. In these sections, The Mannville, Nisku, Ireton, Cooking Lake, and Beaverhill Lake formations display essentially the same seismic attributes as the baseline seismic sections. Positive time structure below the reef still exists in the pre-stack time-migrated data but is corrected in the pre-stack depth-migrated data (Figure 4.33).

Terminations of the Upper-Leduc and Middle-Leduc events are noticeable on the 2D synthetic seismic sections with some enhancements on the depth section at the reef margin, and the Upper Leduc event shows the rim build-up (Figure 4.32 and Figure 4.33). A higher amplitude reflection at the base of the Upper-Leduc member is evident near the reef margin, compared to the baseline sections, due to CO₂ saturation, and this event becomes weaker toward the interior facies. This is because of the porosity differences and resulting impedance differences between the foreslope facies in the reef rim and lagoonal facies within the central region of the reef.

Figure 4.34 and Figure 4.35 present the PSTM and PSDM seismic sections respectively, with 40% CO₂ saturation in the Leduc rim zone only, based on finite difference modeling. All the formations display basically the same seismic attributes as the ray

trace modelling sections. Also, positive time structure corrected to nearly flat in the pre-stack depth-migrated section.

Figure 4.36 shows the time-lapse seismic section, based on ray trace modeling, for PSDM seismic data before and after 40% CO₂ saturation (Lawton and Sodagar, 2009). There are high amplitude reflections at the top of Upper-Leduc member, top of the rim, and base of upper-Leduc near the reef edge as predicted. A comparative time-lapse seismic section was also produced using finite difference numerical modeling before and after CO₂ saturation (Figure 4.37). Few differences between the two time-lapse sections using both methods of modelling are due to mainly the smoothing of the velocity model in the finite difference approach. Also, the amplitude events at the top of the rim and base of Upper-Leduc near the reef edge are weaker in the time-lapse finite difference section compared to ray tracing section.

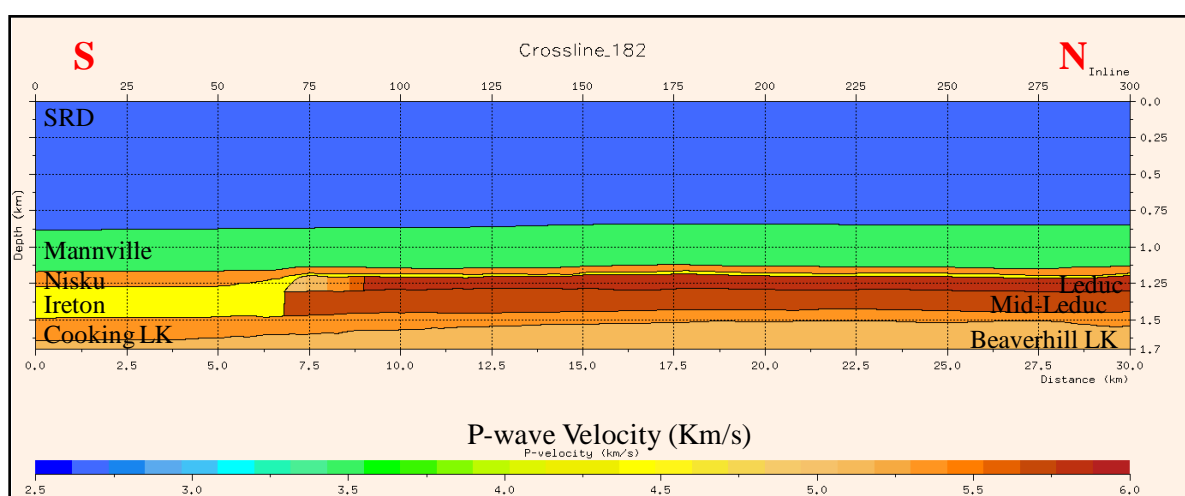


Figure 4.31: 2D geological model with CO₂ fluid substitution in the rim of Upper Leduc member along Line A, across the southern margin of the Redwater reef, showing P-wave interval velocities of the various formations.

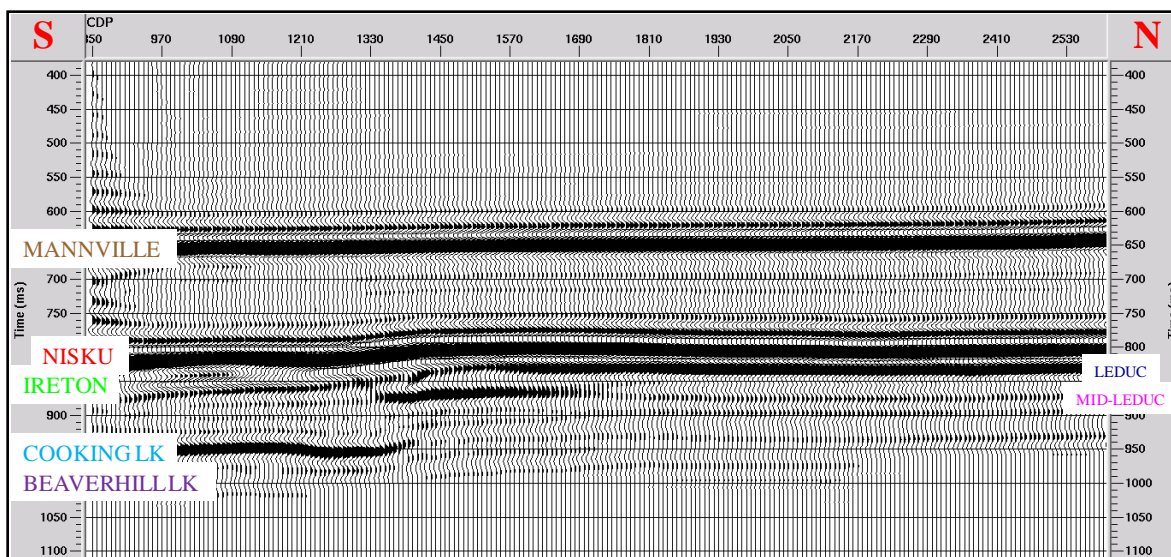


Figure 4.32: 2D ray traced numerical seismic section after CO₂ fluid substitution in the rim of Upper Leduc member and PSTM, Line A.

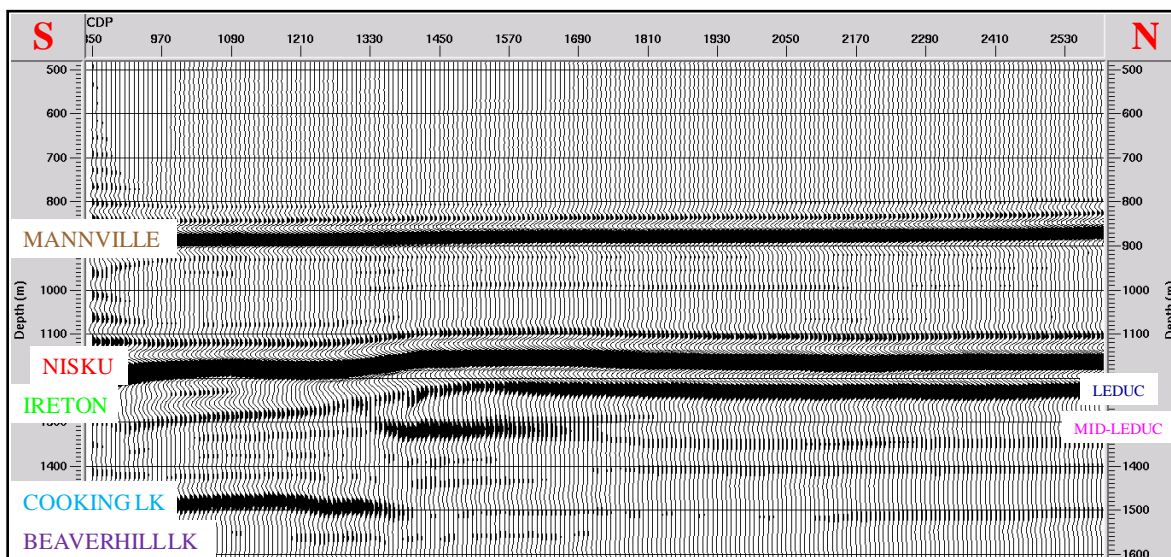


Figure 4.33: 2D ray traced numerical seismic section after CO₂ fluid substitution in the rim of Upper Leduc member and PSDM, Line A.

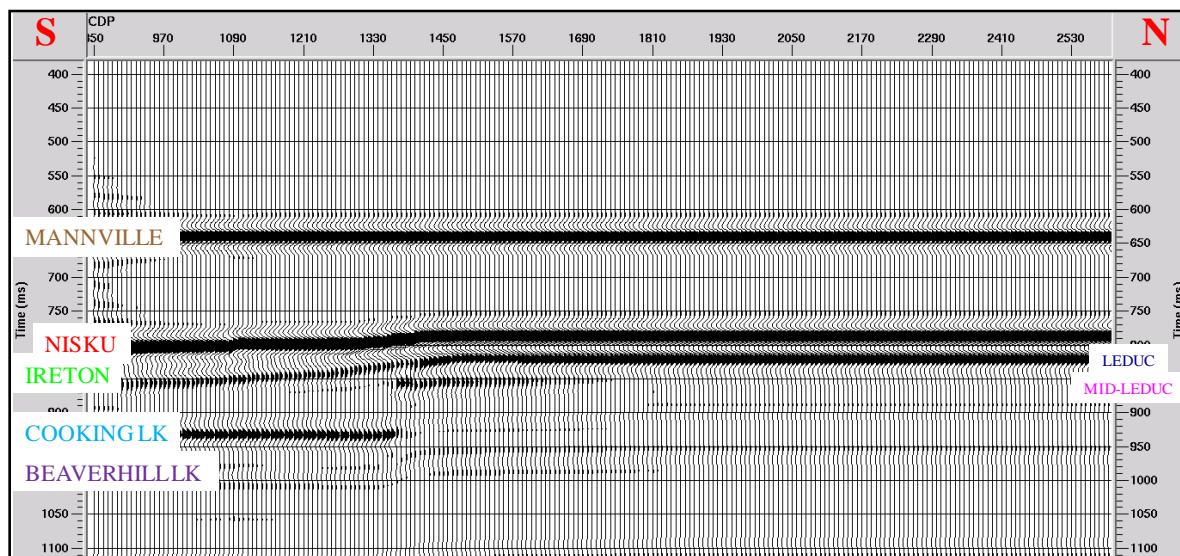


Figure 4.34: 2D finite difference numerical seismic section after CO₂ fluid substitution in the rim of Upper Leduc member and PSTM, Line A.

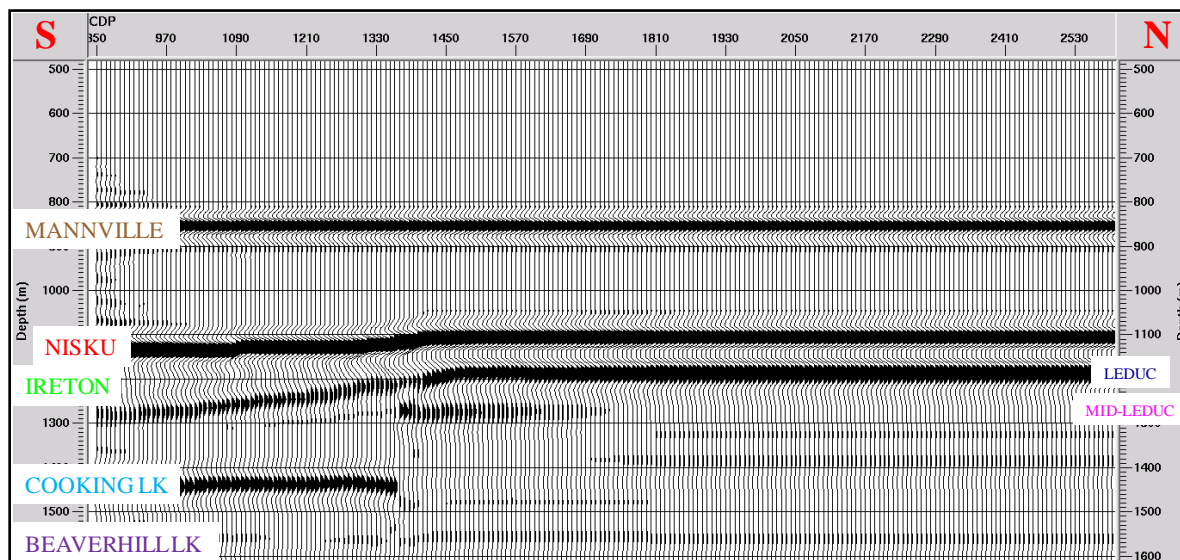


Figure 4.35: 2D finite difference numerical seismic section after CO₂ fluid substitution in the rim of Upper Leduc member and PSDM, Line A.

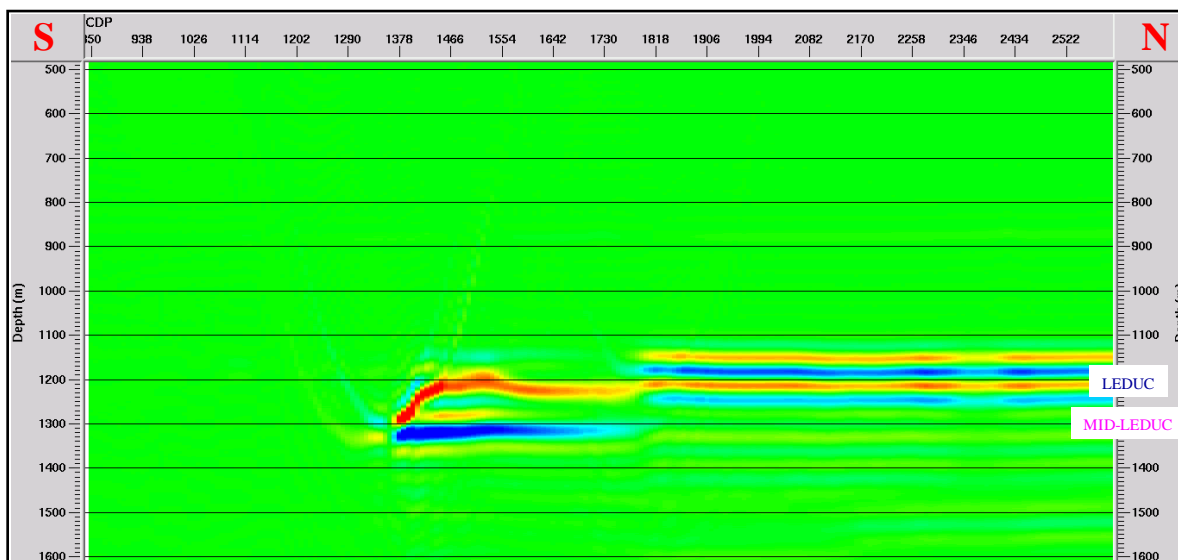


Figure 4.36: Time-lapse difference seismic section before and after CO₂ substitution in the rim target zone, Line A (ray trace modeling and PSDM).

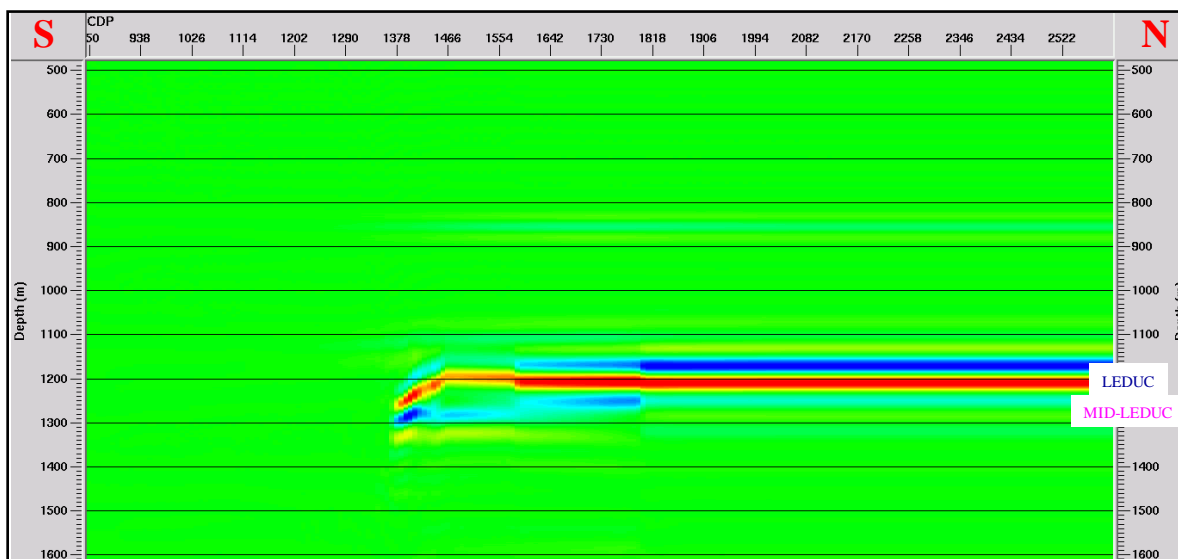


Figure 4.37: Time-lapse difference seismic section before and after CO₂ substitution in the rim target zone, Line A (finite difference modeling and PSDM).

4.4 Results – Line B

4.4.1 East-west Model including Duvernay Embayment

This section (Line B) is oriented in east-west direction and extends from the lagoonal facies within the central region of the reef to off-reef (Figure 4.1). The difference with Line A is that Line B has a Duvernay Formation shale embayment at the Mid-Leduc member level. The 2D geological model developed is shown in Figure 4.38. Interfaces in depth were transformed to event blocks and then P-wave velocities and densities were assigned to these blocks using average values from wells. These properties of the model are shown in Figure 4.39 and Figure 4.40. The reef rim region was modelled as a separate block. In this block, the velocity and density values had a lateral gradient associated with an average porosity of 4% in the tidal flat lagoonal facies to an average porosity 9% in the foreslope facies at the rim of the reef (Figure 4.38 through Figure 4.40). The Duvernay shale embayments were modeled by invasion of shales inside the reef in the Middle and Lower Leduc members. Beside the embayment, there is a transition block of 500 m with a lateral gradient of velocity and density values from the shale to inner reef facies (Figure 4.38 through Figure 4.40). In the Leduc Formation, original pore fluid (100% water) was replaced homogeneously by 40% CO₂ saturation (Sodagar and Lawton, 2009) in the Upper Leduc member. The P-wave velocities and densities after fluid saturation were recalculated using Gassmann equation (Gassmann, 1951).

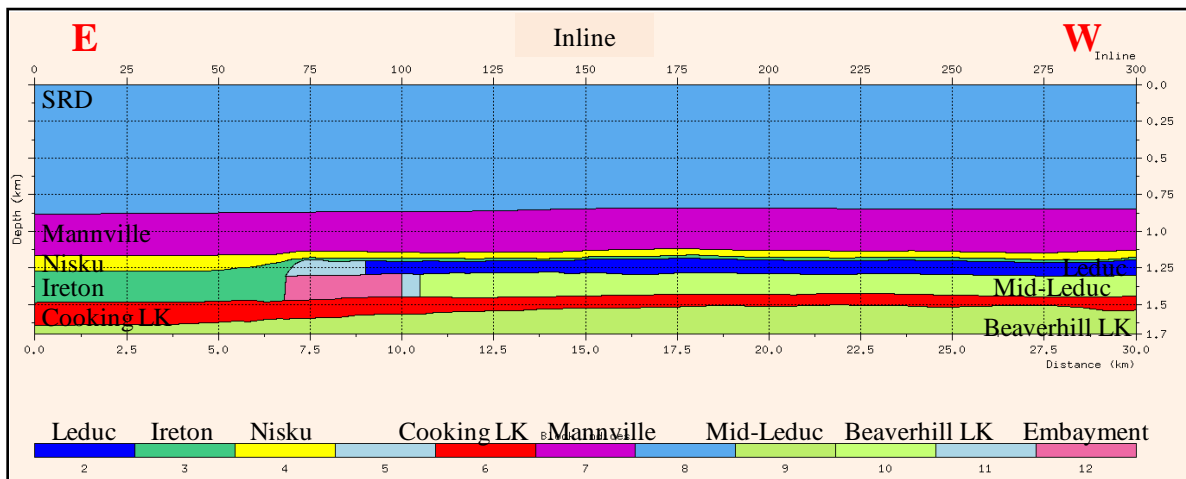


Figure 4.38: 2D geological model along Line B, where crosses the eastern margin of the Redwater reef, showing the formations included in the model.

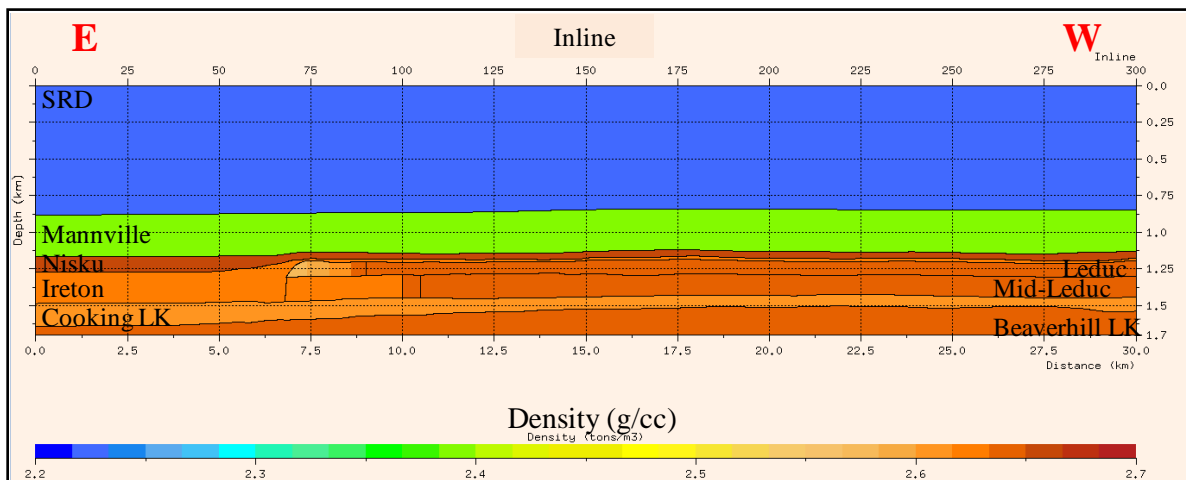


Figure 4.39: Density values of the 2D model along Line B.

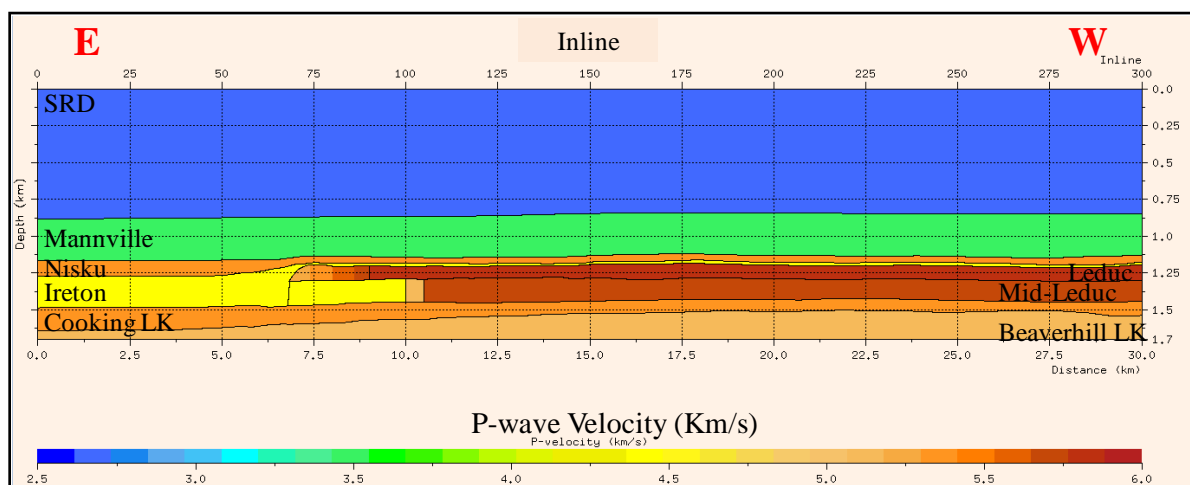


Figure 4.40: P-wave velocities of the 2D model along Line B.

Figure 4.41 and Figure 4.42 illustrate the pre-stack time-migrated and depth-migrated seismic sections respectively, using ray trace modeling. In the time section, the Mannville event is a strong peak, the Nisku event is also a moderate amplitude peak, the Ireton shale event is a trough and the Cooking Lake Formation correlates to a moderate amplitude trough in the central region of the reef but has higher amplitude peak off-reef and on-reef below the Duvernay embayment. This is because the Cooking Lake carbonates, when overlain by Ireton or Duvernay shale, yield a large impedance contrast and a high-amplitude reflection. The Beaverhill Lake event is a fairly weak trough due to the small impedance contrast at the interface between the Cooking Lake and Beaverhill Lake carbonate units.

Reflections from the Cooking Lake and Beaverhill Lake formations exhibit positive time structure below the reef at the time section with less pull-up below the shale embayments. This velocity pull-up is due to a lateral velocity change from the on-reef carbonate strata

(Leduc Formation) to the adjacent, lower velocity off-reef shale strata (Ireton Formation). Both formations are essentially flat in the depth model (Figure 4.38 through Figure 4.40).

Terminations of the Upper Leduc and Middle Leduc events are clear on the 2D synthetic seismic sections at the reef margin, and the Upper Leduc event shows the rim build-up. A moderate to high amplitude reflection at the base of upper-Leduc member is evident near the reef margin and it continuous across the embayment but weakens toward the interior facies (Figure 4.43). This is because of the porosity differences and consequently velocity and density differences between the foreslope facies in the reef rim and lagoonal facies within the central region of the reef and the shale embayments. It is noteworthy that this event on the modeled seismic data is similar to that observed on the processed field data where an embayment is interpreted (Figure 4.44), and thus may be a direct indicator of the embayment. Figure 4.45 displays the velocity model super-imposed on the pre-stack depth migration seismic section, showing the match between the velocity model and the seismic depth image.

Figure 4.46 and Figure 4.47 present the pre-stack time-migrated and depth-migrated seismic sections respectively using finite difference modeling. All the formations display basically the same seismic attributes as the ray tracing modeling sections. Also, positive time structure corrected to nearly flat in the pre-stack depth-migrated data.

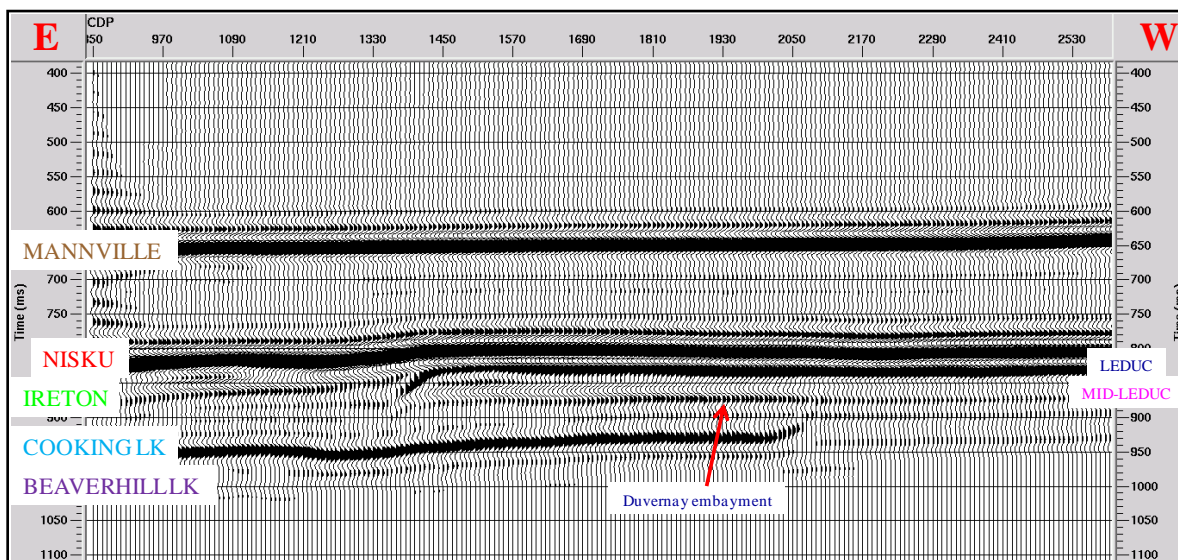


Figure 4.41: 2D ray traced numerical seismic section after pre-stack time migration, Line B. Arrow shows Duvernay embayment event encroaching into the reef.

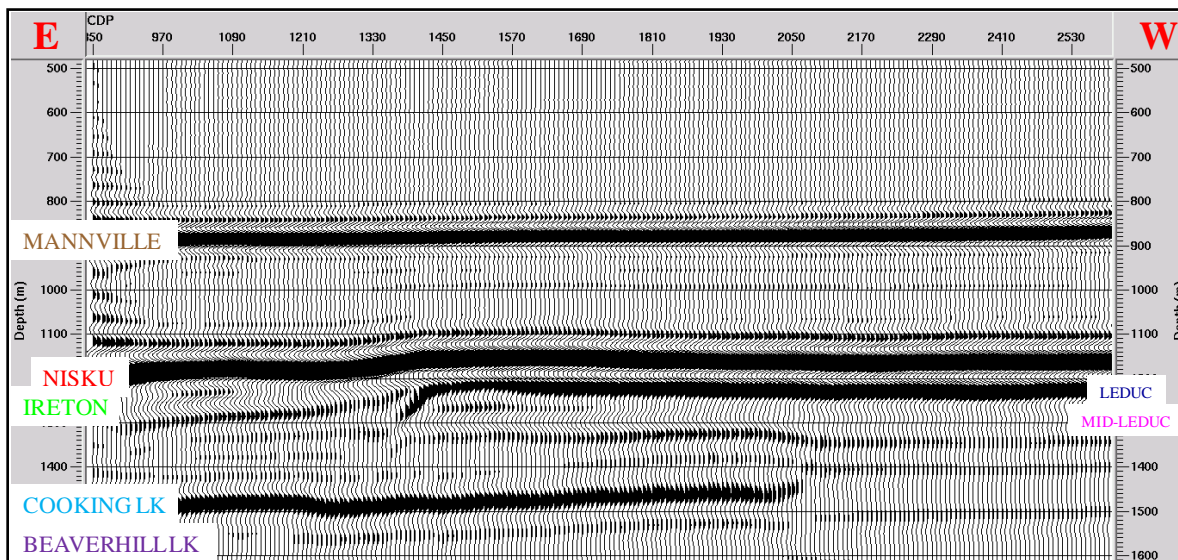


Figure 4.42: 2D ray traced numerical seismic section after pre-stack depth migration, Line B. Note the litho-facies impedance contrast at the base of Upper Leduc and Duvernay invasion as well as thinning at the top of the reef rim.

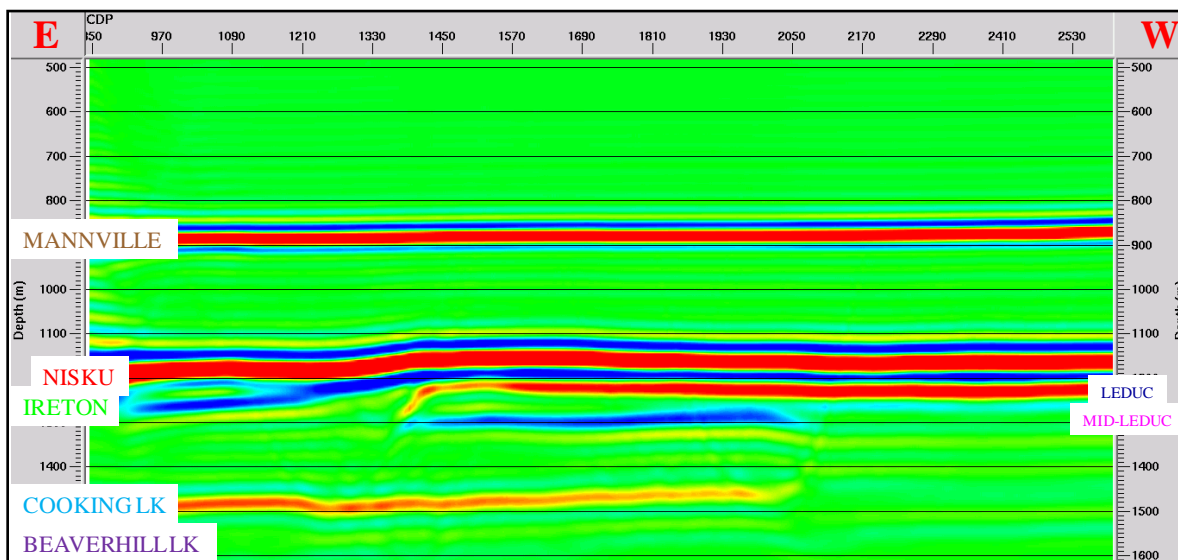


Figure 4.43: Colored pre-stack depth migrated section from Line B, showing the litho-facies impedance contrast at the top, base of Upper Leduc and Duvernay invasion as well as thinning across the top of the reef rim.

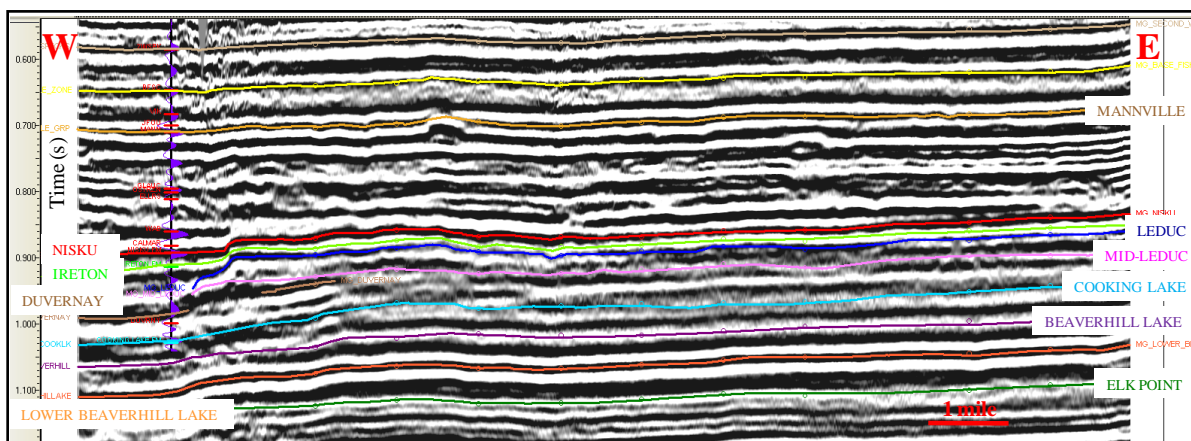


Figure 4.44: Interpreted west-east seismic section near Line B. This line shows the reef edge clearly and a limited Duvernay embayment event encroaching into the reef buildup from the west. Tie with well 11-24 is shown.

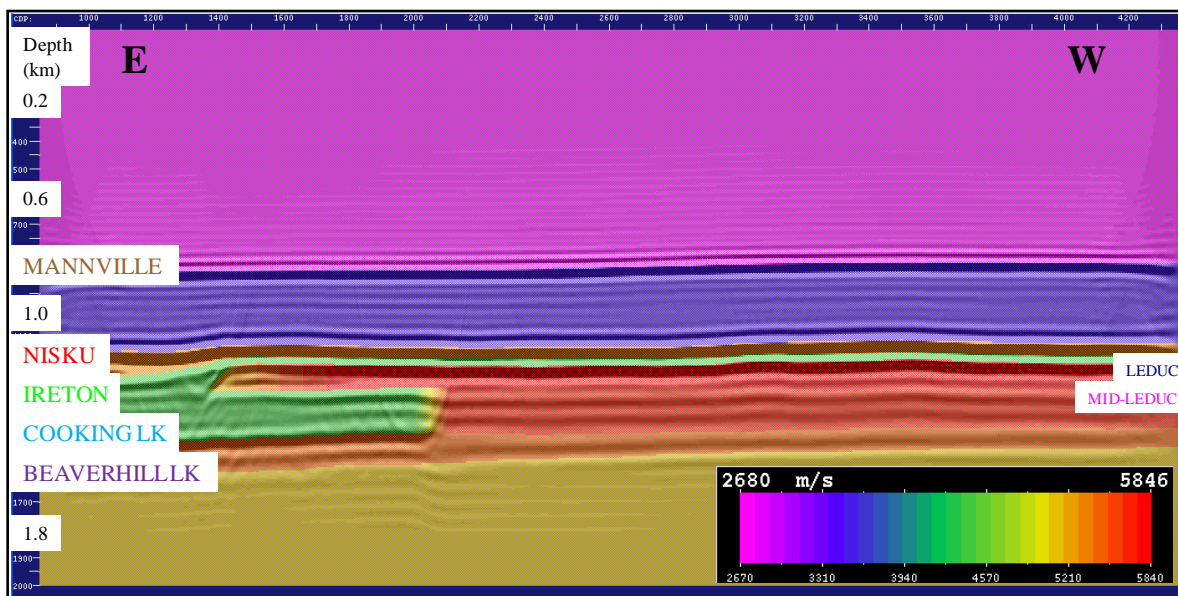


Figure 4.45: Colored velocity model super-imposed on pre-stack depth migration seismic section, Line B.

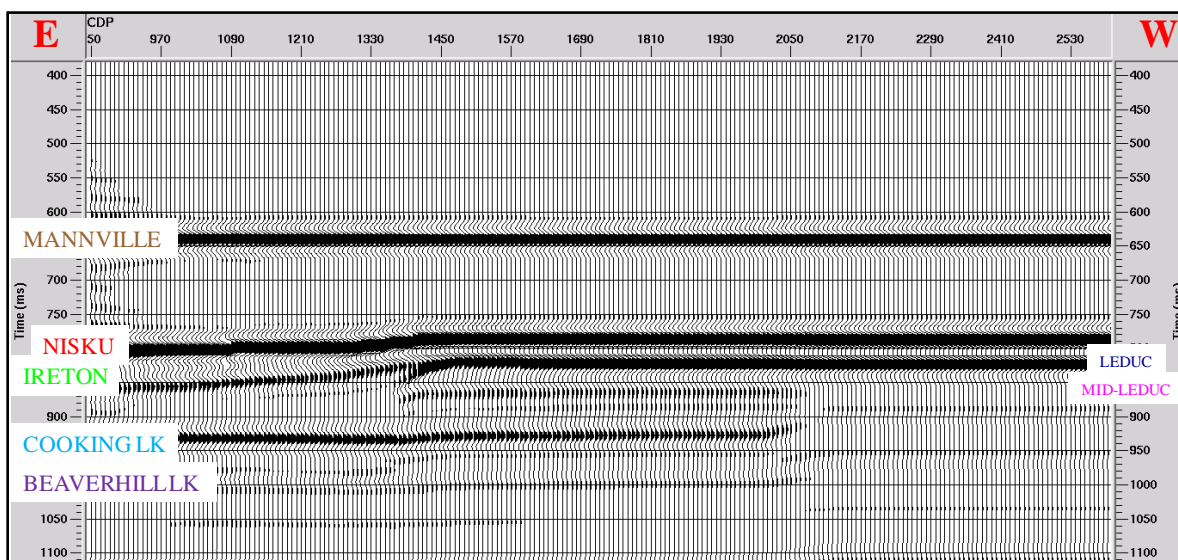


Figure 4.46: 2D finite difference numerical seismic section after pre-stack time migration, Line B, with interfaces identified on the section.

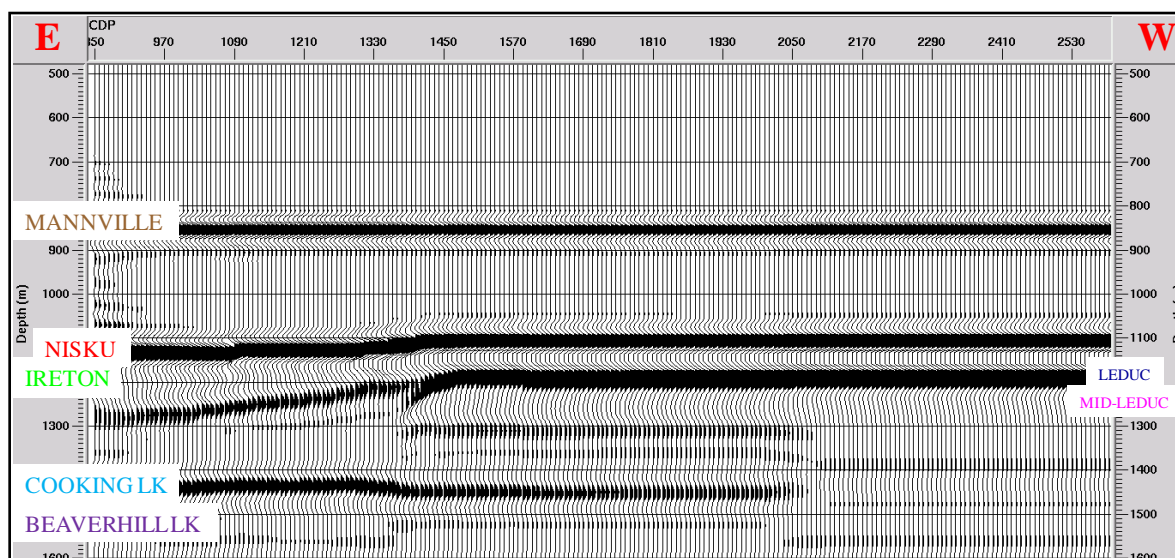


Figure 4.47: 2D finite difference numerical seismic section after pre-stack depth migration, Line B, showing the Duvernay embayment event encroaching into the reef buildup.

4.4.2 East-west Geological Model after CO₂ Fluid Replacement

The 2D geological model including embayment with CO₂ replacing natural pore water in the Upper-Leduc member is shown in Figure 4.48 including P-wave interval velocities. Figure 4.49 and Figure 4.50 illustrate the pre-stack time-migrated (PSTM) and depth-migrated (PSDM) seismic sections respectively with 40% CO₂ saturation in the Upper-Leduc member interval, based on ray tracing. In these sections, The Mannville, Nisku, Ireton, Cooking Lake, and Beaverhill Lake formations display essentially the same seismic attributes and characterizations as the baseline seismic sections. Positive time structure below the reef exists in the pre-stack time-migrated data but is corrected in the pre-stack depth-migrated data (Figure 4.50).

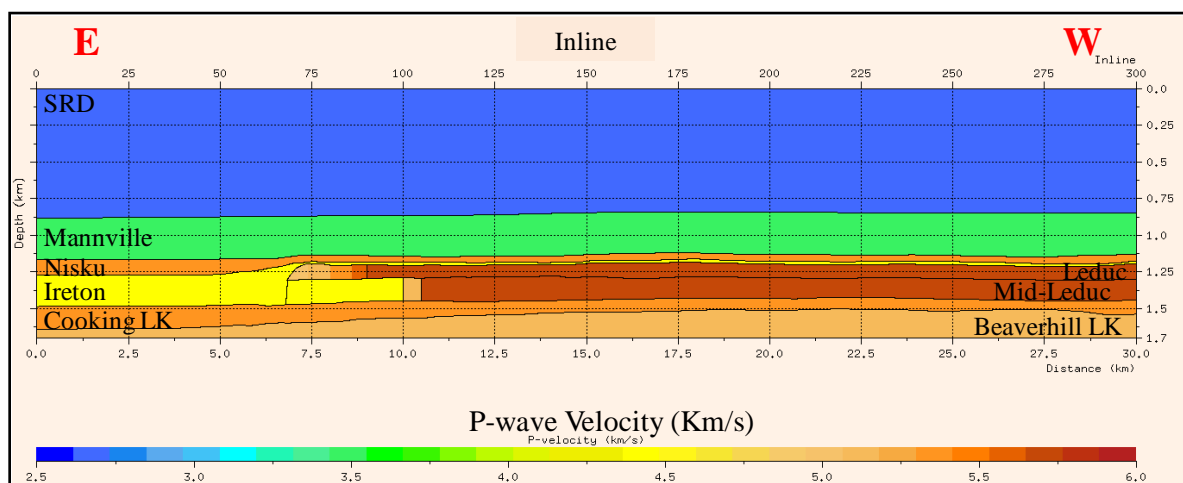


Figure 4.48: 2D geological model with CO₂ fluid substitution in the Upper Leduc member along Line B, across the eastern margin of the Redwater reef, showing P-wave interval velocities of the various formations.

Terminations of the Upper-Leduc and Middle-Leduc events are apparent on the 2D synthetic seismic sections with some enhancements on the depth section at the reef margin, and the Upper Leduc event shows the rim build-up (Figure 4.49 and Figure 4.50). Due to CO₂ replacement, a low to moderate amplitude reflection at the base of upper-Leduc member is apparent close to the reef margin and gets improved toward the embayment invasion trimmings. This event becomes even weaker toward the interior facies compared to baseline sections as a result of CO₂ saturation. This is because of the lateral porosity gradient and consequently velocity and density differences between the foreslope facies in the reef rim and lagoonal facies within the central region of the reef and the Duvernay shale embayments.

Figure 4.51 and Figure 4.52 demonstrate the pre-stack time-migrated (PSTM) and depth-migrated (PSDM) seismic sections respectively with 40% CO₂ saturation in the Upper

Leduc member zone, based on finite difference modeling. All the formations display basically the same seismic attributes as the sections based on ray tracing. Also, positive time structure is corrected in the depth sections.

Time-lapse analysis was applied to examine the effect of 40% CO₂ saturation on seismic reflectivity and attributes (Lawton and Sodagar, 2009). Figure 4.53 shows the time-lapse seismic section using ray trace numerical modeling and PSDM seismic data. This difference section is before and after 40% CO₂ saturation. It is noticed that there are high amplitude reflection at the top of upper-Leduc member, top of the rim, and base of upper-Leduc near the reef edge where gets improved toward the embayment invasion ends as expected. In comparison, Figure 4.54 shows time-lapse seismic section produced using finite difference modeling and PSDM seismic data before and after CO₂ saturation. There are few differences between the time-lapse sections because of the smoothing of the velocity model in the finite difference method. The amplitude events at the base of Upper-Leduc near the reef edge, the top of Cooking Lake Formation and Duvernay embayment below the reef are weaker in the time-lapse finite difference seismic section compared to the time-lapse ray tracing section. Figure 4.55 illustrates the velocity model in colour super-imposed on the PSDM seismic section with 40% CO₂ saturation in the Upper Leduc. It shows a very good match between the original model (formation interfaces and velocities, Figure 4.48) and the depth seismic image.

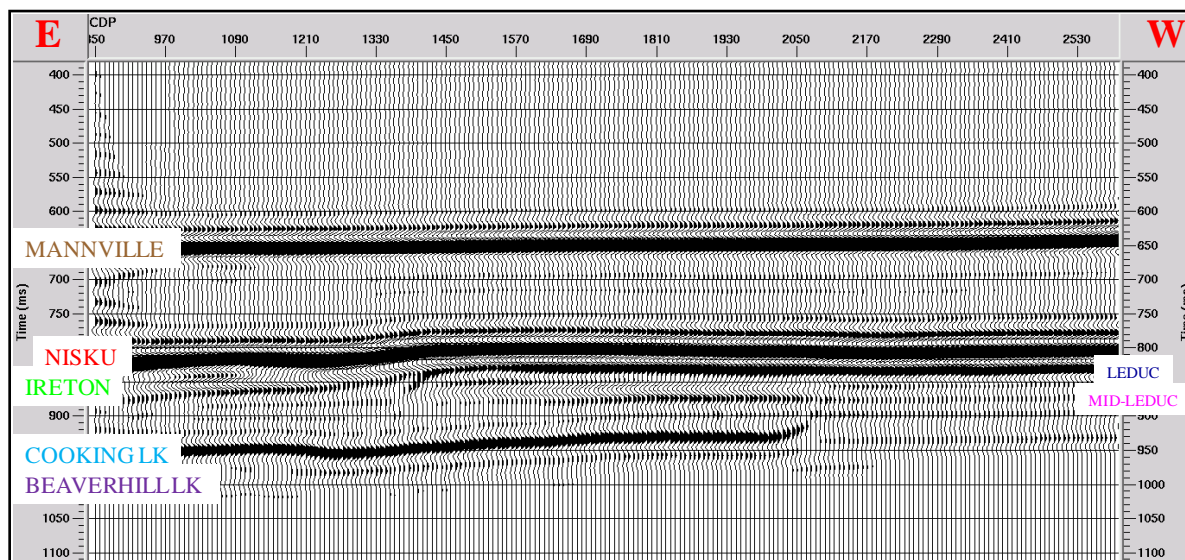


Figure 4.49: 2D ray traced numerical seismic section after CO₂ fluid substitution and PSTM, Line B.

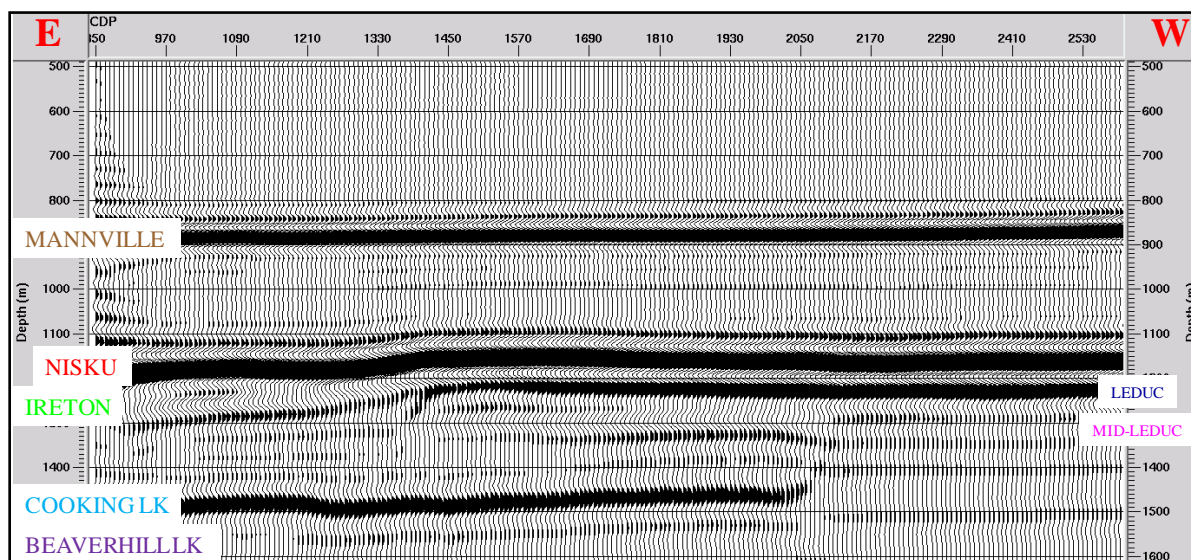


Figure 4.50: 2D ray traced numerical seismic section after CO₂ fluid substitution and PSDM, Line B.

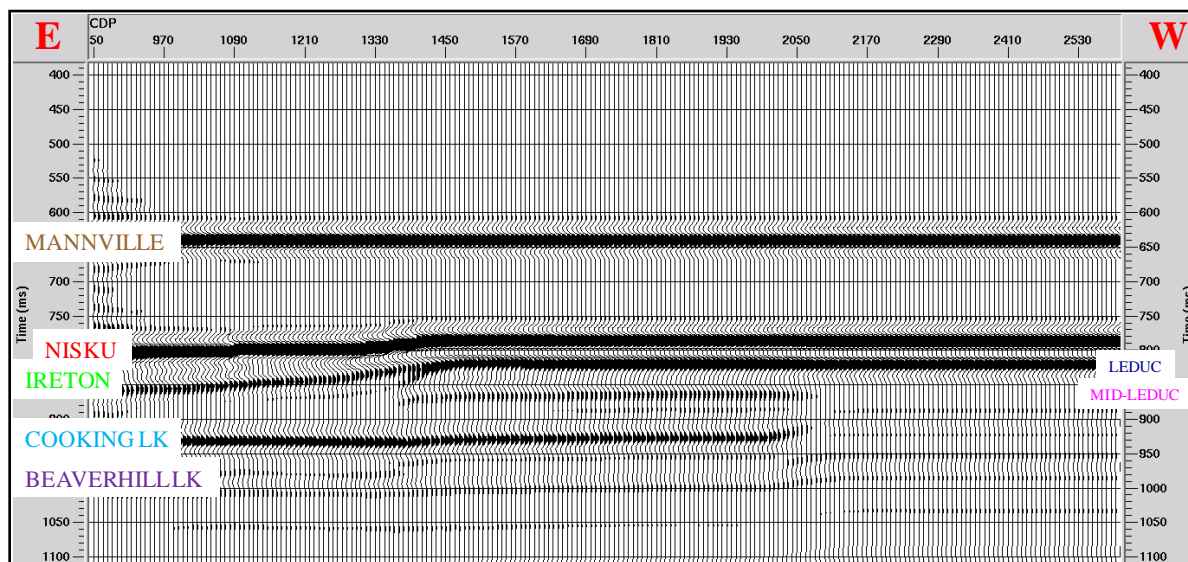


Figure 4.51: 2D finite difference numerical seismic section after CO₂ fluid substitution and PSTM, Line B.

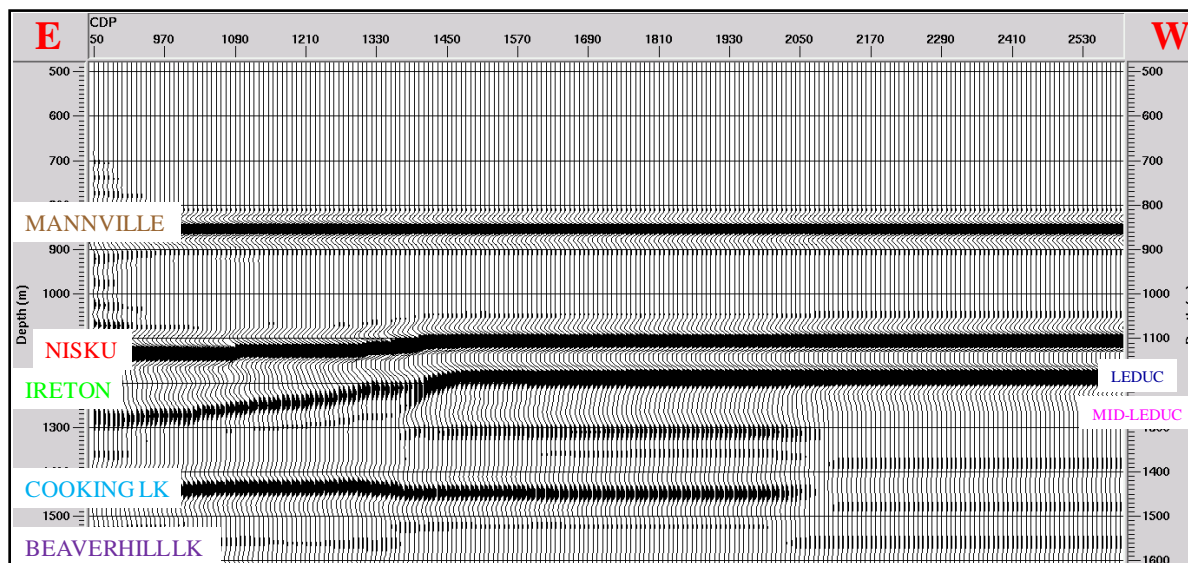


Figure 4.52: 2D finite difference numerical seismic section after CO₂ fluid substitution and PSDM, Line B.

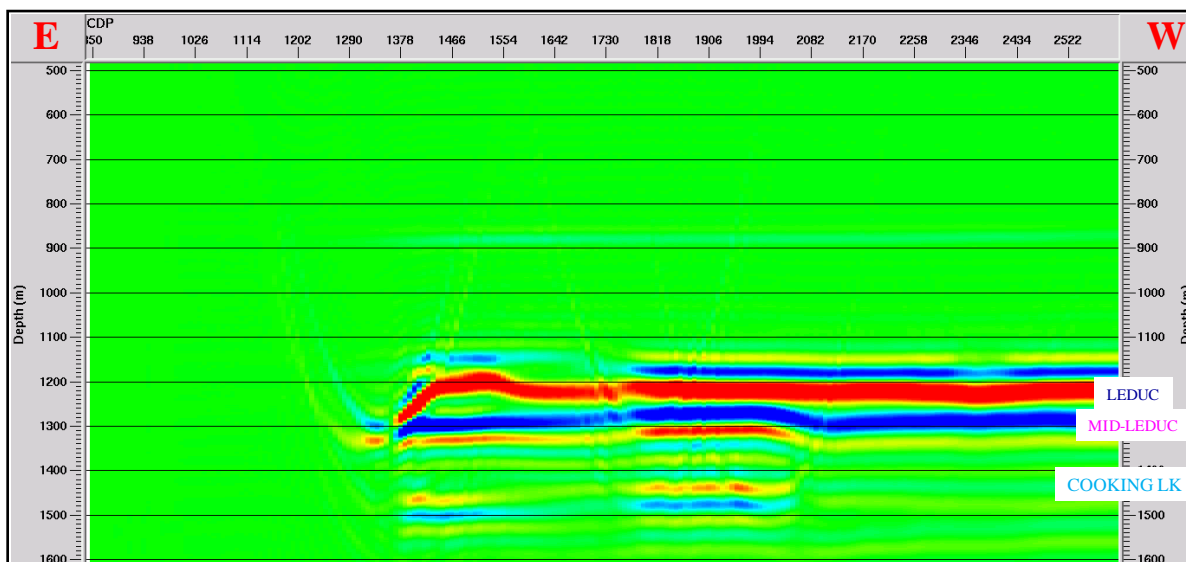


Figure 4.53: Time-lapse difference seismic section before and after CO₂ substitution in the Upper Leduc member, Line B (ray trace modeling and PSDM).

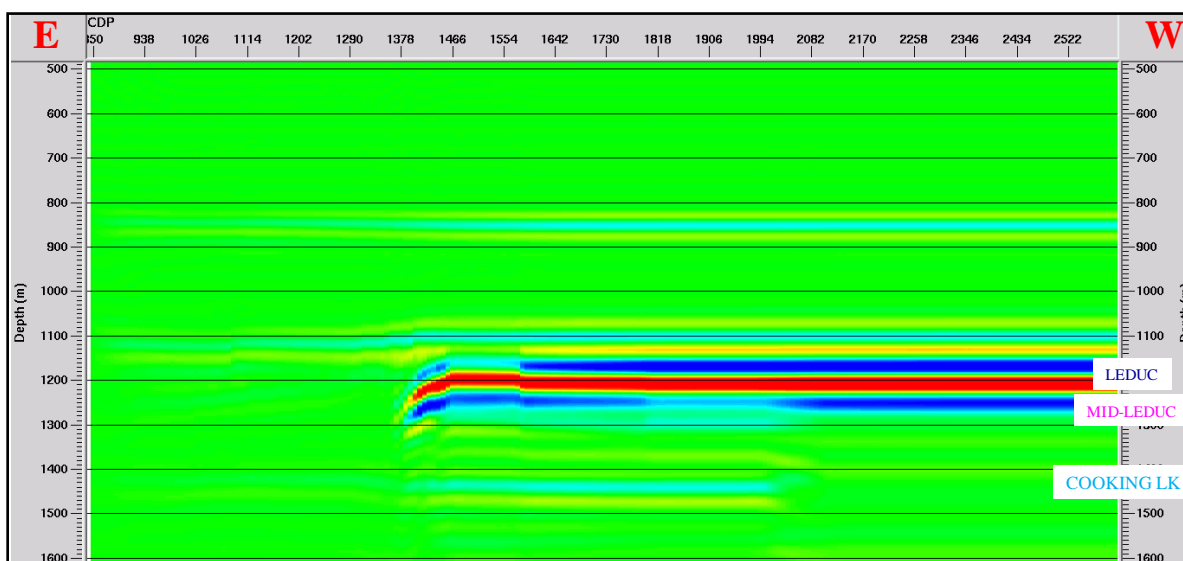


Figure 4.54: Time-lapse difference seismic section before and after CO₂ substitution in the Upper Leduc member, Line B (finite difference modeling and PSDM).

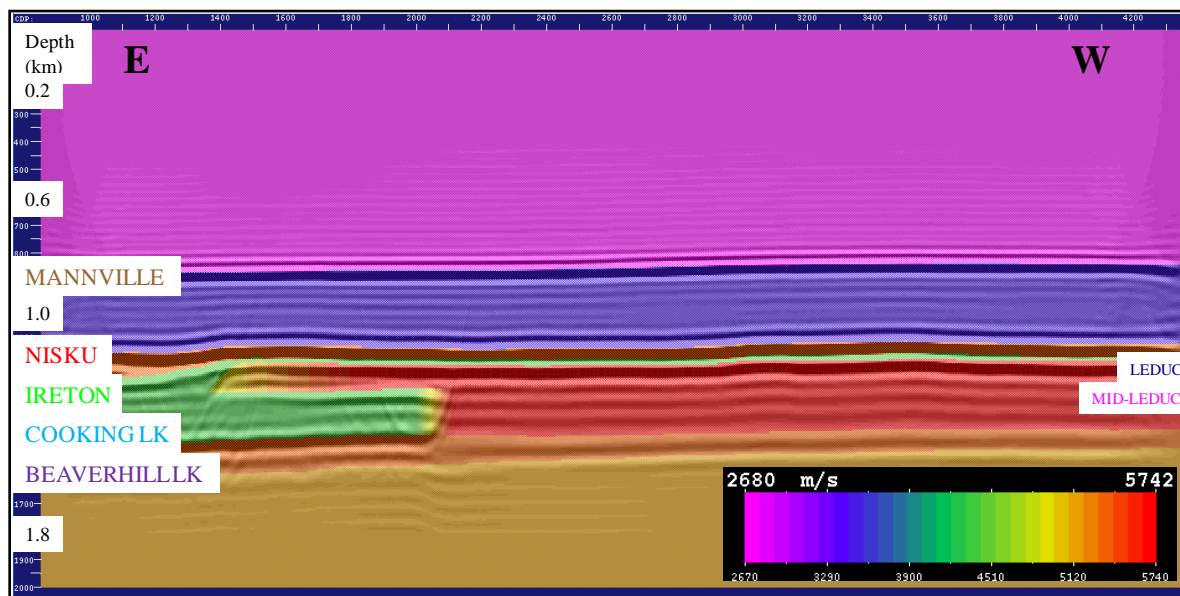


Figure 4.55: Colored velocity model super-imposed on the PSDM seismic section after CO₂ fluid substitution, Line B.

4.5 Results – Time-lapse of converted wave seismic modeling

4.5.1 Baseline Modeling, Line A

The 2D geological model along Line A with the seismic properties is shown in Figure 4.2 through Figure 4.4. Figure 4.56 and Figure 4.57 show examples of the radial component seismic shot gathers of the ray tracing modeling method after geometry and sorting but Figure 4.57 shows the shot gather after polarity reversing for the trailing traces. Figure 4.58 and Figure 4.59 illustrate the pre-stack time-migrated (PSTM) and pre-stack depth-migrated (PSDM) seismic sections respectively for PS dataset along Line A. Generally, the Mannville event is a high-amplitude peak, the Nisku event is also a moderate to high amplitude peak, the Ireton shale event is a trough and the Cooking Lake Formation correlates to a moderate amplitude trough on-reef but has higher amplitude peak off-reef. This is because the Cooking Lake carbonates, when overlain by Ireton shale, yield a large

impedance contrast and a high-amplitude reflection (Sodagar and Lawton, 2010e, f, and g). The Beaverhill Lake Formation reflection is a rather weak trough due to the small impedance contrast at the interface between the two carbonate units.

Reflections from the Cooking Lake and Beaverhill Lake formations exhibit positive time structure below the reef in the time section for the converted wave data (Figure 4.58).

This velocity pull-up is due to a lateral velocity change from the on-reef carbonate strata (Leduc Formation) to the adjacent, lower velocity off-reef shale strata (Ireton Formation).

Both formations are essentially flat in the depth model (Figure 4.2 through Figure 4.4).

This velocity pull-up is corrected to being nearly flat in the pre-stack depth-migrated data (Figure 4.59).

Terminations of the Upper Leduc and Middle Leduc events are clear on the 2D synthetic seismic sections at the reef margin, and the Upper Leduc event shows the rim build-up with some enhancement in PSDM section (Figure 4.58 and Figure 4.59). A high-amplitude reflection at the base of Upper-Leduc member is evident near the reef margin and but this event becomes weaker and diminishes toward the interior facies. This is because of the modeled porosity differences and consequently impedance differences between the foreslope facies in the reef rim and lagoonal facies within the central region of the reef (Figure 4.60). All the horizons dip gently to the south on the 2D synthetic seismic section.

It is noteworthy that the seismic attributes and character on the radial component of converted wave (PS) seismic data are comparable to that on the vertical component (PP) seismic data in this part of the reef along Line A, and thus may be supportive as a potential porosity indicator. Figure 4.61 shows the registration and comparison between PP time section and the PS time section (scaled approximately to PP time) where they show a fairly perfect tie for the seismic events with higher frequency in P-P section as expected. The PSTM seismic section for PS presents at a scale of 0.69 times than that of the PP section to align equivalent seismic events (Figure 4.61). This scale value is derived from the V_p/V_s ratio of 1.9 that directs to an interval time on the PS section of 1.45 times than that of the PP section. In the PSDM section, PP and PS sections are displayed at the same depth scale and match very well with only a small error of 0-10 m due to smoothing the velocity required for migration (Figure 4.62).

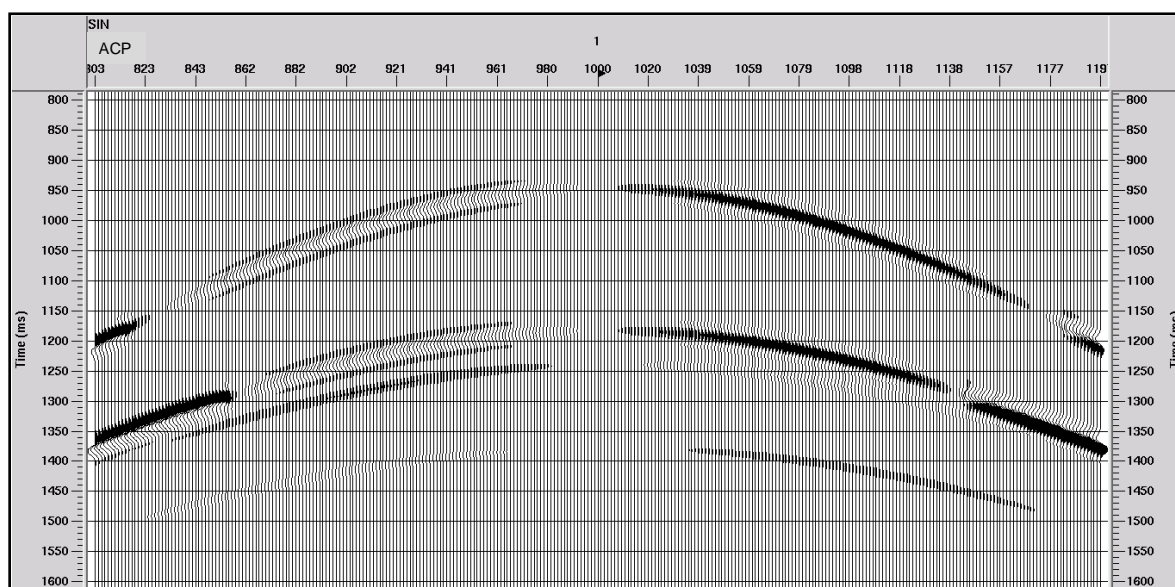


Figure 4.56: Radial component of converted wave (PS) ray tracing numerical shot gather after geometry and sorting from the Line A model.

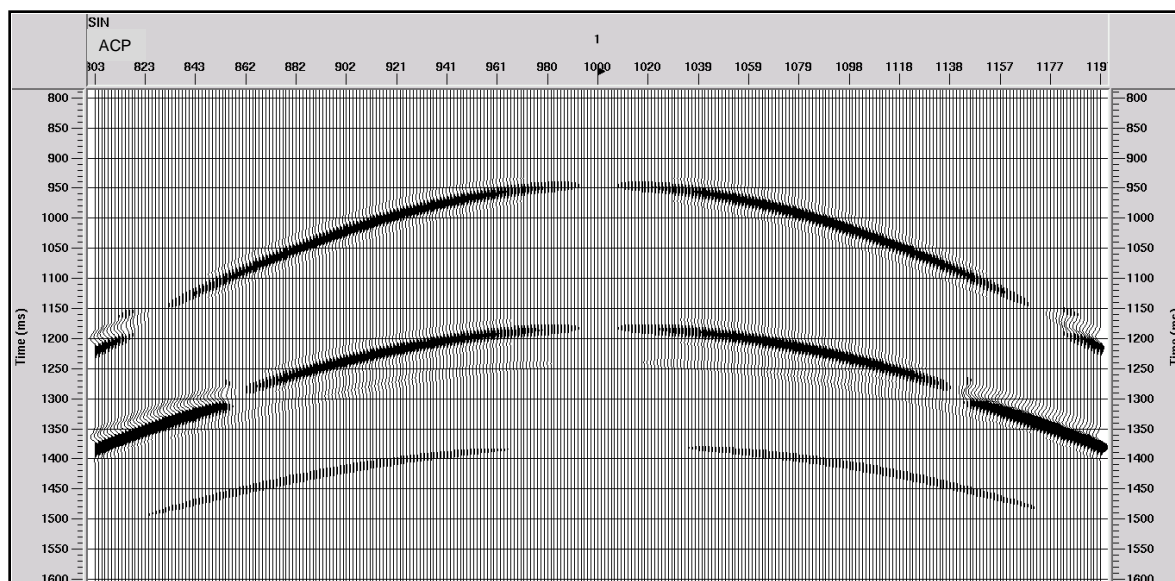


Figure 4.57: Radial component of converted wave (PS) ray tracing numerical shot gather after geometry sorting and trailing trace polarity reverse from the Line A model.

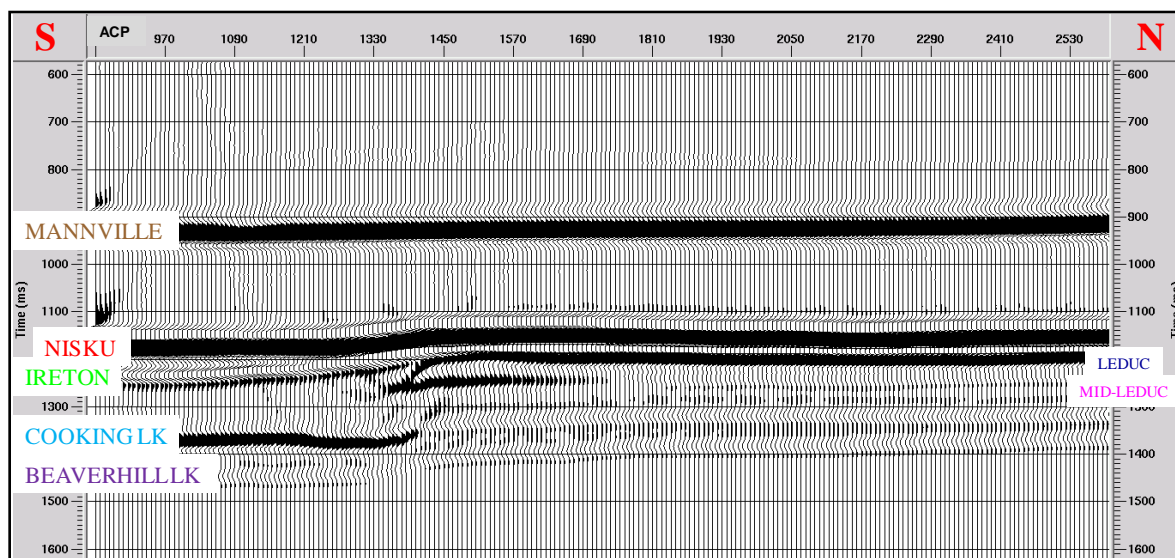


Figure 4.58: Radial component of converted wave (PS) seismic section after pre-stack time migration, Line A, with interfaces identified on the section.

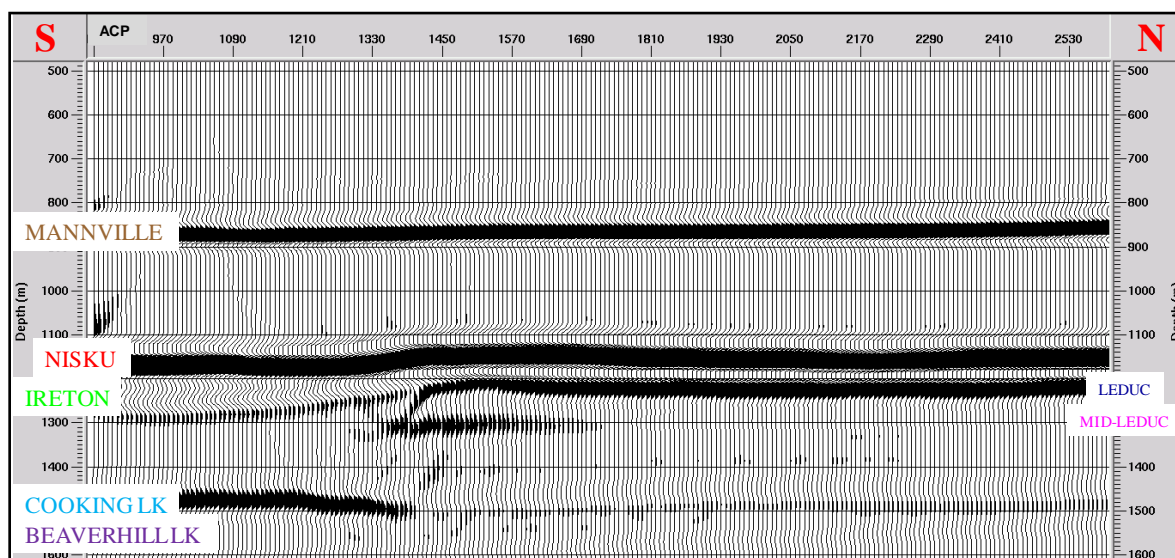


Figure 4.59: Radial component of converted wave (PS) seismic section after pre-stack depth migrated section, Line A.

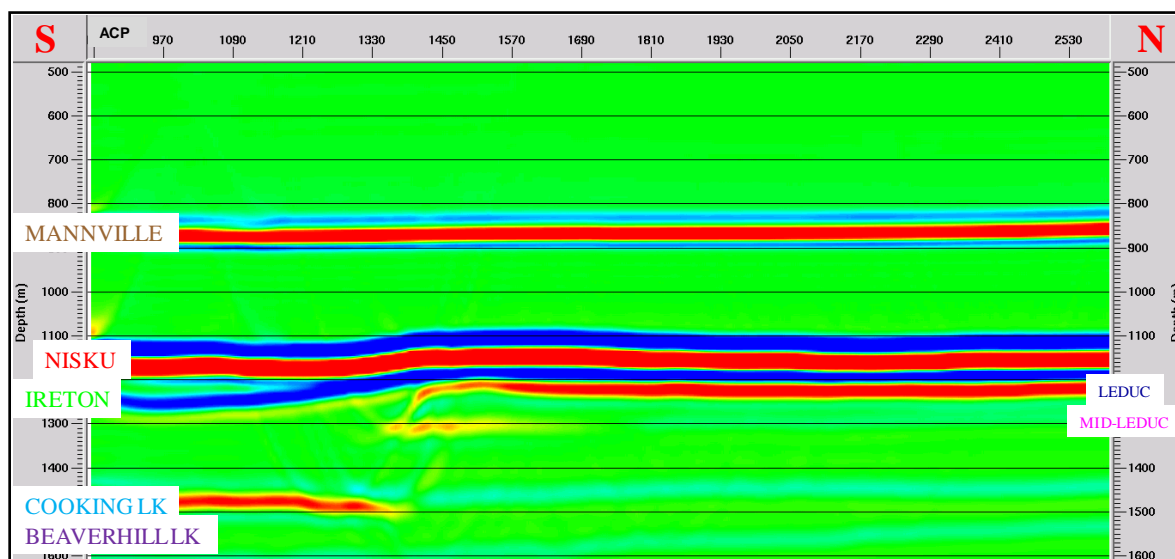


Figure 4.60: PS colored pre-stack depth migrated section from Line A, showing the litho-facies impedance contrast at the top and base of Upper Leduc as well as thinning across the top of the reef rim.

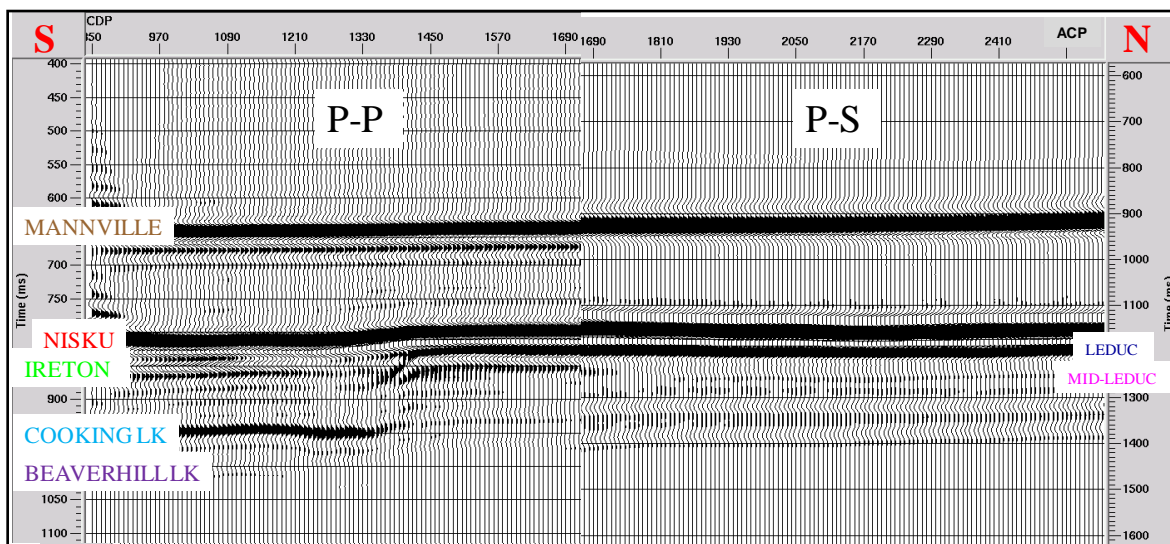


Figure 4.61: Registration and Comparison of the events between the PP wave and PS wave PSTM seismic sections from the Line A.

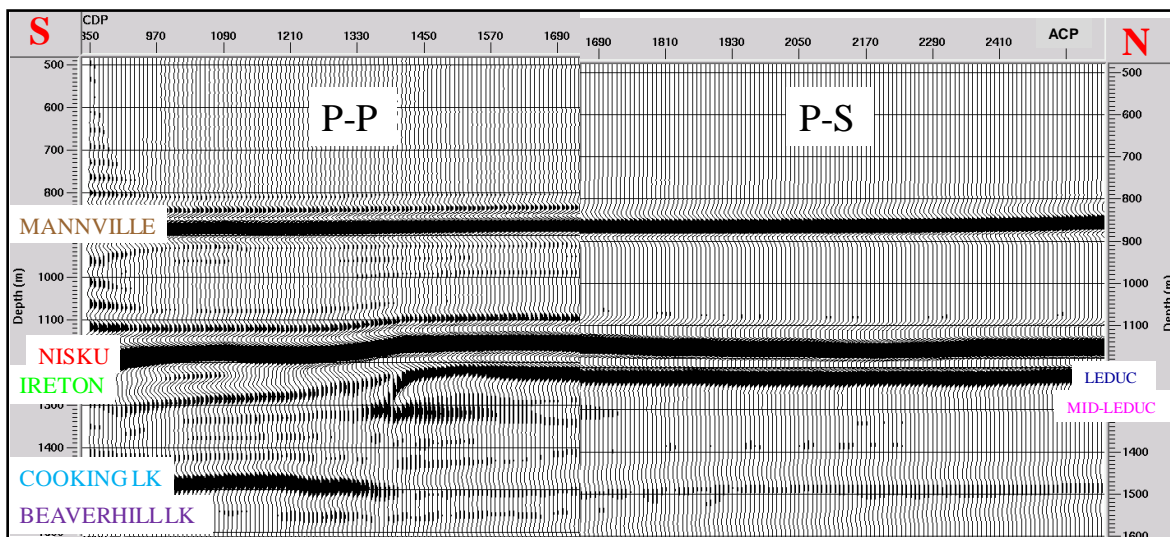


Figure 4.62: Comparison and matching the events between PP wave and PS wave PSDM seismic sections from the Line A.

4.5.2 CO₂ Fluid Substitution, Line A

The 2D geological model of Line A with a homogeneous 40% CO₂ fluid substitution in the Upper-Leduc member was shown in Figure 4.16. Figure 4.63 and Figure 4.64

demonstrate the pre-stack time-migrated (PSTM) and depth-migrated (PSDM) seismic sections respectively for PS data generated from ray tracing modeling. In these sections, The Mannville, Nisku, Ireton, Cooking Lake, and Beaverhill Lake formations display essentially the same seismic attributes as the baseline seismic sections. Positive time structure below the reef exists in the pre-stack time-migrated data but is corrected in the pre-stack depth-migrated section (Figure 4.64).

Terminations of the Upper-Leduc and Middle-Leduc events are apparent on the 2D synthetic seismic sections with a modest improvement on the depth section at the reef margin, and the Upper Leduc event shows the rim build-up with lower amplitude compared to the baseline sections (Figure 4.58 and Figure 4.59) because of the brine replacement with 40% CO₂ (Figure 4.63 and Figure 4.64). A stronger and higher amplitude reflection at the base of Upper-Leduc member is evident near the reef margin compared to the baseline sections. This event becomes weaker toward the interior facies due to the lateral porosity gradient and consequently velocity and density differences between the foreslope facies in the reef rim and lagoonal facies within the central region of the reef.

The registration and comparison between PP wave and PS wave PSTM and PSDM seismic sections with CO₂ fluid substitution in the Upper Leduc member show a fairly good tie for the seismic events with a lower frequency in PS section as expected (Figure 4.65 and Figure 4.66). In the PSDM section, PP and PS sections are displayed at the same

depth scale and match very well with only a small error of 5-15 m due to smoothing the velocity required for migration (Figure 4.66).

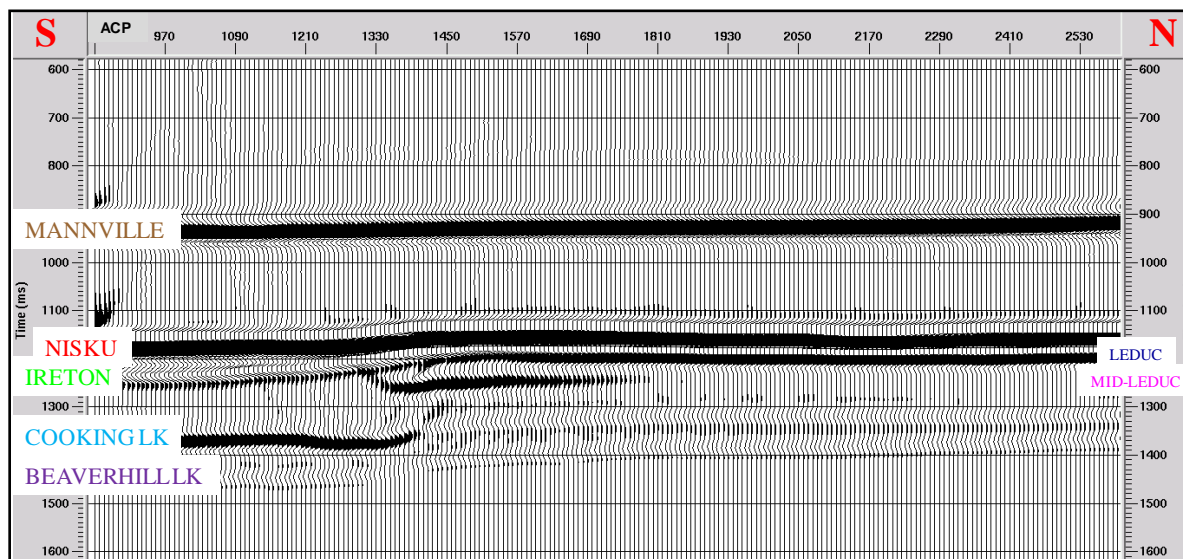


Figure 4.63: Radial converted wave seismic section after CO₂ fluid substitution and PSTM, Line A.

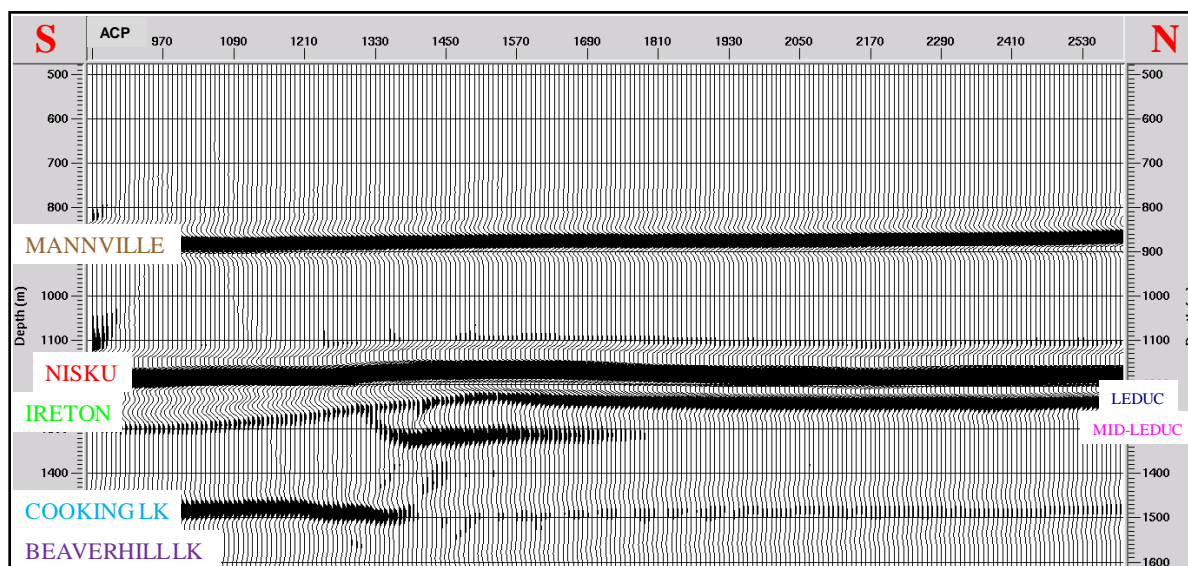


Figure 4.64: Radial converted wave seismic section after CO₂ fluid substitution and PSDM, Line A.

Time-lapse analysis has applied to examine the effect of CO₂ saturation on the radial converted wave seismic reflectivity and attributes (Lawton and Sodagar, 2009). Figure 4.67 shows the PS difference seismic section after pre-stack depth migration, before and after 40% CO₂ saturation. Notice that there are good reflections at the top of upper-Leduc member, around the reef rim, and at the top of the mid-Leduc member near the reef edge, as expected. This difference anomaly on the PS data is attributed to a slight increase in S-wave velocity due to reduction in bulk density after brine replacement with CO₂.

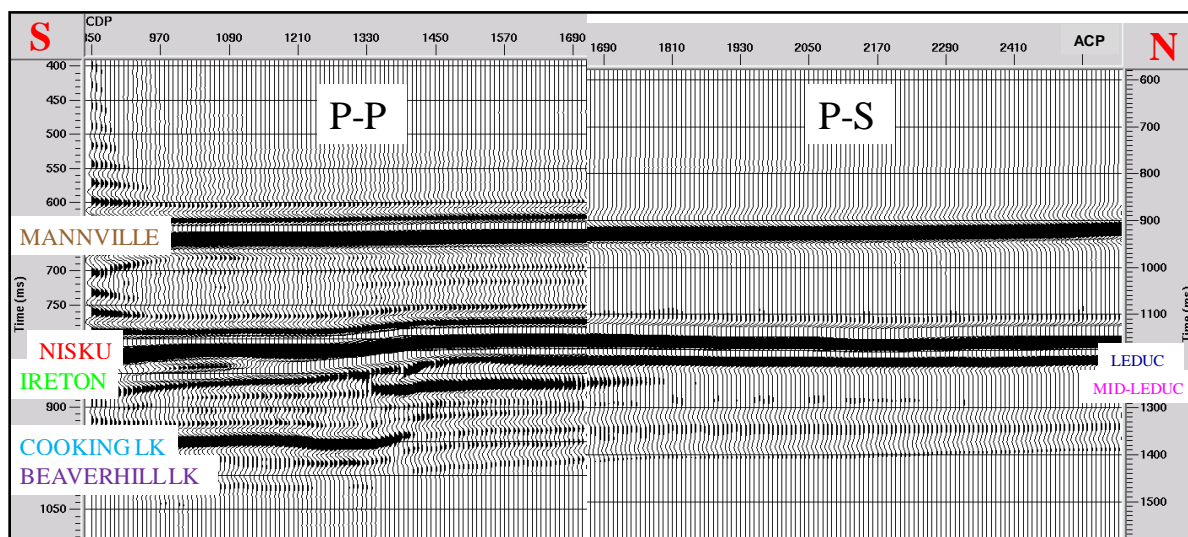


Figure 4.65: Registration and Comparison of the events between the PP wave and PS wave PSTM seismic sections from the Line A, after CO₂ replacement in the Upper Leduc member.

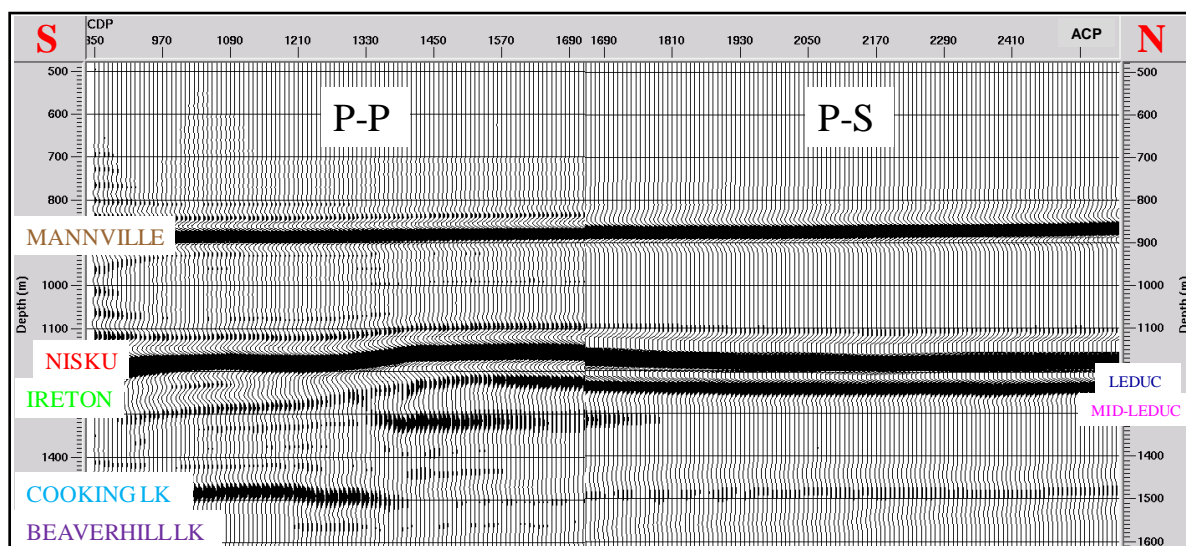


Figure 4.66: Comparison and matching the events between PP wave and PS wave PSDM seismic sections from the Line A, after CO₂ replacement in the Upper Leduc member.

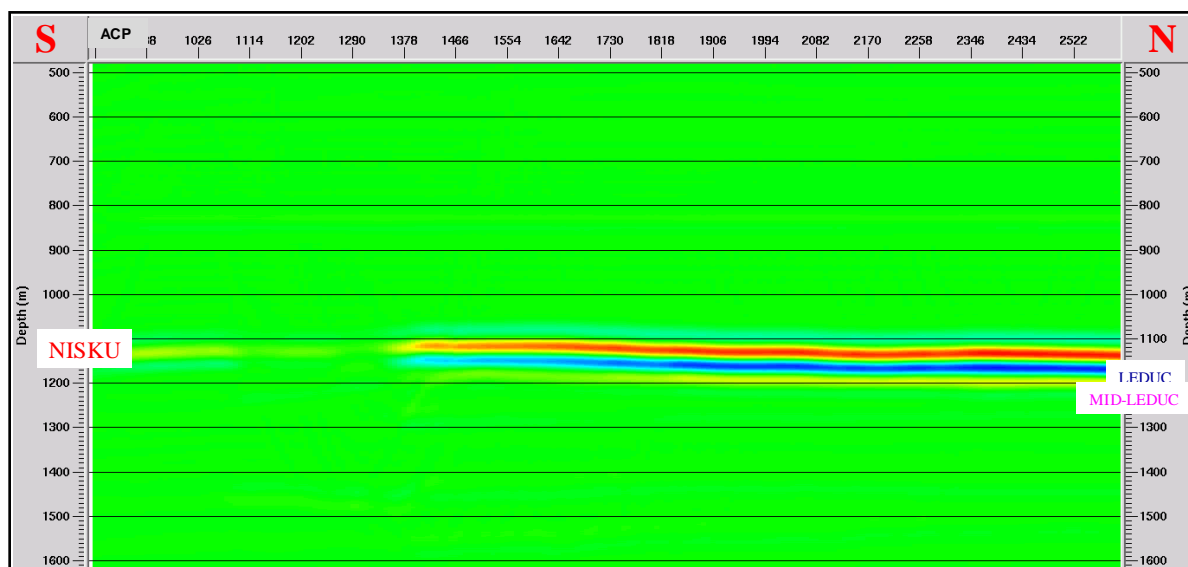


Figure 4.67: Time-lapse difference seismic section before and after CO₂ substitution in the Upper Leduc member, Line A (radial converted wave ray trace modeling and PSDM).

4.6 Conclusions

Synthetic seismic sections based on ray trace and finite difference modeling along Line A and B as well as ray traced synthetic PS seismic sections along Line A demonstrate similar seismic attributes for the Mannville, Nisku, Ireton, Cooking Lake and Beaverhill Lake formations as well as with CO₂ saturations. The Cooking Lake and Beaverhill Lake formations display positive time structure below the reef in time sections due to a lateral velocity change. Both formations are corrected after depth migration.

Terminations and the lateral position of the Upper Leduc and Middle Leduc events are obvious on the post-stack time migration synthetic seismic section and enhanced on the pre-stack time and depth-migrated seismic sections for both geological models along Line A and B as well as with CO₂ saturations. The reef rim reflection is observed clearly at the reef margin. High reflection amplitudes for PP and even stronger for PS at the base of Upper-Leduc member are evident at the reef edge due to porosity differences between the foreslope facies in the reef rim and tidal flat lagoonal facies within the central region of the reef. Therefore, PS seismic characters efficiently recognize Redwater reef lithofacies because they are more sensitive to lithology.

There is a time difference of 45 ms between the events in the ray traced and finite difference synthetic seismic data and equivalent events on the field surface seismic data. This difference is because of the slight change in the seismic reference datum (SRD) of the numerical and field seismic data, combined with assumptions about the near-surface replacement velocity in the numerical seismic model. The registration and comparison

between PP wave and PS wave shows an excellent tie of the seismic events with a higher frequency in PP section. There are few differences in seismic attributes between the Line A and B for some events. Base of Upper Leduc reflection at the reef margin is weaker in Line B than in A. Also, Cooking Lake reflection is modest trough in Line A, while is a strong peak on-reef below the Duvernay embayment in Line B.

Numerical multichannel time-lapse analysis shows an amplitude difference for the Upper Leduc reflection and a travelttime delay for the Mid-Leduc event in the seismic data before and after CO₂ fluid substitution, using both ray-tracing (for PP and PS data) and finite-difference (for PP data) modelling methods. The timelapse seismic response shows an event at the top of upper-Leduc, particularly around the reef rim, and at the base of upper-Leduc as the reef edge is approached. After 40% CO₂ saturation in the Upper Leduc Formation, the average P-wave interval velocity decreases by about 3.3% and the impedance decreases by about 3.6%, yielding a reflectivity difference of about 14%. The two-way travel-time delay through the Upper Leduc interval following the CO₂ fluid substitution is about 1.6 ms. These results suggest that the time-lapse seismic surveys will be appropriate for monitoring the CO₂ plume within the Redwater Leduc Reef.

Chapter Five: **4D MULTICOMPONENT SEISMIC MODELING OF CO₂ FLUID SUBSTITUTION IN THE REDWATER DEVONIAN REEF**

5.1 Introduction

After 2D multicomponent seismic modeling across the southern margin of the reef, to examine the seismic response before and after CO₂ saturation for the Upper Leduc interval had been completed, time-lapse 3D seismic modeling was undertaken for multicomponent seismic data analysis (PP and PS data) in southern part of the reef (Figure 5.1).

The main objective of the study was to map facies variations within the Redwater Leduc reef, based on seismic character, and to characterize the reef members and formations below the reef by creating a 3D geological model at the southern margin of the Redwater reef. 3D multicomponent seismic modeling was then undertaken to generate a 3D synthetic seismic data (PP and PS data) to study the 3D seismic response of the different formations of the Redwater Reef, particularly the Leduc Formation. The primary goal was to undertake time-lapse 3D multicomponent seismic modeling with a harmonized 40% CO₂ saturation in the Devonian Upper Leduc member interval, based on fluid substitution using a Gassmann (1951) approach, to evaluate 3D seismic surveys to monitor the CO₂ saturation.

For the 3D multicomponent synthetic seismic modeling discussed in this chapter, full common-shot ray tracing was used to produce the PP and PS numerical seismic responses of the reef. The model is based on available well data and depth-converted seismic data

from the seismic interpretation study discussed in chapter 2. The seismic data were processed and migrated to evaluate the reflection image of the reef edge as well as the internal reef litho-facies within the 3D model.

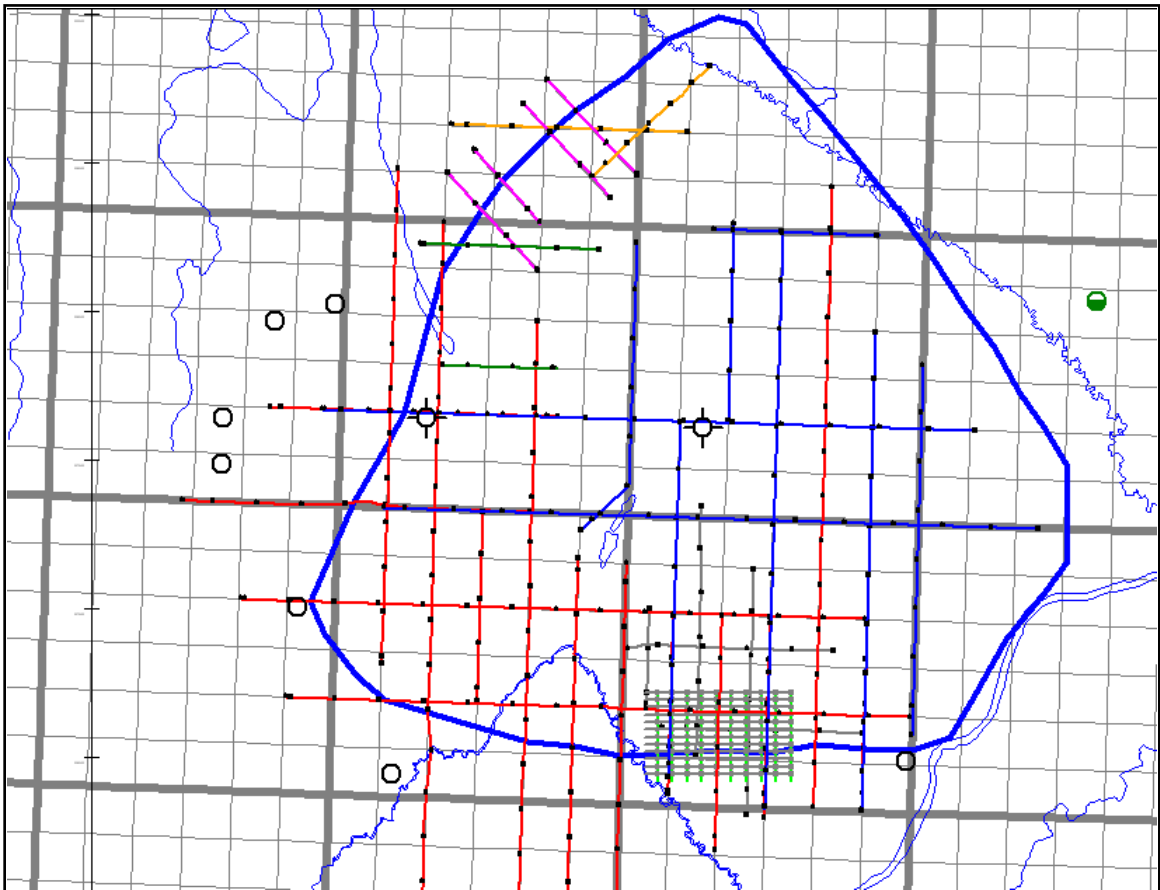


Figure 5.1: Redwater reef map showing the wells that penetrate the Cooking Lake Formation and have sonic logs and also showing the distribution of all the 2D seismic data available for the project. The colours depict different vintages of data purchased. The location of the synthetic 3D survey is shown in the southern margin of the Redwater reef. The eastern boundary marks the edge of data, not the edge of the reef.

5.2 Methodology

5.2.1 Common Shot Surface Seismic Modeling

A large number of wells penetrate the Upper Leduc Fm, especially along the eastern margin of the Redwater reef, but only a small number of wells penetrate the Cooking Lake Formation and few of these have sonic and density logs. Figure 5.1 shows three wells inside the reef and six wells off-reef that penetrate the Cooking Lake Formation in the general study area. Of these, three on-reef and four off-reef wells were used to assist in the generation of the velocity and density model used for the seismic modelling project. The 3D model is oriented in the southern part of the Redwater reef and includes the lagoonal facies within the reef to off-reef facies (Figure 5.1).

A 3D geological model of the Redwater reef area was constructed from the interpretation of available vintage 2D surface seismic data within the study area as well as available well data. The full 3D geological model was extracted from the 3D gridded time structure maps of geological formations including Mannville, Nisku, Ireton, Leduc, Mid-Leduc, Cooking Lake and Beaverhill Lake events for the entire Redwater reef (Sodagar and Lawton, 2010a, b, and c). These time structure maps were converted to depth maps using a gradient velocity at the well locations and the final model is shown in Figure 5.2. Errors in the calculated depth were within 1m at the well locations for all formations picked for the geological model.

The geological model developed for the 3D seismic modeling is shown in Figure 5.3. Interfaces in depth were transformed to event blocks and P-wave velocities and densities

were assigned to these blocks using average values from the wells and equivalent for properties used for the 2D modeling. These properties of the model are shown in Figure 5.4 through Figure 5.7. S-wave velocities were assigned using $V_p/V_s = 1.9$, calculated from a single existing dipole well on the eastern side of the reef. The Leduc reef rim region was modelled as a separate block (Figure 5.3 through Figure 5.7). In this block, the velocity and density values had a lateral gradient associated with an average porosity of 4% in the tidal flat lagoonal facies, to an average porosity 9% in the foreslope facies at the rim of the reef (Figure 5.3 and Figure 5.4). The original pore fluid of the Leduc Formation (100% water) was replaced uniformly by CO₂ at a saturation level of 40% (Lawton and Sodagar, 2009 and Sodagar and Lawton, 2009) in the Upper Leduc member since it was found that there are no significant changes in the seismic velocities occurred between 40% and 100% CO₂ saturation (Sodagar and Lawton, 2010d). The P-wave velocities and densities were recalculated using Gassmann equation (Gassmann, 1951), after fluid substitution, similar to the approach used for 2D modelling.

5.2.2 Seismic Survey Parameters

Common shot ray tracing for primary PP wave and PS wave events were performed with a shot interval of 100 m and receiver interval of 50 m from a SRD (Seismic Reference Datum) of 750 m above sea-level. The survey was undertaken with an orthogonal geometry with parallel receiver lines as well as parallel source lines (Figure 5.8). The survey dimension is 3 x 5 km (Sodagar and Lawton, 2011b). Table 5.1 lists the full survey design parameters that were used in the seismic modeling. Seismic shot gathers were generated by convolving the reflectivity functions at the computed arrival times

with a zero-phase 40 Hz Ricker wavelet for PP data and a 20 Hz Ricker wavelet for the PS data. The seismic wavelet was extracted from the reprocessed 2D surface seismic data at a well location.

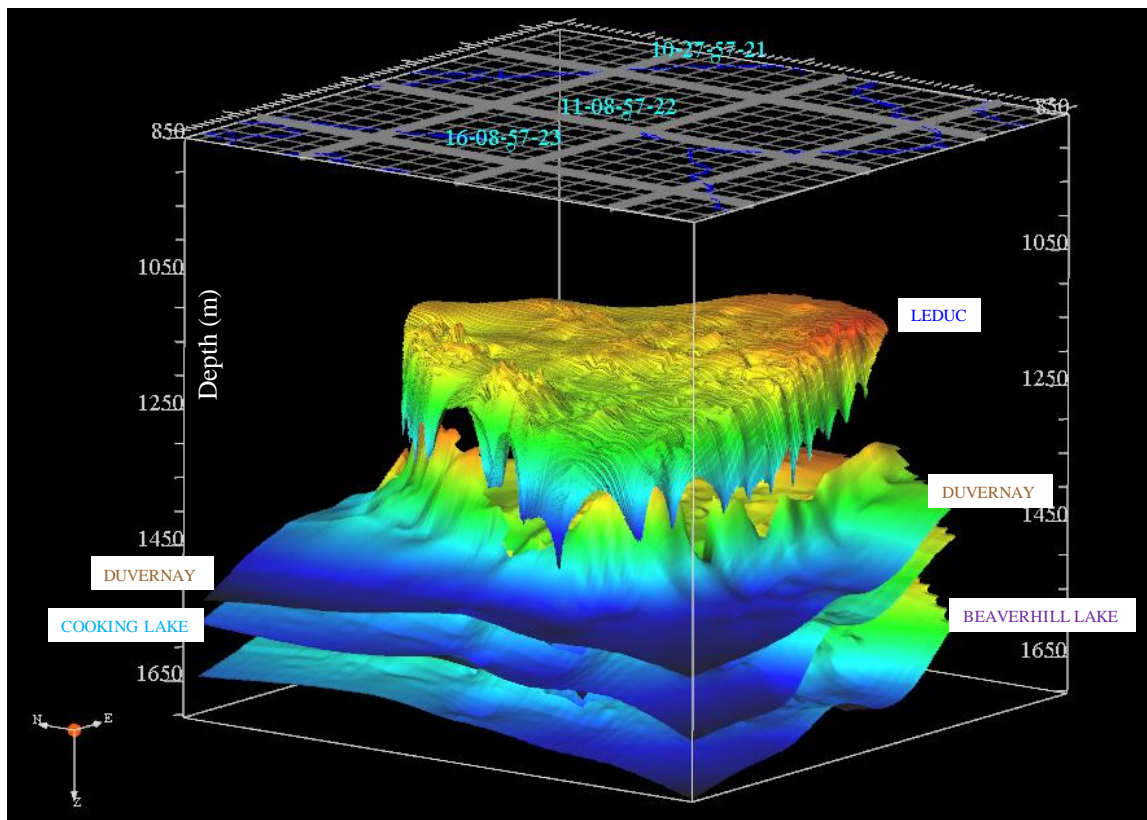


Figure 5.2: 3D view of the gridded depth structure maps of the Redwater reef, showing the Leduc, Duvernay, Cooking Lake, and Beaverhill Lake formations that included in the 3D model.

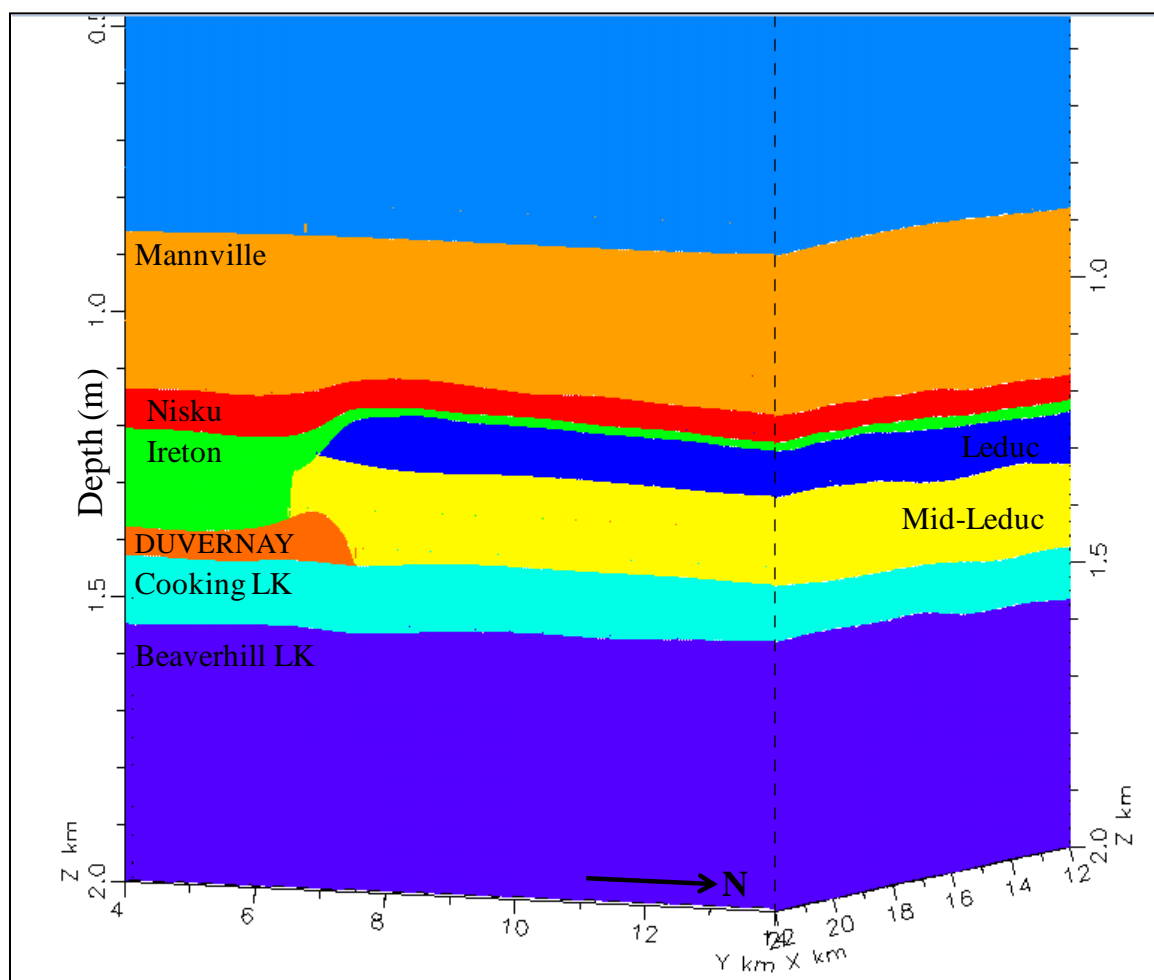


Figure 5.3: 3D geological model at the southern margin of the Redwater reef, showing the formations included in the model.

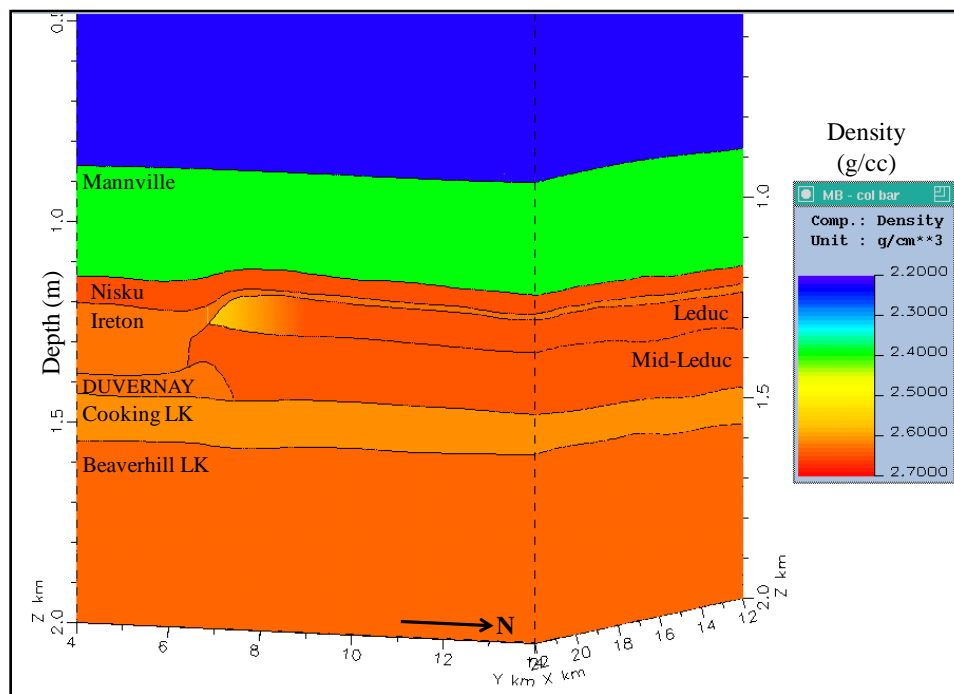


Figure 5.4: 3D geological model at the southern margin of the Redwater reef, showing densities of the various formations (brine saturation).

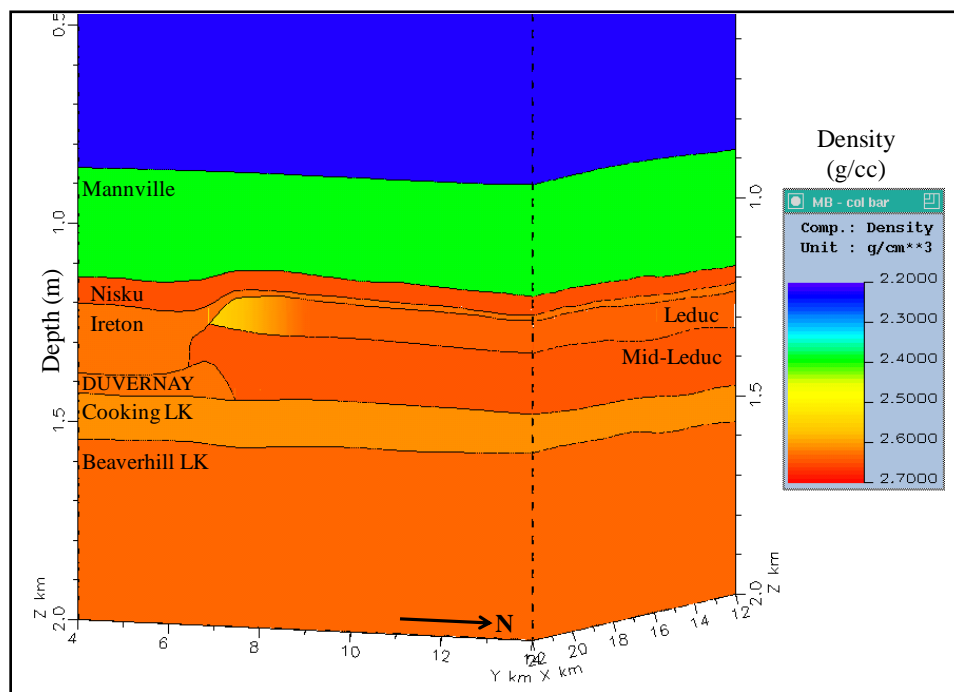


Figure 5.5: 3D geological model at the southern margin of the Redwater reef, showing densities of the various formations after CO₂ saturation in Upper Leduc member.

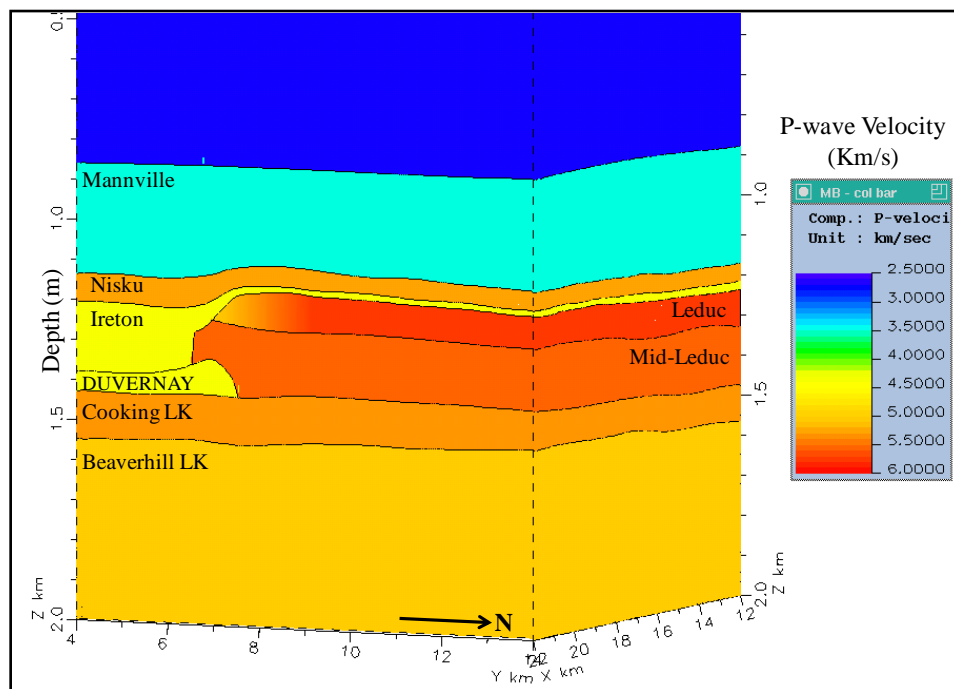


Figure 5.6: 3D geological model at the southern margin of the Redwater reef, showing P-wave interval velocities of the various formations (brine saturation).

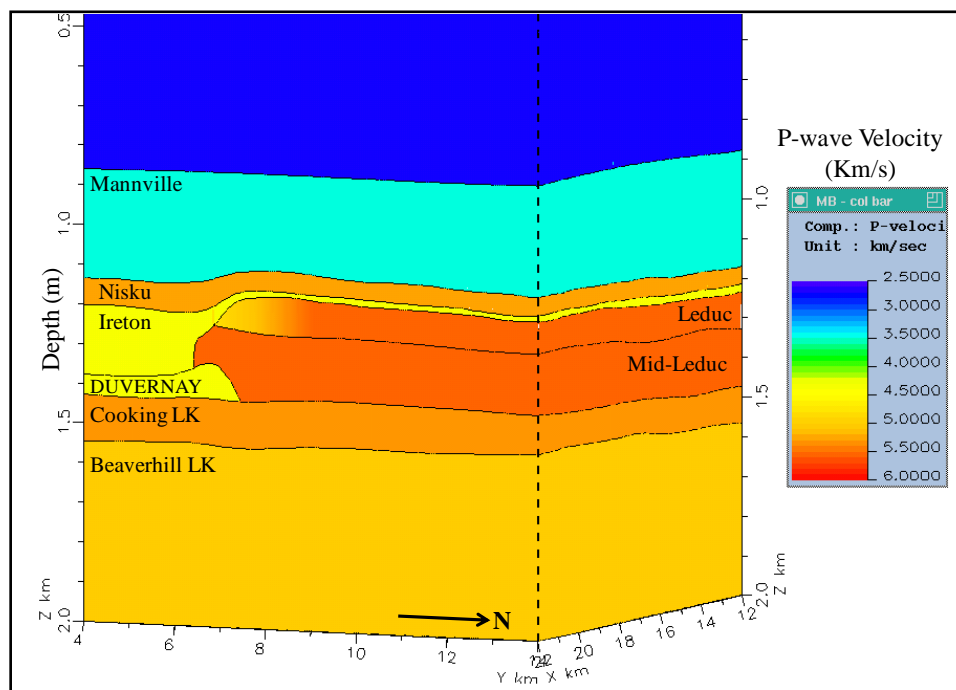


Figure 5.7: 3D geological model at the southern margin of the Redwater reef, showing P-wave interval velocities of the various formations after CO₂ saturation in Upper Leduc member.

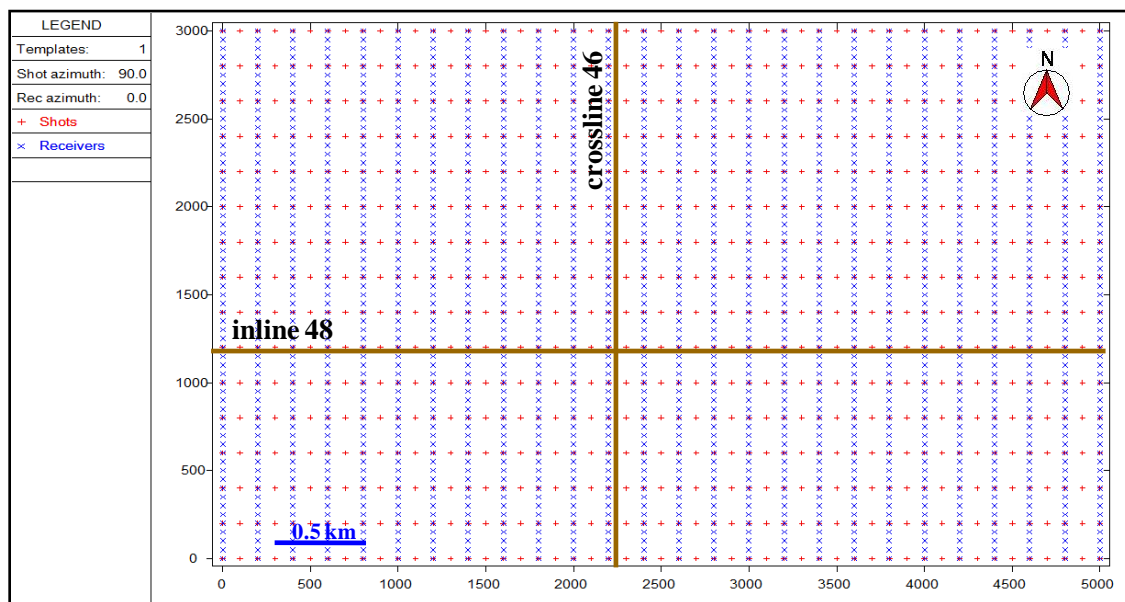


Figure 5.8: 3D survey design showing the source and receiver layout, parallel source and receiver lines every 200m, the source line in the east-west direction and shot every 100m, the receiver line in north-south direction, and the station every 50m.

Table 5.1: 3D survey design parameters used for the 3D seismic modeling in the Redwater reef area.

3D SURVEY DESIGN	PARAMETERES
Source interval	100 meters
Source line interval	200 meters
Source line direction	East- West
Total number of source lines	16 lines
Total number of shots per source line	51 shots
Total number of shots	816 shots
Receiver interval	50 meters
Receiver line interval	200 meters
Receiver line direction	North-South
Total number of receiver lines	26 lines
Total number of receivers per receiver line	61 receivers
Total number of receivers	1586 receivers
Total number of CDP	12221 CDPs
CDP grid bin	25x50 meters
CDP Fold	396 traces
Minimum offset	50 meters
Maximum offset	5830 meters
Total number of traces	1294176 traces

5.2.3 Seismic Data Processing

The synthetic shot gather seismic data were processed and migrated to image the reef margin and the internal reef facies (Figure 5.9). This processing involved converting the trace headers from shot point to CDP (Common Depth Point) domain for the PP data and converting the trace headers from common midpoint (CMP) to ACP (Asymptotic Conversion Point) domain and reversing the polarity of trailing traces in the shot gathers for the PS data, CDP gather, normal moveout (NMO) correction, and stack, followed by 3D Kirchhoff post-stack migration, 3D Kirchhoff pre-stack time migration (PSTM), and 3D Kirchhoff pre-stack depth migration (PSDM). The PP and PS velocity model used for the migration was created by converting the interval velocities from the input geological model into rms velocities in time.

5.2.4 Software

NORSAR3D software was used to create the 3D blocks, perform common shot ray tracing for PP and PS data, and generate the multicomponent synthetic shot gathers (NORSAR, 2008). ProMax software was used for geometry sorting, polarity reversal for PS data, velocity conversion, CDP gather, NMO correction, stack, 3D post-stack time migration, and 3D pre-stack time migration. Paradigm GeoDepth software was used for 3D pre-stack depth migration for PP and PS data.

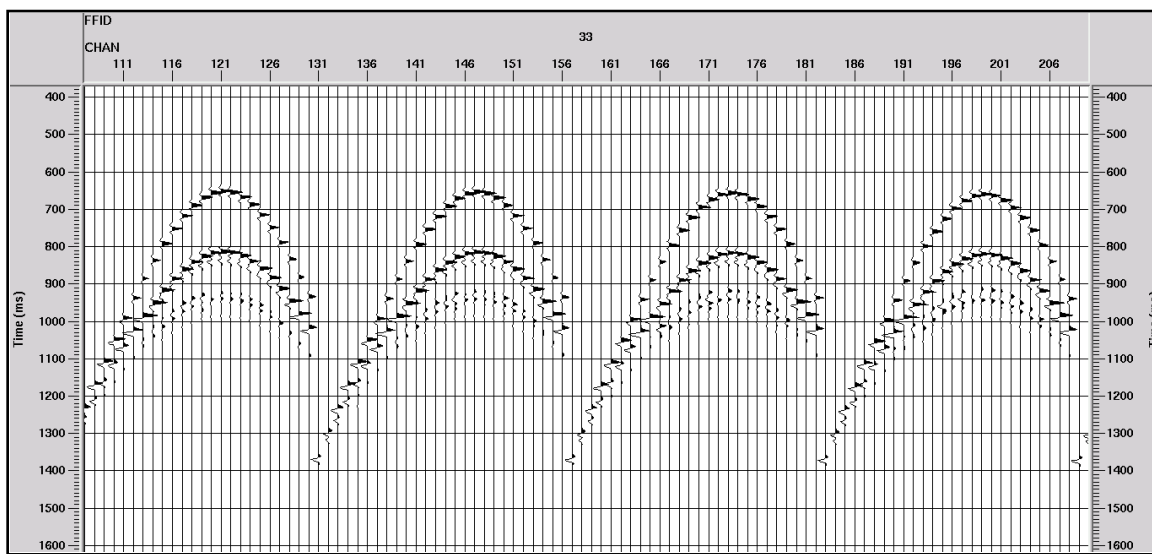


Figure 5.9: 3D ray tracing numerical seismic shot gather data.

5.3 Results

The processed 3D seismic volumes for the PP and PS data were interpreted manually line by line for maximum accuracy of the picked horizons. The interpreted horizons included Mannville, Nisku, Ireton, Leduc (upper and middle members), Duvernay, Cooking Lake, and Beaverhill Lake formations. The interpretation results of the 3D multicomponent seismic data before and after CO₂ saturation are presented in seismic sections and attribute maps, to examine the CO₂ saturation effects on the 3D multicomponent seismic response.

The 3D multicomponent seismic volumes were processed with the same general workflow but using three different migration methods. The migration types were Kirchhoff post-stack time migration, Kirchhoff pre-stack time migration (PSTM), and Kirchhoff pre-stack depth migration (PSDM). PP and PS seismic data were examined

after the different kinds of migration were applied, before and after CO₂ saturation in Upper Leduc member. Time-lapse analysis was undertaken to examine the effect of 40% CO₂ fluid substitution on seismic reflectivity and attributes.

5.3.1 Seismic section interpretation

5.3.1.1 Post-stack time migrated seismic section interpretation

Figure 5.10 illustrates the 3D ray traced numerical seismic volume data after CDP stack and after post-stack Kirchhoff migration respectively where the migration effect is clear in Figure 5.10B at the reef margin. Figure 5.11 demonstrates an example of the PP Kirchhoff post-stack time-migrated seismic section at inline (48) from 3D ray tracing (Figure 5.8). Figure 5.12 illustrates the PP Kirchhoff post-stack time-migrated seismic section at crossline (46) which is very close to the line extracted in the 2D modeling in chapter 4 (Figure 5.8), so the comparison can be evaluated between the 2D and 3D ray tracing sections. In this section, the Mannville and Nisku events are high amplitude peaks, the Ireton shale event is a trough and the Cooking Lake Formation correlates to a weak amplitude trough on-reef but is a higher amplitude peak off-reef (Figure 5.12). This is because the Cooking Lake carbonates, when overlain by Ireton shale, yield a large impedance contrast and a high-amplitude reflection. The Beaverhill Lake event is a fairly weak trough due to the small impedance contrast at the interface between the two carbonate units. The Duvernay shale embayment event is a moderate trough invading the carbonate reef.

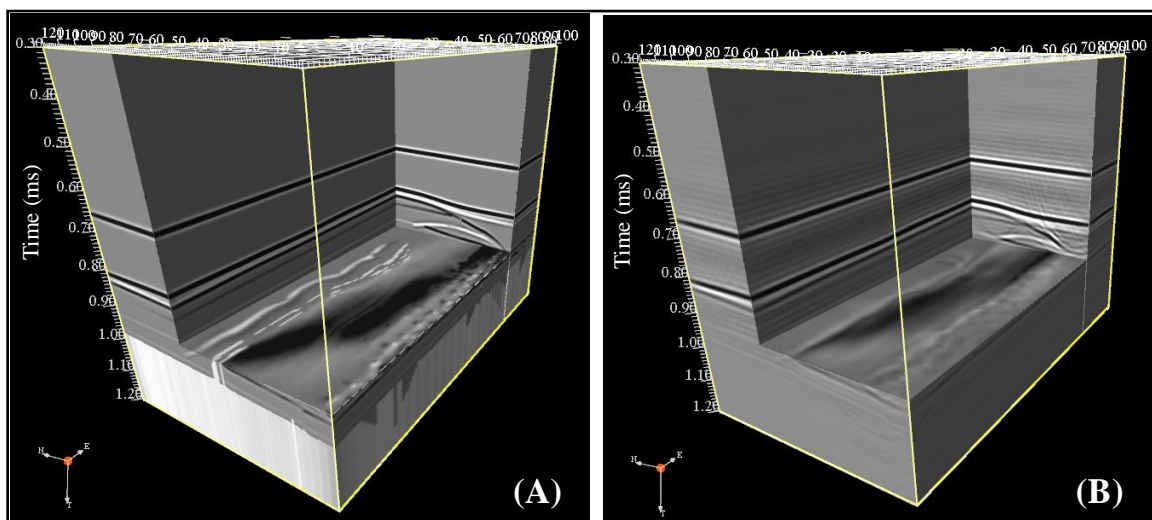


Figure 5.10: 3D ray traced numerical seismic volume (A) after CDP stack and (B) after post-stack time migration.

Reflections from the Cooking Lake and Beaverhill Lake formations exhibit positive time structure below the reef on the time section shown in Figure 5.12. This velocity pull-up is due to a lateral velocity change from the on-reef carbonate strata (Leduc Fm.) to the adjacent, lower velocity off-reef shale strata (Ireton Fm.). Both formations are essentially flat in the depth model (Figure 5.3). This velocity pull-up is removed in the PP pre-stack depth-migrated section show later (Figure 5.24).

Terminations of the Upper Leduc and Middle Leduc events are clear on the synthetic seismic section at the reef margin, and the Upper Leduc event shows the rim build-up (Figure 5.12). A high- amplitude reflection at the base of upper-Leduc member is evident near the reef margin and but this event becomes weaker toward the interior facies. This is due to the modelled porosity differences and consequently velocity and density differences between the foreslope facies in the reef rim and lagoonal facies within the

central region of the reef. All the horizons dip gently to the southwest in the seismic volume. These 3D results display essentially the similar visual seismic attributes as those on 2D section with some enhancements on 3D volume.

Figure 5.13 illustrates the PP post-stack time-migrated seismic section with 40% CO₂ saturation in the Upper Leduc member, based on 3D ray tracing. All the formations display essentially the same seismic attributes as the baseline seismic section. Positive time structure below the reef still exists but is corrected in the pre-stack depth-migrated data (Figure 5.25). It is observed that there is a reduction in the amplitude of the reflection from the top of Upper Leduc member, and increase in amplitude at the base of Upper Leduc near the reef edge, as predicted due to CO₂ saturation. After 40% CO₂ saturation in the Upper Leduc Formation, the average P-wave interval velocity was found to decrease by about 3.3% and its impedance decreases by 3.6%, yielding a reflection amplitude difference of about 14%. The two-way travel-time delay through the Upper Leduc Formation following CO₂ substitution is about 1.6 ms.

Figure 5.14 shows the time-lapse seismic section for PP post-stack time migration seismic data before and after 40% CO₂ saturation. It is noticeable that there are high amplitude reflections at the top of Upper Leduc member, the top of the rim, and at the base of Upper Leduc near the reef edge, as expected.

Figure 5.15 and Figure 5.16 illustrate the PS Kirchhoff post-stack time-migrated seismic sections, using 3D ray tracing, before and after 40% CO₂ fluid substitution in the Upper

Leduc member respectively. All the formations display mainly the same seismic attributes as the PP seismic sections, but have lower frequency. Also, high amplitude reflection at the base of upper-Leduc member and terminations of the Upper-Leduc and Middle-Leduc events are apparent on the PS seismic sections. Positive time structure below the reef still exists but is corrected in the pre-stack depth-migrated sections (Figure 5.27 and Figure 5.28).

In the PS post-stack time-migrated seismic section with 40% CO₂ saturation, there are less reduction in amplitude reflection at the top of upper-Leduc member, and less increase in amplitude at base of upper-Leduc compared to the PP seismic section with 40% CO₂ saturation. Time-lapse method has been applied on the radial converted wave seismic data to examine the effect of CO₂ saturation. Figure 5.17 shows the PS difference after post-stack time migration before and after CO₂ saturation. There are good reflection differences at the top of upper-Leduc member, top of the rim, and base of upper-Leduc near the reef edge. This difference anomaly on the PS data is attributed to a slight increase in S-wave velocity due to reduction in bulk density after brine replacement with CO₂.

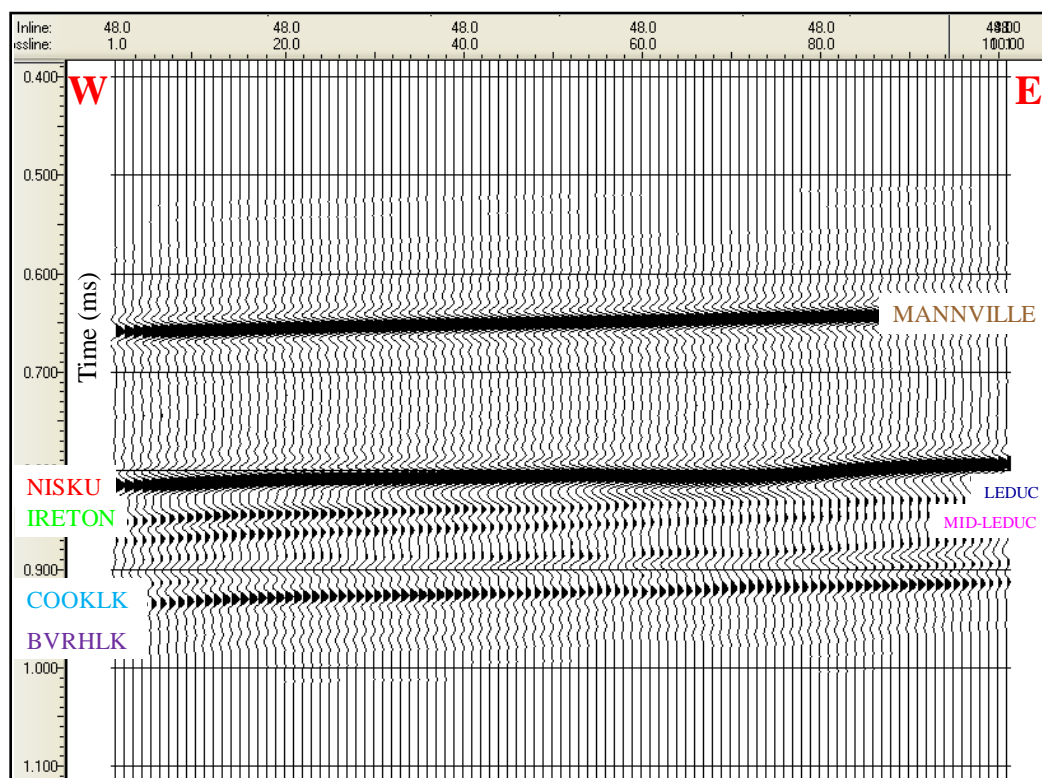


Figure 5.11: Vertical component (PP) seismic section (inline 48) after post-stack time migration, with interfaces identified on the section.

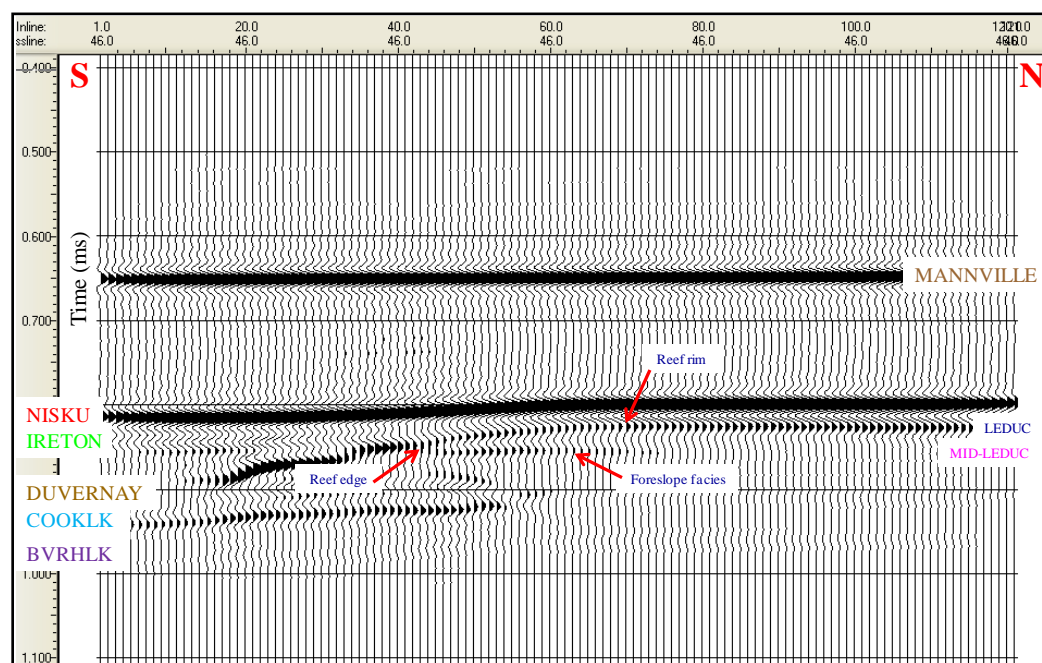


Figure 5.12: Vertical component (PP) seismic section (crossline 46) after post-stack time migration, with interfaces identified on the section.

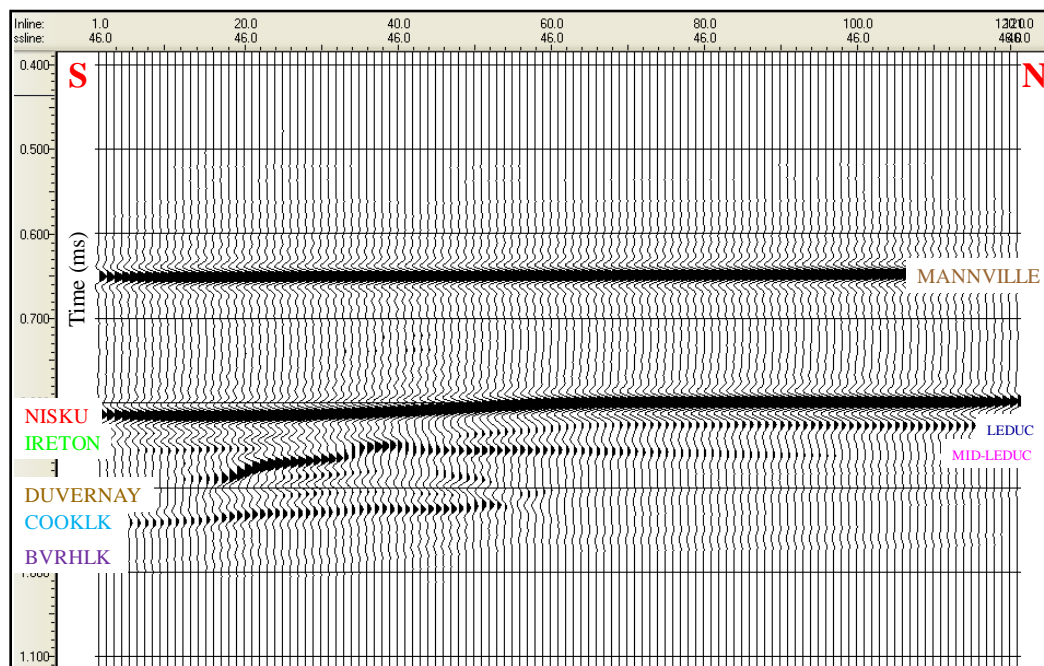


Figure 5.13: Vertical component (PP) post-stack time migrated seismic section (crossline 46) after CO₂ fluid substitution in Upper Leduc member.

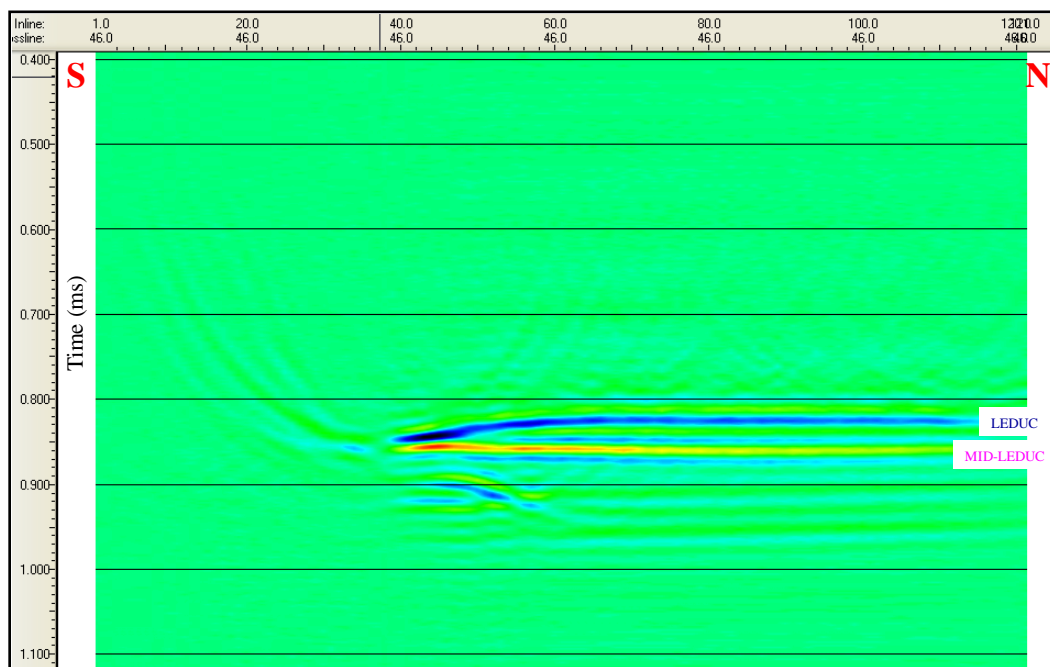


Figure 5.14: PP difference after post-stack time migration (crossline 46) before and after CO₂ fluid substitution.

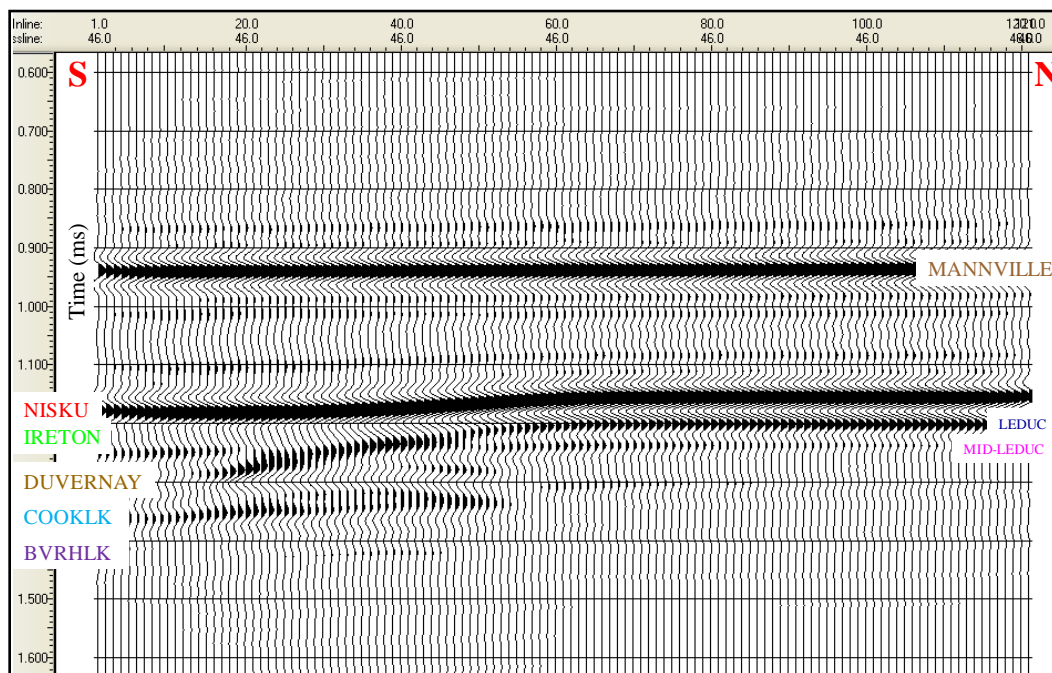


Figure 5.15: Radial component (PS) seismic section (crossline 46) after post-stack time migration, with interfaces identified on the section.

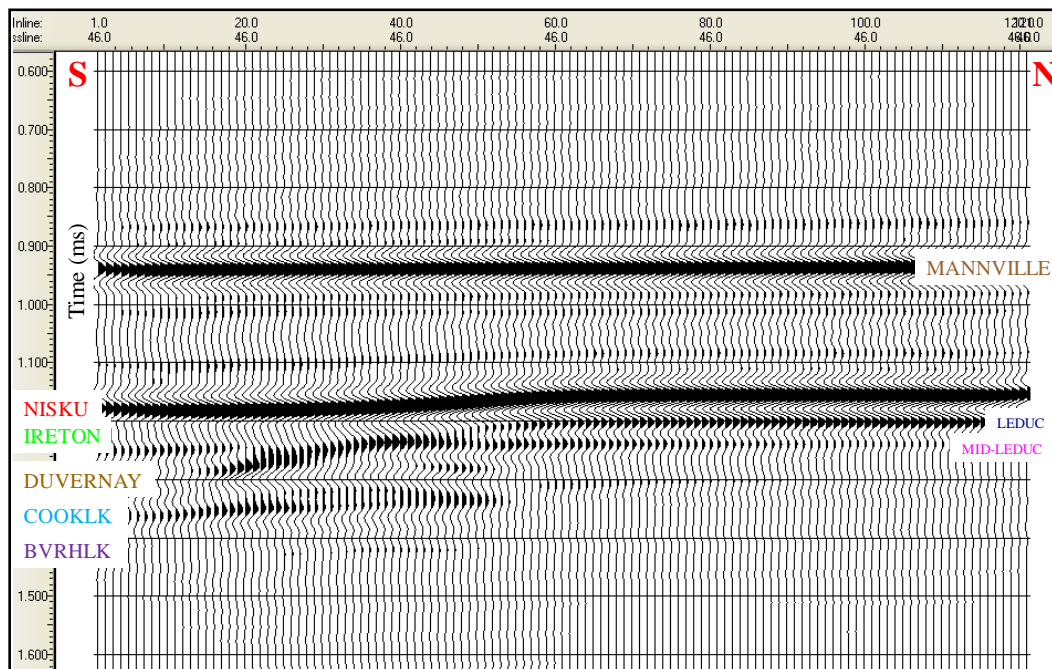


Figure 5.16: Radial component (PS) post-stack time migrated seismic section (crossline 46) after CO₂ fluid substitution in Upper Leduc member.

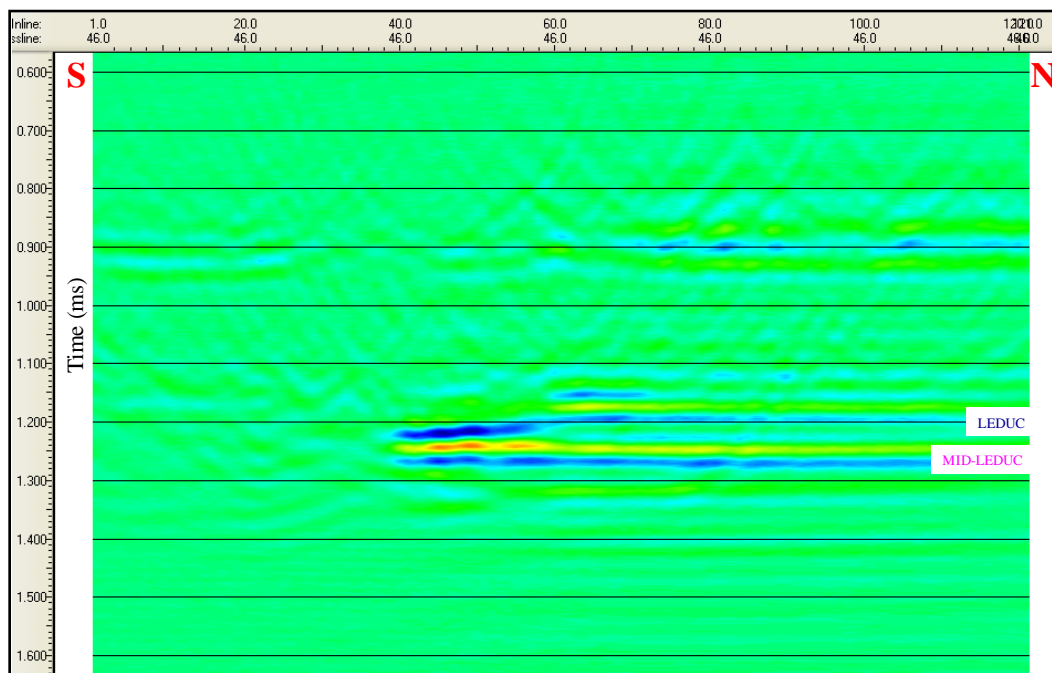


Figure 5.17: PS difference after post-stack time migration (crossline 46) before and after CO₂ fluid substitution. Color amplitude scale is 2 times of PP.

5.3.1.2 Pre-stack time migrated seismic section interpretation

Figure 5.18 and Figure 5.19 illustrate the PP pre-stack time-migrated seismic sections before and after 40% CO₂ fluid substitution in the upper Leduc member. All the formations display essentially the same seismic attributes as the PP post-stack time-migrated seismic sections, but with a little improvement. Also, a high amplitude reflection at the base of the Upper Leduc member and terminations of the Upper Leduc and Middle-Leduc events are enhanced. Positive time structure below the reef is still observed but compensated in the depth section (Figure 5.24 and Figure 5.25). A reduction in amplitude of the reflection at the top of Upper Leduc member, and an increase in the amplitude at the base of Upper Leduc near the reef edge are observed in the PP pre-stack time-migrated seismic section after CO₂ fluid substitution (Figure 5.19).

Figure 5.20 shows the time-lapse difference section for PP pre-stack time migrated seismic data before and after brine replaced with 40% CO₂ saturation. It is observed that there are higher amplitude difference at the top of upper-Leduc member, top of the rim, and base of upper-Leduc near the reef edge compared to PP time-lapse difference after post-stack time-migration, due to the enhancement of PSTM data.

Figure 5.21 and Figure 5.22 illustrate the PS pre-stack time-migrated seismic sections before and after CO₂ fluid substitution in the Upper Leduc member. All the formations display generally the same seismic attributes as the PP seismic sections but with lower frequency. Also, the high amplitude reflection at the base of upper-Leduc member and terminations of the Upper-Leduc and Middle-Leduc events are apparent on the PS seismic sections. Positive time structure below the reef still exists but corrected in the depth sections (Figure 5.27 and Figure 5.28).

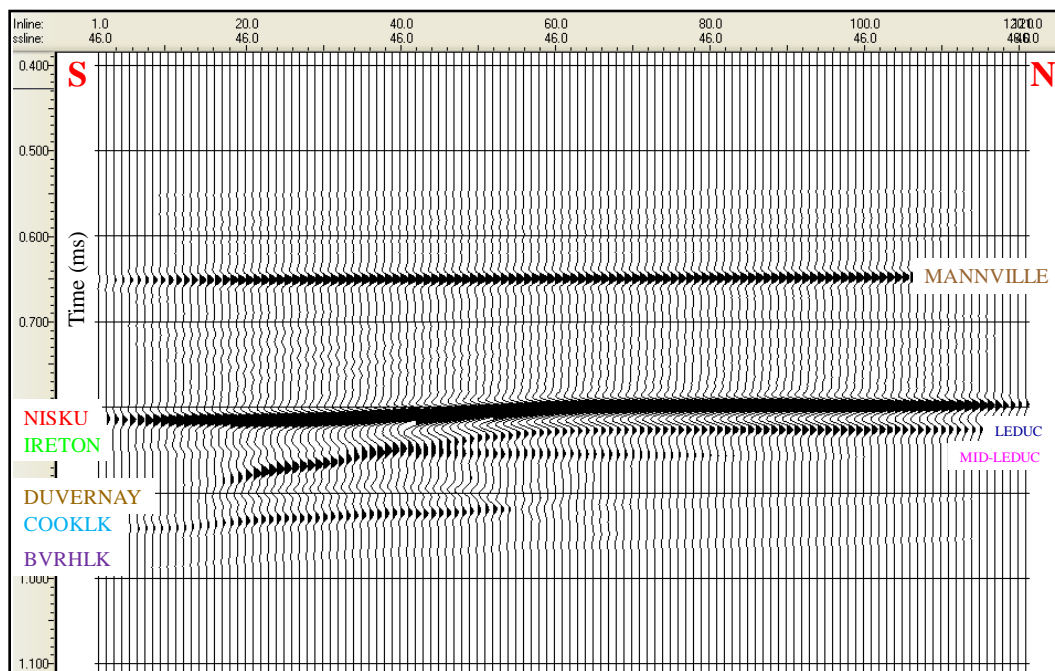


Figure 5.18: Vertical component (PP) seismic section (crossline 46) after pre-stack time migration, with interfaces identified on the section.

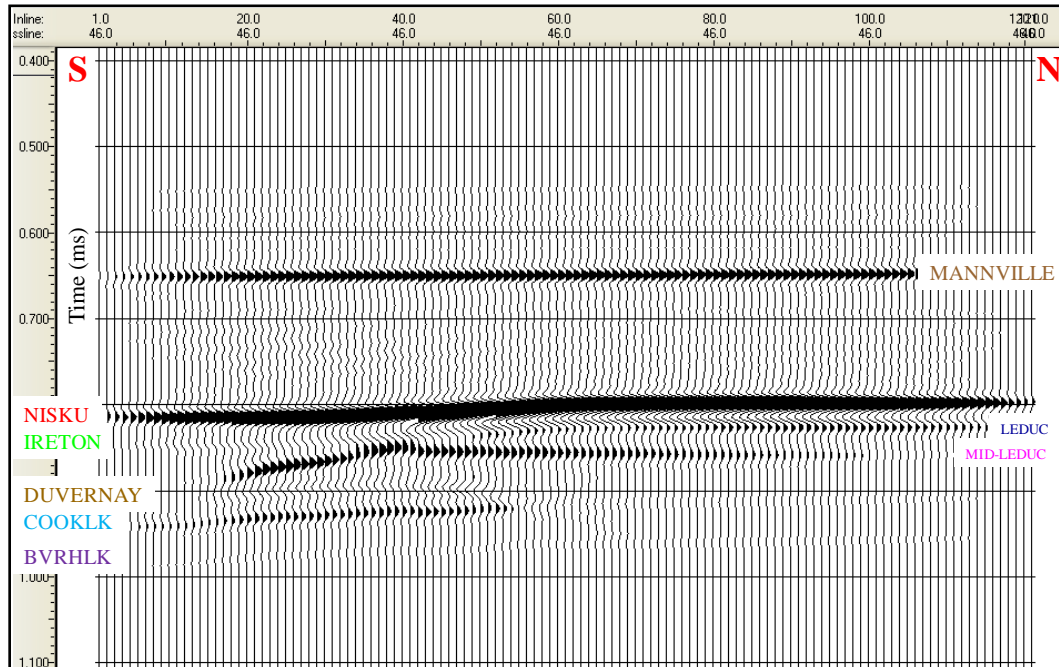


Figure 5.19: Vertical component (PP) pre-stack time migrated seismic section (crossline 46) after CO₂ fluid substitution in Upper Leduc member.

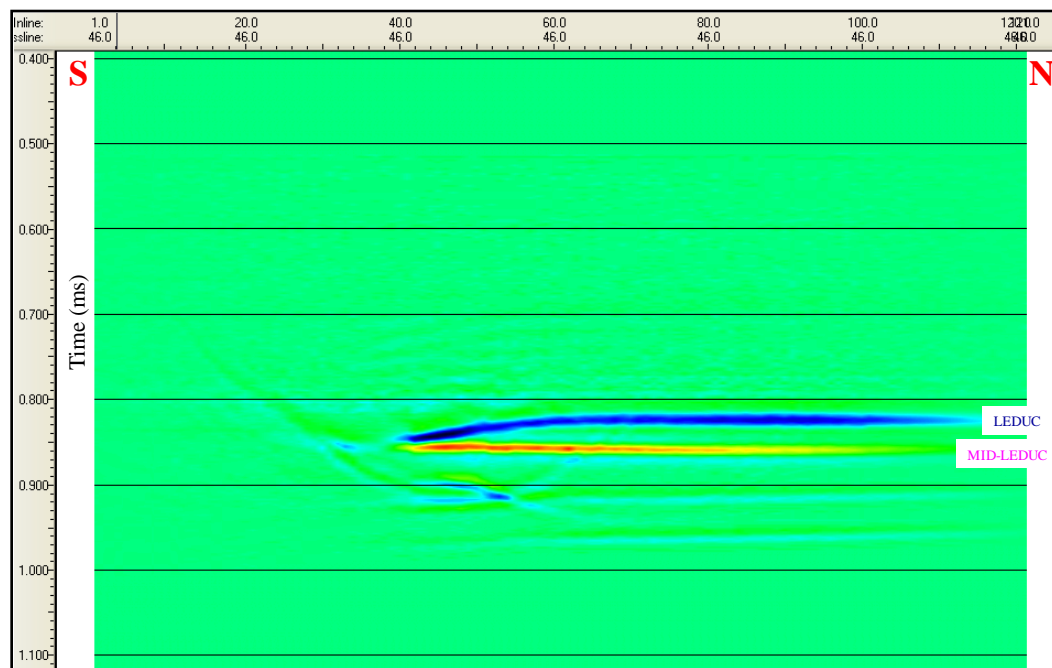


Figure 5.20: PP difference after pre-stack time migration (crossline 46) before and after CO₂ fluid substitution.

In the PS pre-stack time-migrated seismic section after brine replacement with CO₂, it is still noticed that there is less reduction in amplitude of the reflection from the top of Upper Leduc member, and a smaller increase in amplitude at base of upper-Leduc compared to the PP seismic section with 40% CO₂ saturation. Figure 5.23 shows the PS difference before and after CO₂ saturation after pre-stack time migration. There are significant differences at the top of Upper Leduc member, top of the rim, and base of Upper Leduc near the reef edge with some enhancements compared to PS time-lapse section after post-stack time-migration.

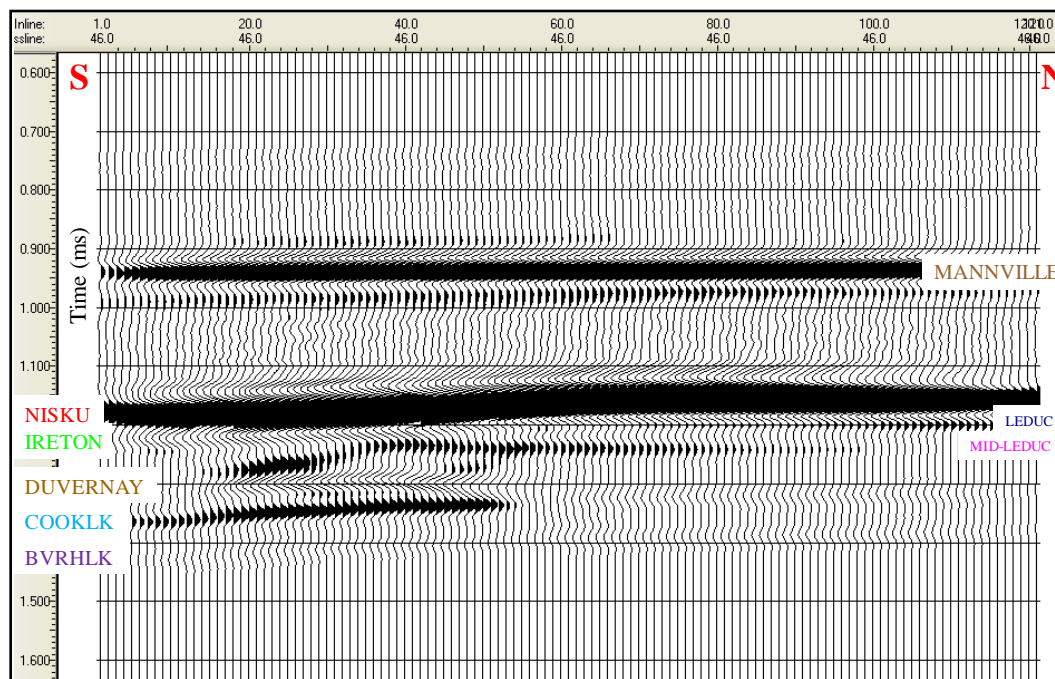


Figure 5.21: Radial component (PS) seismic section (crossline 46) after pre-stack time migration, with interfaces identified on the section.

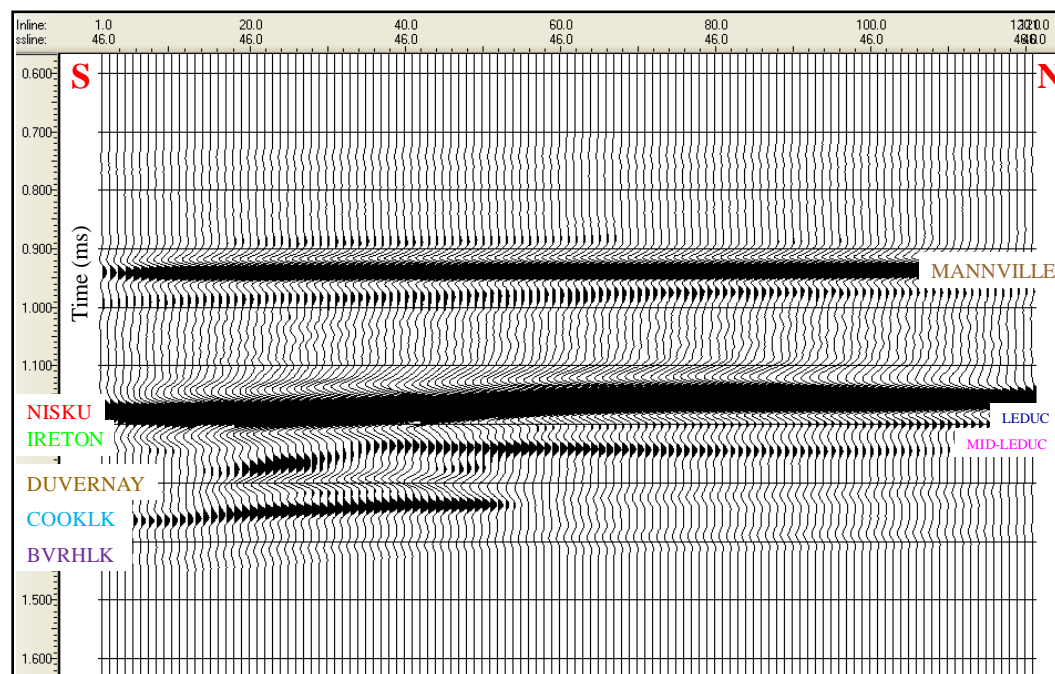


Figure 5.22: Radial component (PS) pre-stack time migrated seismic section (crossline 46) after CO₂ fluid substitution in Upper Leduc member.

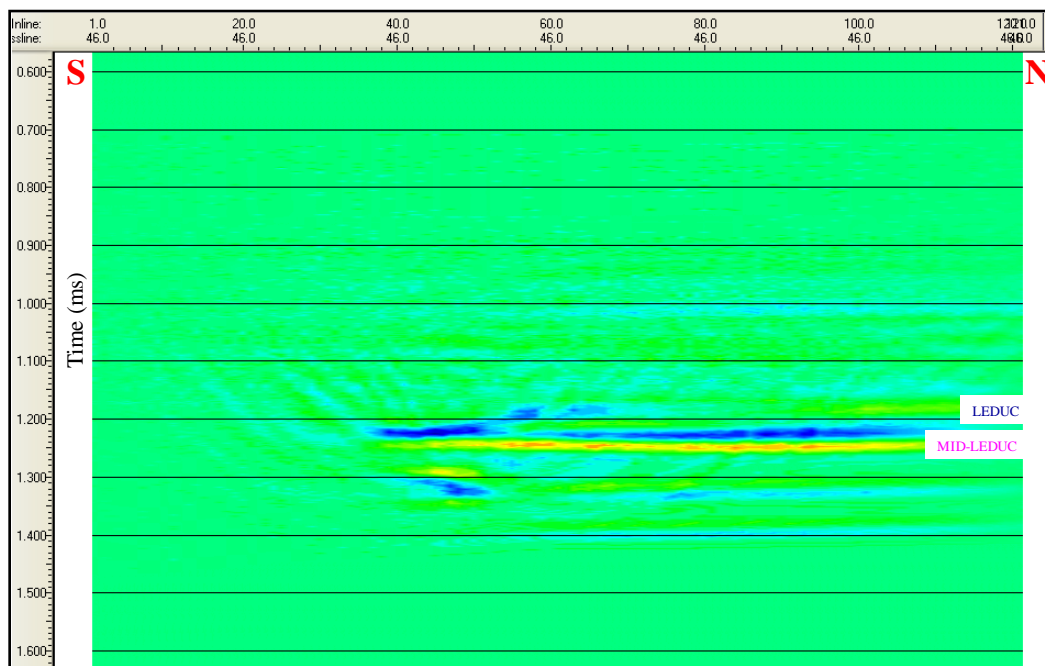


Figure 5.23: PS difference after pre-stack time migration (crossline 46) before and after CO₂ fluid substitution. Color scale is 4 times of PP.

5.3.1.3 Pre-stack depth migrated seismic section interpretation

Figure 5.24 and Figure 5.25 illustrate PP pre-stack depth-migrated seismic sections before and after CO₂ fluid substitution in the upper Leduc member. The Mannville, Nisku, Ireton, Leduc, Duvernay, Cooking Lake, and Beaverhill Lake events display generally the same seismic attributes as the PP time seismic sections. Also, a high amplitude reflection at the base of Upper Leduc member and terminations of the Upper Leduc and Middle-Leduc events are clear. Positive time structure below the reef is now corrected to being almost flat in depth. A decrease in reflection amplitude at the top of Upper Leduc member, and an increase in amplitude at the base of Upper Leduc near the reef edge are observed in the PP pre-stack depth-migrated seismic section after brine replacement with 40% CO₂ saturation (Figure 5.25).

Figure 5.26 shows the time-lapse difference section for PP pre-stack depth migration seismic data before and after CO₂ saturation. It is clear that there are high amplitude difference at the top of Upper Leduc member, top of the rim, and base of Upper Leduc near the reef edge. The high amplitude difference at Nisku Formation and formations below the reef is due to seismic migration artefacts using Paradigm GeoDepth software for 3D pre-stack depth migration processing work flow for PP and PS data.

Figure 5.27 and Figure 5.28 illustrate the PS pre-stack depth-migrated seismic sections before and after CO₂ fluid substitution. All the formations display mainly the same seismic attributes as the PP seismic sections. A high amplitude reflection at the base of the Upper Leduc member and terminations of the Upper-Leduc and Middle-Leduc events are apparent on the PS seismic sections. Also, positive time structure below the reef is now corrected in depth.

In the PS pre-stack depth-migrated seismic section after brine replacement with CO₂, it is noticed that there are reduction in reflection amplitude at the top of Upper Leduc member, and an increase in amplitude at base of Upper Leduc but less in effect than those in the PP seismic sections after CO₂ saturation. This is because of the small increase in S-wave velocity in the PS data with CO₂ saturation due to reduction in bulk density when brine replaced with CO₂ fluid.

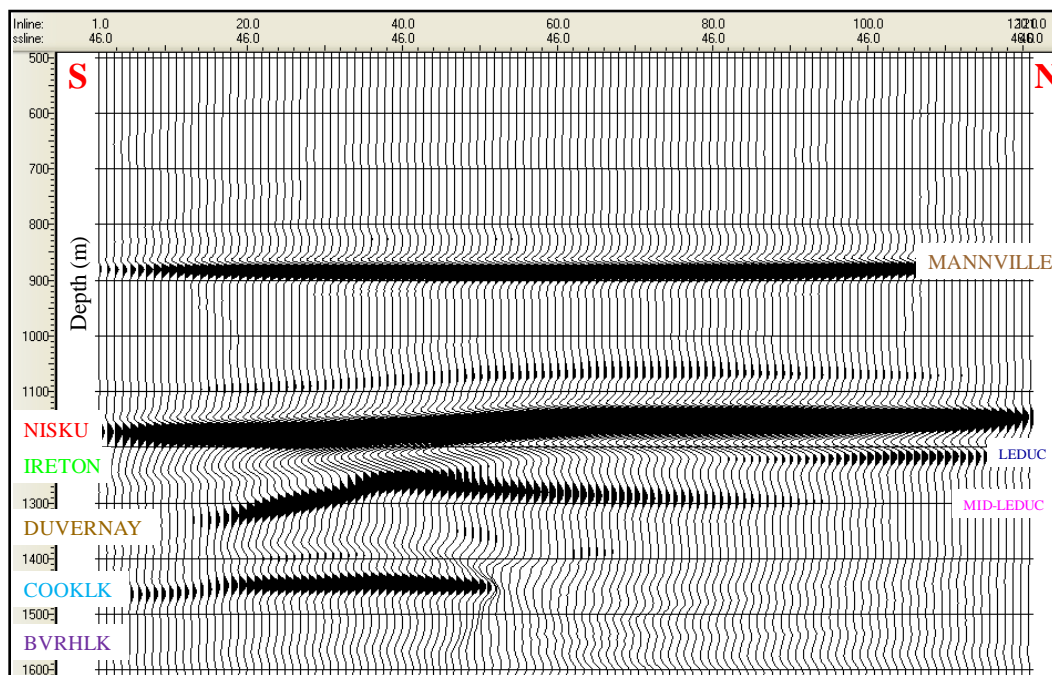


Figure 5.24: Vertical component (PP) seismic section (crossline 46) after pre-stack depth migration, with interfaces identified on the section.

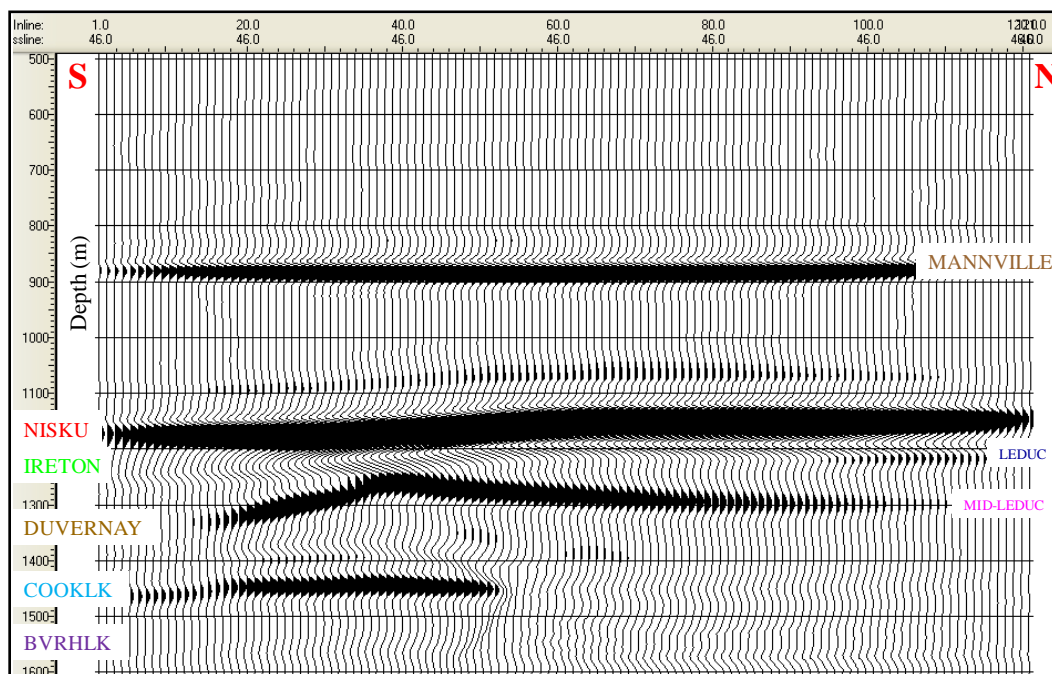


Figure 5.25: Vertical component (PP) pre-stack depth migrated seismic section (crossline 46) after CO₂ fluid substitution in Upper Leduc member.

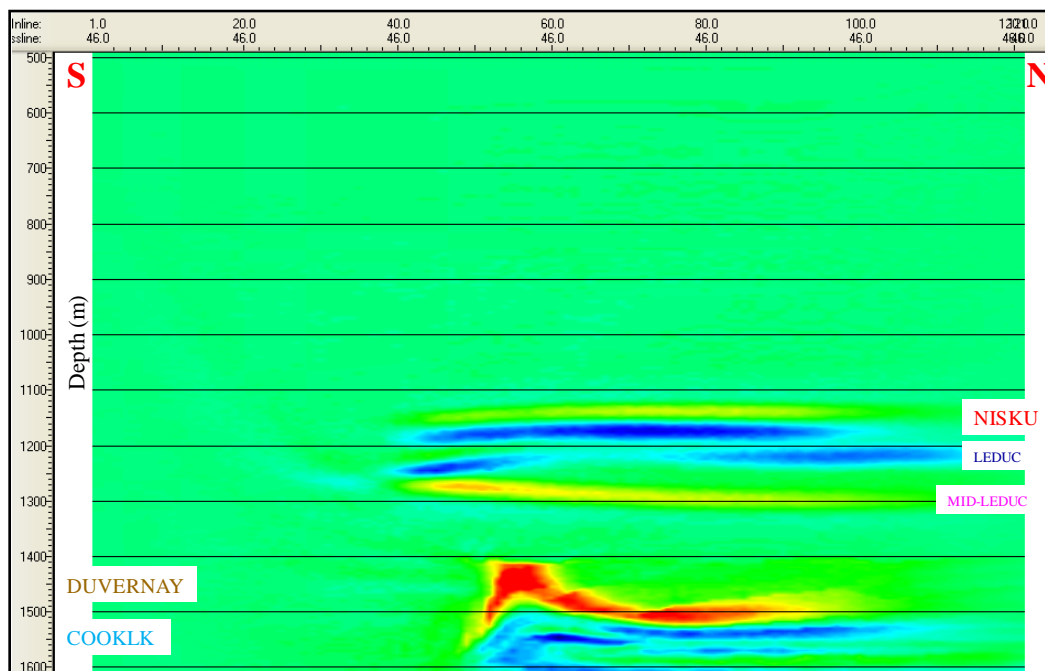


Figure 5.26: PP difference after pre-stack depth migration (crossline 46) before and after CO₂ fluid substitution.

Figure 5.29 shows the PS difference after pre-stack depth migration before and after 40% CO₂ fluid substitution. There are weak to moderate reflection differences at the top of upper-Leduc member, top of the rim, and base of upper-Leduc near the reef edge. This small difference is also due to a minor increase in S-wave velocity because of the bulk density reduction after brine replacement with CO₂.

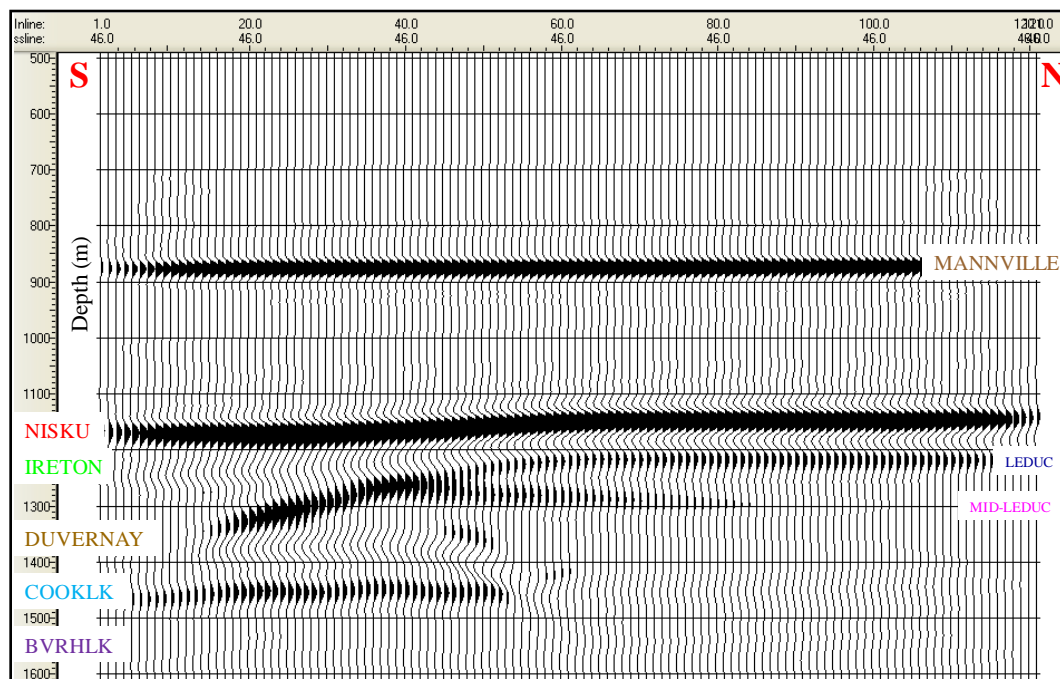


Figure 5.27: Radial component (PS) seismic section (crossline 46) after pre-stack depth migration, with interfaces identified on the section.

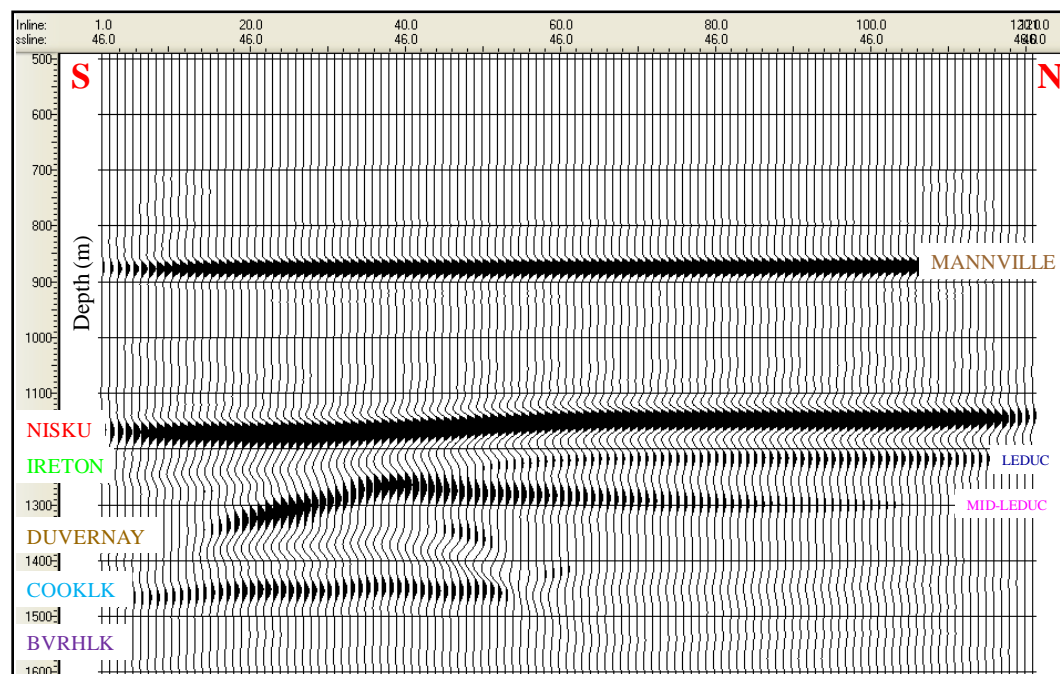


Figure 5.28: Radial component (PS) pre-stack depth migrated seismic section (crossline 46) after CO₂ fluid substitution in Upper Leduc member.

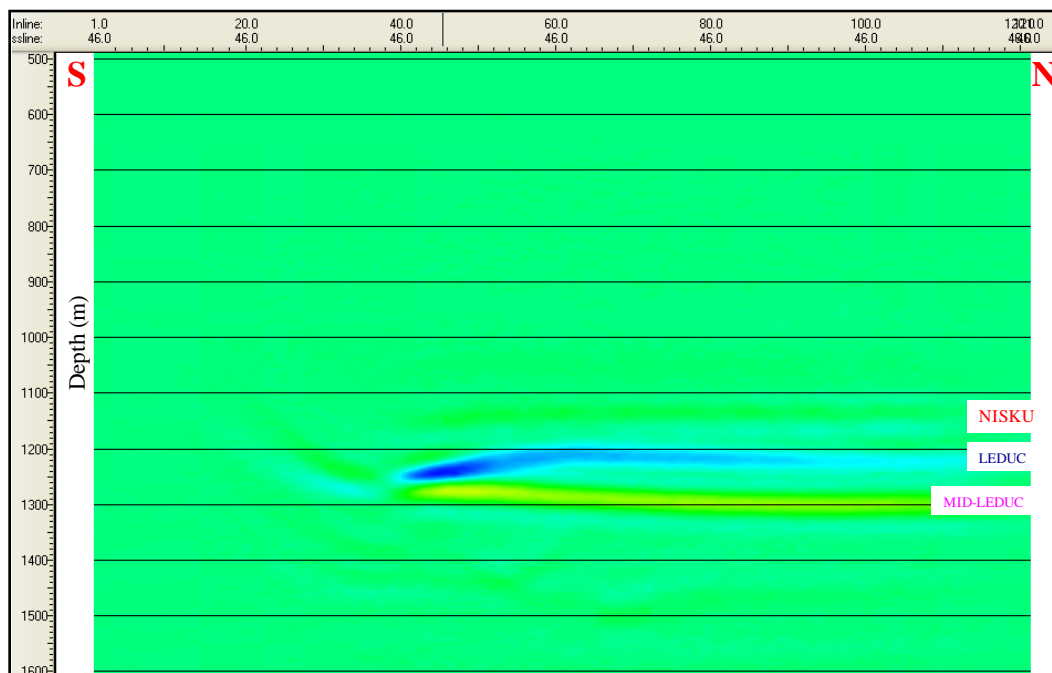


Figure 5.29: PS difference after pre-stack depth migration (crossline 46) before and after CO₂ fluid substitution.

5.3.2 Seismic attribute map interpretation

The 3D multicomponent seismic volumes were interpreted, and the Mannville, Nisku, Ireton, Leduc (Upper and Middle members), Duvernay, Cooking Lake and Beaverhill Lake events were picked. Then, amplitude maps of Leduc horizon (top of Upper Leduc Formation) and Mid-Leduc horizon (base of Upper Leduc Formation and top of Mid-Leduc member) were extracted to evaluate the seismic peak amplitude attribute for the top of upper-Leduc member, top of the rim, and the base of Upper Leduc near the reef edge for the lithofacies indication.

Time-lapse analysis was undertaken to examine the effect of 40% CO₂ fluid substitution on the horizon amplitude maps by taking the difference between two horizon amplitude

maps before and after replacement of brine with CO₂ at a 40% saturation level. The amplitude maps are shown in the PSTM and PSDM domain for both PP and PS seismic data before and after CO₂ saturation in Upper Leduc member as well as difference maps.

5.3.2.1 PSTM amplitude map interpretation

Figure 5.30 and Figure 5.31 illustrate the PP Leduc horizon amplitude maps after PSTM before and after 40% CO₂ fluid substitution in the upper Leduc member. The amplitude increases from the reef edge (south) toward the reef interior (north) due to the modelled porosity differences and consequently velocity and density differences between the foreslope facies in the reef rim and lagoonal facies within the central region of the reef. Figure 5.31 shows that there is an overall reduction in amplitude value by using the amplitude color scale as expected due to CO₂ saturation in Upper Leduc carbonate where the impedance contrast with the overlain Ireton shale is reduced. To identify the CO₂ saturation seismically, a difference amplitude map of Leduc horizon was undertaken by subtracting the Leduc horizon amplitude maps before and after CO₂ saturation where it shows a fairly good amplitude difference and therefore it is quite apparent to observe the CO₂ saturation in the target zone (Figure 5.32).

Figure 5.33 and Figure 5.34 illustrate the PP amplitude maps for the Mid-Leduc horizon, after PSTM, before and after CO₂ fluid substitution. A high amplitude is evident near the reef margin and but this event becomes weaker toward the interior facies due to the porosity differences between the reef rim and the internal reef. It is generally noticed that there is an overall increase in amplitude in Figure 5.34 due to CO₂ saturation in Upper

Leduc underlain by Mid-Leduc carbonate causing an increase in the impedance contrast. Figure 5.35 shows the amplitude difference map of Mid-Leduc horizon where the strong and significant amplitude differences demonstrates the feasibility of monitoring of CO₂ storage in Upper Leduc Formation.

Figure 5.36, Figure 5.37, Figure 5.39 and Figure 5.40 illustrate the PS Leduc and Mid-Leduc horizon amplitude maps after PSTM before and after CO₂ saturation in the upper Leduc member respectively. In Figure 5.36 and Figure 5.37, the amplitude increases from the reef edge toward the reef interior for Leduc horizon while decreases for Mid-Leduc horizon (Figure 5.39 and Figure 5.40) similar to PP amplitude maps. Figure 5.37 shows a lower reduction in amplitude values for Leduc horizon whereas there is a lesser increase in amplitude in Figure 5.40 for Mid-Leduc horizon compared to PP amplitude maps due to CO₂ saturation in Upper Leduc. This small anomaly in impedance contrast is because that the PS data is due to a slight increase in S-wave velocity due to reduction in bulk density after brine replacement with CO₂. The anomaly in Figure 5.36 is interpreted to be due to a differential tuning effect between Upper Leduc and Mid-Leduc members, where Mid-Leduc member is almost flat while the Upper Leduc member has topography relief causing this anomaly (Figure 5.11).

Difference amplitude maps of Leduc and Mid-Leduc horizons for PS data show reasonable amplitude differences and as a result they, along with the PP maps, verify the feasibility of monitoring the CO₂ saturation in Upper Leduc Formation by time-lapse multicomponent seismic surveys (Figure 5.38 and Figure 5.41).

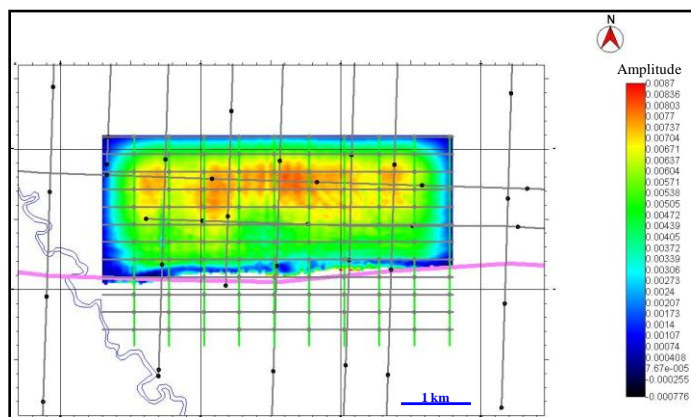


Figure 5.30: Amplitude map of Leduc horizon of (PP) PSTM seismic data. The pink color line is the Redwater reef southern edge.

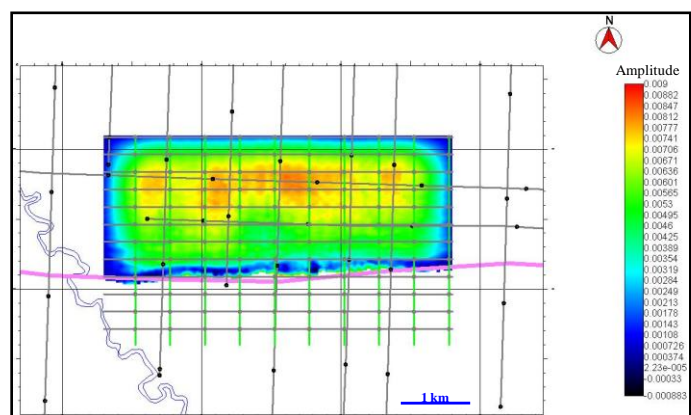


Figure 5.31: Amplitude map of Leduc horizon of (PP) PSTM seismic data after CO₂ fluid substitution in Upper Leduc member.

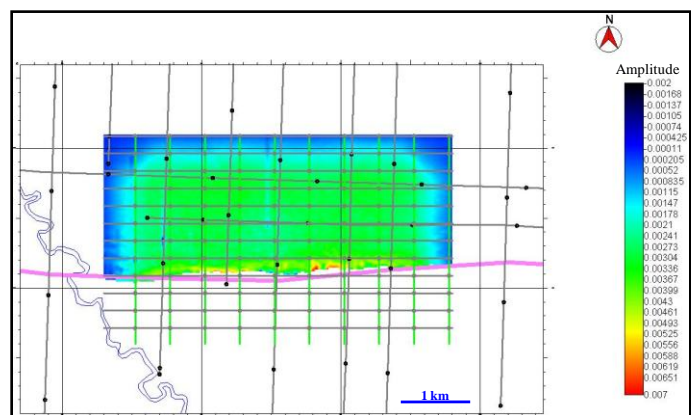


Figure 5.32: Amplitude map of Leduc horizon of PP difference after PSTM before and after CO₂ saturation.

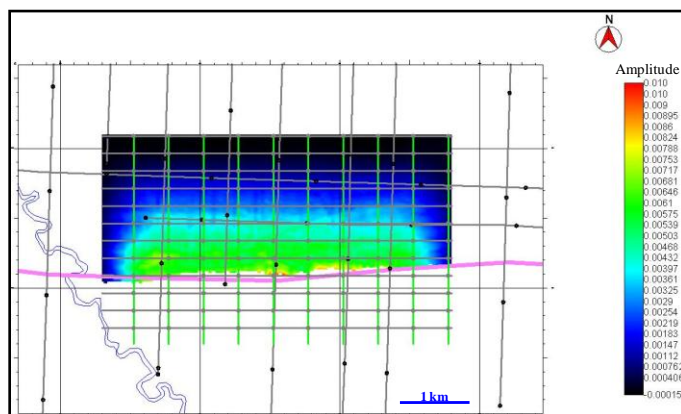


Figure 5.33: Amplitude map of Mid-Leduc horizon of (PP) PSTM seismic data.

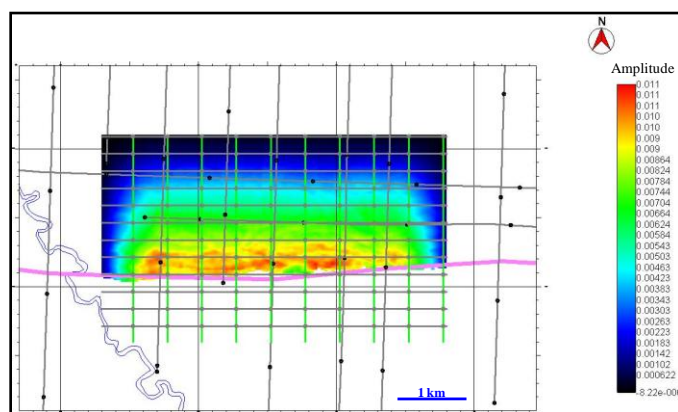


Figure 5.34: Amplitude map of Mid-Leduc horizon of (PP) PSTM seismic data after CO₂ fluid substitution in Upper Leduc member.

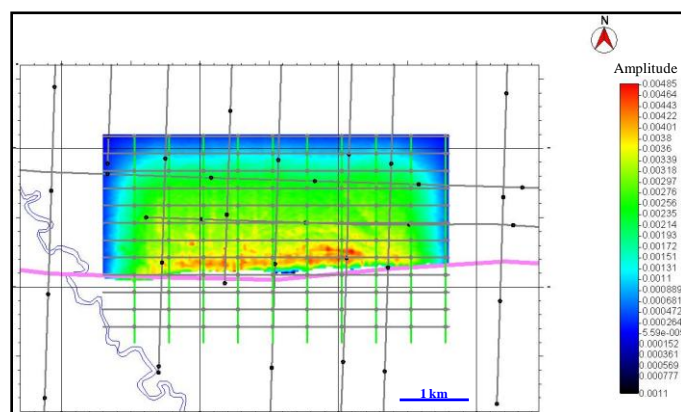


Figure 5.35: Amplitude map of Mid-Leduc horizon of PP difference after PSTM before and after CO₂ saturation.

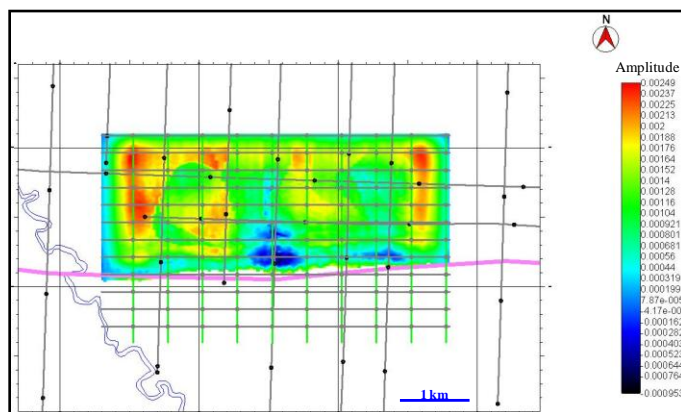


Figure 5.36: Amplitude map of Leduc horizon of (PS) PSTM seismic data.

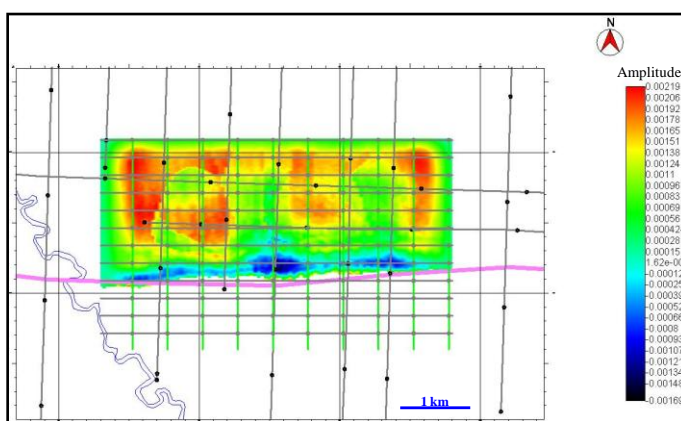


Figure 5.37: Amplitude map of Leduc horizon of (PS) PSTM seismic data after CO₂ fluid substitution in Upper Leduc member.

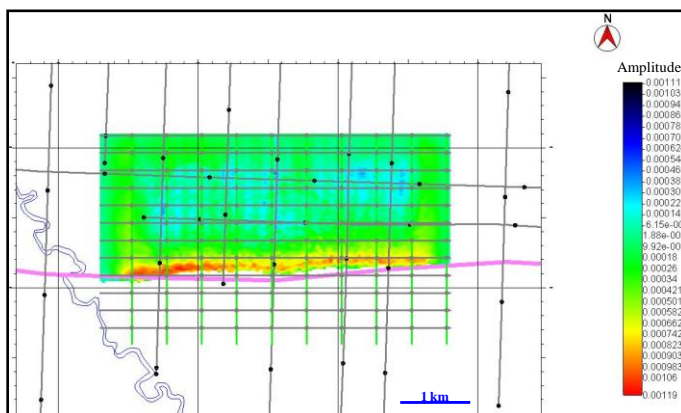


Figure 5.38: Amplitude map of Leduc horizon of PS difference after PSTM before and after CO₂ saturation.

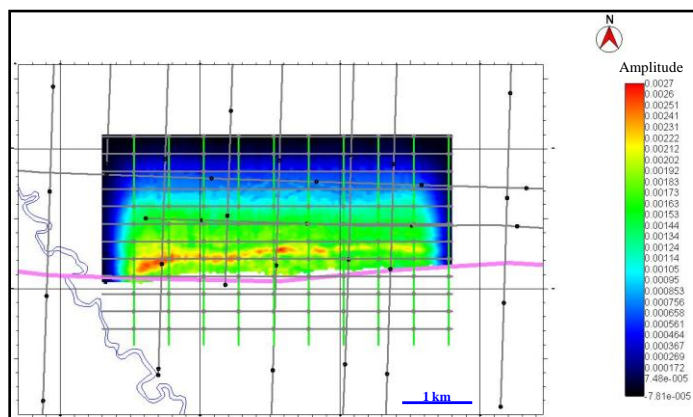


Figure 5.39: Amplitude map of Mid-Leduc horizon of (PS) PSTM seismic data.

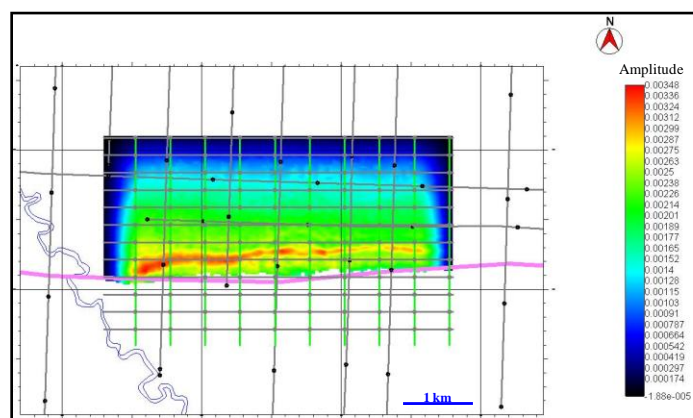


Figure 5.40: Amplitude map of Mid-Leduc horizon of (PS) PSTM seismic data after CO₂ fluid substitution in Upper Leduc member.

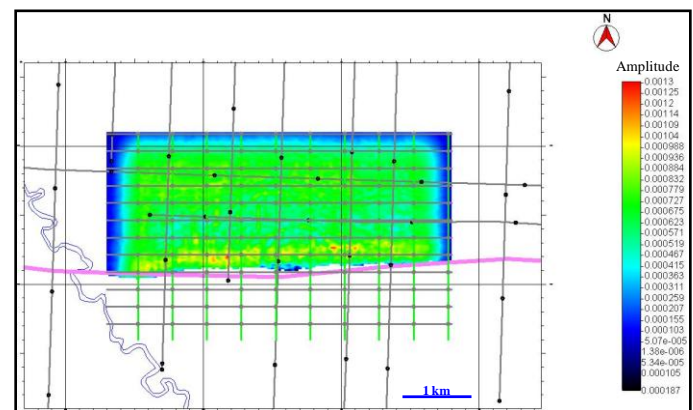


Figure 5.41: Amplitude map of Mid-Leduc horizon of PS difference after PSTM before and after CO₂ saturation.

5.3.2.2 PSDM amplitude map interpretation

Figure 5.42 and Figure 5.43 illustrate the PP Leduc horizon amplitude maps after PSDM before and after 40% CO₂ fluid substitution in the Upper Leduc member. The event amplitudes still increase from the reef edge toward the reef interior, similar to PSTM data. Figure 5.43 shows also an overall reduction in amplitude value due to CO₂ saturation in Upper Leduc interval and Figure 5.44 shows the amplitude difference map of the Leduc horizon. The amplitude differences after PSDM confirm the feasibility of monitoring CO₂ storage in Upper Leduc Formation.

Figure 5.45 and Figure 5.46 illustrate the PP amplitude maps of Mid-Leduc horizon after PSDM, before and after CO₂ fluid substitution. High amplitude are apparent near the reef margin but become weaker toward the interior facies similar to results after PSTM. It is also observed that there is an increase in amplitude value in Figure 5.46 due to CO₂ saturation in Upper Leduc zone. Difference amplitude map of the Mid-Leduc horizon shows strong and significant amplitude differences which is comparable to PSTM data (Figure 5.47).

Figure 5.48, Figure 5.49, Figure 5.51 and Figure 5.52 demonstrate the PS Leduc and Mid-Leduc horizon amplitude maps after PSDM, before and after CO₂ saturation in the Upper Leduc member respectively. In Figure 5.48 and Figure 5.49, the amplitude increases from the reef margin to the reef interior for Leduc horizon but decreases for the Mid-Leduc horizon (Figure 5.51 and Figure 5.52) similar to PSTM data. Figure 5.49 shows a less decrease in amplitude value for Leduc horizon while a lower amplitude increase is shown

in Figure 5.52 for the Mid-Leduc horizon when compared to the PP amplitude maps due to CO₂ saturation. This is just because only the reduction in bulk density influences the PS data when brine is replaced with CO₂.

Figure 5.50 and Figure 5.53 illustrate the PS difference amplitude maps of Leduc and Mid-Leduc horizons after PSDM and show fairly good amplitude differences and therefore they are similar to the PP amplitude maps in demonstrating the monitoring potential to evaluate of CO₂ saturation using 4D multicomponent seismic data. It is noticed that there are some stripes in the horizon amplitude maps. This anomaly is possibly due to acquisition footprint, as illustrated from the effective fold for a synthetic 3C 3D survey design acquired with an effective maximum offset of 1500m (Figure 5.54).

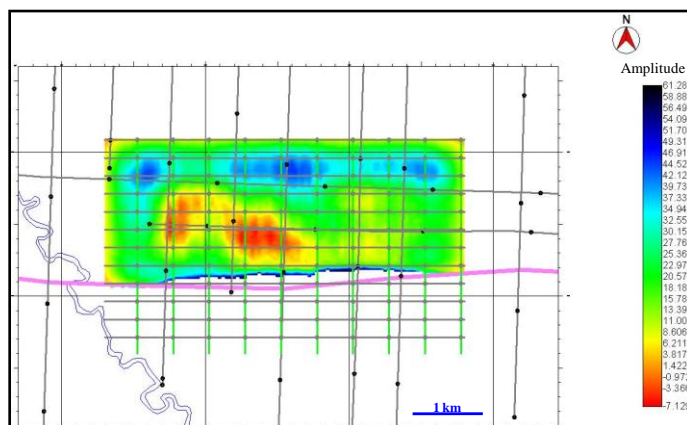


Figure 5.42: Amplitude map of Leduc horizon of (PP) PSDM seismic data.

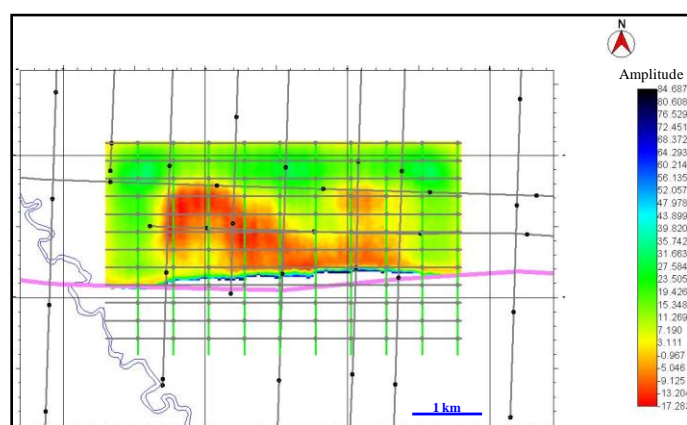


Figure 5.43: Amplitude map of Leduc horizon of (PP) PSDM seismic data after CO₂ fluid substitution in Upper Leduc member.

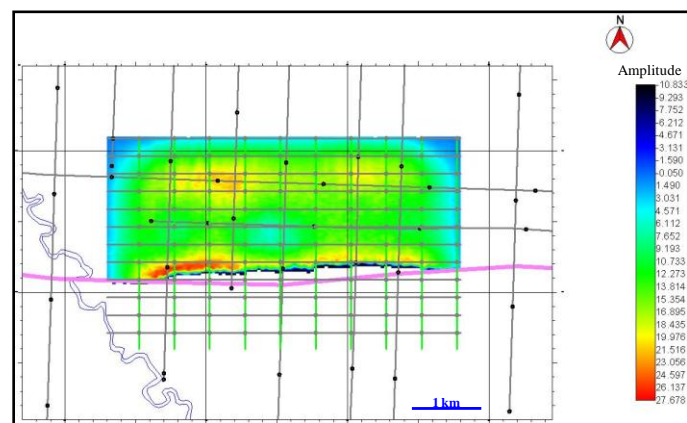


Figure 5.44: Amplitude map of Leduc horizon of PP difference after PSDM before and after CO₂ saturation.

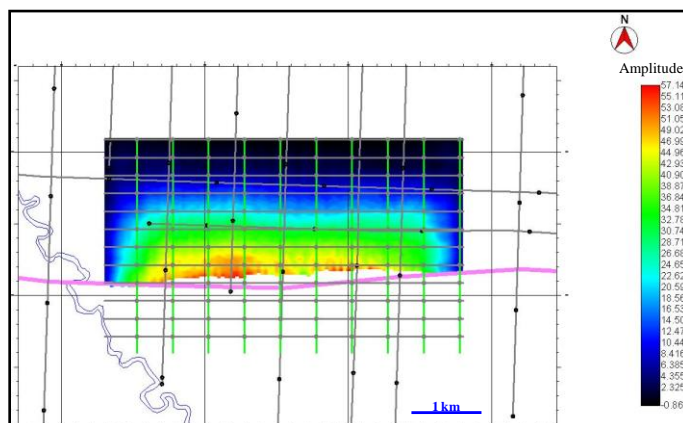


Figure 5.45: Amplitude map of Mid-Leduc horizon of (PP) PSDM seismic data.

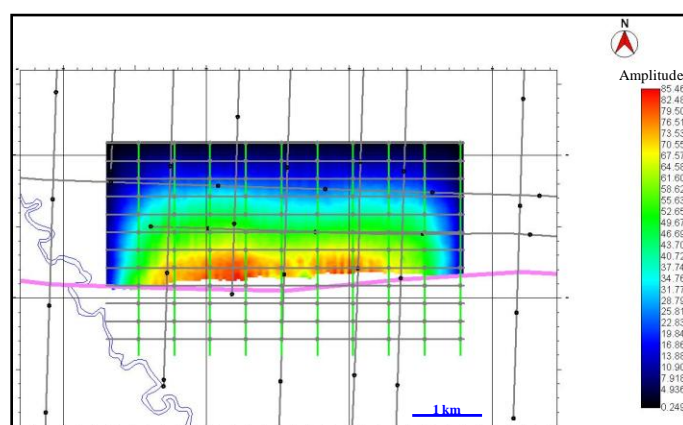


Figure 5.46: Amplitude map of Mid-Leduc horizon of (PP) PSDM seismic data after CO₂ fluid substitution in Upper Leduc member.

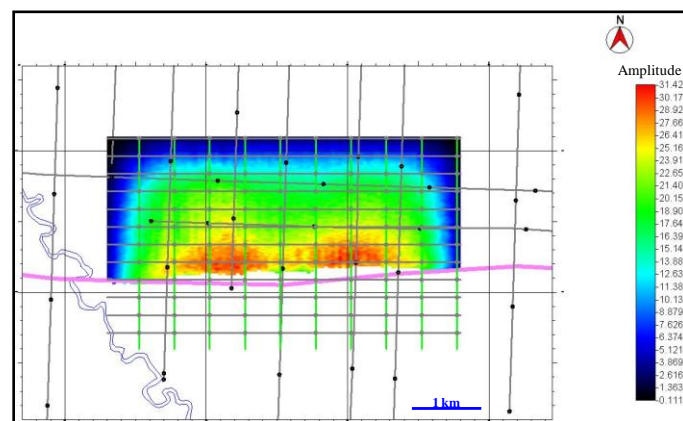


Figure 5.47: Amplitude map of Mid-Leduc horizon of PP difference after PSDM before and after CO₂ saturation.

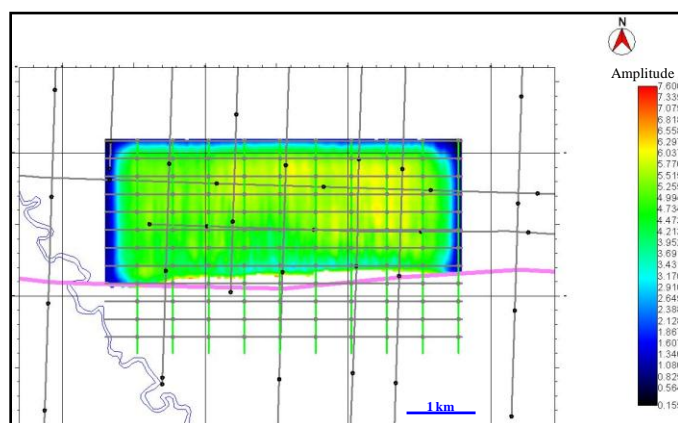


Figure 5.48: Amplitude map of Leduc horizon of (PS) PSDM seismic data.

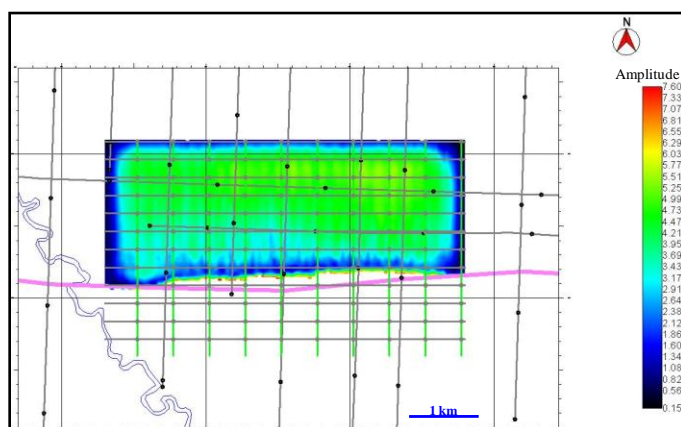


Figure 5.49: Amplitude map of Leduc horizon of (PS) PSDM seismic data after CO₂ fluid substitution in Upper Leduc member.

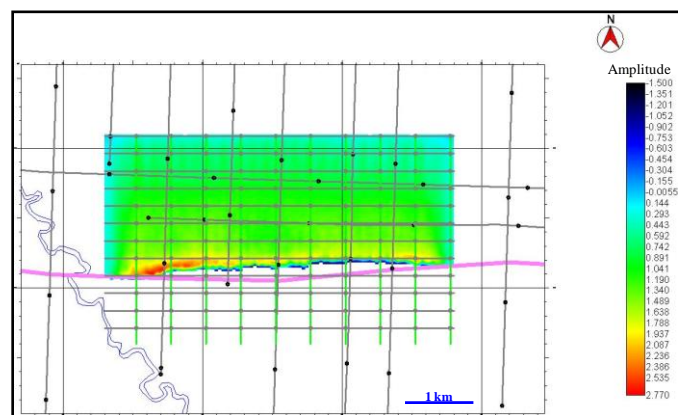


Figure 5.50: Amplitude map of Leduc horizon of PS difference after PSDM before and after CO₂ saturation.

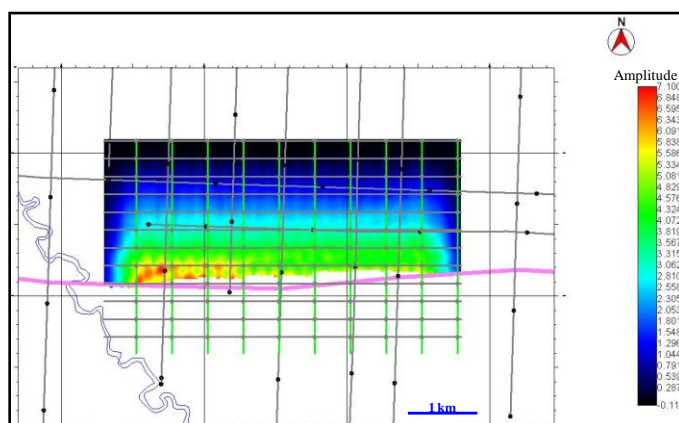


Figure 5.51: Amplitude map of Mid-Leduc horizon of (PS) PSDM seismic data.

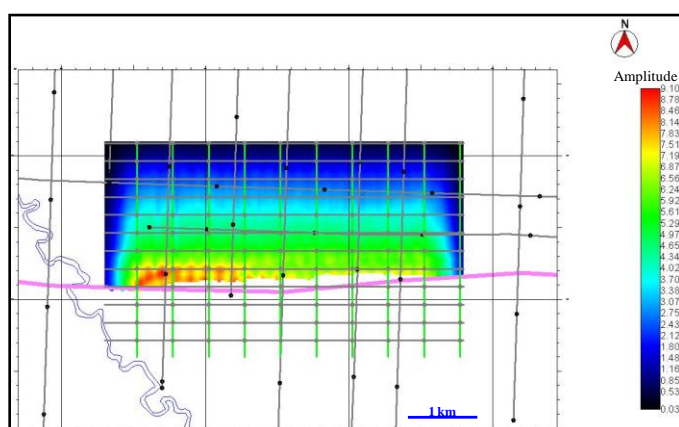


Figure 5.52: Amplitude map of Mid-Leduc horizon of (PS) PSDM seismic data after CO₂ fluid substitution in Upper Leduc member.

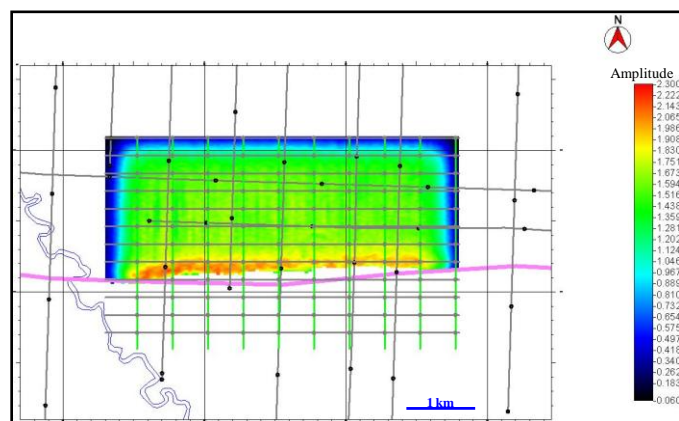


Figure 5.53: Amplitude map of Mid-Leduc horizon of PS difference after PSDM before and after CO₂ saturation.

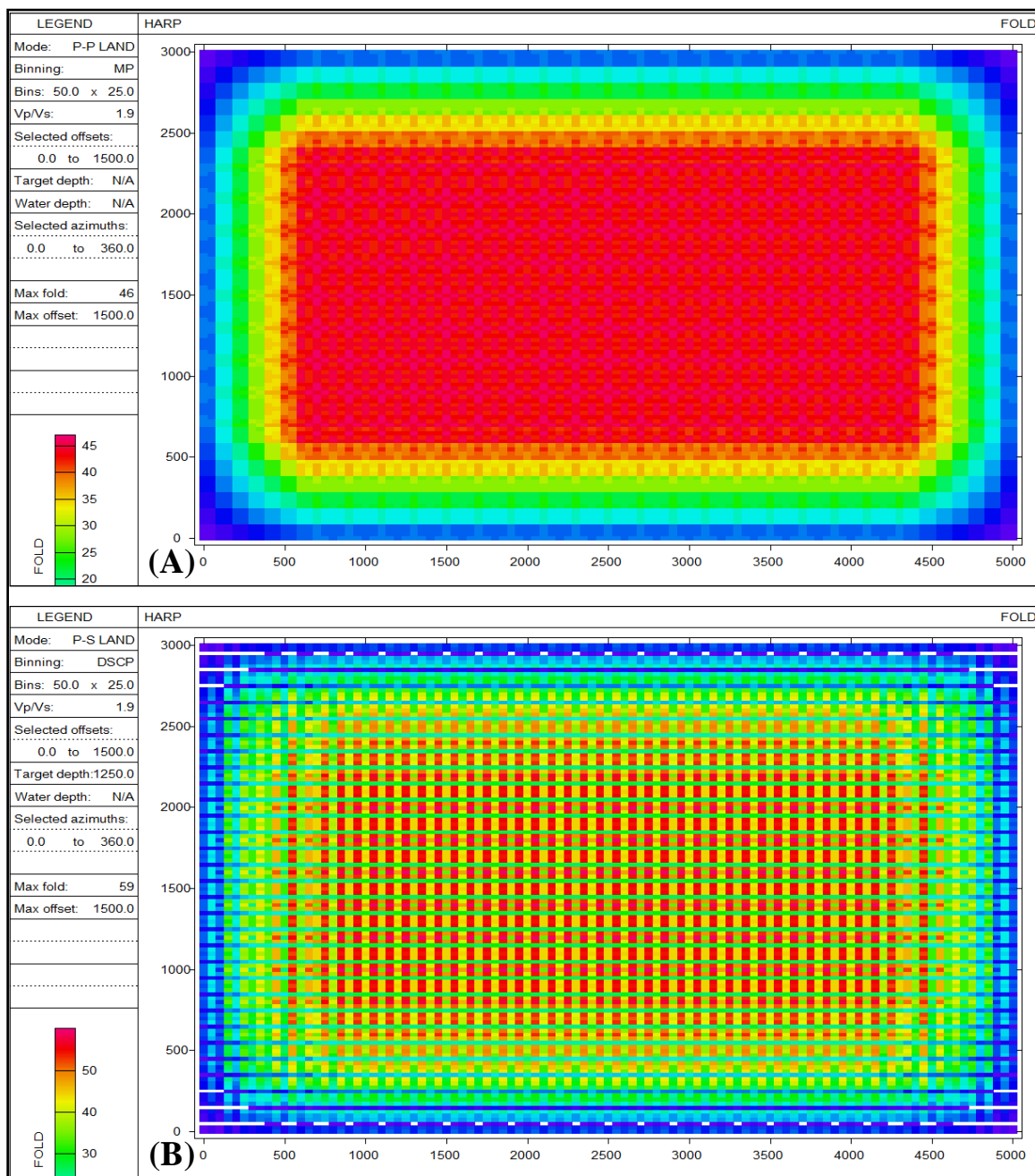


Figure 5.54: Fold distribution maps of (A) PP and (B) PS acquisition survey with maximum offset of 1500m.

5.4 Conclusions

The 3D multicomponent synthetic seismic sections after post-stack time migration, pre-stack time migration and pre-stack depth migration demonstrate similar seismic attributes for the Mannville, Nisku, Ireton, Leduc (Upper Leduc and Mid-Leduc members), Duvernay, Cooking Lake, and Beaverhill Lake formations before and after CO₂ saturation. The Cooking Lake and Beaverhill Lake Formations display positive structure below the reef in the PP and PS time sections due to a lateral velocity change. This structure is apparent on time sections and is compensated to being nearly flat after PSDM.

Terminations and the lateral position of the Upper Leduc and Middle Leduc events are evident on the PP and PS seismic sections after post-stack time migration and are enhanced on the PSTM and PSDM sections. The reef rim is observed clearly at the reef margin. Amplitude increase for the Upper Leduc and amplitude decrease for the Mid-Leduc members toward the interior reef are evident on both PP and PS seismic sections and horizon amplitude maps due to porosity differences between the foreslope facies in the reef rim and tidal flat lagoonal facies in the central region of the reef.

In the PP sections and horizon amplitude maps after CO₂ saturation, there is a reduction in amplitude for Leduc horizon and an increase in Mid-Leduc horizon compared to baseline due to CO₂ saturation in Upper Leduc interval. The PS CO₂ saturated sections and horizon amplitude maps illustrate a lower reduction in amplitude for the Leduc horizon and a smaller increase in amplitude for the Mid-Leduc horizon compared to PP

monitor sections and amplitude maps. This small anomaly is because that the PS data is simply influenced only by a reduction in bulk density after replacement of brine with CO₂.

Time-lapse analysis after PSTM and PSDM shows significant amplitude differences for the Upper Leduc and Mid-Leduc members before and after 40% CO₂ saturation for both PP and PS seismic sections and horizon amplitude maps. The 4D multicomponent synthetic seismic data results illustrate that it is feasible to monitor the CO₂ saturation within the Redwater Reef by repeated 3D multicomponent seismic surveys.

Chapter Six: **DISCUSSION AND CONCLUSIONS**

6.1 Introduction

One objective of this chapter was to discuss the capacity of CO₂ storage in Redwater Devonian reef in detail with different scenarios and circumstances. In this section, the suitable ranges of the storage efficiency factor and the determination of the CO₂ storage capacity for the entire Redwater reef as well as for each interval are discussed. This is followed by conclusions of the dissertation with discussions about the surface 2D seismic data, time-lapse 2D and 3D multicomponent seismic modeling of fluid substitution and the feasibility to monitor the CO₂ saturation within the Redwater Leduc Reef.

Assumptions, limitations, implementations of the dissertation and comparison of the results with other CCS projects are also summarized. Finally, several recommendations for future work for the HARP project to be implemented are provided.

6.2 CO₂ storage capacity in the Redwater Leduc reef

Storage capacity of CO₂ is very important resource for industrial and commercial projects. According to Kaldi and Bachu (2009), there is a difference between theoretical pore volume (the total amount of pore space that can store CO₂ in the subsurface geological formations) and storage capacity (the pore volume restricted by some factors like technical, engineering, economic or regulatory feasibility limitations). The storage efficiency factor for the suitable formation explains the fraction of total pore space available for CO₂ storage controlled by heterogeneity, buoyancy effects, residual water saturation (Bachu and Adams, 2003).

The current method involves estimating storage capacity of open formations from which the local fluid can easily escape laterally and make space for the injected CO₂ allowing for a larger effective storage efficiency factor to take place (Doughty and Pruess, 2004; Holloway et al., 1996; Shafeen et al., 2004; and Van der Meer, 1995). The large amount of local brine laterally displaced by the CO₂ in the open system may have a hydrological and geochemical impact on shallow groundwater resources (Birkholzer et al., 2007; and Zhou et al., 2008). On the other hand, when a reservoir bounded vertically by impermeable seals or surrounded on all sides by barriers of very low permeability, then this reservoir operates as a closed system yielding to a smaller effective storage efficiency factor (Muggeridge et al., 2004; Neuzil, 1995; Puckette and Al-Shaieb, 2003).

Deep reservoirs illustrate higher storage efficiency factor compared to shallow reservoirs (Kopp et al., 2008). The typical storage efficiency factor ranges from 5 – 40 % in carbonate and clastic formations (Anthonsen et al., 2009; and EU GeoCapacity Project, 2009). Volumetric equation for the calculation of CO₂ storage capacity in geological formations (DOE, 2006) is given by:

$$M_{CO_2} = A \cdot h \cdot \phi \cdot \rho \cdot E$$

where:

M_{CO₂} is mass estimate of CO₂ storage capacity of brine geological formation,

A is geographical area that defines the region assessed for CO₂ storage-capacity,

h is gross thickness of brine formations within the region defined by **A** assessed for CO₂ storage-capacity,

φ is average porosity of brine formation within the region defined by **A** and **h** assessed for CO₂ storage-capacity,

ρ is density of CO₂ evaluated at pressure and temperature that represents storage conditions anticipated for a specific geologic unit averaged over **h**,

E is CO₂ storage (sweep) efficiency factor that reflects the fraction of the total pore volume filled by CO₂.

This equation was used to estimate the CO₂ storage capacity in the full Redwater Leduc reef. The result shows that the CO₂ storage capacity is about 800 Mt CO₂ using the full reef area (blue line) of 527 km² (Figure 6.1) taking in to consideration the latest seismic interpretation (Sodagar and Lawton, 2010h), average thickness of 270 m, assuming a reef average porosity of 6%, CO₂ density of 0.4676 g/cc and storage efficiency factor of 20%. This result is for the entire Redwater reef (including the oil-leg and water-leg) but since this dissertation has focussed on the water-leg area (including wells and formation maps), detailed storage capacity of CO₂ has been calculated for the different Redwater reef intervals (Table 6.1) with different CO₂ storage efficiency factors ranging from 10% to 40%.

The Redwater Leduc reef was divided geologically to three members (Upper Leduc, Mid-Leduc and Lower Leduc). The CO₂ storage capacity was determined for each member.

Furthermore, the Upper Leduc was separated into the reef rim (high porosity and thick) and the central region of the reef (low porosity and thin) for more precise estimation of storage capacity (Figure 6.1). The CO₂ storage capacity of the water-leg area in the Upper Leduc member only is 163 Mt, and in the full Redwater Leduc reef is 352 Mt for the average of storage efficiency factor of 20% (Table 6.1). Furthermore, the CO₂ storage capacity of the Cooking Lake Formation below the water-leg area is estimated by 124 Mt, and below the total area of Redwater Leduc reef is 174 Mt for the same storage efficiency factor of 20%.

After estimating the CO₂ storage capacity using the average values of the volumetric equation parameters such as the area, thickness and porosity of each member interval, uncertainties were also considered by calculating the standard deviation for each interval zone (Table 6.1). Firstly, the CO₂ storage capacity was estimated for each interval using the high values of the volumetric equation parameters. Secondly, it was again estimated using the low values of the parameters. Then, the standard deviation of the CO₂ storage capacity values was computed for each interval to estimate the error and give an estimate of the variation from the average value in each case.

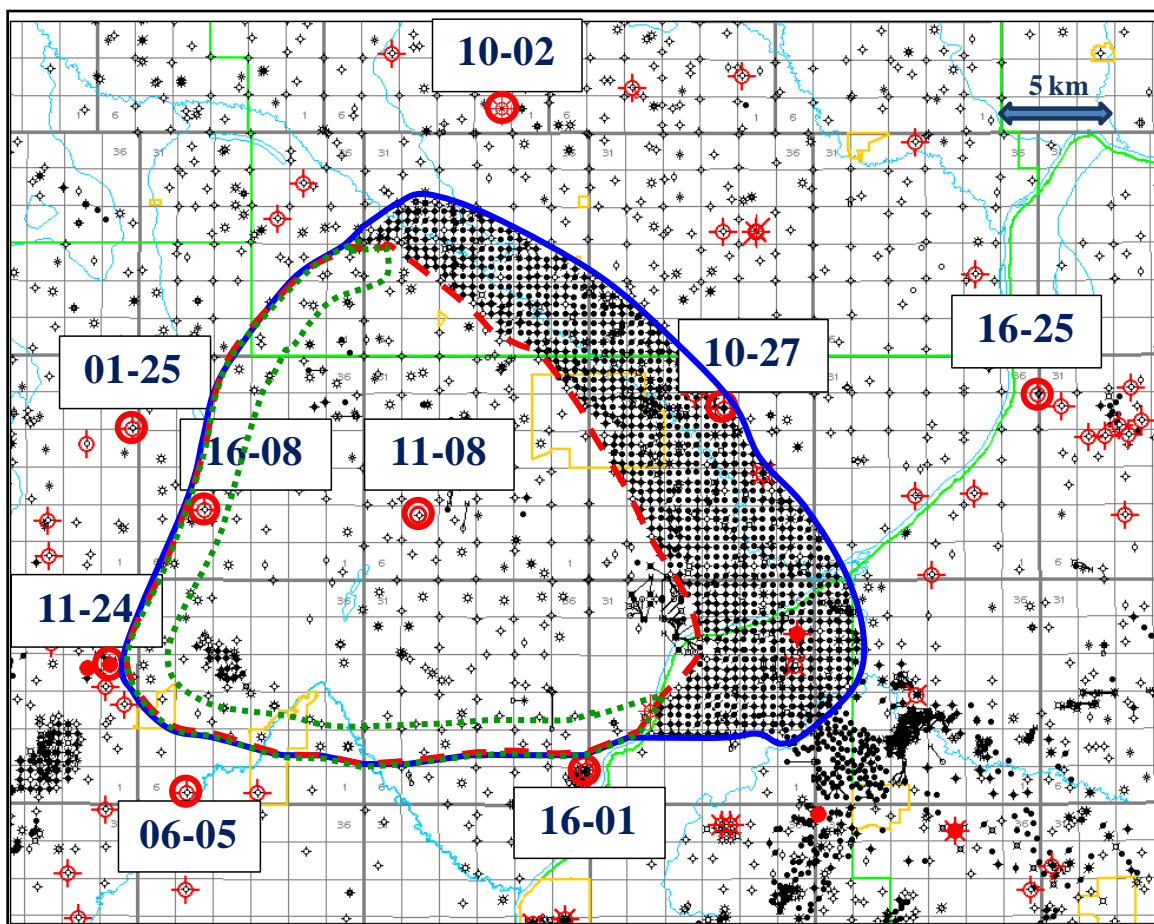


Figure 6.1: Redwater reef map showing all wells. Those wells that penetrate the Cooking Lake Formation and have sonic logs are highlighted in red. The blue color line presents the Redwater reef margin, the dashed red line outlines the reef water-leg scope and the dotted green line delineates the Redwater reef rim in the water-leg region.

Table 6.1: Redwater reef calculated CO₂ storage capacity with different scenarios

Water-leg reef intervals	Area (km ²)	Thickness (m)	Porosity	CO ₂ Storage Capacity (Mt) (E=0.1)	CO ₂ Storage Capacity (Mt) (E=0.2)	CO ₂ Storage Capacity (Mt) (E=0.4)
Upper Leduc member (reef center only)	308.6	101	0.03	44 ± 8	88 ± 16	176 ± 32
Upper Leduc member (reef rim only)	67.4	132	0.09	37.5 ± 7	75 ± 14	150 ± 28
Upper Leduc member	376	101-132	0.03-0.09	181.5 ± 15	163 ± 30	326 ± 60
Mid-Leduc member	345	98	0.04	63.5 ± 16	127 ± 32	254 ± 64
Lower-Leduc member	345	55	0.035	31 ± 5	62 ± 10	124 ± 20
Mid-Leduc and Lower-Leduc members	345	153	0.035-0.4	94.5 ± 21	189 ± 42	378 ± 84
Full Leduc reef	345-376	254-285	0.03-0.09	176 ± 36	352 ± 72	704 ± 144
Cooking Lake Formation	376	88	0.04	62 ± 9	124 ± 18	248 ± 36

6.3 Discussion about assumptions used in the Dissertation

Some assumptions were considered for the fluid substitution modeling. First, the rock is assumed to be homogeneous. Second, all the pores are in communication and the pores are filled with a frictionless fluid. Third, the un-drained rock-fluid system is assumed to be closed, and the pore fluid will not soften or harden the rock frame. Fourth, the shear modulus stays constant during fluid substitution when using the Gassmann's equations. This means that the shear modulus for an isotropic and homogeneous media does not depend on the pore fluids, but if the pores are not in communication or cracks happen in the reservoir, this assumption would be violated.

In addition, during the fluid substitution process an equilibrium saturation model (end-state situation or final stage) was assumed. However, during the CO₂ injection, the equilibrium distribution of fluids will be disturbed and employing a patchy saturation model would perhaps be more practical and realistic than the equilibrium saturation model used. Furthermore, the effects of the pressure, temperature and viscosity variations in the reservoir were also not taken in consideration. All of these variables were not included in the fluid substitution modeling because of the lack of this information at Redwater reef. This was due to termination of the HARP project which impacted the acquiring of new field data such as surface seismic data, VSP, logs, cores, cuttings and rock properties. In addition, some issues related to confidentiality and data licencing agreements restricted access to reservoir data and reservoir simulations.

The seismic modeling analysis done in the dissertation was to compare a baseline scenario with seismic results that would be achieved at the end of the project; for example when the reef pore space had been filled with CO₂. Time-lapse seismic modeling to show development of the plume during the injection phase was not undertaken because of uncertainties in the flow model of CO₂ within the Leduc Formation.

Identifying the Redwater reef margin, delineating the reef rim thickening and the inner reef region thinning, and mapping the Duvernay embayment were implemented in this dissertation to understand the reef geometry and facies to help the HARP project management make the right decision for the best location for CO₂ injection and storage.

The significant results from the seismic amplitude differences before and after CO₂ saturation using the seismic time-lapse analysis were implemented to possibly monitor the CO₂ saturation within the Redwater Leduc Reef. The capacity of CO₂ storage of about 974 Mt in the Redwater Leduc reef and Cooking Lake Formation below the reef is significant if the HARP project is resumed to reduce the CO₂ emissions into the atmosphere.

In comparison of the Redwater reef carbonates in the HARP project in Alberta with other CCS projects in carbonates like Weyburn field project in Saskatchewan, there are similarities in the results between the time-lapse multicomponent seismic modeling of Devonian Redwater reef and time-lapse multicomponent seismic data measurements and modeling of Mississippian carbonate reservoir in the Weyburn field. The P-wave velocity decreased by 4-6% with a corresponding 15-20% change in reflection amplitude and S-wave velocity change by 5-10% in Weyburn carbonates due to CO₂ sequestration (Davis et al., 2003). The time-lapse multicomponent analysis demonstrates significant amplitude difference for P-waves and less difference for S-waves for Weyburn reservoir interval due to CO₂ injection, as well as a time delay up to 2 ms in P-wave (Davis et al., 2003, Li, 2003, Terrell et al., 2002 and Herawati and Davis, 2003). These results show agreement between HARP project and Weyburn project and give more confidence in the dissertation outcomes.

One main difference between the two projects is the change in S-wave velocity where it is predicted to be less than 1% in Redwater reef after CO₂ saturation. This is due to some

differences in rock composition, properties and fluid contents in both projects. The Weyburn carbonate has higher average porosity of 15-26%, lower average permeability of 0.1-0.2 Darcy and it is oil bearing reservoir (Whittaker and Gilboy, 2003 and Davis and Benson, 2004), yielding changes in S-wave velocity of 5-10%.

6.4 Conclusions

6.4.1 Surface 2D seismic data interpretation

Interpretation of 400 line km of vintage 2D seismic data was accomplished for this study. The seismic data quality is good. Six wells were used to generate zero-offset synthetic seismograms to tie the seismic data to formation tops. The correlation between the synthetic seismograms and the migrated seismic data were good. The key horizons including the Mannville, Nisku, Leduc, Mid-Leduc, Cooking Lake, Beaverhill Lake, Lower Beaverhill Lake formations are gridded and mapped as well as the Basement event. All the formations dip towards the south-west and no observable faults were indentified in the study area. Time structure of formations younger than the Leduc Formation exhibits compactional drape over the reef, and this decreases upwards.

Reflections below the reef exhibit significant positive time structure due to the lateral velocity change that compensated in depth maps. Terminations of the Upper Leduc and Middle Leduc events are clear and were used to define the reef margin. Isochron and Isopach maps between the Upper Leduc and deeper formations delineate thickening of the reef rim, and thinning in the inner reef region. A Duvernay embayment was mapped encroaching into the reef along the northern part of the north-western reef flank, and also

around the southwestern corner of the reef. A loss of coherence in reflectivity along some seismic lines near the western edge of the reef was interpreted to be an indicator of dolomitization in the Middle Leduc and Cooking Lake formations.

6.4.2 Well-based fluid substitution seismic modeling

Fluid replacement modeling using the Gassmann approach is an effective method to model seismic time-lapse differences that would be caused by CO₂ injection. For both well 16-08-57-23W4 and well 11-08-57-22W4, a distinct P-wave velocity decrease occurs between 0% and 40% of CO₂ saturation by about 2.3% and 4.1% respectively. From 40% to 100% of CO₂ saturation, the P-wave velocity changes are slightly. In contrast, the S-wave velocity increases almost linearly with increasing CO₂ saturation by about 0.65% and 0.44% respectively. V_p/V_s decreases by about 2.9% and 4.5% and the P-wave impedance also decreases by 3.5% and 4.9% respectively.

Zero-offset ray tracing synthetic seismograms were generated for both wells before and after fluid substitution. There are changes in amplitudes between the wet in-situ reservoir reflections and the fluid substitution modeling reflections of Leduc formation. The time shift is obviously observed at the base of the Leduc reservoir of about 2.5 ms and 4.2 ms respectively. The maximum time shift at the base of the Leduc reservoir and the highest amplitude difference changes are recognized at about 40% CO₂ saturation.

6.4.3 Time-lapse 2D and 3D multicomponent seismic modeling of CO₂ fluid substitution in the Redwater Leduc reef

The 2D and 3D multicomponent synthetic seismic data demonstrate similar seismic attributes for the key formations including Mannville, Nisku, Ireton, Leduc, Duvernay, Cooking Lake, and Beaverhill Lake Formations before and after CO₂ saturations.

Reflections below the reef such as the Cooking Lake and Beaverhill Lake Formations display positive structure in the time seismic data conform to the real seismic data. This apparent structure is compensated to being flat in depth-migrated seismic data. The reef rim is observed at the reef margin. Terminations and the lateral position of the Upper Leduc and Middle Leduc events are evident on the 2D and 3D multicomponent seismic sections. After CO₂ saturation in the Upper Leduc member, the P-wave interval velocity decreases by about 3.3% and the impedance decreases by about 3.6%, yielding a reflectivity difference of about 14%. The time shift at the base of Upper Leduc member is about 1.6 ms.

The 2D and 3D vertical component (PP) CO₂ saturated synthetic seismic data display a reduction in amplitude for Leduc Formation and an increase in amplitude in Mid-Leduc member compare to baseline, while the radial component (PS) CO₂ saturated seismic data display a less reduction for Leduc and less increase for Mid-Leduc amplitudes compared to PP monitor seismic data. The 2D and 3D time-lapse analysis of multicomponent synthetic seismic data demonstrate significant amplitude differences for the Upper Leduc and Mid-Leduc members before and after 40% CO₂ saturation recommending that it is

possible to monitor the CO₂ saturation within the Redwater Leduc Reef by repeated 2D or 3D multicomponent seismic surveys.

The CO₂ storage capacity is about 800 Mt CO₂ for the entire Redwater reef (including the oil-leg and water-leg) for the storage efficiency factor of 20%. The CO₂ storage capacity of the water-leg area in the Upper Leduc member only is 163 Mt and in the full Redwater Leduc reef is 352 Mt. The CO₂ storage capacity of the Cooking Lake Formation below the water-leg area is estimated by 124 Mt, and below the total area of Redwater Leduc reef is 174 Mt.

6.5 Recommendations for future work

The plans of phase-I of HARP project were the site characterization of the Redwater reef using the 2D seismic data and to evaluate the CO₂ saturation in the Devonian Leduc reservoir. 2D and 3D multicomponent seismic modeling of fluid substitution and time-lapse analysis were generated to validate the feasibility of monitoring the CO₂ storage seismically. The plans for Phase-II of HARP project are to drill exploratory well for injectivity test and acquire baseline and monitor surface seismic surveys.

A 3D 3C seismic survey is recommended in Redwater area for subsurface CO₂ monitoring with dipole sonic logs acquired if possible. Construction of V_p / V_s maps by producing isochron maps between the Upper Leduc and Cooking Lake formations for PP and PS before and after CO₂ saturation is also suggested. Also, following the same seismic data acquisition parameters and processing work flow with the same software for

baseline and monitor surveys are strongly recommended to avoid any artefacts. The patchy saturation model should be taken in consideration to simulate the actual CO₂ injection in the Redwater reef. Finally, the comparison between the future acquired seismic data and the modeled seismic data implemented in this dissertation is a key to recognize the seismic characterization of CO₂ saturation in the Redwater Leduc reef by analyzing the similarity and contrast of seismic attributes.

References

- Anderson, N. L., White, D., and Hinds, R., 1989, Woodbend Group Reservoirs in: Geophysical Atlas of Western Canada Hydrocarbon Pools: Canadian Society of Exploration Geophysicists and Canadian Society of Petroleum Geologists, p.101-132.
- Andrichuk, J. M., 1958, Stratigraphy and facies analysis of Upper Devonian reefs in Leduc, Stettler and Redwater areas, Alberta: AAPG Bulletin, vol. 42, Number 1, 1-93.
- Anthonsen K. L., Vangkilde-Pedersen T., and Vangkilde-Pedersen L. H., 2009, Estimates of CO₂ storage capacity in Europe: IOP Conf Ser Earth Environ Sci., 6, 172006.
- Arts, R., Eiken, O., Chadwick, A., Zweigel, P., Meer, L., and Zinszner, B., 2002, Monitoring of CO₂ injected at Sleipner using time lapse seismic data: Abstracts of the 6th international conference on greenhouse gas control technology (GHGT-6).
- Atchley, S. C., West, L.W., and Sluggett, J. R., 2006, Reserves growth in a mature oil field: The Devonian Leduc Formation at Innisfail field, south-central Alberta, Canada: AAPG Bulletin, vol. 90, Number 8, 1153–1169.
- Bachu, S., Adams, J. J., 2003, Sequestration of CO₂ in geological media in response to climate change: capacity of deep saline aquifers to sequester CO₂ in solution: Energy Convers, Manage, 44, 3151–3175.
- Bachu, S., Buschkuehle, M., Haug, K. and Michael, K., 2008, Subsurface characterization of the Edmonton-area acid-gas injection operations: Energy Resources Conservation Board, ERCB/AGS Special Report 092, 134 p.
- Bachu, S., 2000, Suitability of the Alberta subsurface for carbon-dioxide sequestration in geological media: Alberta Geological Survey, Alberta Energy and Utilities Board, Earth Sciences Report 00-11.
- Bakhorji, A. and Schmitt, D., 2008, Velocity of P- and S-Waves in Arab-D and WCSB Carbonates: Expanded abstract in CSEG 2008 Conference and Exhibition, Calgary, Canada.
- Batzle, M., and Wang, Z., 1992, Seismic properties of pore fluids: Geophysics, 57, 1396-1408.

- Birkholzer, J. T., Zhou, Q., Rutqvist, J., Jordan, P., Zhang, K., Tsang, C. F., 2007, Research project on CO₂ geological storage and groundwater resources: large-scale hydrogeological evaluation and impact on groundwater systems: Report LBNL-63544, Lawrence Berkeley National Laboratory, Berkeley, CA, USA.
- Brown, L.T., Davis, T.L., and Batzle, M., 2002, Integration of rock physics, reservoir simulation, and time-lapse seismic data for reservoir characterization at Weyburn Field, Saskatchewan: Society of Exploration Geophysicists Expanded Abstract, 21, p. 1708-1711.
- Daley, T. M., Myer, L., Hoversten, G., and Peterson, J., 2005, Borehole Seismic Monitoring of Injected CO₂ at the Frio Site: American Geophysical Union, 2005.
- Dashtgard, S. E., Buschkuehle, M. B. E., Berhane, M., and Fairgrieve, B., 2006, Local-Scale Baseline Geological Report for the Pembina-Cardium CO₂-Enhanced Oil Recovery Site: Alberta Geological Survey.
- Davis, T. L., Terrell, M. J., Benson, R. D., Cardona, R., Kendall R. R., and Winarsky, R., 2003, Multicomponent seismic characterization and monitoring of the CO₂ flood at Weyburn Field, Saskatchewan: The Leading Edge, Vol. 22, 696-697.
- Davis, T. L., and Benson, R. D., 2004, Weyburn Field Seismic Monitoring Project: SEG expanded abstract, Vol. 23, 2255-2258.
- Del Pino, S., Levinson, R., and Larsen, J., 2006, Hot Climate, Cool Commerce: A Service Sector Guide to Greenhouse Gas Management.
- DOE, 2006, Proposed Methodology for Construction of a 2006 National Geological Carbon Sequestration Capacity Assessment: Final Draft Prepared by the Capacity and Fairways Subgroup of the Geologic Working Group of the DOE Carbon Sequestration Regional Partnerships, October 1, 2006.
- Doughty, C., Pruess, K., 2004, Modeling supercritical carbon dioxide injection in heterogeneous porous media: Vadose Zone J., 3, 837-847.
- EIA, World Energy Projection System Plus, 2010, International Energy Statistics database (November 2009), web site www.eia.doe.gov/oiaf/ieo/emissions.html.
- EU GeoCapacity Project, 2009, Assessing European Capacity for Geological Storage of Carbon Dioxide: Sixth Framework Programme of the European Community for Research, D16 WP2 Report Storage Capacity.

- Gassmann, F., 1951, *Über die Elastizität poröser Medien: Vierteljahrsschrift der Naturforschenden Gesellschaft Zürich*, vol. 96, 1–23.
- Gassmann, F., 1951, Elastic waves through a packing of spheres: *Geophysics*, 16, 673-685.
- Gunter, B., and Bachu, S., 2007, *The Redwater Reef in the Heartland Area, Alberta; A Unique Opportunity for Understanding and Demonstrating Safe Geological Storage of CO₂: ARC and AEUB Document on Heartland Redwater CO₂ Storage opportunities.*
- Gunter, W.D., Bachu, S., Palombi, D., Lakeman, B., Sawchuk, W., Bonner, D., 2009, *Heartland Area Redwater reef saline aquifer CO₂ storage project: Energy Procedia*, Vol. 1, 3943–3950.
- Herawati, I., and Davis, T. L., 2003, *The Use of Time-Lapse P-wave Impedance Inversion to monitor CO₂ Flood at Weyburn Field, Saskatchewan, Canada: SEG expanded abstract*, Vol.22, 1350-1353.
- Hashin, Z. and Shtrikman, S., 1963, A variational approach to the theory of elastic behavior of multiphase materials: *J. Mech. Phys. Solids*, 11, 127-140.
- Holloway, S., Heederik, J. P., van der Meer, L. G. H., Czernichowski-Lauriol, I., Harrison, R., Lindeberg, E., Summerfield, I. R., Rochelle, C., Schwarzkopf, T., Kaarstad, O., Berger, B., 1996, *The underground disposal of carbon dioxide: summary report: JOULE II Project No. CT92-0031. British Geological Survey, Keyworth, UK.*
- Houghton, J. T., Filho, L. G. M., Bruce, J., Lee, H., Callander, B. A., Haites, E., Harris, N. and Maskell, K., 1994, *Radiative Forcing of Climate Change and An Evaluation of the IPCC IS92 Emission Scenarios: Cambridge University Press*, pp 339.
- Intergovernmental Panel on Climate Change (IPCC), 2005, *IPCC Special Report on Carbon Dioxide Capture and Storage: Prepared by Working Group III of the Intergovernmental Panel on Climate Change [Metz, B., O. Davidson, H. C. de Coninck, M. Loos, and L. A. Meyer (eds.)]*, Cambridge University Press.
- Kaldi, J. and Bachu, S., 2009, *Site Selection and Storage Capacity for Geosequestration of Carbon Dioxide: AAPG/SEG/SPE Hedberg conference, in Vancouver, Canada, AAPG search and discovery 2010 article no. 90103.*

- Klovan, J. E., 1974, Development of Western Canadian Devonian Reefs and Comparison with Holocene Analogues: AAPG Bulletin, vol. 58, Number 5, 787–799.
- Klovan, J. E., 1964, Facies analysis of the Redwater Reef complex. Alberta, Canada: Bulletin of Canadian Petroleum Geology, vol. 12, 1-100.
- Kopp, A., Probst, P., Class, H., and Helmig, R., 2008, Estimation of CO₂ Storage Capacity Coefficients in Geologic Formations: GHGT9.
- Lawton, D. C. and Sodagar, T. M., 2009, CO₂ Fluid Replacement Seismic Modeling of the Devonian Leduc Reef in Redwater Area, Alberta: SEG 2009 Summer Research Workshop of CO₂ Sequestration Geophysics, in Banff, Canada.
- Li, G., 2003, 4D seismic monitoring of CO₂ flood in a thin fractured carbonate reservoir: The Leading Edge, Vol. 22, 690-695.
- Mathieson, A., Wright, I., Robert, D., and Ringrose, P., 2008, Satellite Imaging to monitor CO₂ movement at Krechba, Algeria: Abstracts of the 9th international conference on greenhouse gas control technology (GHGT-9), Paper 307.
- Mavko, G., Mukerji, T., and Dvorkin, J., 1998, The rock physics handbook, tools for seismic analysis in porous media: Cambridge University press, New York, 329 p.
- Michael, K., Bachu, S., Buschkuehle, B., Haug, K., and Talman, S., 2008, Comprehensive Characterization of a Potential Site for CO₂ Geological Storage in Central Alberta, Canada: AAPG Manuscript, 40 p.
- Mossop, G. D., 1972, Origin of the peripheral rim, Redwater reef, Alberta: Bulletin of Canadian Petroleum Geology, vol. 20, 238-280.
- Muggeridge, A., Abacioglu, Y., England, W., Smalley, C., 2004, Dissipation of anomalous pressures in the subsurface: J. Geophys. Res. 109, B11104, doi:10.1029/2003JB002922.
- Neuzil, C. E., 1995, Abnormal pressures as hydrodynamic phenomena: Am. J. Sci. 295, 742–786.
- NORSAR Innovation AS, 2007, NORSAR-2D User's Guide: www.norsar.com.
- NORSAR Innovation AS, 2008, NORSAR-3D User's Guide: www.norsar.com.

- Piri, M., Prevost, J. H., and Fuller, R., 2005, Carbon Dioxide Sequestration in Saline Aquifers: Evaporation, Precipitation and Compressibility Effects: Fourth Annual Conference on Carbon Capture and Sequestration DOE/NETL.
- Puckette, J., Al-Shaieb, Z., 2003, Naturally underpressured reservoirs: applying the compartment concept to the safe disposal of liquid waste., In: Search and Discovery Article 40071, Online Adaptation of Presentation at American Association of Petroleum Geologists, Southwest Section Meeting, Fort Worth, TX, USA, March, 2003, (www.southwestsection.org).
- Riddiford, F., Akretche, S., and Tourqui, A., 2003, Storage and Sequestration of CO₂ in the In Salah Gas Project: World Gas Conference, Tokyo.
- Shafeen, A., Croiset, E., Douglas, P. L., Chatzis, I., 2004, CO₂ sequestration in Ontario, Canada. Part I. Storage evaluation of potential reservoirs: Energy Convers. Manage., 45, 2645–2659.
- Smith, T. M., Sondergeld, C. H., and Rai, C. S., 2003, Gassmann fluid substitutions: a tutorial: Geophysics, 68, 430-440.
- Sodagar, T. M., and Lawton, D. C., 2009, Seismic modeling of fluid substitution in Redwater Reef, Alberta: CREWES Research Report, Volume 21.
- Sodagar, T.M., and Lawton, D.C., 2010a, 2D Seismic modeling of the Redwater Leduc Reef, Alberta: Expanded abstract in GeoCanada 2010 Conference and Exhibition, Calgary, Canada.
- Sodagar, T.M., and Lawton, D.C., 2010b, Timelapse seismic modelling of CO₂ fluid substitution in the Redwater Leduc Reef, Alberta: Expanded abstract in 72nd EAGE Conference and Exhibition 2010, Barcelona, Spain.
- Sodagar, T.M., and Lawton, D.C., 2010c, 2D Seismic Modeling of CO₂ Fluid Replacement of the Redwater Leduc Reef for CO₂ Storage Project, Alberta: Abstract in AAPG International Conference and Exhibition 2010, Calgary, Canada.
- Sodagar, T.M., and Lawton, D.C., 2010d, Seismic modeling of CO₂ fluid substitution for the Heartland Area Redwater CO₂ Storage Project (HARP), Alberta, Canada: Expanded abstract in GHGT-10 Conference, Amsterdam, Netherlands.

- Sodagar, T.M., and Lawton, D.C., 2010e, Time-lapse multi-component seismic modeling of CO₂ fluid replacement in Redwater Leduc Reef, Alberta: Expanded abstract in SEG Annual Conference and Exhibition 2010, Denver, USA.
- Sodagar, T.M., and Lawton, D.C., 2010f, Time-lapse multi-component seismic modeling of CO₂ fluid substitution in the Redwater Devonian Reef, Alberta, Canada: *The Leading Edge*, Vol. 29, no 10, 1266-1276.
- Sodagar, T. M., and Lawton, D. C., 2010g, Time-lapse of multi-component seismic modeling of CO₂ fluid replacement in Redwater Leduc Reef, Alberta: CREWES Research Report, Volume 22.
- Sodagar, T. M., and Lawton, D. C., 2010h, Seismic interpretation of the Redwater Leduc Reef, Alberta: CREWES Research Report, Volume 22.
- Sodagar, T.M., and Lawton, D.C., 2011a, Seismic modeling of CO₂ fluid substitution for the Heartland Area Redwater CO₂ Storage Project (HARP), Alberta, Canada: *Elsevier International Journal, Energy Procedia*, Vol. 4, 3338-3345.
- Sodagar, T.M., and Lawton, D.C., 2011b, 4D multicomponent seismic modeling of CO₂ fluid substitution in the Redwater Devonian Reef, Alberta, Canada: Abstract in AAPG Annual Conference and Exhibition 2011, Houston, USA.
- Stoakes, F. A., 1980, Nature and control of shale basin fill and its effect on reef growth and termination: Upper Devonian Duvernay and Ireton Formations of Alberta, Canada: *Bulletin of Canadian Petroleum Geology*, vol. 28, 345-410.
- Stoakes, F. A., and Foellmer, K., 2008, Geological Model of the Cooking Lake– Leduc at Redwater, Central Alberta: Stoakes Consulting Group (SCG) LTD unpublished report.
- Terrell, M. J., Davis, T. L., Brown, L., and Fuck, R., 2002, Seismic monitoring of a CO₂ flood at Weyburn field, Saskatchewan, Canada: demonstrating the robustness of time-lapse seismology: SEG expanded abstract, Vol. 21, 1673-1676.
- Van der Meer, L. G. H., 1995, The CO₂ storage efficiency of aquifers: *Energy Convers. Manage.*, 36 (6–9), 513–518.
- Verwer, K., Braaksma, H., and Kenter, J. A., 2008, Acoustic properties of carbonates: Effects of rock texture and implications for fluid substitution: *Geophysics*, 73, 51-65.

- Wang, Z., 2001, Fundamentals of seismic rock physics: *Geophysics*, 66, 398-412.
- Wendte, J. C., Stoakes, F. A., and Campbell, C. V., 1992, Devonian - Early Mississippian carbonates of the Western Canada Sedimentary Basin: a sequence stratigraphic framework: *SEPM Society for Sedimentary Geology Short Course No. 28*, p. 163-206.
- Whittaker, S., and Gilboy C., 2003, IEA Weyburn CO₂ Monitoring and Storage Project: Geoscience Framework update: *in* Summary of Investigations 2003, Volume 1, Saskatchewan Geological Survey, Sask. Industry Resources, Misc. Rep. 2003-4.1, CD-ROM, Paper A-7, 9p.
- Yu, H., Zhou, G., Fan, W., and Ye, J., 2006, Predicted CO₂ enhanced coalbed methane recovery and CO₂ sequestration in China: *International Journal of Coal Geology*, 71, 345-357.
- Zhou, Q., Birkholzer, J. T., Tsang, C. F., Rutqvist, J., 2008, A method for quick assessment of CO₂ storage capacity in closed and semi-closed saline formations: *international journal of greenhouse gas control*, Vol. 2, 626-639.